UNIVERSITY OF OKLAHOMA

GRADUATE COLLEGE

DEVELOPMENT AND APPLICATION OF SINGLE CELL MASS SPECTROMETRY TECHNIQUES FOR NON-ADHERENT CELL ANALYSIS

A DISSERTATION

SUBMITTED TO THE GRADUATE FACULTY

in partial fulfillment of the requirement for the

Degree of

DOCTOR OF PHILOSOPHY

By

Yanlin Zhu

Norman, Oklahoma

2020

Downloaded from SHAREOK. Persistent Handle URL: https://hdl.handle.net/11244/325290

DEVELOPMENT AND APPLICATION OF SINGLE CELL MASS SPECTROMETRY TECHNIQUES FOR NON-ADHERENT CELL ANALYSIS

A DISSERTATION APPROVED FOR THE DEPARTMENT OF CHEMISTRY AND BIOCHEMISTRY

By THE COMMITTEE CONSISTING OF

Dr. Zhibo Yang

Dr. Mark A. Nanny

Dr. Rakhi Rajan

Dr. Yihan Shao

© Copyright by YANLIN ZHU 2020
All Rights Reserved.

I dedicate this dissertation to my family.

Acknowledgments

First of all, I want to thank my advisor, Dr. Yang, for helping me to conceive new ideas, develop novel methods, and overcome the challenges of our research during these five years. Without his patience and guidance, I probably cannot finish these projects successfully in five years. Besides, He teaches me a lot of skills to maintain MS, such as replacing multipliers, pump oil, MS cooling fans, and voltage output ports, which are useful for my future careers. Furthermore, Dr. Yang is always willing to support us to attend various conferences to learn the most advanced MS technology and build our network with other experts. After getting along with Dr. Yang for five years, I think he is my role model, and I will keep following his example after graduation.

Secondly, I would love to thank all the members of my committee, including Dr. Mark A. Nanny, Dr. Yihan Shao, Dr. Rakhi Rajan, and the former committee members, Dr. Shaorong Liu and Dr. Robert Thomson for providing advice for my General Exam and daily research.

Last but not least, I need to thanks all the lab members, Xingxiu Chen, Zou Zhu, Zongkai Peng, Yunpeng Lan, Tra Ngyuen, Zhihao Ma and Dan Chen, and previous lab members, Dr. Ning Pan, Dr. Wei Rao, Dr. Renmeng Liu, Dr. Mei Sun, Dr. Shawna Standke, Dr. Xiang Tian, and Jonathan Pope. They are the kindest people that I have never seen before. It’s my honor to work with them.

Table of Contents

Chapter 1. Introduction 1

1.1 Single-cell analysis 1

1.2 Single-cell mass spectrometry analysis (SCMS) 2

1.2.1 Ambient MS for single-cell analysis 3

1.2.1.1 Ambient MS technologies requiring cell attachment 5

1.2.1.1.1 The Single-probe MS 6

1.2.1.1.2 The T-probe MS 7

1.2.1.1.3 Live single-cell video-MS 8

1.2.1.1.4 Capillary microsampling ESI-MS 11

1.2.1.1.5 Cell pressure probe MS 12

1.2.1.1.6 Internal electrode capillary pressure probe ESI-MS 14

1.2.1.1.7 Nanomanipulation-coupled nanospray MS 15

1.2.1.1.8 Probe electrospray ionization (PESI) MS 15

1.2.1.1.9 Direct sampling probe (DSP) MS 17

1.2.1.1.10 Surface-coated probe nanoelectrospray Ionization (SCP-nanoESI-MS) 18

1.2.1.1.11 Desorption electrospray ionization (DESI) MS 19

1.2.1.1.12 Laser ablation electrospray ionization (LAESI) MS 19

1.2.1.1.13 Laser desorption/ionization droplet delivery (LDIDD) MS 20

1.2.1.2 Ambient MS technologies for non-adherent single cells..... 21

1.2.1.2.1 Integrated cell manipulation platform combined with the Single-probe MS 21

1.2.1.2.2 Easy Ambient Sonic-Spray Ionization (EASI) MS 22

1.2.1.2.3 Drop-on-demand inkjet printing combined with Probe Electrospray Ionization (PESI)-MS 23

1.2.1.2.4 Mass cytometry..... 25

1.2.1.2.5 Redesigned T-probe MS..... 26

1.2.1.2.6 Micropipette needle MS 26

1.2.2 Non-ambient MS techniques for single-cell analysis 27

1.2.2.1 Non-ambient MS technologies which require cell attachment..... 27

1.2.2.1.1 Time of Flight (ToF)- secondary ion mass spectrometry (SIMS).... 27

1.2.2.1.2 Matrix-assisted laser desorption/ionization (MALDI)-MS..... 28

1.2.2.1.3 Nanostructure initiator MS (NIMS)..... 28

1.2.2.2 Non-ambient MS technologies for non-adherent cells..... 28

1.2.2.2.1 Nanopost arrays (NAPA) based-LDI-MS 28

Reference..... 30

Chapter 2. Research Overview 34

Reference..... 36

Chapter 3. Redesigning the T-probe for mass spectrometry analysis of online lysis of non-adherent single cells 37

3.1 Abstract..... 37

3.2 Introduction 38

3.3 Experimental Design and Data Processing..... 43

3.3.1 Fabrication and test of the T-probe..... 43

3.3.2 SCMS Experiments 45

3.3.3 SCMS Data Analysis 46

3.4 Results and discussion 47

3.4.1 Sampling solvent selection 47

3.4.2 Molecular Analysis of Single Cells in the Control and Drug Treatment Groups 47

3.4.3 Changes of Metabolomic Profiles after Drug Treatment..... 50

3.5 Conclusion 52

Reference..... 54

Chapter 4. Combining Mass Spectrometry with Paternò-Büchi Reaction to Determine Double-bond Positions in Lipids at the Single-cell Level. 59

4.1 Abstract..... 59

4.2 Introduction 60

4.2.1 Lipids 60
4.2.2 Classification of lipids 61
4.2.2.1 Classification of lipids base on their composition 61
4.2.2.2 Classification of lipids base on their functions 63
4.2.3 Significance of unsaturated lipid isomers 64
4.2.4 Identification of unsaturated lipid isomers 64
4.2.4.1 Current methods for unsaturated lipid isomers identification 64
4.2.4.2 The novel approach for unsaturated lipid isomers identification at single-cell level 65
4.3 Method 69
4.3.1 Fabrication of the micropipette needle 69
4.3.2 Preparation of SCMS solutions 69
4.3.3 Reactive SCMS experiments 70
4.3.4 Cells culture and sample preparation 71
4.4 Result and Discussion 72
4.4.1 Sampling solvent selection 72
4.4.2 Characterization of the micropipette needle 73
4.4.3 Workflow of data analysis 73
4.4.4 Determination of C=C bond locations in unsaturated lipids of single cells . 75
4.4.5 Comparison studies of cell lysates and single cells 80

4.5 Conclusion 81

Reference 84

Appendix I: Support Information of Chapter 3 88

Fabrication of the redesigned T-probe 88

Cells culture and SCMS sample preparation 89

Cell lysis 90

Data pre-treatment 91

Supporting Tables 92

Supporting Figures 96

References 108

Appendix II: Support Information of Chapter 4 109

Cell lysis preparation 109

Lipids C=C bond identification using cell lysate 109

Supporting Tables 111

Supporting Figures 161

References 174

Appendix III: Copyrights 175

Copyrights of Chapter 1 175

Copyrights of Chapter 3 190

Copyrights of Chapter 4 191

List of Tables

Chapter 1

Table 1-1..... 4

Chapter 3

Table 3-1..... 48

Chapter 4

Table 4-1..... 75

Appendix I

Table S3-1. 92

Table S3-2. 93

Table S3-3. 94

Table S3-4. 95

Appendix II

Table S4-1. 111

Table S4-2. 112

Table S4-3. 114

Table S4-4. 115

Table S4-5. 116

Table S4-6. 117

Table S4-7. 119

Table S4-8. 121

Table S4-9. 123

Table S4-10. 125

Table S4-11. 129

Table S4-12. 137

Table S4-13. 140

Table S4-14. 142

Table S4-15. 143

Table S4-16. 145

Table S4-17. 151

Table S4-18. 152

Table S4-19. 154

Table S4-20. 156

Table S4-21. 158

Table S4-22. 160

List of Figures

Chapter 1

Figure 1-1. 6

Figure 1-2. 9

Figure 1-3. 10

Figure 1-5. 13

Figure 1-6. 14

Figure 1-7. 16

Figure 1-8. 17

Figure 1-9. 18

Figure 1-10. 20

Figure 1-11. 22

Figure 1-12. 23

Figure 1-13. 24

Figure 1-14. 25

Figure 1-15. 29

Chapter 3

Figure 3-1. 41

Figure 3-2. 44

Figure 3-3. 49

Figure 3-4. 52

Chapter 4

Figure 4-1. 62
Figure 4-2. 67
Figure 4-3. 68
Figure 4-4. 71

Appendix I

Figure S3-1. 96
Figure S3-2. 97
Figure S3-3 98
Figure S3-4. 99
Figure S3-5. 100
Figure S3-6. 101
Figure S3-7. 102
Figure S3-8. 103
Figure S3-9. 105
Figure S3-10. 106

Appendix II

Figure S4-1. 161
Figure S4-2. 162
Figure S4-3. 163
Figure S4-4. 164
Figure S4-5. 165
Figure S4-6. 166
Figure S4-7. 168

Figure S4-8. 170

Figure S4-9. 171

Figure S4-10. 173

Abstract

Mass spectrometry (MS) analysis of biological samples is traditionally carried out using extractions from large populations of cells, concealing the information from individual cells. In contrast, the drawbacks of traditional methods can be overcome by single cell MS (SCMS) methods, and this approach is particularly suitable to study rare types of cells that are hard to achieve or culture, including primary cells, stem cells, and patient-derived cells. Due to the super capability of MS technique, a series of SCMS methods have been rapidly developed to investigate undiscovered cellular mechanisms of a broad range of cells. My studies led to the development of two novel sampling and ionization devices for analyzing non-adherent single cells in ambient conditions: the redesigned T-probe and micropipette needle. The redesigned T-probe can be applied for real-time SCMS analysis of live single cells, without losing cell content during the analysis. In addition, this device allows for relatively long ion signal acquisition time for more molecular structure identification. The development and application of this device are described in Chapter 3. The micropipette needle is another technology for non-adherent single cell analysis. Particularly, this device can be used for reactive SCMS experiments, in which chemical reactions between cellular species and reagents can be performed prior to MS analysis, allowing for versatile experimental designs. In Chapter 4, the micropipette device was used to conduct both regular and reactive SCMS analysis of the same single cell to identify double bond locations of unsaturated lipid isomers, which are critical for the understanding of lipid biochemistry and therapeutic targets in diseases.

Chapter 1. Introduction

1.1 Single-cell analysis

Traditional studies of tissues or cells are based on pooled assays to achieve averaged results using bulk samples (i.e., cell lysis and tissue extraction) with the assumption that the weighted average can represent the population's cellular constituents.[1] However, numerous single-cell studies recently find that cellular heterogeneity is presented in multicellular organisms, including any single tissue, which is apparent homogeneous.[1, 2] The differences may appear in cell functions, morphologies, and gene expression profiles. These differences can influence the health and features of the entire cellular population.[3] Therefore, cellular heterogeneities cannot be ignored, and the behaviors of any individual cell cannot be studied based on behaviors of population cells.[2]

Cells receive and respond to signals from the surrounding environment using their signaling molecules. However, each individual cell responds differently to the same message, and a portion of cells may exhibit incorrect or unexpected responses because of random signal transduction noise.[4] Cellular heterogeneity is also related to the expression of genes, proteins, and metabolites.[5] Recent studies indicated that cellular heterogeneity is a fundamental feature of cancer cells. For example, cell heterogeneity can affect cancer cell growth, which cannot be detected using pooled assays. Besides, previous studies point out that high levels of cellular heterogeneity exist in most unstable cancer cell populations.[6] Investigating cellular heterogeneity can improve the understanding of the communication and responsibility of cells for both healthy and

disease states. Therefore, investigation of cellular heterogeneity is significant for cellular biology, especially for cancer cell populations.

In contrast to bulk analysis, cell heterogeneity in multicellular organisms (i.e., organs, tissues, and cell culture) can be investigated using single-cell analysis.[3] Various single-cell analyses have been carried out in genomics, transcriptomics, proteomics, and metabolomics studies.[5] Among all these single-cell "omics" studies, single-cell metabolomics studies are able to provide molecular information that more directly reflect the functions, status, and dynamics of individual cells. However, due to the intrinsic characteristics of metabolites, including rapid (e.g., a few seconds or less) dynamic change of abundances, vast structural diversity, broad ranges of concentrations, incapable amplification of quantities, and the absence of non-interfering labeling technique (e.g., commonly used fluorescent tags can alter metabolites' functions), single-cell metabolomics is a very challenging area.[7] Currently, the major technologies used for single-cell metabolomics studies include mass spectrometry (MS), capillary electrophoresis (CE), optical spectroscopy, and fluorescence biosensors. With the development of the single-cell metabolomics study, it can be applied in broad areas, such as cancer cell study, systems biology, and drug resistance.[7]

1.2 Single-cell mass spectrometry analysis (SCMS)

A number of analytical techniques, such as single-cell transcriptomics[8], flow cytometry[9], fluorescence microscopy[10], Raman spectroscopy[10, 11], and electrochemical assays,[12] have been used for single-cell analysis. However, broad applications of these techniques are limited by their own drawbacks, including the requirement of using molecular labels (e.g., fluorescence-based methods), incapability of simultaneous detection of broad types

of molecules, limited sensitivity, inadequate resolution, and unsatisfied reproducibility.[13] Hence, a label-free method with high sensitivity, high selectivity, and high resolution would be more suitable for single-cell analysis. Compared with the above technologies, MS can provide several advantages, such as high sensitivity at femtomolar level, high selectivity, high resolution, high throughput, rich chemical information, and no requirement of labels. Particularly, owing to its high sensitivity, the sample consumption of MS measurement is very low, indicating it is suitable for single cell analysis.[13, 14] Presently, a variety of MS techniques have been developed as effective, powerful, and reliable devices for single cell analysis focusing on various types of molecules (i.e., proteins, peptides, lipids, and metabolites).[13, 15] The summary of these SCMS techniques are shown in Table 1-1.

1.2.1 Ambient MS for single-cell analysis

Ambient MS techniques, which can be used in ambient conditions for sampling and ionization, allow for direct analysis of components and metabolites of cellular or subcellular under open-air status with little or no sample preparation or separation.[14, 16] The significance of ambient MS is that it enables a direct, rapid, real-time, and straightforward analysis of samples.[14] This is particularly important for studies of live cells under their normal growing conditions. In addition, ambient MS technologies retain the advantages of MS, including high throughput, high selectivity, and high sensitivity. Nowadays, a number of ambient MS technologies have been applied in *in situ* or *in vivo* single-cell studies through direct, real-time analysis.[14]

Table 1-1. Summary of SCMS techniques

SCMS technologies	Require cell attachment	Types	Pros/Cons
The Single-probe MS[17]	Y	Ambient	Real-time analysis; able to conduct reactive SCMS/Limited throughput; no separation
The T-probe MS[18]	Y	Ambient	Real-time analysis/Limited throughput, no separation
Live single-cell video-MS[19]	Y	Ambient	Easy assemble process/Limited throughput, no separation
Capillary microsampling ESI-MS[20]	Y	Ambient	Similar to Live single-cell video MS; Post-ionization separation (coupled with ion mobility separation)/Limited throughput, no separation
Cell pressure probe MS[21]	Y	Ambient	Able to conduct quantitative SCMS/Limited throughput, no separation
Internal electrode capillary pressure probe ESI-MS[22]	Y	Ambient	Similar to the cell pressure probe; internal electrode which can provide stable ionization voltage/Limited throughput, no separation
Nanomanipulation-coupled nanospray MS[23]	Y	Ambient	A second nanopositioner was used to puncture the cell membrane to avoid clogging of the probe/Limited throughput, no separation
Probe electrospray ionization (PESI) MS[24]	Y	Ambient	Analytes enrichment inside the probe/Limited throughput, no separation
Direct sampling probe (DSP) MS[25]	Y	Ambient	Cellular contents can be withdrawn in to probe spontaneously due to the hydrophilic surface of the probe and positive pressure inside of plant cells/ Limited throughput, no separation, limited signal duration time
Surface-coated probe nanoelectrospray Ionization (SCP-nanoESI-MS)[26]	Y	Ambient	Similar to Direct sampling probe; surface-coated probe can absorb target analytes/Limited throughput, no separation
Desorption electrospray ionization (DESI) MS[27]	Y	Ambient	High throughput; less sample preparation/Limited spatial resolution
Laser ablation electrospray ionization (LAESI) MS[28]	Y	Ambient	High throughput; less sample preparation/Limited spatial resolution
Laser desorption/ionization droplet delivery (LDIDD) MS[29]	Y	Ambient	Similar to LAESI (the wavelength of LDIDD is different from LAESI)
Integrated cell manipulation platform combined with the Single-probe MS[30]	N	Ambient	Real-time analysis/Limited throughput; no separation; limited signal duration time

Easy Ambient Sonic-Spray Ionization (EASI) MS[31]	N	Ambient	High throughput/large spatial resolution
Drop-on-demand inkjet printing combined with Probe Electrospray Ionization (PESI)-MS[32]	N	Ambient	High throughput; automatic sampling/no separation; limited signal duration time
Mass cytometry[33]	N	Ambient	High throughput; automatic; able to analyze the mixture of different types of cells/limited signal duration time; no separation
Redesigned T-probe MS[34]	N	Ambient	Real-time analysis; High throughput; online cell lysis system inside the probe/Limited throughput; no separation
Micropipette needle MS[35]	N	Ambient	Longer signal duration time; long reactive time for the chemical reaction; able to conduct reactive SCMS/Limited throughput; no separation
Time of Flight (ToF)-secondary ion mass spectrometry (SIMS)[36]	Y	Non-ambient	High spatial resolution; little sample consumption/complex sample preparation; extensive fragments
Matrix-assisted laser desorption/ionization (MALDI)-MS[15]	Y	Non-ambient	High throughput/complex sample preparation; large spatial resolution
Nanostructure initiator MS[37]	Y	Non-ambient	No matrix effect/requirement of spatial substrates;
Nanopost arrays (NAPA) based-LDI-MS[38]	N	Non-ambient	No matrix effect/requirement of spatial substrates;

1.2.1.1 Ambient MS technologies requiring cell attachment

These ambient MS technologies require single cell adherence on a smooth surface, such as glass slides, plastic slides, and well plates, for extraction of cellular contents, or desorption of analyte from single cells.[14] Some of the ambient MS technologies are listed below.

1.2.1.1.1 The Single-probe MS

The Single-probe works as a multifunctional sampling and ionization tool, which can be coupled with MS directly for real-time, *in situ* metabolomics analysis of living single cells. The single-probe is made up of three ingredients, which are a laser-pulled dual-bore quartz needle, a silica capillary, and a nano-ESI emitter. Both the nano-ESI emitter and the fused silica capillary, which works as solvent providing capillary, are embedded into a laser-pulled dual-bora quartz needle to combine a Single-probe. The diameter of

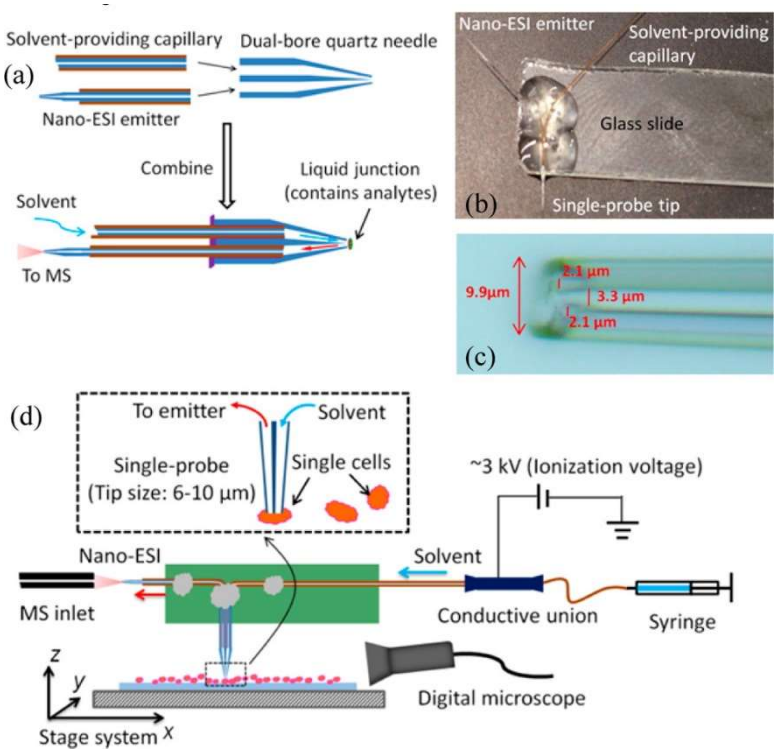


Figure 1-1. *Single-probe MS technology. (a) Fabrication processes of Single-probe; (b) Photograph of a Single-probe; (c) Tip of the Single-probe under magnification (40x); (d) Setup of Single-probe MS (Pan, N.; Rao, W.; Kothapalli, N. R.; Liu, R.; Burgett, A. W.; Yang, Z., The single-probe: a miniaturized multifunctional device for single cell mass spectrometry analysis. Analytical chemistry 2014, 86 (19), 9376-9380.* Copyright

permission is obtained from American Chemical Society, and the detail is shown in Appendix III.*)*

the Single-probe tip is around 6-10 μm, which can be inserted into a mammalian cell. Since the materials of these parts are inexpensive, the total cost of a Single-probe is around 5 dollars. [17] The stability and reproducibility of the Single-probe have been demonstrated through a series of studies such as metabolomics studies of alga cells,[39] cancer stem cells,[40] and tumor spheroids.[41] Besides, the Single-probe is used for MS imaging studies. [42] The principle and structure of the Single-probe are shown in Figure 1-1.

During the sampling procedure, cells are attached to a glass slide. An XYZ-translational stage system, which is controlled by the LabView software, is used to insert the tip of the Single-probe into a target cell under a digital microscope. The solvent (methanol/water or acetonitrile) is continuously provided through the solvent providing capillary to the dual-bore quartz needle (flow rate: ~25 nL/min). A liquid junction, which is generated between two bores at the quartz needle tip, can extract the analytes from the target cell. Then, driven by a self-aspiring suction force generated by the ESI process, cellular contents dissolved in the solvent are withdrawn into the nano-ESI emitter. During the experiment, ~3 kV ionization voltage is transmitted to the nano-ESI emitter using a conductive union and solvent. The nano-ESI emitter is positioned in front of the inlet of a mass spectrometer (e.g., Thermo LTQ Orbitrap XL) for direct analysis of cellular contents in real-time.[17]

1.2.1.1.2 The T-probe MS

The T-probe is a sampling device with miniaturized multifunction that allows cellular contents extraction and ionization for SCMS. A T-probe is produced using thermal binding,

from which two polycarbonate slides are fused to sandwich three capillaries arranged in a T-shape. These capillaries work as a sampling probe, a solvent-providing capillary, and a nano-ESI emitter, respectively, during SCMS analysis. The tip size of the sampling probe is around 5-8 μm, which is small enough to insert into a mammalian cell. During the SCMS experiment, the sampling solvent (methanol: water 1:1 (v/v) with 0.1% formic acid) is delivered (flow rate: 0.2 μL/min) through the solvent providing capillary from a syringe. The sampling probe is controlled by an XYZ-stage to insert in a targeted cell. Similar to the Single-probe, a suction force, which is generated via the ESI mechanisms, at the tip of the sampling probe draws the cellular contents into T-probe and mixed with the solvent at the T-junction. The mixture is then delivered and ionized at the nano-ESI emitter. 4 kV ionization voltage is transmitted to the nano-ESI emitter via a conductive union. Because the sampling probe only has one channel, the tip size of the sampling probe can be minimized under 1 μm, which can be potentially used for Single-cell analysis at the subcellular-level. Coupled with a mass spectrometer (e.g., Thermo LTQ Orbitrap XL MS) during single-cell sampling, the T-probe enables for online, *in situ,* and real-time analysis of individual live cells. Due to the high sensitivity and high reproducibility of the T-probe, it can be applied for a variety of species of single-cell metabolomics studies.[18] The working mechanisms and photos of the T-probe are illustrated in Figure 1-2.

1.2.1.1.3 Live single-cell video-MS

In this design, a video-microscope combined with a commercially available gold-coated nanospray tip was used to conduct SCMS analysis. Cell contents can be sucked into

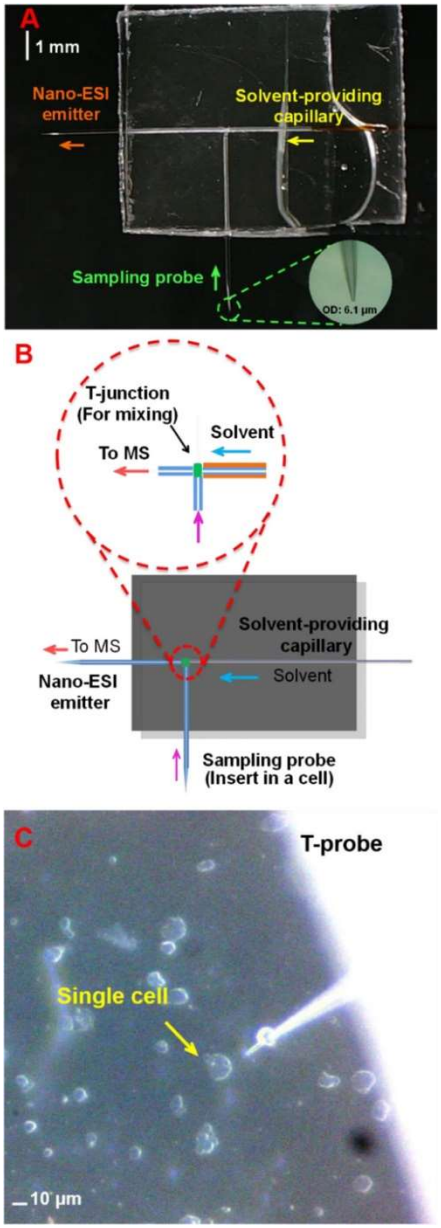


Figure 1-2. *T-probe technology for SCMS experiments. (A) Photography of T-probe; (B) Working mechanism and fluid flow direction of T-probe; (C) The photography of using T-probe sample a single cell under the microscope (x40). (Liu, R.; Pan, N.; Zhu, Y.; Yang, Z., T-probe: an integrated microscale device for online in situ single cell analysis and metabolic profiling using mass spectrometry. Analytical chemistry 2018, 90 (18), 11078-*

11085. Copyright permission is obtained from American Chemical Society, and the detail is shown in Appendix III.*)*

the nanospray tip (ID: 1-2 μm) under the video microscope using a piston syringe. After single-cell sampling, acetonitrile with 0.5% formic acid (ionization solvent) is added into the nanospray tip, which is then set up in front of the nano-ESI source of the mass spectrometer for analysis (Figure 1-3).[14, 19, 43] This technique has been used to study multiple cell lines, including Swiss 3T3 cells, RBL 2H3 cells, and TIG-3 cells. Hundreds of small metabolites were analyzed in a single cell. Statistical analysis methods, including PCA and t-test, were used for data interpretation.[19]

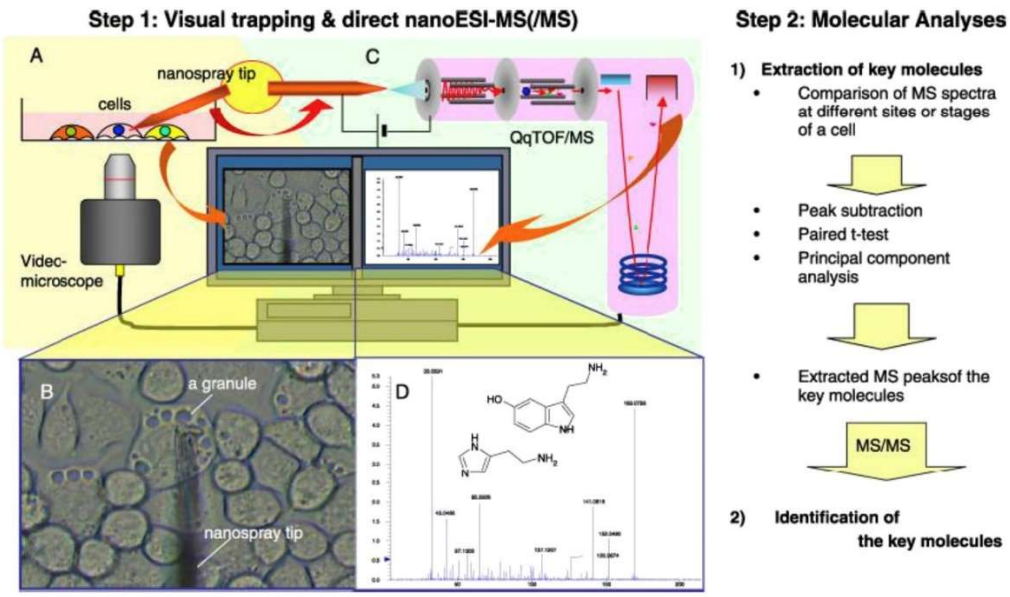


Figure 1-3. *Two steps of live single-cell video mass spectrometry using nanospray tip. In the first step: (A) Schematic diagram of live single-cell sampling; (B) Photo of Cells under video microscope; (C) Ionization of live single-cell video mass spectrometry; (D)Single-cell data acquisition and analysis. The second step is the workflow of molecular analyses. (Mizuno, H.; Tsuyama, N.; Harada, T.; Masujima, T., Live single-cell video-*

mass spectrometry for cellular and subcellular molecular detection and cell classification. Journal of mass spectrometry 2008, 43 (12), 1692-1700. Copyright permission is obtained from John Wiley and Sons, and the detail is shown in Appendix III.*)*

1.2.1.1.4 Capillary microsampling ESI-MS

The sampling procedure of capillary microsampling ESI-MS is similar to the above live single-cell video-MS. A nanospray tip (ID: 1 μm) is used to inject into a single cell and draw cell contents. After single-cell sampling, the electrospray solution (methanol and

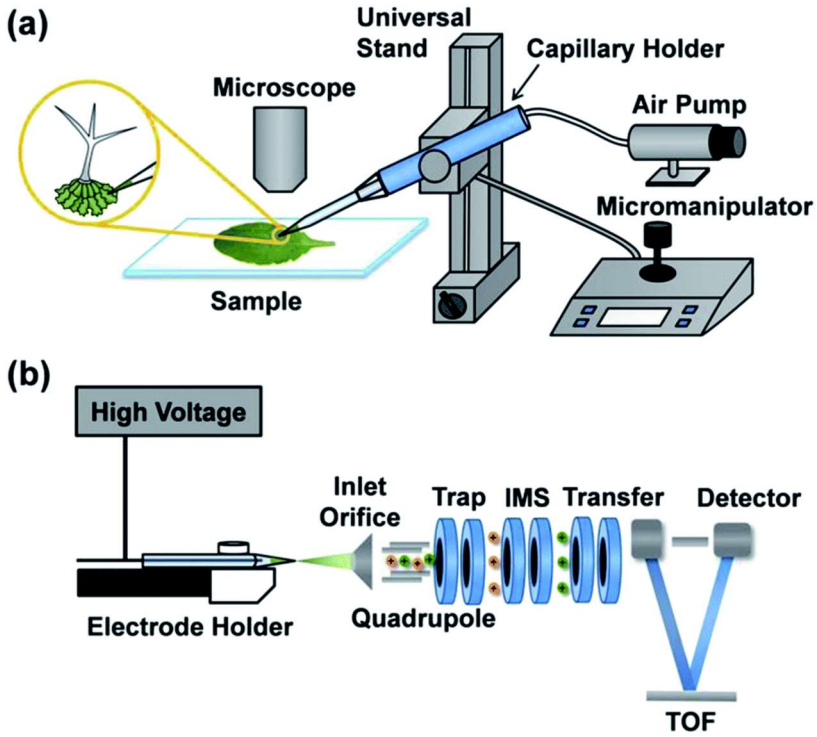


Figure 1-4. *(a) Schematic diagram of single-cell capillary microsampling. The nanospray capillary is controlled by a micromanipulator under a microscope. An air pump is used for controlling nanospray tip to extract cell contents; (B) Schematic diagram of ESI-IMS-MS analysis of single cells. (Zhang, L.; Foreman, D. P.; Grant, P. A.; Shrestha, B.; Moody, S. A.; Villiers, F.; Kwak, J. M.; Vertes, A., In Situ metabolic analysis of single plant cells by capillary microsampling and electrospray ionization mass spectrometry with*

ion mobility separation. Analyst 2014, 139 (20), 5079-5085. Copyright permission is obtained from Royal Society of Chemistry, and the detail is shown in Appendix III*)*

water (1:1) with 0.2% acetic acid, 1 μL) is backfilled into the nanospray tip. Then, this tip is positioned with the ion source of the mass spectrometer, and the ionization voltage (2 KV) is applied to a platinum wire, which is installed into the nanospray tip and to transfer the voltage to the solution and induce electrospray for analysis. In this specific study, the mass spectrometer utilizes ion mobility separation (IMS), (Figure 1-4) [20], which allows for post-ionization separation of ions due to the mobility in the gas-phase. This technique has been used to conduct analysis of different types of cells such as plant cells[20] and human hepatocytes.[44] Owing to the capability of ions separation, hundreds of metabolites and lipids were analyzed in these cells. Specifically, this technology has been used to investigate the lipids turnover rates, the energy charge of single cells, and the difference in energy charge between normal cells and drug-treated cells.[14]

1.2.1.1.5 Cell pressure probe MS

In this design, a quartz capillary with the tip size around 3-7 μM, which is fulfilled with a mixture of silicon oil and engine oil (9:1, v/v), is used as a sampling probe. The volume of the oil mixture is controlled by moving a rod back-and-forth with a motorized micrometer. After the capillary tip is inserted into a single cell, a pressure transducer is connected with the capillary tip to monitor and record the hydrostatic pressure inside the capillary. The piezo-manipulator controls and determines the location of the tip via a hydraulic continuity test. Because the sampling procedure is performed under a digital microscope, the volume of the cellular contents inside the capillary can be photographed and calculated. After cell sampling, the capillary is coupled to a mass spectrometer, and an ionization

voltage is applied on the capillary to create electrospray ionization (Figure 1-5).[21, 45] Because the cell sampling volume can be calculated, this technology can be applied for quantitative analysis of species in single cells. In the reported studies, several types of metabolites, such as sugars, amino acids, vitamins, and fatty acids, are rapidly detected. Besides, the pressure probe is coupled with hydrogen flame desorption ionization mass spectrometer (HFDI–MS) to quantitate metabolites at the single-cell level.

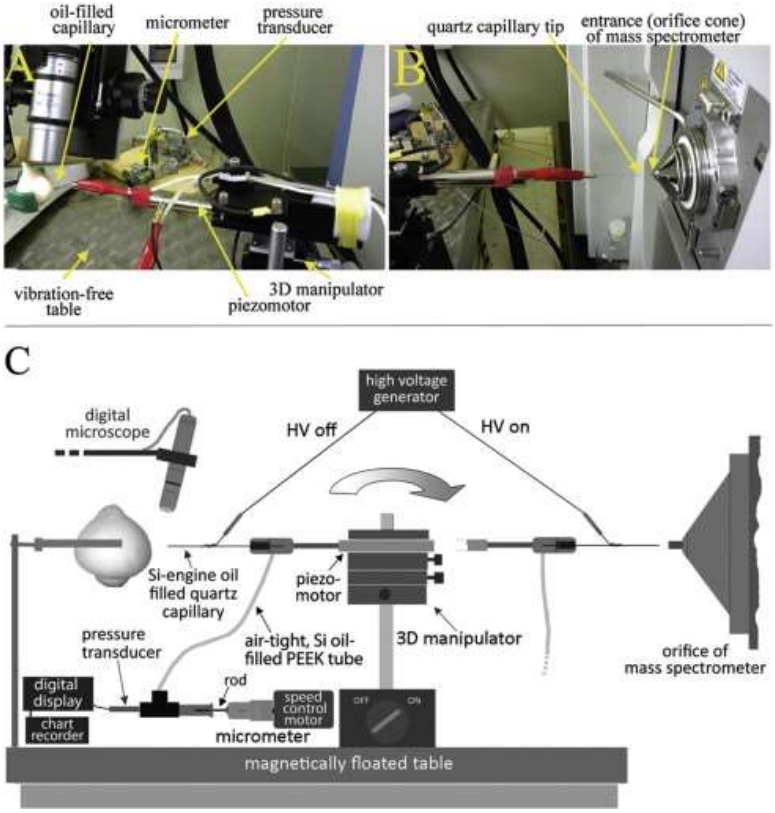


Figure 1-5. *(A) Photo of single-cell sampling using cell pressure probe. (B) Photo of cell pressure probe MS ionization and detection setup. (C) Scheme of the cell pressure probe instruments setup. (Gholipour, Y.; Erra-Balsells, R.; Hiraoka, K.; Nonami, H., Living cell manipulation, manageable sampling, and shotgun picoliter electrospray mass spectrometry for profiling metabolites. Analytical biochemistry 2013, 433 (1), 70-78.*

Copyright permission is obtained from ELSEVIER, and the detail is shown in Appendix III.*)*

1.2.1.1.6 Internal electrode capillary pressure probe ESI-MS

The working mechanism, including the sampling procedure, of the internal electrode capillary pressure probe is similar to the cell pressure probe. The major difference between them is that a titanium wire (0.3 mm I.D.), which is pre-embedded inside the capillary before sampling, is used as the internal wire electrode. The set-up of this device

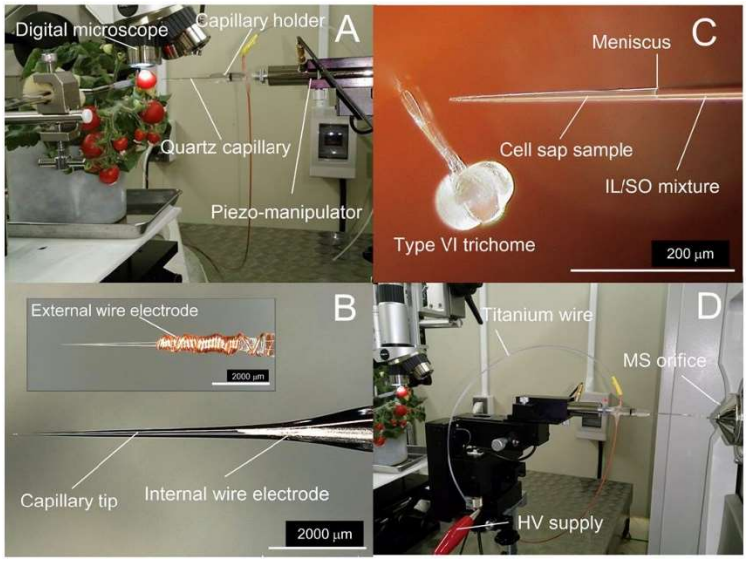


Figure 1-6. *(A) setup of the internal electrode capillary pressure probe. (B) the probe tip and a single cell under the microscope. (C) Photo of probe tip under the microscope. (D) The setup of subsequent ionization and detection using Orbitrap. (Nakashima, T.; Wada, H.; Morita, S.; Erra-Balsells, R.; Hiraoka, K.; Nonami, H., Single-cell metabolite profiling of stalk and glandular cells of intact trichomes with internal electrode capillary pressure probe electrospray ionization mass spectrometry. Analytical chemistry 2016, 88*

(6), 3049-3057. Copyright permission is obtained from American Chemical Society, and the detail is shown in Appendix III.*)*

is shown in Figure 1-6, and the location of the internal electrode is detailed in Figure 1-6C.[22]

1.2.1.1.7 Nanomanipulation-coupled nanospray MS

This system contains two nanopositioners to extract cellular contents, such as extract lipids (especially for triacylglycerols (TGs)), from individual cells.[23] In the reported studies, adipocytes are analyzed using this instrument. A Pd/Au-coated nanospray emitter (tip size: 1 ± 0.2 μm), which is prefilled with 10 μL of solution (chloroform: methanol 2:1 (v/v) with 0.1% NH_4OAc), is controlled by the first nanopositioner and inserted into the target adipocyte to extract cellular contents form cells with gentle suction (five psi pressure) for 500 ms. Because the tip size of the nanospray emitter is tiny, clogging by cell membrane can easily occur. Therefore, the authors use the second nanopositioner to hold a quartz probe (tip size: 8 μm) to puncture the cell membrane prior to sampling of cellular contents, minimizing the clogging issues. The sampling solvent and cellular species (e.g., TGs extraction) are drawn into the nanospray emitter to conduct subsequent detection using a mass spectrometer (Figure 1-7).[23] In particular, they investigated the dissimilarity of the TGs between normal and tumorous adipocytes and identified them as potential biomarkers.[23] In addition, they observed heterogeneity of TGs among large and small lipids droplets of normal adipocyte.[46]

1.2.1.1.8 Probe electrospray ionization (PESI) MS

The PESI-MS set-up uses a tungsten probe (tip size: 1 μm) as a sampling probe to insert into a single cell under the control of a three-dimensional manipulator. In order to enrich

metabolites, the probe is kept inside of the target cell for 30 s for surface absorption. After enrichment, the probe is coupled to the ion source of a mass spectrometer for subsequent ionization. Specifically, the sprayed-assistant solvent is used to wet the probe tip, and then an ionization voltage (~ 2.5 kV) is applied to the probe for ionization.[24] Due to the

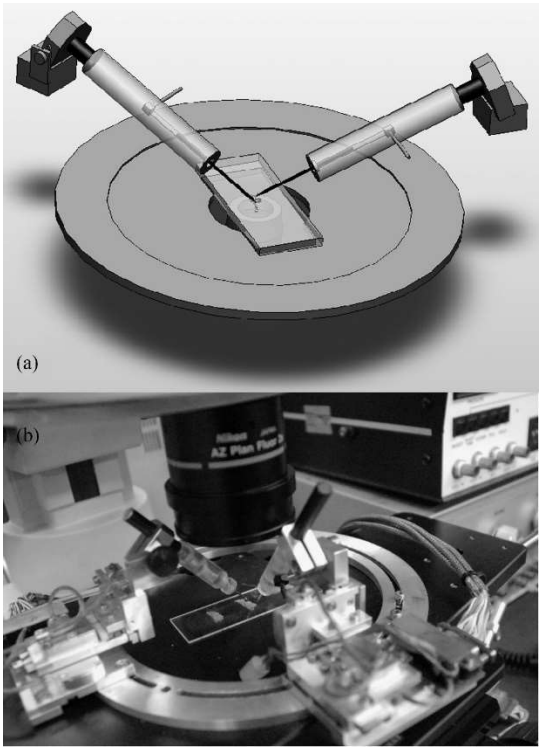


Figure 1-7. *(a) Scheme of single-cell sampling using a two-positioner nanomanipulator. (b) Photo of the two-positioner nanomanipulator.* (*Phelps, M.; Hamilton, J.; Verbeck, G. F., Nanomanipulation-coupled nanospray mass spectrometry as an approach for single cell analysis. Review of Scientific Instruments 2014, 85 (12), 124101.* Copyright permission is obtained from AIP Publishing, and the detail is shown in Appendix III.*)*

metabolite enrichment, this method is able to enhance signal intensity for 30 folds comparing with nanoESI-MS.[14]

1.2.1.1.9 Direct sampling probe (DSP) MS

In this set-up, a piezomicro-manipulator is used to control the direct sampling probe (tip size: 150 nm), which is oxidized to obtain the hydrophilic surface, and insert the probe tip inside an individual plant cell. Because of the positive turgor pressure inside the plant cell and the hydrophilic surface of the probe, the cellular contents can naturally leak out and spontaneously be absorbed by the probe tip. Then, the probe is coupled with the time-of-flight (TOF) mass spectrometer. The absorbed analytes are desorbed using auxiliary solvent droplets (acetonitrile and water, 50/50 (v/v)), which are generated by an inkjet head, and then an ionization voltage is applied to create electrospray for MS detection (Figure 1-8). Various metabolites of different plant single cells are detected and identified using this method.[25]

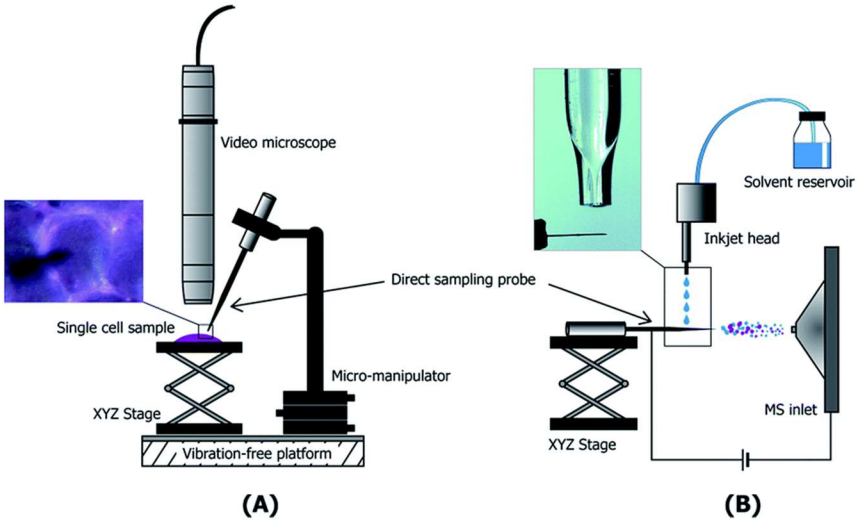


Figure 1-8. *(A) Scheme of single-cell sampling using DSP. (B) Scheme of DSP-MS setup. (Yu, Z.; Chen, L. C.; Ninomiya, S.; Mandal, M. K.; Hiraoka, K.; Nonami, H., Piezoelectric inkjet assisted rapid electrospray ionization mass spectrometric analysis of metabolites in plant single cells via a direct sampling probe. Analyst 2014, 139 (22), 5734-*

5739. Copyright permission is obtained from Royal Society of Chemistry, and the detail is shown in Appendix III.*)*

1.2.1.1.10 Surface-coated probe nanoelectrospray Ionization (SCP-nanoESI-MS)

Although the working mechanisms of the SCP device are similar to those of DSP, the SCP has two modifications.[26] First, the surface of a fine tungsten probe is coated using a solvent mixture (30% sulfuric acid with 30 mg/mL potassium permanganate and 15 mg/mL potassium dichromate; 30% sodium hydroxide) to improve the capability of absorbing target analytes such as perfluorinated compounds (PFCs). Second, a nanospray tip is used for the ionization of analytes. The sampling procedure of both techniques is nearly identical. After sampling, the SCP is installed into a nanospray tip, which is prefilled with desorption/spray solvent (1 μL of methanol) for 30 s to dissolve analytes for the surface of SCP. Then, an ionization voltage is applied to the SCP to induce the electrospray ionization for subsequent MS detection (Figure 1-9).[26] PFCs are detected and quantified from single *Daphnia magna's* egg cells using this method.

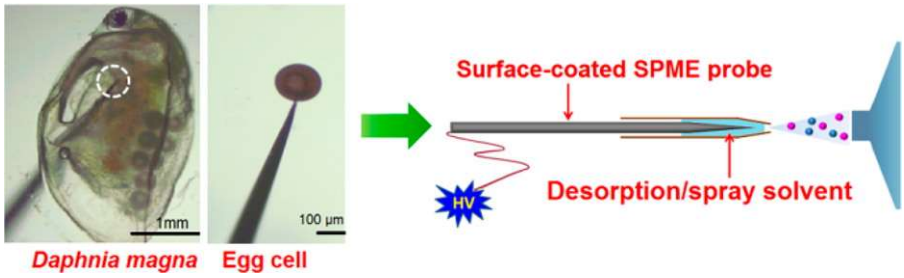


Figure 1-9. *Photo of Daphnia magna and Egg cell; Scheme of SCP-nanoESI-MS setup. (Deng, J.; Yang, Y.; Xu, M.; Wang, X.; Lin, L.; Yao, Z.-P.; Luan, T., Surface-coated probe nanoelectrospray ionization mass spectrometry for analysis of target compounds in individual small organisms. Analytical chemistry 2015, 87 (19), 9923-9930.* Copyright

permission is obtained from American Chemical Society, and the detail is shown in Appendix III.*)*

1.2.1.1.11 Desorption electrospray ionization (DESI) MS

DESI directly applies the electrospray mist on the surface of samples, which are dried on the insulated surfaces. Then, the desorbed and ionized analytes with the splashed droplets are carried to the MS for detection.[47, 48] In the study performed by Cooks *et al*., individual target cells (e.g., oocyte or embryo) are attached to the glass slide and dried at room temperature. A spray solvent, which contains ethanol (or acetonitrile) and dimethylformamide (50/50, v/v), is used to desorb and ionize lipids of single cells for MS analysis.[49] In another study, this technique has been utilized to analyze unfertilized oocytes, two- and four-cell embryos, and blastocysts. A significant difference in lipids among these samples was discovered through the principal component analysis (PCA) of experimental data.[27] In the other study, the dynamics of lipid composition change of single bovine oocytes and preimplantation embryos were obtained using this method combined with linear discriminant analysis and PCA.[50]

1.2.1.1.12 Laser ablation electrospray ionization (LAESI) MS

LAESI MS uses mid-IR laser pulses, which is conducted through a GeO2-based glass fiber, to ablate a single cell that is placed on a microscope glass slide. The ablated analytes are then ionized using electrospray and detected using MS.[51] This technology has been broadly used for metabolomics studies at the single-cell level,[28] including the metabolic variation of Allium cepa's epidermal cells and Narcissus pseudo narcissus bulb, [51] and metabolic and lipidomic changes of embryogenesis at early stages.[52]

1.2.1.1.13 Laser desorption/ionization droplet delivery (LDIDD) MS

The working mechanisms of LDIDD are similar to the LAESI, whereas the major difference is that LDIDD utilizes UV light for desorption. LDIDD uses 266 nm UV laser beam to desorb samples, where the wavelength of IR laser used by LAESI is 2.94 μm.[14, 53] During the sampling process, target cells are placed on a glass slide, and then attached single cells are desorbed and ionized by the laser beam (15 Hz, 266 nm). Meantime, liquid droplets are applied to the laser focusing area to carry the desorbed analyte to the MS for analysis under ambient conditions (Figure 1-10).[29] Because LDIDD MS combines laser photoionization and electrospray ionization together, it provides higher sensitivity compared with using pulsed laser alone.[29] Zare's group used this approach to investigate the difference of lipids in the healthy and apoptotic Human Embryonic Kidney cells.[29]

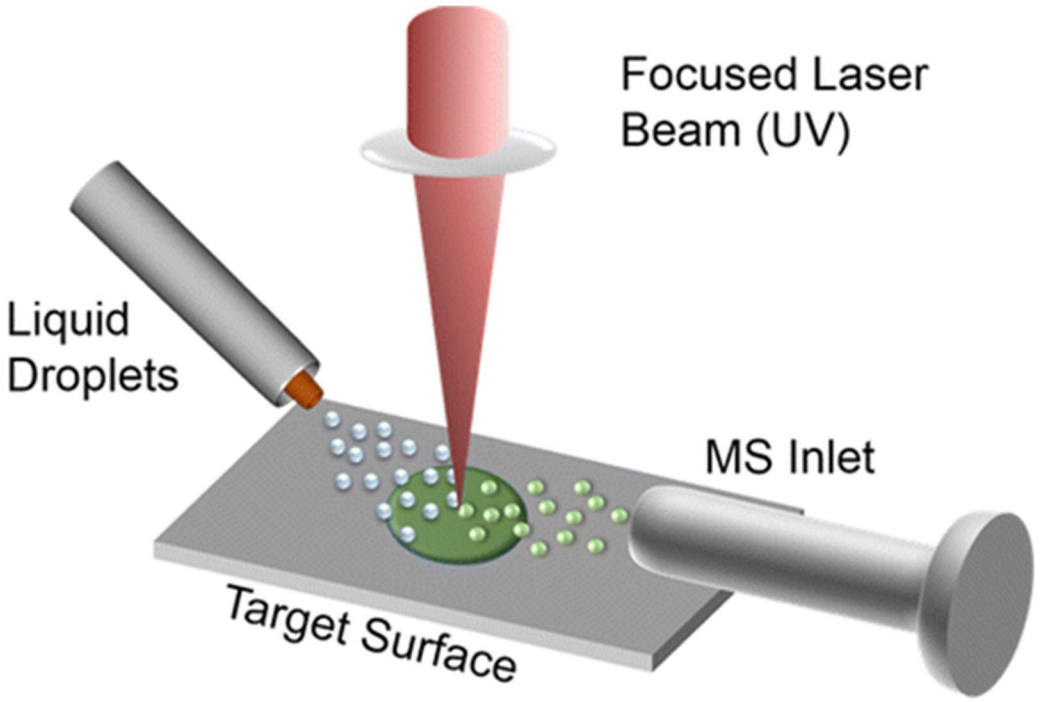


Figure 1-10. *Scheme of LDIDD MS. (Lee, J. K.; Jansson, E. T.; Nam, H. G.; Zare, R. N., High-resolution live-cell imaging and analysis by laser desorption/ionization droplet*

delivery mass spectrometry. Analytical chemistry 2016, 88 (10), 5453-5461. Copyright permission is obtained from American Chemical Society, and the detail is shown in Appendix III.*)*

1.2.1.2 Ambient MS technologies for non-adherent single cells

1.2.1.2.1 Integrated cell manipulation platform combined with the Single-probe MS

The Single-probe developed by our group has been primarily used for the analysis of adherent cells, which are attached to the substrate prior to MS analysis. We recently extended its application to the non-adherent cell by coupling it with an integrated cell manipulation platform (ICMP) to conduct real-time analysis of suspended cells. This multifunctional cell manipulation platform is used to control a Single-probe and the cell-selection probe. During the single-cell sampling, the cell-selection probe is used to capture a suspended cell (through a gentle suction) at its tip, and the cell is then transferred to the tip of the Single-probe using the manipulator. Because the Single-probe can generate a liquid junction at its tip, rapid microscale lysis of the single cell occurs once the cell meets the liquid, which is composed of high-concentration acetonitrile. The released cellular species are then ionized by the nano-ESI emitter of the Single-probe for MS detection in real-time (Figure 1-11).[30]

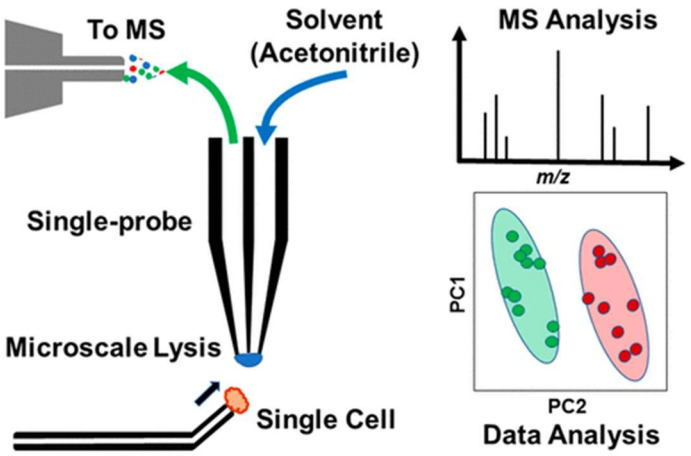


Figure 1-11. *Scheme of ICMP coupled with Single-probe MS.(Standke, S. J.; Colby, D. H.; Bensen, R. C.; Burgett, A. W.; Yang, Z., Mass spectrometry measurement of single suspended cells using a combined cell manipulation system and a single-probe device. Analytical chemistry 2019, 91 (3), 1738-1742.* Copyright permission is obtained from American Chemical Society, and the detail is shown in Appendix III.*)*

For example, this technique has been used to illustrate the metabolites difference of control and Taxol treated (100 nM, 24 h) K562 cells.

1.2.1.2.2 Easy Ambient Sonic-Spray Ionization (EASI) MS

EASI-MS is able to generate charged droplets of analytes for desorption and ionization for MS detection using sonic-spray ionization.[31, 54] To apply this technique for SCMS studies, cells are resuspended and pipetted onto the sterilized membrane filters. Due to the absence of ionization voltage between the sample and EASI ion source inlet, this technique can eliminate electric field disturbance during the analysis. Besides, the EASI-MS analysis is under room temperature, and live cells can be used for real-time analysis (Figure 1-12). Zhao's group used this technique to investigate acidic lipids changes of unicellular and filamentous cyanobacteria at the single-cell level. They detected

metabolites and lipids of cyanobacteria and discovered several various species of cyanobacteria using PCA of experimental data.[54]

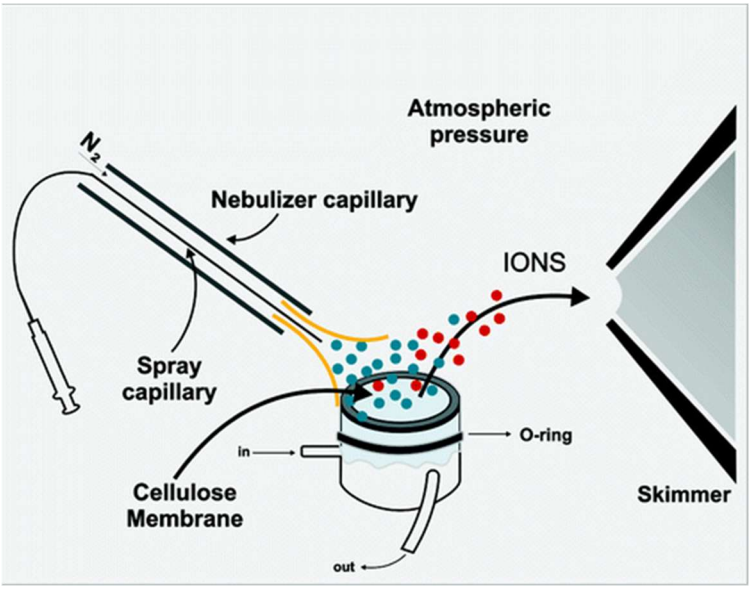


Figure 1-12. *Scheme of EASI-MS. (Haddad, R.; Sparrapan, R.; Kotiaho, T.; Eberlin, M. N., Easy ambient sonic-spray ionization-membrane interface mass spectrometry for direct analysis of solution constituents. Analytical chemistry 2008, 80 (3), 898-903.* Copyright permission is obtained from American Chemical Society, and the detail is shown in Appendix III.*)*

1.2.1.2.3 Drop-on-demand inkjet printing combined with Probe Electrospray Ionization (PESI)-MS

In this method, drop-on-demand inkjet works as a cell sorting and separation device to print a free-flying droplet on the tip of a tungsten probe, and PESI is used to ionize the droplet. Prior to sampling, a cell suspension reservoir is connected with the inkjet to provide cells, and the inkjet head is coupled with an electric system to control the volume of a droplet. Using a homebuilt magnetic stirring device with optimized cell density in the

cell suspension reservoir, even distribution of suspended cells can be obtained to improve the production efficiency of single-cell-droplet. During the sampling, the position of inkjet is controlled by a precise automatic XY stage to manage the single-cell-droplet drip on the tip of the tungsten probe for subsequent MS analysis using PESI (Figure 1-13).[32] In this study, cellular heterogeneity between several cells, such as human umbilical vein endothelial cells, NIH 3T3 cells, and MCF-7 breast cancer cells, was investigated using this method.

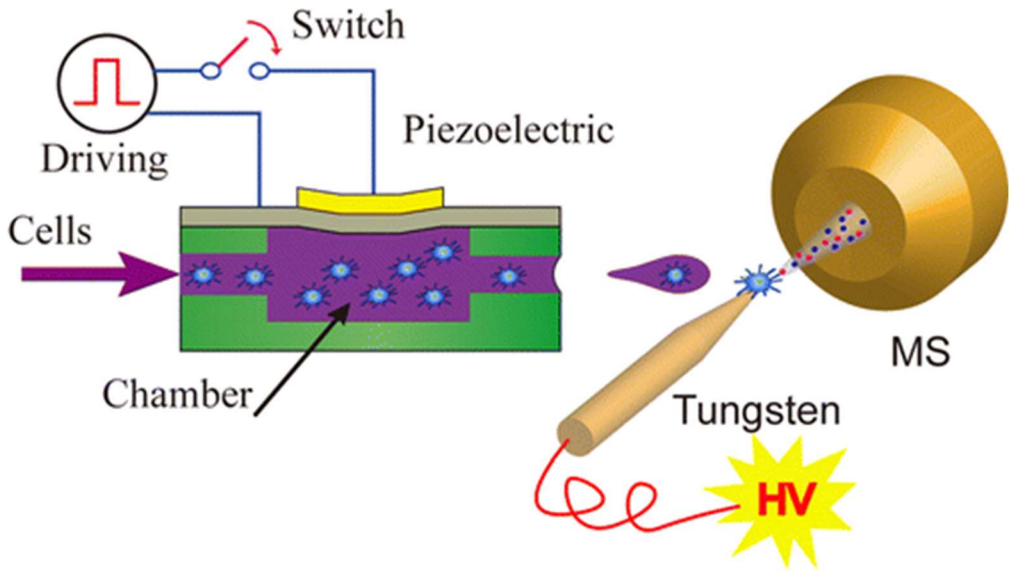


Figure 1-13. *Scheme of Drop-on-demand inkjet printing combined with PESI-MS. (Chen, F.; Lin, L.; Zhang, J.; He, Z.; Uchiyama, K.; Lin, J.-M., Single-cell analysis using drop-on-demand inkjet printing and probe electrospray ionization mass spectrometry. Analytical chemistry 2016, 88 (8), 4354-4360.* Copyright permission is obtained from American Chemical Society, and the detail is shown in Appendix III.*)*

1.2.1.2.4 Mass cytometry

Mass cytometry blends flow cytometry and elemental mass spectrometry together. A major advantage of using MS as a detector is that MS is able to simultaneously detect multiple cellular parameters with high accuracy. Before the analysis using mass cytometry, a stain is used to label and eliminate single dead cells. Multiple cell samples can be pooled together and barcoded with heavy metal isotopes before staining. These attached metal ions serve as reporters to express the target cells. Antibodies conjugated with metal ions are used for incubation with cells to target specific proteins on the cell surface. Cells are then nebulized into droplets containing single cells, atomized (e.g., using inductively coupled plasma (ICP)) into metal ions for MS detection (Figure 1-14).[33, 55]

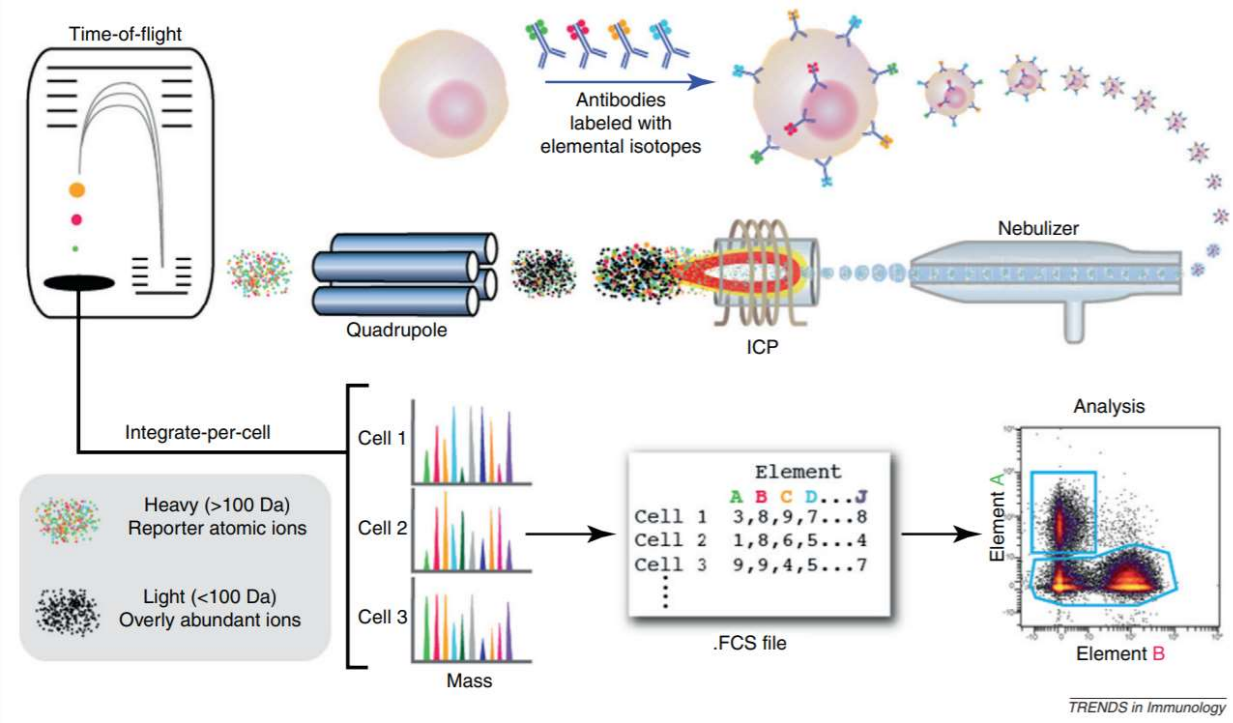


Figure 1-14. *The workflow of mass cytometry. (Bendall, S. C.; Nolan, G. P.; Roederer, M.; Chattopadhyay, P. K., A deep profiler's guide to cytometry. Trends in immunology*

2012, 33 (7), 323-332. Copyright permission is obtained from ELSEVIER, and the detail is shown in Appendix III.*)*

1.2.1.2.5 Redesigned T-probe MS

The redesigned T-probe, a device developed by our group, has a similar structure to the T-probe except for two features.[34] First, the orifice of the sampling probe of the redesigned T-probe (~14 μm) is slightly larger than the original T-probe (~6 μm). Therefore, a whole single cell can be drawn into the probe for measurement. Second, the nano-ESI emitter of the redesigned T-probe (5.5 cm) is much longer than the T-probe (~0.5 cm), providing sufficient time (~15 s) for online single-cell lysis by the sampling solvent (acetonitrile with 0.1% formic acid (FA)) inside the nano-ESI emitter. To conduct the experiment, cells are resuspended in the culture medium. A target cell can be drawn into the redesigned T-probe for rapid lysis followed by MS analysis (more details of the redesigned T-probe are provided in Chapter 3).

1.2.1.2.6 Micropipette needle MS

In order to conduct regular (no chemical reactions) and reactive (with chemical reactions) SCMS for the same single cell, the micropipette needle is developed by our group. It is produced by combining a pulled glass capillary needle (tip size ~15 um) with a fused silica capillary. The solvent is loaded into the micropipette needle to play the role of the cell lysis solvent. Particularly, this technique allows for more versatile studies such as reactive SCMS analysis.[35] For example, acetone or acetonitrile (containing 5 mM benzophenone) was used as both cell lysis solvent and the Paternò-Büchi (PB) reagents in the reactive SCMS experiments to assist the identification of unsaturated lipids. In our studies, the micropipette needle was connected to a syringe pump to draw a suspension cell, which

underwent rapid lysis, and then coupled to a mass spectrometer for detection. Using the micropipette needle as a nano-ESI emitter, both regular and reactive (with PB reactions induced by 15-min UV irradiation) SCMS analysis of the same cell can be achieved. Double bond locations were identified from MS scan and MS/MS analysis of PB products assisted by the Python program. The details of this study are shown in Chapter 4.

1.2.2 Non-ambient MS techniques for single-cell analysis

In contrast to ambient SCMS methods, non-ambient techniques require samples to be placed in vacuum conditions, indicating they cannot be used for live cell analysis. In addition, most of these non-ambient SCMS technologies, except for some matrix-free laser desorption/ionization (LDI)-MS method, require complex sample preparation and cell attachment. However, as a major advantage, the vacuum environment generally provides higher detection sensitivity than those ambient SCMS methods.

1.2.2.1 Non-ambient MS technologies which require cell attachment

1.2.2.1.1 Time of Flight (ToF)- secondary ion mass spectrometry (SIMS)

SIMS uses the primary ion beam, which is generated by an ion gun, to focus on the surface of single-cell samples under high vacuum conditions, to generate secondary ion for subsequent ToF-MS analysis. The spatial resolution of SIMS is around 100 nm, allowing for molecular imaging of subcellular structures. In addition, SIMS is able to provide morphological information of samples. However, due to the non-ambient MS, this method requires elaborate sample preparation, such as frozen-hydrated samples.[15, 36]

1.2.2.1.2 Matrix-assisted laser desorption/ionization (MALDI)-MS

MALDI-MS has been widely applied in numerous studies. Similar to conventional MALDI experiments, SCMS analysis using this technique requires careful sample preparation. Before sampling, single cells are attached to the solid surface and embedded in the matrix. The UV laser pulse is then applied to desorb cellular contents. During the ablation, the matrix molecules transfer the analytes to the gas phase, and protonation (deprotonation) of the analytes occurs for MS detection. MALDI-MS has previously used for the analysis of single-cell, tissued-embedded cells, and unicellular organisms.[15]

1.2.2.1.3 Nanostructure initiator MS (NIMS)

Due to the matrix effect (i.e., hard to analyze small molecules (<1,000 m/z) because of matrix interference.[56]) and complicated sample preparation of matrix-assisted MS methods, matrix-free laser desorption/ionization techniques are developed to increase the sensitivity and efficiency of MS detection. NIMS is one of the matrix-free LDI methods.

Both NIMS and MALDI share certain similarities. However, the major difference is that NIMS uses a nanoporous silicon material to absorb the laser energy and trap an initiator compound, which can desorb and ionize analytes inside nanopores.[15] Siuzdak's group used NIMS to investigate changes of metabolites induced by chemotherapy at the single-cell level.[37]

1.2.2.2 Non-ambient MS technologies for non-adherent cells

1.2.2.2.1 Nanopost arrays (NAPA) based-LDI-MS

Similar to NIMS, NAPA (instead of the matrix) is used to decrease the matrix effect and simplify the sample preparation procedure. Because the silicon NAPA can produce

nanophotonic ionization of analytes, which is generated by the interaction between the laser pulse and a commensurate dimension and wavelength of the nanostructure, cell suspensions can be placed on the NAPA for direct LDI-MS analysis (Figure 1-15). The NAPA can increase the ionization efficiencies and enable to detect ~800 zmol of verapamil.[38] Several metabolites of single S. cerevisiae cells were analyzed and identified using this method.[57]

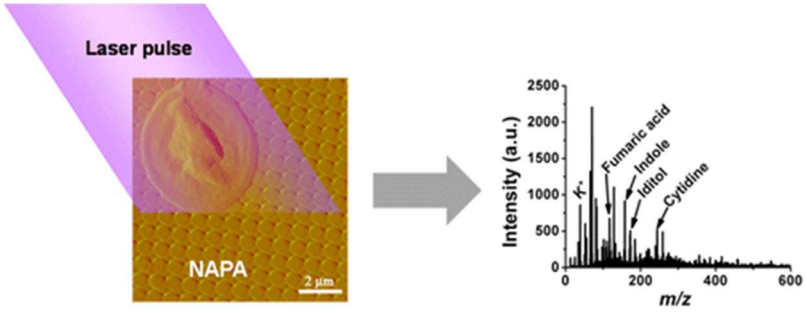


Figure 1-15. *Scheme of single-cell sampling using Nanopost arrays (NAPA) based-LDI-MS. (Walker, B. N.; Stolee, J. A.; Vertes, A., Nanophotonic ionization for ultratrace and single-cell analysis by mass spectrometry. Analytical chemistry 2012, 84 (18), 7756-7762.* Copyright permission is obtained from American Chemical Society, and the detail is shown in Appendix III.*)*

Reference

1. Yuan, G.-C.; Cai, L.; Elowitz, M.; Enver, T.; Fan, G.; Guo, G.; Irizarry, R.; Kharchenko, P.; Kim, J.; Orkin, S., Challenges and emerging directions in single-cell analysis. *Genome biology* 2017, *18* (1), 84.
2. Altschuler, S. J.; Wu, L. F., Cellular heterogeneity: do differences make a difference? *Cell* 2010, *141* (4), 559-563.
3. Hodzic, E., Single-cell analysis: Advances and future perspectives. *Bosnian journal of basic medical sciences* 2016, *16* (4), 313.
4. Habibi, I.; Cheong, R.; Lipniacki, T.; Levchenko, A.; Emamian, E. S.; Abdi, A., Computation and measurement of cell decision making errors using single cell data. *PLoS computational biology* 2017, *13* (4), e1005436.
5. Wang, D.; Bodovitz, S., Single cell analysis: the new frontier in 'omics'. *Trends in biotechnology* 2010, *28* (6), 281-290.
6. Abdallah, B. Y.; Horne, S. D.; Stevens, J. B.; Liu, G.; Ying, A. Y.; Vanderhyden, B.; Krawetz, S. A.; Gorelick, R.; Heng, H. H., Single cell heterogeneity: why unstable genomes are incompatible with average profiles. *Cell Cycle* 2013, *12* (23), 3640-3649.
7. Zenobi, R., Single-cell metabolomics: analytical and biological perspectives. *Science* 2013, *342* (6163), 1243259.
8. Klein, A. M.; Mazutis, L.; Akartuna, I.; Tallapragada, N.; Veres, A.; Li, V.; Peshkin, L.; Weitz, D. A.; Kirschner, M. W., Droplet barcoding for single-cell transcriptomics applied to embryonic stem cells. *Cell* 2015, *161* (5), 1187-1201.
9. Davey, H. M.; Kell, D. B., Flow cytometry and cell sorting of heterogeneous microbial populations: the importance of single-cell analyses. *Microbiol. Mol. Biol. Rev.* 1996, *60* (4), 641-696.
10. van Manen, H.-J.; Kraan, Y. M.; Roos, D.; Otto, C., Single-cell Raman and fluorescence microscopy reveal the association of lipid bodies with phagosomes in leukocytes. *Proceedings of the National Academy of Sciences* 2005, *102* (29), 10159-10164.
11. Schuster, K. C.; Urlaub, E.; Gapes, J., Single-cell analysis of bacteria by Raman microscopy: spectral information on the chemical composition of cells and on the heterogeneity in a culture. *Journal of Microbiological Methods* 2000, *42* (1), 29-38.
12. Murata, T.; Yasukawa, T.; Shiku, H.; Matsue, T., Electrochemical single-cell gene-expression assay combining dielectrophoretic manipulation with secreted alkaline phosphatase reporter system. *Biosensors and Bioelectronics* 2009, *25* (4), 913-919.
13. Yin, L.; Zhang, Z.; Liu, Y.; Gao, Y.; Gu, J., Recent advances in single-cell analysis by mass spectrometry. *Analyst* 2019, *144* (3), 824-845.
14. Yang, Y.; Huang, Y.; Wu, J.; Liu, N.; Deng, J.; Luan, T., Single-cell analysis by ambient mass spectrometry. *TrAC Trends in Analytical Chemistry* 2017, *90*, 14-26.
15. Zhang, L.; Vertes, A., Single‐Cell Mass Spectrometry Approaches to Explore Cellular Heterogeneity. *Angewandte Chemie International Edition* 2018, *57* (17), 4466-4477.
16. Huang, M.-Z.; Cheng, S.-C.; Cho, Y.-T.; Shiea, J., Ambient ionization mass spectrometry: a tutorial. *Analytica chimica acta* 2011, *702* (1), 1-15.

17. Pan, N.; Rao, W.; Kothapalli, N. R.; Liu, R.; Burgett, A. W.; Yang, Z., The single-probe: a miniaturized multifunctional device for single cell mass spectrometry analysis. *Analytical chemistry* 2014, *86* (19), 9376-9380.
18. Liu, R.; Pan, N.; Zhu, Y.; Yang, Z., T-probe: an integrated microscale device for online in situ single cell analysis and metabolic profiling using mass spectrometry. *Analytical chemistry* 2018, *90* (18), 11078-11085.
19. Mizuno, H.; Tsuyama, N.; Harada, T.; Masujima, T., Live single - cell video - mass spectrometry for cellular and subcellular molecular detection and cell classification. *Journal of mass spectrometry* 2008, *43* (12), 1692-1700.
20. Zhang, L.; Foreman, D. P.; Grant, P. A.; Shrestha, B.; Moody, S. A.; Villiers, F.; Kwak, J. M.; Vertes, A., In situ metabolic analysis of single plant cells by capillary microsampling and electrospray ionization mass spectrometry with ion mobility separation. *Analyst* 2014, *139* (20), 5079-5085.
21. Gholipour, Y.; Erra-Balsells, R.; Hiraoka, K.; Nonami, H., Living cell manipulation, manageable sampling, and shotgun picoliter electrospray mass spectrometry for profiling metabolites. *Analytical Biochemistry* 2013, *433* (1), 70-78.
22. Nakashima, T.; Wada, H.; Morita, S.; Erra-Balsells, R.; Hiraoka, K.; Nonami, H., Single-cell metabolite profiling of stalk and glandular cells of intact trichomes with internal electrode capillary pressure probe electrospray ionization mass spectrometry. *Analytical chemistry* 2016, *88* (6), 3049-3057.
23. Phelps, M.; Hamilton, J.; Verbeck, G. F., Nanomanipulation-coupled nanospray mass spectrometry as an approach for single cell analysis. *Review of Scientific Instruments* 2014, *85* (12), 124101.
24. Gong, X.; Zhao, Y.; Cai, S.; Fu, S.; Yang, C.; Zhang, S.; Zhang, X., Single cell analysis with probe ESI-mass spectrometry: detection of metabolites at cellular and subcellular levels. *Analytical chemistry* 2014, *86* (8), 3809-3816.
25. Yu, Z.; Chen, L. C.; Ninomiya, S.; Mandal, M. K.; Hiraoka, K.; Nonami, H., Piezoelectric inkjet assisted rapid electrospray ionization mass spectrometric analysis of metabolites in plant single cells via a direct sampling probe. *Analyst* 2014, *139* (22), 5734-5739.
26. Deng, J.; Yang, Y.; Xu, M.; Wang, X.; Lin, L.; Yao, Z.-P.; Luan, T., Surface-coated probe nanoelectrospray ionization mass spectrometry for analysis of target compounds in individual small organisms. *Analytical chemistry* 2015, *87* (19), 9923-9930.
27. Ferreira, C. R.; Pirro, V.; Eberlin, L. S.; Hallett, J. E.; Cooks, R. G., Developmental phases of individual mouse preimplantation embryos characterized by lipid signatures using desorption electrospray ionization mass spectrometry. *Analytical and bioanalytical chemistry* 2012, *404* (10), 2915-2926.
28. Stolee, J. A.; Vertes, A., Toward single-cell analysis by plume collimation in laser ablation electrospray ionization mass spectrometry. *Analytical chemistry* 2013, *85* (7), 3592-3598.
29. Lee, J. K.; Jansson, E. T.; Nam, H. G.; Zare, R. N., High-resolution live-cell imaging and analysis by laser desorption/ionization droplet delivery mass spectrometry. *Analytical chemistry* 2016, *88* (10), 5453-5461.
30. Standke, S. J.; Colby, D. H.; Bensen, R. C.; Burgett, A. W.; Yang, Z., Mass spectrometry measurement of single suspended cells using a combined cell manipulation system and a single-probe device. *Analytical chemistry* 2019, *91* (3), 1738-1742.

31. Haddad, R.; Sparrapan, R.; Kotiaho, T.; Eberlin, M. N., Easy ambient sonic-spray ionization-membrane interface mass spectrometry for direct analysis of solution constituents. *Analytical Chemistry* 2008, *80* (3), 898-903.
32. Chen, F.; Lin, L.; Zhang, J.; He, Z.; Uchiyama, K.; Lin, J.-M., Single-cell analysis using drop-on-demand inkjet printing and probe electrospray ionization mass spectrometry. *Analytical chemistry* 2016, *88* (8), 4354-4360.
33. Bendall, S. C.; Nolan, G. P.; Roederer, M.; Chattopadhyay, P. K., A deep profiler's guide to cytometry. *Trends in immunology* 2012, *33* (7), 323-332.
34. Zhu, Y.; Liu, R.; Yang, Z., Redesigning the T-probe for mass spectrometry analysis of online lysis of non-adherent single cells. *Analytica chimica acta* 2019, *1084*, 53-59.
35. Zhu, Y.; Wang, W.; Yang, Z., Combining Mass Spectrometry with Paternò-Büchi Reaction to Determine Double-bond Positions in Lipids at the Single-cell Level. *Analytical Chemistry* 2020, *DOI: 10.1021/acs.analchem.0c02245*.
36. Jungnickel, H.; Laux, P.; Luch, A., Time-of-flight secondary ion mass spectrometry (ToF-SIMS): a new tool for the analysis of toxicological effects on single cell level. *Toxics* 2016, *4* (1), 5.
37. O'Brien, P. J.; Lee, M.; Spilker, M. E.; Zhang, C. C.; Yan, Z.; Nichols, T. C.; Li, W.; Johnson, C. H.; Patti, G. J.; Siuzdak, G., Monitoring metabolic responses to chemotherapy in single cells and tumors using nanostructure-initiator mass spectrometry (NIMS) imaging. *Cancer & metabolism* 2013, *1* (1), 1-14.
38. Walker, B. N.; Stolee, J. A.; Vertes, A., Nanophotonic ionization for ultratrace and single-cell analysis by mass spectrometry. *Analytical chemistry* 2012, *84* (18), 7756-7762.
39. Sun, M.; Yang, Z.; Wawrik, B., Metabolomic fingerprints of individual algal cells using the single-probe mass spectrometry technique. *Frontiers in Plant Science* 2018, *9*, 571.
40. Sun, M.; Yang, Z., Metabolomic studies of live single cancer stem cells using mass spectrometry. *Analytical chemistry* 2018, *91* (3), 2384-2391.
41. Sun, M.; Tian, X.; Yang, Z., Microscale mass spectrometry analysis of extracellular metabolites in live multicellular tumor spheroids. *Analytical chemistry* 2017, *89* (17), 9069-9076.
42. Rao, W.; Pan, N.; Yang, Z., High resolution tissue imaging using the single-probe mass spectrometry under ambient conditions. *Journal of The American Society for Mass Spectrometry* 2015, *26* (6), 986-993.
43. Tsuyama, N.; Mizuno, H.; Tokunaga, E.; Masujima, T., Live single-cell molecular analysis by video-mass spectrometry. *Analytical Sciences* 2008, *24* (5), 559-561.
44. Zhang, L.; Vertes, A., Energy charge, redox state, and metabolite turnover in single human hepatocytes revealed by capillary microsampling mass spectrometry. *Analytical chemistry* 2015, *87* (20), 10397-10405.
45. Gholipour, Y.; Erra-Balsells, R.; Nonami, H., In situ pressure probe sampling and UV-MALDI MS for profiling metabolites in living single cells. *Mass Spectrometry* 2012, *1* (1), A0003-A0003.
46. Phelps, M. S.; Verbeck, G. F., A lipidomics demonstration of the importance of single cell analysis. *Analytical Methods* 2015, *7* (9), 3668-3670.
47. Takats, Z.; Wiseman, J. M.; Cooks, R. G., Ambient mass spectrometry using desorption electrospray ionization (DESI): instrumentation, mechanisms and applications in forensics, chemistry, and biology. *Journal of mass spectrometry* 2005, *40* (10), 1261-1275.
48. Takáts, Z.; Wiseman, J. M.; Gologan, B.; Cooks, R. G., Mass spectrometry sampling under ambient conditions with desorption electrospray ionization. *Science* 2004, *306* (5695), 471-473.

49. Ferreira, C.; Eberlin, L.; Hallett, J.; Cooks, R., Single oocyte and single embryo lipid analysis by desorption electrospray ionization mass spectrometry. *Journal of Mass Spectrometry* 2012, *47* (1), 29-33.
50. González-Serrano, A. F.; Pirro, V.; Ferreira, C. R.; Oliveri, P.; Eberlin, L. S.; Heinzmann, J.; Lucas-Hahn, A.; Niemann, H.; Cooks, R. G., Desorption electrospray ionization mass spectrometry reveals lipid metabolism of individual oocytes and embryos. *PloS one* 2013, *8* (9).
51. Shrestha, B.; Vertes, A., In situ metabolic profiling of single cells by laser ablation electrospray ionization mass spectrometry. *Analytical Chemistry* 2009, *81* (20), 8265-8271.
52. Shrestha, B.; Sripadi, P.; Reschke, B. R.; Henderson, H. D.; Powell, M. J.; Moody, S. A.; Vertes, A., Subcellular metabolite and lipid analysis of Xenopus laevis eggs by LAESI mass spectrometry. *PLoS One* 2014, *9* (12).
53. Stopka, S. A.; Khattar, R.; Agtuca, B. J.; Anderton, C. R.; Paša-Tolić, L.; Stacey, G.; Vertes, A., Metabolic noise and distinct subpopulations observed by single cell LAESI mass spectrometry of plant cells in situ. *Frontiers in plant science* 2018, *9*, 1646.
54. Liu, Y.; Zhang, J.; Nie, H.; Dong, C.; Li, Z.; Zheng, Z.; Bai, Y.; Liu, H.; Zhao, J., Study on variation of lipids during different growth phases of living cyanobacteria using easy ambient sonic-spray ionization mass spectrometry. *Analytical chemistry* 2014, *86* (14), 7096-7102.
55. Spitzer, M. H.; Nolan, G. P., Mass cytometry: single cells, many features. *Cell* 2016, *165* (4), 780-791.
56. Peterson, D. S., Matrix-free methods for laser desorption/ionization mass spectrometry. *Mass spectrometry reviews* 2007, *26* (1), 19-34.
57. Walker, B. N.; Antonakos, C.; Retterer, S. T.; Vertes, A., Metabolic differences in microbial cell populations revealed by nanophotonic ionization. *Angewandte Chemie International Edition* 2013, *52* (13), 3650-3653.

Chapter 2. Research Overview

During my Ph.D. studies, my research has been focused on the development and application of two SCMS technologies, redesigned T-probe and micropipette needle, for non-adherent single cell analysis. The detailed information of the Redesigned T-probe and micropipette needle are shown in Chapters 3 and 4, respectively.

Currently, the majority of the SCMS technologies require cell attachment onto substrates prior to analysis. However, numerous types of cells, including lymphoblast, leucocyte, monocytes, and neutrophils,[1-4] are non-adherent and suspended in biofluids such as blood, cerebrospinal fluid, and urine. These cells are related to serval diseases, such as blood cancer and chronic inflammatory diseases.[5] However, only a few SCMS technologies, including ambient and non-ambient technologies, were developed for the studies of single cells in suspension. Among them, the redesigned T-probe and micropipette needle could solve the potential problems and overcome the limitations of current technologies for non-adherent single cell analysis. The redesigned T-probe has an online cell lysis system inside the probe for high throughput and real-time single cell analysis of non-adherent cells. To perform molecular structure identification, adequately long signal duration time can benefit tandem MS (MS/MS) analysis of ions of interest. The signal duration time (~15 to 20 seconds) is longer than some of the current SCMS methods for non-adherent cells, including the Integrated cell manipulation platform combined with the Single-probe MS and Drop-on-demand inkjet printing combined with PESI-MS.

The micropipette needle is reported as the first SCMS technique allowing for both regular SCMS and reactive SCMS, in which chemical reactions can be induced between cellular molecules and reagents, analysis of the same single cell.[6] The reactive SCMS can extend the detection range of molecules and provide more structure information. Here are some examples. Using dicationic ion-pairing reagents in the Single-probe SCMS measurement can detect negative ions, such as phosphatidylethanolamines (PE), phosphatidylglycerol (PG), and phosphatidylserine (PS), under the positive ion mode. Paternò-Büchi reactions can be performed to identify lipids double bond locations at the single-cell level. The development of these two SCMS techniques can be potentially coupled with other chemical reactions. For example, Norrish reaction can be used to identify C=O location of metabolites. With further development, our novel technologies can be potentially utilized for the investigation of wider types of non-adherent cells in both fundamental studies and clinical applications.

Reference

1. Tsang, M.; Gantchev, J.; Ghazawi, F. M.; Litvinov, I. V., Protocol for adhesion and immunostaining of lymphocytes and other non-adherent cells in culture. *BioTechniques* 2017, *63* (5), 230-233.
2. Keller, H.; Cottier, H., Crawling-like movements and polarisation in non-adherent leucocytes. *Cell Biology International Reports* 1981, *5* (1), 3-7.
3. de Mulder, P.; van Rennes, H.; Mier, P.; Bergers, M.; De Pauw, B.; Haanen, C., Characterization of monocyte maturation in adherent and suspension cultures and its application to study monocyte differentiation in Hodgkin's disease. *Clinical and experimental immunology* 1983, *54* (3), 681.
4. Suzuki, T.; Yanai, M.; Kubo, H.; Kanda, A.; Sasaki, H.; Butler, J. P., Interaction of non-adherent suspended neutrophils to complement opsonized pathogens: a new assay using optical traps. *Cell research* 2006, *16* (11), 887-894.
5. Walker, H. K.; Hall, W. D.; Hurst, J. W., *Peripheral Blood Smear--Clinical Methods: The History, Physical, and Laboratory Examinations*. Butterworths: 1990.
6. Zhu, Y.; Wang, W.; Yang, Z., Combining Mass Spectrometry with Paternò-Büchi Reaction to Determine Double-bond Positions in Lipids at the Single-cell Level. *Analytical Chemistry* 2020, *DOI: 10.1021/acs.analchem.0c02245*.

Chapter 3. Redesigning the T-probe for mass spectrometry analysis of online lysis of non-adherent single cells

Author Contributions: The study of Chapter 3 is majorly conducted by Yanlin Zhu. Renmeng Liu participated in Redesigned T-probe fabrication.

Copyright permission: The material in chapter 3 is adapted from Zhu, Yanlin, Renmeng Liu, and Zhibo Yang. “Redesigning the T-probe for mass spectrometry analysis of online lysis of non-adherent single cells.” Analytica chimica acta 1084 (2019): 53-59. Copyright permission is obtained from Elsevier, and the detail is shown in Appendix III.

3.1 Abstract

Single cell mass spectrometry (SCMS) allows for molecular analysis of individual cells while avoiding the inevitable drawbacks of using cell lysate prepared from populations of cells. Based on our previous design of the T-probe, a microscale sampling and ionization device for SCMS analysis, we further developed the device to perform online, and real-time lysis of non-adherent live single cells for mass spectrometry (MS) analysis at ambient conditions. This redesigned T-probe includes three parts: a sampling probe with a small tip to withdraw a whole cell, a solvent-providing capillary to deliver lysis solution (i.e., acetonitrile), and a nano-ESI emitter in which rapid cell lysis and ionization occur followed by MS analysis. These three components are embedded between two polycarbonate slides and are jointed through a T-junction to form an integrated device. Colon cancer cells (HCT-116) under control and treatment (using anticancer drug irinotecan) conditions

were analyzed. We detected a variety of intracellular species, and structural identification of selected ions was conducted using tandem MS (MS2). We further conducted statistical analysis (e.g., PLS-DA and t-test) to gain biological insights of cellular metabolism. Our results indicate that the influence of anticancer drugs on cellular metabolism of live non-adherent cells can be obtained using the SCMS experiments combined with statistical data analysis.

3.2 Introduction

The basic structural, functional, and biological units of life are cells. Great efforts have been devoted in recent decades to study the dynamic nature of cells, and to understand their roles in complex biological systems.[1, 2] However, a particular cell is an individual unit with unique genomic and phenotypic traits, and thus distinguishes itself from other seemingly identical cells that reside in adjacent regions.[3] Such phenomenon termed as cell-to-cell heterogeneity poses a great challenge for clinical and biological studies, as a majority of conventional methods are based on cell populations, which result in averaged results of the cohort analyzed.[4] Facing such challenges, single cell based techniques that can differentiate such cell-to-cell heterogeneity are desired to gain insights into the nature of cells. Currently, a variety of studies at the single-cell level have been conducted, and they have fundamentally enhanced our understandings of cells through single-cell genomics,[5] single-cell transcriptomics,[6] single-cell proteomics,[7] and single-cell metabolomics.[8] These studies provide chemical and biological information of target systems that is otherwise lost in traditional analyses using samples prepared from bulk populations of cells.[3] Among those single-cell “omics” approaches, single-cell

metabolomics focuses on changes of cellular metabolites corresponding to the altered microenvironment and thus provides direct clues towards cellular metabolism.[9]

Mass spectrometry (MS), as a powerful analytical approach, satisfies prerequisites of single-cell metabolomic analysis due to its abilities to analyze trace amounts of samples, resolve cellular metabolites from the complex matrix,[10] and identify species of interest.[11] A variety of different single cell MS (SCMS) techniques, which fall into non-ambient or ambient method (i.e., non-ambient, ambient), according to their sampling and ionization environment, have been developed and applied to analyses of a broad range of cells (plant cells, mammalian cells, yeasts, etc.).[12-14]

Non-ambient SCMS methods are primarily based on two ionization techniques: secondary ion MS (SIMS) and matrix-assisted desorption/ionization (MALDI) MS. Techniques based on SIMS and MALDI MS use high-energy ion beams or UV laser to ablate and ionize molecules in cells, such as metabolites, lipids, and pharmaceuticals, for sensitive and reproducible analysis at the single-cell level.[13, 15] In contrast to vacuum-based techniques, ambient SCMS methods allow for sampling and ionization of cells with little or no sample preparation.[16-18] A variety of ambient SCMS techniques, such as live single-cell video-MS,[19] laser ablation electrospray ionization (LAESI) MS,[20] nanospray desorption electrospray ionization (nano-DESI) MS,[21], induced nanoESI (InESI) MS,[22] probe electrospray ionization (PESI),[23, 24] and techniques coupled to microfluidic chips [25] and flow cytometry (i.e., mass cytometry).[26, 27] In addition, we have previously developed the Single-probe,[28-31] which was also used for MS imaging [29, 32-34] of tissues and MS analysis of extracellular molecules in live spheroids[35], and the T-probe [36] to capture chemical information of single live cells. These approaches hold promising potentials

towards studies of fundamental cell biology and translational applications in clinical practice.[12]

Due to the extremely small amount of contents from a single cell (e.g., a single cell volume can be as low as a few pLs, with a few types of cells being smaller than 1 pL),[37, 38] sample separation, which can potentially result in analyte dilution and loss, is not performed in most SCMS methods. On the other hand, suitable separation techniques can be coupled with MS techniques to improve sensitivity and identification. These separation techniques include micro-separation prior to ionization (e.g., capillary electrophoresis[39] and microscale liquid chromatography[40, 41]) and post-ionization (i.e., ion mobility separation[42]). These techniques have been applied to *in situ* metabolic analysis of single plant cells[43] and quantifying translational cell heterogeneity in the frog embryo.[44]

Despite great efforts contributed, two major limitations still exist in most of SCMS techniques mentioned above. First, these methods require cell immobilization or attachment to a particular substrate.[45] Second, loss of cellular contents may occur during sample preparation or sampling processes. The former prevents sampling from inherently non-adherent cells, whereas the latter renders a loss of molecular information of cellular contents.

To address the above limitations, we provided a new design of the T-probe that enables rapid lysis of live non-adherent single cells followed by immediate MS analysis. This new design was based on our previously reported T-probe device.[36] They both have three capillaries (i.e., a solvent-providing capillary, a sampling probe, and a nano-ESI emitter) that are joint to form a T-shaped junction and sandwiched by two polycarbonate slides (Figure 3-1B). The working mechanisms of both designs are similar. During the SCMS

experiment, the sampling solvent is provided a solvent pump and delivered to the solvent-providing capillary, which is connected to a conductive union. A DC ionization voltage is applied on the conductive union and transmitted through the solvent inside the capillaries to generate ionization at the nano-ESI emitter. Under well-tuned conditions (e.g., suitable solvent flowrate and ionization voltage), a suction force can be generated at the sampling probe. Although the exact mechanisms are unclear, the generation of the suction force is likely due to the capillary action in the sampling probe induced by continuous consumption of solvent in the nano-ESI emitter.[36]

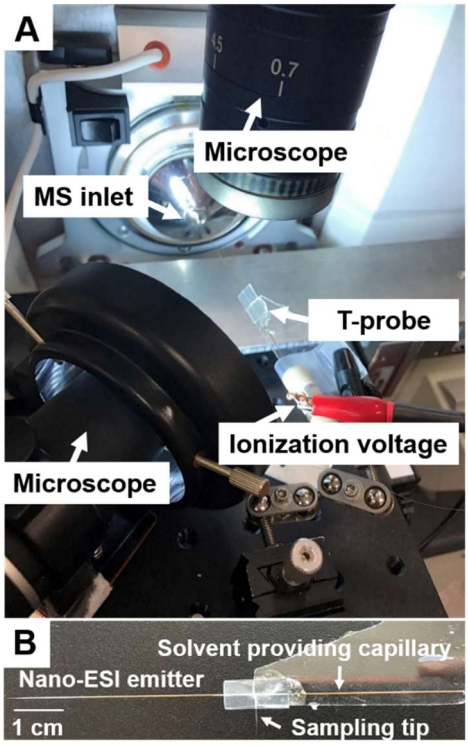


Figure 3-1. *(A) Experimental set-up of the redesign T-probe for SCMS analysis. Two microscopes were used to provide a visual guide during the experiment, and the XYZ-stage was utilized to precisely target single cells. Ionization voltage was applied on the conductive union, and the MS analysis was conducted using a LTQ Orbitrap XL mass*

spectrometer. (B) Photo of a T-probe, in which a solvent-providing capillary, a cell sampling probe, and a nano-ESI emitter were sandwiched by two polycarbonate slides.

The novelty of the T-probe used in the current study includes two major aspects. First, it is designed for the analysis of suspension cells. Although the majority of existing SCMS techniques, including the T-probe device, only allow for analyzing cells attached to substrates, methods based on mass cytometry [27], PESI [24], and microfluid chip devices[46] have been developed to analyze suspension cells. The capability of analyzing suspension cells is particularly important for clinical investigations, in which suspension cells, including primary blood cells (e.g., lymphocytes, macrophages, dendritic cells), lymph node cells (T-cells and B-cells), bone marrow cells, circulating tumor cells, can be analyzed for cell-based therapy and diagnostics.[47-50] Our group has recently reported an integrated cell manipulation platform (ICMP) for MS analysis of single suspension cells.[51] Compared with this technique, the redesigned T-probe is a relatively simple device allowing for higher throughput analysis. Second, the new design allows for the analysis of an entire cell undergoing online, rapid lysis. A cell can be withdrawn from the solution and followed by rapid lysis inside the nano-ESI emitter of the device to avoid the loss of cellular contents, which can potentially occur during the sampling process of other techniques. Compared with the previously reported T-probe, the new design accordingly has two major features. First, because the new design aims to sample an entire non-adherent cell, its sampling probe has an orifice (~14 μm) slightly larger than that of the T-probe (~6 μm). Second, its nano-ESI emitter (5.5 cm) is much longer than that of the T-probe (~0.5 cm), allowing for adequate time (~15 s) to induce online cell lysis inside the

nano-ESI emitter upon the cell contacting the solvent (99.9% acetonitrile with 0.1% formic acid (FA)) at the T-junction.

3.3 Experimental Design and Data Processing

3.3.1 Fabrication and test of the T-probe

Although the general fabrication workflows of both designs are similar,[36] the major differences between them include the length of nano-ESI emitter and tip size of the sampling probe. The fabrication work is illustrated in Figure S3-1, and detailed information is provided in the Support Information. Briefly, three capillaries (a solve-providing capillary, a cell sampling probe, and nano-ESI emitter) were joint at a T-shaped junction and sandwiched by two polycarbonate slides, which were coated with a hydrophobic material and then bond together through a thermal binding process to form an integrated device (Figure 3-2). We have conducted experiments using a series of tip sizes, and we selected a tip size of ~14 μm for both the sampling probe and the nano-ESI emitter to achieve the optimized performance. In addition, the lengths of the sampling probe (8 mm) and the nano-ESI emitter (5.5 cm) were carefully selected. Ideally, the length of the sampling probe should be short enough to minimize the amount of cell culture medium drawn along with a cell (i.e., minimized matrix effect),[24] but long enough to maintain a strong mechanical strength of the polycarbonate bond structure. On the other hand, with two major functions (i.e., online cell lysis and ionization) of the nano-ESI emitter, its length needs to be long enough to provide space and time for rapid cell lysis occurring upon the cell entering the T-junction and mixing with the solvent. However, an excessively long emitter can reduce the experimental throughput and result in difficulties of probe fabrication.

The performance of all devices was tested prior to the SCMS experiments. Simply, a small droplet of a prepared solution containing a standard testing compound (e.g., leucine enkephalin, 1 μM) was added to a vial, followed by immersion of the sampling probe tip into the solution. A stable

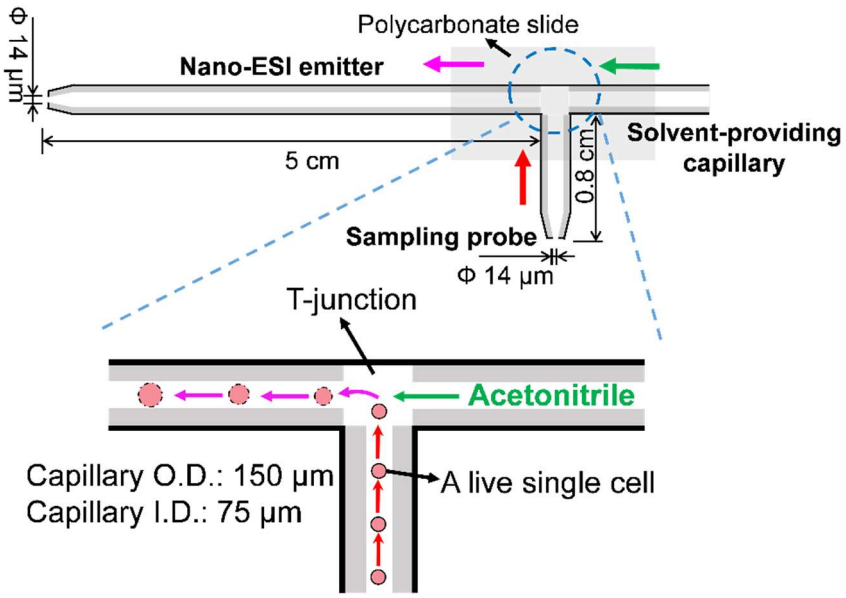


Figure 3-2. *Schematic of the T-probe and mechanisms of SCMS analysis. The inset shows the single cell withdrawn into the cell sapling probe undergoes a rapid (within a few seconds) lysis. The single-cell lysate is immediately ionized through the nano-ESI emitter for MS analysis.*

ion signal of leucine enkephalin can be observed shortly (~15 s) after the probe immersion (Figure S3-2). The sampling probe tip was then removed from the prepared solution, and the sampling solvent was continuously delivered to rinse the probe until the ion signal of the testing compound completely disappeared. To evaluate the sensitivity of the redesigned T-probe, we measured the limit of detection (LOD) of multiple standard compounds relevant to our studies. As a result, LODs were 0.1, 0.1, and 10 nM for

irinotecan, leucine enkephalin, and phosphatidylcholine (PC (16:0/18:1)), respectively (Figure S3-3). These results indicated that the new design has similar sensitivities compared with the original T-probe, the Single-probe, and standard nano-ESI source results.[36, 52] (Table S3-1).

3.3.2 SCMS Experiments

During the SCMS analysis, the redesigned T-probe was coupled to our in-home developed SCMS platform employed in our previous SCMS studies using the Single-probe[28, 30, 35] and the original T-probe.[36] Briefly, this platform includes an XYZ-translational stage system, two digital microscopes, and a Thermo LTQ Orbitrap XL mass spectrometer (Figure 3-1A).[28] Cells in both control and drug treatment groups were used for the SCMS experiments (detailed sample preparation procedures are described in the Supporting Information). Irinotecan is a common anticancer drug for the treatment of colon cancer[53] that inhibits the function of *Topoisomerase I*, leading to DNA damage and cell apoptosis.[53, 54] This drug compound was selected to treat live HCT-116 colorectal cells in our experiments to demonstrate the change of cellular metabolites upon the treatment of anticancer agent. Specifically, cells were first treated using 18 μM irinotecan for 45 min, and then rinsed and detached using trypsinization. Afterward, a droplet of cell suspension solution was placed onto a glass slide, which was attached to the XYZ-stage system controlled by a LabView software package (incremental step size = 0.1 μm).[55] Using two digital microscopes as the visual guide, the sampling probe tip initially located above the sample plate was submerged into the solution containing cells by lifting the Z-stage. Upon selecting a target cell, the sampling probe can precisely draw the target cell with visual guidance (Figure S3-4). The XYZ-stage was then immediately lowered down

to free the sampling probe tip from the culture medium and stop the suction of culture medium. Due to the complex composition of the cell culture medium that may affect the detection sensitivity,[10]caution should be taken to minimize its amount withdrawn during cell sampling. This is particularly important for future analysis of patient cells suspended in complex biological fluids such as blood, urine, saliva, and cerebrospinal fluid (CSF). After a single cell was withdrawn, the solvent provided through the solvent-providing capillary (flowrate = 0.5 μL/min) mixed with the cell at the T-junction, and cell lysis rapidly occurred inside the nano-ESI emitter. In our SCMS analysis, an ionization voltage (+4 kV) was applied to the conductive union and transmitted throughout the solution inside the solvent-providing capillary and the nano-ESI emitter to ionize the cell lysis for MS analysis.

3.3.3 SCMS Data Analysis

A comprehensive data analysis procedure was performed following SCMS analysis to gain biological insights. Specifically, we conducted data pre-treatment, including removal of background (i.e., species detected in the sampling solvent, the culture medium, and any dissolved polycarbonate oligomers), reduction of instrumental noise, ion signal normalization, and peak alignment (see the Supporting Information and Figure S3-5 for details).[56] We performed statistical analyses, including Partial Least Squares-discriminant Analysis (PLS-DA) and two-sample *t*-test (hereinafter referred to as *t*-test), using an online metabolomics analysis tool, MetaboAnalyst.[57] PLS-DA is a multivariate statistical method for data analysis and visualization, and it has been widely applied to classification and regression of metabolomics data.[58] In addition, *t*-test is generally used to determine if there is a statistically significant difference between results from two groups of cells. In our work, we employed both methods to study the change of cellular metabolomic profiles

upon drug treatment. Furthermore, two online metabolome databases, METLIN[59] and HMDB[60], were used to tentatively assign the detected metabolites based on their accurate *m/z* values. More confident identification of species of interest was performed using MS/MS fragmentation patterns.

3.4 Results and discussion

3.4.1 Sampling solvent selection

A key feature of the new design of the T-probe is to induce rapid cell lysis during the transport of a cell from the T-junction to the tip of the nano-ESI emitter. It is critical to select MS-compatible solvents with the desired composition for the SCMS experiments. To rapidly screen the solvent composition to be used in the SCMS analysis for optimal performance, we used a microscope (Micromaster, Fisher Scientific, MA) to monitor the lysis process of HCT-116 cells upon adding the lysis solution. A number of solvents commonly used in MS experiments (e.g., acetonitrile, methanol, and methanol/water) with a variety of compositions were tested as the lysis solution (Table 3-1). Our experiments indicated that cell lysis rapidly occurred (< 15 s) in the solution containing high concentrations of acetonitrile (> 80%) (Figure S3-6). Considering that a small amount of culture media would also be drawn along with a cell into the T-probe and therefore dilute the concentration of cellular contents, we used a sampling solvent composed of pure acetonitrile (with 0.1% FA to improve ionization efficiency) for our SCMS experiments.

3.4.2 Molecular Analysis of Single Cells in the Control and Drug Treatment Groups

During the SCMS analysis, the ion signals of cellular species were usually observed within 15 s upon the selected cell entering the sampling probe tip. We analyzed 25 cells

Table 3-1. Influence of solvent composition (acetonitrile/cell culture medium) on cell lysis rate.

Percentage of acetonitrile (%)	Cell lysis rate (s)
20	> 120
40	> 60
60	≥ 60
80	10–15
90	< 3
95	< 3

in the control group and 19 cells in the drug treated group, and a total number of ~400 cellular metabolites were detected (Figure 3-3). As expected, irinotecan ($[C_{33}H_{38}N_4O_6 + H]^+$, *m/z* 587.2881) was only detected in the drug treated cells. By accomplishing the tentative assignment of detected species, we found that cellular species detected in the control group include phosphatidylcholine (PC), metabolites of vitamin D_3, phosphatidylethanolamide (PE), prostaglandin (PG), and PE-ceramide (PE-cer). For cells in the drug treated group, PC, PG, and PE were the major species. The forms of the detected species include protonated, sodiated, and potassiated species. Furthermore, the ion signal of one cell usually lasted for 15 to 20 seconds, which was adequate to conduct MS/MS analysis of a selected ion with relatively higher abundance (e.g., $>10^5$) at the single-cell level. Among all abundant cellular species (e.g., the top 30 most abundant species in the control and treatment groups), six of them were further identified by MS/MS analysis at the single-cell level (Tables S3-2 and S3-3, Figure S3-7 and Figure

S3-8). However, the signal intensities of the rest species were inadequate for MS/MS analysis at the single-cell level due to multiple factors, including a very limited amount of

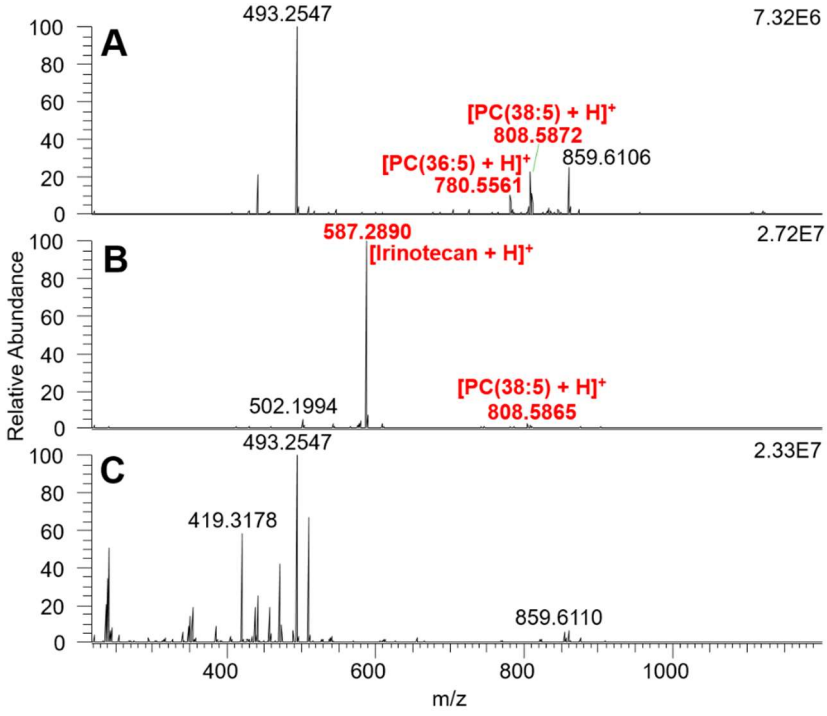


Figure 3-3. *Mass spectra of (A) a cell in the control group, (B) a cell in the drug treatment groups, and (C) background.*

cellular contents, the ionization suppression by salts (from cell culture medium), and pronounced background signals. Therefore, we used traditional nanoESI-MS/MS to analyze cell lysate samples as a complementary method (see the Support Information for detailed procedures of the lysate preparation and MS analysis). For example, the identification of irinotecan has been confirmed by MS/MS analysis in single cells (Figure S3-7), cell lysate (Figure S3-10), and the standard irinotecan solution. In addition, five cellular species were detected in both control and drug treatment groups, and they were identified as PC(36:5), PC(38:5), PC(34:1), PC(36:1), and TEI 9647 (Figure S3-8) from

online MS/MS analysis at the single cell level. Using the cell lysate, 12 species from the control group were further identified as PC(36:5), PC(34:1), PC(36:3), PC(38:6), PC(38:5), PC(38:4), PC(40:4), PC(38:7), TEI-9647, Coenzyme Q4, PC(40:6), and PC(40:7) (Figure S3-9). Among them, the first seven species were also detected in the lysate sample prepared using irinotecan treated cells (Figure S3-10).

Interestingly, the antagonist of VDR (vitamin D_3 nuclear receptor), TEI-9647 [61-63], was only present in control cells. As previously reported, vitamin D can hinder the progression of colon cancer[64, 65] through its active form 1,25-dihydroxyvitamin D_3 (1,25D), which induces growth arrest and apoptosis of cancer cells.[63] Importantly, activating VDR in cancer cells is needed for effective treatment using 1,25D.[63, 66] Our experimental results can likely provide rationales to these observations in previous studies. Producing TEI-9647 seems to be a protection mechanism of cancer cells against their undesired chemical environment, and this antagonist can suppress the activity of VDR to disable the anticancer functions of 1,25D. The absence of TEI-9647 in cancer cells upon irinotecan treatment likely indicates this anticancer drug may hinder synthetic pathways of TEI-9647, which can potentially be a new mechanism in addition to its known inhibition function of topoisomerase[67]. However, comprehensive studies are still needed to verify our hypothesis.

3.4.3 Changes of Metabolomic Profiles after Drug Treatment

Lipid metabolism is regulated by several cellular processes, including cell growth, proliferation, apoptosis, chemotherapy response, and drug resistance.[68] To illustrate the influence of anticancer drug treatment on cellular metabolism, we conducted the statistical analysis of the SCMS data. Specifically, PLS-DA was conducted to illustrate

the difference of overall metabolomic profiles between two groups of cells,[69] followed by the permutation test to validate the results.[70] We then used *t*-test to compare metabolites' abundances before and after treatment. Intuitively, visual discrimination of chemical profiles between two groups can be observed from the PLS-DA score plot (Figure 3-4), and the corresponding permutation test indicates that the difference is statistically significant (p-value < 0.001). Through the *t*-test, we discovered that a few types of lipids, including PC, PG, phosphatidylserine (PS), PE, and triglycerides (TG), were significantly changed (most of them were downregulated) due to drug treatment (Table S3-4). From a biological perspective, phosphatidic acid (PA) is the precursor for the biosynthesis of TGs and other phospholipids such as PC, PG, and PE.[71, 72] The suppressed production of PA upon the exposure to irinotecan, which was also reported in other studies,[73] can likely result in reduced synthesis of down-stream metabolites, such as TGs and phospholipids.

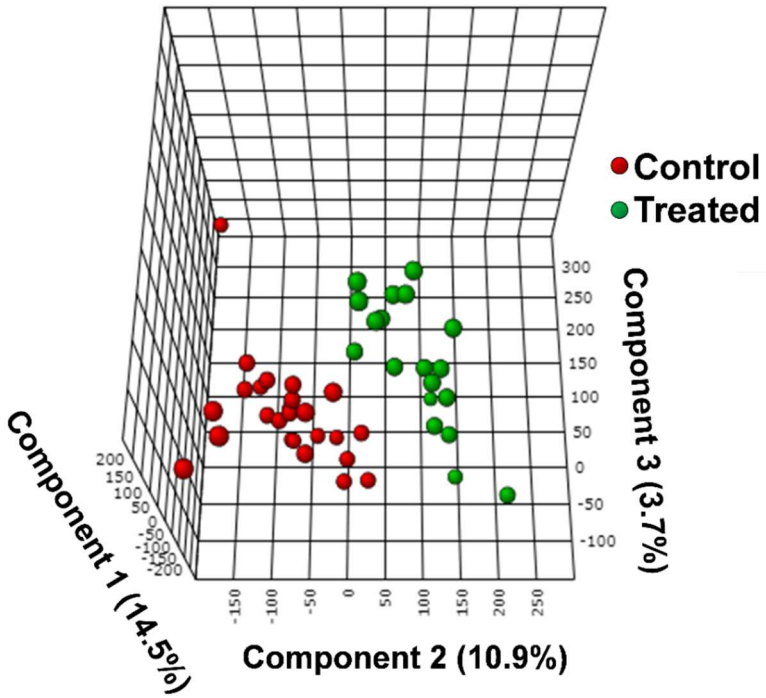


Figure 3-4. *3D PLS-DA plot illustrating the metabolomic difference of cells between the control (red dots) and the treatment (green dots) groups. Each dot represents the overall metabolomic profile of a single cell.*

In addition, a number of abundant species, including PE-Cer(d40:2) (*m/z* 781.5588) and SM(d37:1) (*m/z* 783.5758), were only detected from single cells rather than cell lysates (Tables S3-2 and S3-3), indicating that these cellular species are rapidly altered due to changes of cell microenvironment, or they are too labile to survive from multi-step sample preparation procedures. Due to the minimum sample preparation and rapid analysis, our technology allows for the detection of cellular species reflecting the status of live cells with minimum perturbation of cell microenvironment.

3.5 Conclusion

We reported a redesigned T-probe that can be coupled to a mass spectrometer to conduct rapid, in situ SCMS analysis of entire live single cells in suspension. HCT-116 cell line was used as the model, and cells in control and drug treatment groups were subjected to the SCMS experiments. An individual cell was initially withdrawn into the probe, subsequently subjected to rapid online lysis upon mixing with lysis solvent, and immediately ionized for real-time MS detection. The major advantage of this new design is that this device can be used to analyze non-adherent cells without cellular contents loss, as an entire cell is lysed inside the device. A variety of cellular species, including PC, PS, PE, PG, and TG, were detected from control and irinotecan treated single cells, with some of those further identified through online MS/MS analysis at the single-cell level. Evident changes of metabolomic profiles of single cells after drug treatment were visualized through PLS-DA, and cellular species (i.e., PC, PG, PS, PE, and TG) with

significant changes were discovered through t-test. In addition, we detected a number of species only present in single cells rather than cell lysates, indicating they are likely to be liable metabolites and sensitive to the change of cellular microenvironment. Our techniques can be potentially used for future SCMS analysis of a broader range of non-adherent cell types with different sizes, such as patient cells suspended in biological fluids.

Reference

1. Liu, Z.; Lavis, L. D.; Betzig, E., Imaging live-cell dynamics and structure at the single-molecule level. *Molecular cell* 2015, *58* (4), 644-659.
2. Rué, P.; Arias, A. M., Cell dynamics and gene expression control in tissue homeostasis and development. *Molecular systems biology* 2015, *11* (2), 792.
3. Altschuler, S. J.; Wu, L. F., Cellular Heterogeneity: Do Differences Make a Difference? *Cell* 2010, *141* (4), 559-563.
4. Dettmer, K.; Aronov, P. A.; Hammock, B. D., Mass spectrometry-based metabolomics. *Mass spectrometry reviews* 2007, *26* (1), 51-78.
5. Gawad, C.; Koh, W.; Quake, S. R., Single-cell genome sequencing: current state of the science. *Nature Reviews Genetics* 2016, *17* (3), 175.
6. Kanter, I.; Kalisky, T., Single cell transcriptomics: methods and applications. *Frontiers in oncology* 2015, *5*, 53.
7. Newman, J. R.; Ghaemmaghami, S.; Ihmels, J.; Breslow, D. K.; Noble, M.; DeRisi, J. L.; Weissman, J. S., Single-cell proteomic analysis of S. cerevisiae reveals the architecture of biological noise. *Nature* 2006, *441* (7095), 840.
8. Rubakhin, S. S.; Lanni, E. J.; Sweedler, J. V., Progress toward single cell metabolomics. *Current opinion in biotechnology* 2013, *24* (1), 95-104.
9. Zenobi, R., Single-cell metabolomics: analytical and biological perspectives. *Science* 2013, *342* (6163), 1243259.
10. Zhang, X.-C.; Wei, Z.-W.; Gong, X.-Y.; Si, X.-Y.; Zhao, Y.-Y.; Yang, C.-D.; Zhang, S.-C.; Zhang, X.-R., Integrated droplet-based microextraction with ESI-MS for removal of matrix interference in single-cell analysis. *Scientific reports* 2016, *6*, 24730.
11. Rubakhin, S. S.; Romanova, E. V.; Nemes, P.; Sweedler, J. V., Profiling metabolites and peptides in single cells. *Nature methods* 2011, *8* (4s), S20.
12. Yang, Y.; Huang, Y.; Wu, J.; Liu, N.; Deng, J.; Luan, T., Single-cell analysis by ambient mass spectrometry. *TrAC Trends in Analytical Chemistry* 2017, *90*, 14-26.
13. Zhang, L.; Vertes, A., Single-Cell Mass Spectrometry Approaches to Explore Cellular Heterogeneity. *Angewandte Chemie International Edition* 2018, *57* (17), 4466-4477.
14. Duncan, K. D.; Fyrestam, J.; Lanekoff, I., Advances in mass spectrometry based single-cell metabolomics. *Analyst* 2018.
15. Ibáñez, A. J.; Fagerer, S. R.; Schmidt, A. M.; Urban, P. L.; Jefimovs, K.; Geiger, P.; Dechant, R.; Heinemann, M.; Zenobi, R., Mass spectrometry-based metabolomics of single yeast cells. *Proceedings of the National Academy of Sciences* 2013, *110* (22), 8790-8794.
16. Huang, M.-Z.; Yuan, C.-H.; Cheng, S.-C.; Cho, Y.-T.; Shiea, J., Ambient ionization mass spectrometry. *Annual review of analytical chemistry* 2010, *3*, 43-65.
17. Cooks, R. G.; Ouyang, Z.; Takats, Z.; Wiseman, J. M., Ambient mass spectrometry. *Science* 2006, *311* (5767), 1566-1570.
18. Monge, M. E.; Harris, G. A.; Dwivedi, P.; Fernández, F. M., Mass spectrometry: recent advances in direct open air surface sampling/ionization. *Chemical reviews* 2013, *113* (4), 2269-2308.

19. Tsuyama, N.; Mizuno, H.; Tokunaga, E.; Masujima, T., Live single-cell molecular analysis by video-mass spectrometry. *Analytical Sciences* 2008, *24* (5), 559-561.
20. Shrestha, B.; Vertes, A., In situ metabolic profiling of single cells by laser ablation electrospray ionization mass spectrometry. *Analytical Chemistry* 2009, *81* (20), 8265-8271.
21. Bergman, H.-M.; Lanekoff, I., Profiling and quantifying endogenous molecules in single cells using nano-DESI MS. *Analyst* 2017, *142* (19), 3639-3647.
22. Zhu, H.; Zou, G.; Wang, N.; Zhuang, M.; Xiong, W.; Huang, G., Single-neuron identification of chemical constituents, physiological changes, and metabolism using mass spectrometry. *Proceedings of the National Academy of Sciences* 2017, 201615557.
23. Gong, X.; Zhao, Y.; Cai, S.; Fu, S.; Yang, C.; Zhang, S.; Zhang, X., Single cell analysis with probe ESI-mass spectrometry: detection of metabolites at cellular and subcellular levels. *Analytical chemistry* 2014, *86* (8), 3809-3816.
24. Chen, F.; Lin, L.; Zhang, J.; He, Z.; Uchiyama, K.; Lin, J.-M., Single-cell analysis using drop-on-demand inkjet printing and probe electrospray ionization mass spectrometry. *Analytical chemistry* 2016, *88* (8), 4354-4360.
25. Mao, S.; Zhang, W.; Huang, Q.; Khan, M.; Li, H.; Uchiyama, K.; Lin, J. M., In Situ Scatheless Cell Detachment Reveals Correlation between Adhesion Strength and Viability at Single - Cell Resolution. *Angewandte Chemie International Edition* 2018, *57* (1), 236-240.
26. Naill, M. C.; Roberts, S. C., Flow cytometric analysis of protein content in Taxus protoplasts and single cells as compared to aggregated suspension cultures. *Plant cell reports* 2005, *23* (8), 528-533.
27. Bandura, D. R.; Baranov, V. I.; Ornatsky, O. I.; Antonov, A.; Kinach, R.; Lou, X.; Pavlov, S.; Vorobiev, S.; Dick, J. E.; Tanner, S. D., Mass cytometry: technique for real time single cell multitarget immunoassay based on inductively coupled plasma time-of-flight mass spectrometry. *Analytical chemistry* 2009, *81* (16), 6813-6822.
28. Pan, N.; Rao, W.; Kothapalli, N. R.; Liu, R.; Burgett, A. W.; Yang, Z., The single-probe: a miniaturized multifunctional device for single cell mass spectrometry analysis. *Analytical chemistry* 2014, *86* (19), 9376-9380.
29. Rao, W.; Pan, N.; Yang, Z., Applications of the single-probe: mass spectrometry imaging and single cell analysis under ambient conditions. *Journal of visualized experiments: JoVE* 2016, (112).
30. Sun, M.; Yang, Z.; Wawrik, B., Metabolomic Fingerprints of Individual Algal Cells Using the Single-Probe Mass Spectrometry Technique. *Frontiers in plant science* 2018, *9*.
31. Liu, R.; Zhang, G.; Yang, Z., Towards rapid prediction of drug-resistant cancer cell phenotypes: Single cell mass spectrometry combined with machine learning. *Chemical Communications* 2019, *55* (5), 616-619.
32. Tian, X.; Zhang, G.; Shao, Y.; Yang, Z., Towards enhanced metabolomic data analysis of mass spectrometry image: Multivariate Curve Resolution and Machine Learning. *Analytica chimica acta* 2018, *1037*, 211-219.
33. Tian, X.; Zhang, G.; Zou, Z.; Yang, Z., Anticancer Drug Affects Metabolomic Profiles in Multicellular Spheroids: Studies Using Mass Spectrometry Imaging Combined with Machine Learning. *Anal Chem* 2019, *91* (9), 5802-5809.

34. Rao, W.; Pan, N.; Tian, X.; Yang, Z., High-resolution ambient MS imaging of negative ions in positive ion mode: using dicationic reagents with the single-probe. *Journal of the American Society for Mass Spectrometry* 2016, *27* (1), 124-134.
35. Sun, M.; Tian, X.; Yang, Z., Microscale mass spectrometry analysis of extracellular metabolites in live multicellular tumor spheroids. *Analytical chemistry* 2017, *89* (17), 9069-9076.
36. Liu, R.; Pan, N.; Zhu, Y.; Yang, Z., T-probe: an integrated microscale device for online in situ single cell analysis and metabolic profiling using mass spectrometry. *Analytical chemistry* 2018, *90* (18), 11078-11085.
37. Masujima, T., Live single-cell mass spectrometry. *Analytical Sciences* 2009, *25* (8), 953-960.
38. Carter, D. A.; Fernandes, K. E.; Brockway, A.; Haverkamp, M.; Cuomo, C. A.; Van Ogtrop, F.; Perfect, J. R., Phenotypic variability correlates with clinical outcome in Cryptococcus isolates obtained from Botswanan HIV/AIDS patients. *BioRxiv* 2018, 418897.
39. Onjiko, R. M.; Portero, E. P.; Moody, S. A.; Nemes, P., In situ microprobe single-cell capillary electrophoresis mass spectrometry: metabolic reorganization in single differentiating cells in the live vertebrate (Xenopus laevis) embryo. *Analytical chemistry* 2017, *89* (13), 7069-7076.
40. Sun, L.; Bertke, M. M.; Champion, M. M.; Zhu, G.; Huber, P. W.; Dovichi, N. J., Quantitative proteomics of Xenopus laevis embryos: expression kinetics of nearly 4000 proteins during early development. *Scientific reports* 2014, *4*, 4365.
41. Sun, L.; Dubiak, K. M.; Peuchen, E. H.; Zhang, Z.; Zhu, G.; Huber, P. W.; Dovichi, N. J., Single cell proteomics using frog (Xenopus laevis) blastomeres isolated from early stage embryos, which form a geometric progression in protein content. *Analytical chemistry* 2016, *88* (13), 6653-6657.
42. Cumeras, R.; Figueras, E.; Davis, C.; Baumbach, J. I.; Gracia, I., Review on ion mobility spectrometry. Part 1: current instrumentation. *Analyst* 2015, *140* (5), 1376-1390.
43. Zhang, L.; Foreman, D. P.; Grant, P. A.; Shrestha, B.; Moody, S. A.; Villiers, F.; Kwak, J. M.; Vertes, A., In situ metabolic analysis of single plant cells by capillary microsampling and electrospray ionization mass spectrometry with ion mobility separation. *Analyst* 2014, *139* (20), 5079-5085.
44. Lombard-Banek, C.; Moody, S. A.; Nemes, P., Single-cell mass spectrometry for discovery proteomics: Quantifying translational cell heterogeneity in the 16-cell frog (Xenopus) embryo. *Angewandte Chemie International Edition* 2016, *55* (7), 2454-2458.
45. Lewis, W. G.; Shen, Z.; Finn, M.; Siuzdak, G., Desorption/ionization on silicon (DIOS) mass spectrometry: background and applications. *International Journal of Mass Spectrometry* 2003, *226* (1), 107-116.
46. Mazutis, L.; Gilbert, J.; Ung, W. L.; Weitz, D. A.; Griffiths, A. D.; Heyman, J. A., Single-cell analysis and sorting using droplet-based microfluidics. *Nature protocols* 2013, *8* (5), 870.
47. Pierigè, F.; Bigini, N.; Rossi, L.; Magnani, M., Reengineering red blood cells for cellular therapeutics and diagnostics. *Wiley Interdisciplinary Reviews: Nanomedicine and Nanobiotechnology* 2017, *9* (5), e1454.
48. Liao, J.-C., Cell therapy using bone marrow-derived stem cell overexpressing BMP-7 for degenerative discs in a rat tail disc model. *International journal of molecular sciences* 2016, *17* (2), 147.
49. Potdar, P.; Lotey, N., Role of circulating tumor cells in future diagnosis and therapy of cancer. *Journal of Cancer Metastasis and Treatment* 2015, *1* (2), 44-44.

50. Weisberg, S. P.; Chang, M.; Muranski, P.; Farber, D., Efficient Expansion of Polyfunctional Virus-Specific T Cells from Human Lymph Nodes: Implications for Cellular Therapies. Am Soc Hematology: 2018.
51. Standke, S. J.; Colby, D. H.; Bensen, R. C.; Burgett, A. W.; Yang, Z., Mass spectrometry measurement of single suspended cells using a combined cell manipulation system and a single-probe device. *Analytical chemistry* 2019, *91* (3), 1738-1742.
52. Pan, N.; Rao, W.; Standke, S. J.; Yang, Z., Using dicationic ion-pairing compounds to enhance the single cell mass spectrometry analysis using the single-probe: a microscale sampling and ionization device. *Analytical chemistry* 2016, *88* (13), 6812-6819.
53. Beard Jr, E. L., The american society of health system pharmacists. *JONA'S healthcare law, ethics and regulation* 2001, *3* (3), 78-79.
54. Gupta, E.; Mick, R.; Ramirez, J.; Wang, X.; Lestingi, T. M.; Vokes, E. E.; Ratain, M. J., Pharmacokinetic and pharmacodynamic evaluation of the topoisomerase inhibitor irinotecan in cancer patients. *Journal of Clinical Oncology* 1997, *15* (4), 1502-1510.
55. Lanekoff, I.; Heath, B. S.; Liyu, A.; Thomas, M.; Carson, J. P.; Laskin, J., Automated platform for high-resolution tissue imaging using nanospray desorption electrospray ionization mass spectrometry. *Analytical chemistry* 2012, *84* (19), 8351-8356.
56. Liu, R.; Zhang, G.; Sun, M.; Pan, X.; Yang, Z., Integrating A Generalized Data Analysis Workflow with the Single-probe Mass Spectrometry Experiment for Single Cell Metabolomics. *Analytica Chimica Acta* 2019.
57. Xia, J.; Wishart, D. S., Using MetaboAnalyst 3.0 for comprehensive metabolomics data analysis. *Current protocols in bioinformatics* 2016, *55* (1), 14.10. 1-14.10. 91.
58. Gromski, P. S.; Muhamadali, H.; Ellis, D. I.; Xu, Y.; Correa, E.; Turner, M. L.; Goodacre, R., A tutorial review: Metabolomics and partial least squares-discriminant analysis–a marriage of convenience or a shotgun wedding. *Analytica chimica acta* 2015, *879*, 10-23.
59. Smith, C. A.; O'Maille, G.; Want, E. J.; Qin, C.; Trauger, S. A.; Brandon, T. R.; Custodio, D. E.; Abagyan, R.; Siuzdak, G., METLIN: a metabolite mass spectral database. *Therapeutic drug monitoring* 2005, *27* (6), 747-751.
60. Wishart, D. S.; Jewison, T.; Guo, A. C.; Wilson, M.; Knox, C.; Liu, Y.; Djoumbou, Y.; Mandal, R.; Aziat, F.; Dong, E., HMDB 3.0—the human metabolome database in 2013. *Nucleic acids research* 2012, *41* (D1), D801-D807.
61. Ishizuka, S.; Kurihara, N.; Miura, D.; Takenouchi, K.; Cornish, J.; Cundy, T.; Reddy, S. V.; Roodman, G. D., Vitamin D antagonist, TEI-9647, inhibits osteoclast formation induced by 1α, 25-dihydroxyvitamin D3 from pagetic bone marrow cells. *The Journal of steroid biochemistry and molecular biology* 2004, *89*, 331-334.
62. Peräkylä, M.; Molnár, F.; Carlberg, C., A structural basis for the species-specific antagonism of 26, 23-lactones on vitamin D signaling. *Chemistry & biology* 2004, *11* (8), 1147-1156.
63. Pereira, F.; Larriba, M. J.; Muñoz, A., Vitamin D and colon cancer. *Endocrine-related cancer* 2012, *19* (3), R51-R71.
64. Garland, C. F.; Garland, F. C., Do sunlight and vitamin D reduce the likelihood of colon cancer? *International journal of epidemiology* 1980, *9* (3), 227-231.
65. Lappe, J. M.; Travers-Gustafson, D.; Davies, K. M.; Recker, R. R.; Heaney, R. P., Vitamin D and calcium supplementation reduces cancer risk: results of a randomized trial. *The American journal of clinical nutrition* 2007, *85* (6), 1586-1591.

66. Shah, S.; Islam, M. N.; Dakshanamurthy, S.; Rizvi, I.; Rao, M.; Herrell, R.; Zinser, G.; Valrance, M.; Aranda, A.; Moras, D., The molecular basis of vitamin D receptor and β-catenin crossregulation. *Molecular cell* 2006, *21* (6), 799-809.
67. Mathijssen, R. H.; Loos, W. J.; Verweij, J.; Sparreboom, A., Pharmacology of topoisomerase I inhibitors irinotecan (CPT-11) and topotecan. *Current cancer drug targets* 2002, *2* (2), 103-123.
68. Huang, C.; Freter, C., Lipid metabolism, apoptosis and cancer therapy. *International journal of molecular sciences* 2015, *16* (1), 924-949.
69. Westerhuis, J. A.; Hoefsloot, H. C.; Smit, S.; Vis, D. J.; Smilde, A. K.; van Velzen, E. J.; van Duijnhoven, J. P.; van Dorsten, F. A., Assessment of PLSDA cross validation. *Metabolomics* 2008, *4* (1), 81-89.
70. Golland, P.; Fischl, B. In *Permutation tests for classification: towards statistical significance in image-based studies*, Biennial International Conference on Information Processing in Medical Imaging, Springer: 2003; pp 330-341.
71. Sreenivas, A.; Villa-Garcia, M. J.; Henry, S. A.; Carman, G. M., Phosphorylation of the yeast phospholipid synthesis regulatory protein Opi1p by protein kinase C. *Journal of Biological Chemistry* 2001, *276* (32), 29915-29923.
72. Hsieh, L.-S.; Su, W.-M.; Han, G.-S.; Carman, G. M., Phosphorylation regulates the ubiquitin-independent degradation of yeast Pah1 phosphatidate phosphatase by the 20S proteasome. *Journal of Biological Chemistry* 2015, *290* (18), 11467-11478.
73. Blandizzi, C.; De Paolis, B.; Colucci, R.; Lazzeri, G.; Baschiera, F.; Del Tacca, M., Characterization of a novel mechanism accounting for the adverse cholinergic effects of the anticancer drug irinotecan. *British journal of pharmacology* 2001, *132* (1), 73-84.

Chapter 4. Combining Mass Spectrometry with Paternò-Büchi Reaction to Determine Double-bond Positions in Lipids at the Single-cell Level

Author Contributions: The study of Chapter 4 is primarily conducted by Yanlin Zhu. Wenhua Wang participated in the development of Python scripts.

Copyright permission: The material in chapter 4 is adapted from Zhu, Yanlin, Wenhua Wang, and Zhibo Yang. "Combining Mass Spectrometry with Paternò-Büchi Reaction to Determine Double-bond Positions in Lipids at the Single-cell Level". Copyright permission is obtained from American Chemical Society, and the detail is shown in Appendix III.

4.1 Abstract

Single cell MS (SCMS) techniques are under rapid development for molecular analysis of individual cells among heterogeneous populations. Lipids are basic cellular constituents playing essential functions in energy storage and cellular signaling processes of cells. Unsaturated lipids are characterized with one or multiple carbon-carbon double (C=C) bonds, and they are critical for cell functions and human diseases. Characterizing unsaturated lipids in single cells allows for a better understanding of metabolomic biomarkers and therapeutic targets of rare cells (e.g., cancer stem cells); however, these studies remain challenging. We developed a new technique using a micropipette needle, in which Paternò-Büchi (PB) reactions at C=C bond can be induced,

to determine locations of C=C bonds in unsaturated lipids at the single-cell level. The micropipette needle is produced by combining a pulled glass capillary needle with a fused silica capillary. Cell lysis solvent and PB reagent (acetone or benzophenone) are delivered into the micropipette needle (tip size ~15 um) through a fused silica capillary. The capillary needle plays multiple functions (i.e., single-cell sampling probe, cell lysis container, micro-reactor, and nano-ESI emitter) in the experiments. Both regular (no reaction) and reactive (with PB reaction) SCMS analyses of the same cell can be achieved. C=C bond locations were determined from MS scan and MS/MS of PB products assisted by Python programs. This technique can be potentially used for other reactive SCMS studies to enhance molecular analysis for broad ranges of single cells.

4.2 Introduction

Among all known organisms, cells are the smallest unit of life. The majority of current studies of cells are based on ensemble measurement. However, each individual cell has unique genomic and phenotypic traits that can distinguish itself from other adjacent cells, causing the cell to cell heterogeneity in any population.[1] Numerous studies indicate that small subpopulations of cells are overlooked using population measurements, resulting in the loss of important biology information of rare cells.[1] Therefore, molecular analysis of single cells is an inevitable choice to understand cellular mechanisms that cannot be studied using traditional bulk analysis.[1]

4.2.1 Lipids

Among all cellular molecules, lipids are crucial components of the cell membrane and other cellular compartments, including the endoplasmic reticulum, Golgi apparatus, and nuclear membrane. Lipids are organic compounds that are generally soluble in nonpolar

solvents due to the long hydrophobic hydrocarbon chains.[2] They are also defined as small amphiphilic molecules that enable them to form vesicles, liposomes, and membranes in the aqueous environment. Lipids play crucial roles in the structure and function of living cells such as acting as a structural unit of cell membranes, energy storage, signals, cofactors and pigments.[3]

4.2.2 Classification of lipids

Lipids can be classified into three according to their functions or composition[4, 5]

4.2.2.1 Classification of lipids base on their composition

Base on their composition of lipids, they are divided into simple lipids, complex lipids, and derived lipids.[4, 6] Simple lipids consist of the ester of fatty acids with diverse alcohols, such as fats, waxes, and triglycerides (TG). These lipids belong to heterogeneous nonpolar compounds that are soluble in nonpolar organic solvents.

Complex lipids generally contain sugar moieties and two or more other chemical identities, including glycerol, fatty acids (FA), nucleoside, and the phosphate group. Some of them may only contain one of these identities.[5] Complex lipids can be widely found in plants, bacteria, and animals, and they are the major components of cell membranes. Phospholipids, glycolipids, lipoamino acid, and nucleolipids are the main groups of complex lipids. Phospholipids contain a phosphate residue, one or two fatty acid tails, and one glycerol, amino alcohol, or fatty alcohol. Glycerophospholipids and sphingosylphosphatides are the most common phospholipids. Glycerophospholids contain three components, which are glycerol, two fatty acid tails, and a phosphate ester. Different glycerophospholipids contain variable phosphate esters, and the most common glycerophospholipids include phosphatidic acid (PA), phosphatidylserine (PS),

phosphatidylethanolamine (PE), phosphatidylcholine (PC), phosphatidylinositol (PI), phosphatidylglycerol (PG), and bisphosphatidyl glycerol.[7]

Sphingosylphosphatides, which is another class of phospholipids, consist of sphingosine, one fatty acid tail, and a phosphate ester. Similarly, different sphingosylphosphatides contain variable phosphate esters (Figure 4-1). Sphingosine, ceramide, sphingomyelin (SM), cerebroside, and ganglioside are the common sphingosylphosphatides.[8]

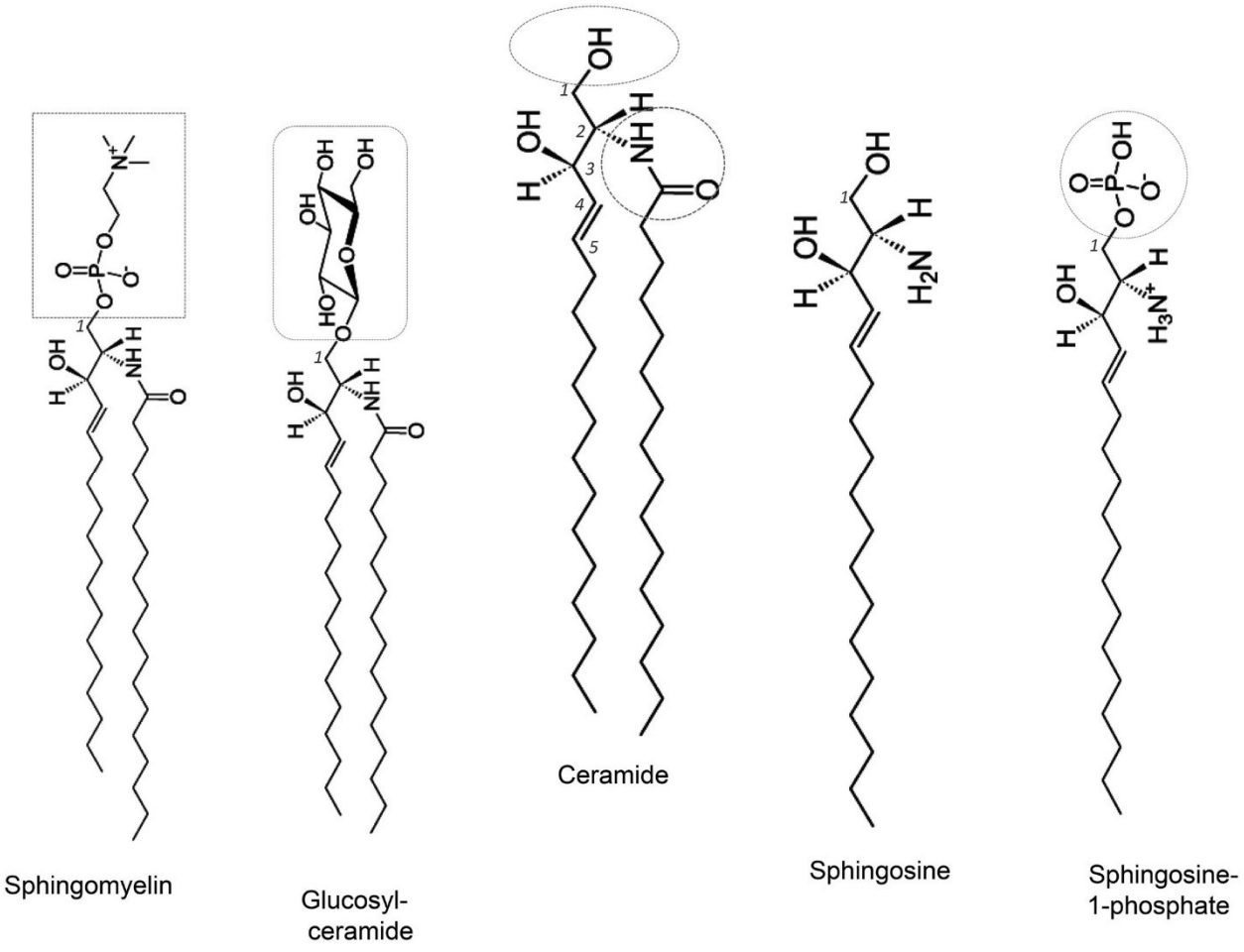


Figure 4-1. *The structure of sphingosylphosphatides contains variable phosphate esters. (Chen, H., Chan, A. Y., Stone, D. U., & Mandal, N. A. (2014). Beyond the cherry-red spot: Ocular manifestations of sphingolipid-mediated neurodegenerative and*

inflammatory disorders. Survey of ophthalmology, 59(1), 64-76. Copyright permission is obtained from ELSEVIER, and the detail is shown in Appendix III.*)*

Derived lipids are the hydrolysis products of simple and complex lipids. FA, monoglycerides (MG), diglycerides (DG), steroids, terpenes, and carotenoids belong to this classification.[5] Among these derived lipids, FAs are the critical unit of lipids of living cells. A FA is composed of a carboxylic acid group and a saturated or unsaturated hydrocarbon chain. Saturated FAs only contain single carbon-carbon bonds of the long hydrocarbon chain, whereas unsaturated FAs contain one or multiple carbon-carbon double bonds (C=C).

4.2.2.2 Classification of lipids base on their functions

According to the functions of lipids, they can be divided into three classifications: storage lipids, structural lipids, and other lipids (e.g., signals, cofactors, and pigment).[5] The storage lipids include FAs and TGs. TGs are energy storage molecules, and FAs work as an energy source of cells.[9] Structural lipids, including phospholipids and non-phosphorylated lipids, are essential components of cell membranes.[10] Other lipids, such as signal, cofactor, and pigment lipids, perform signaling roles.[5] For example, DGs and MGs work as secondary messengers of signaling proteins. Since lipids work as messengers between extracellular and intracellular to control the normal physiology of cells, lipid signaling can cause inflammation, cancer, metabolic, cardiovascular, and degenerative diseases under deregulated conditions.[11]

4.2.3 Significance of unsaturated lipid isomers

The identification of unsaturation sites is critical for understanding lipid biochemistry. For example, previous studies indicate that cancer stem cells have relatively higher levels of unsaturated lipids compared with non-stem cancer cells[12, 13], and higher abundances of unsaturated lipids in cancer stem cells are related to the upregulated of *de novo* fatty acid (FA) synthesis pathway.[12, 14, 15] The unsaturation level of lipids influences many cell physiological properties such as membrane fluidity[16, 17], neurotransmitter release[18, 19], and cardiolipin remodeling.[20] The location of C=C bond in unsaturated lipids is critical for their biological functions. For example, lipid isomers with different C=C bond positions are related to numerous diseases, including cancer, cardiovascular disease, type II diabetes, Barth syndrome, Alzheimer's disease, and Parkinson's disease.[20-22] Thus, determining the C=C bond locations in unsaturated lipids is needed in studies of fundamental cell biology and wide types of diseases.

4.2.4 Identification of unsaturated lipid isomers

4.2.4.1 Current methods for unsaturated lipid isomers identification

Mass spectrometry (MS) has become one of the most effective tools for lipid profiling and quantification.[23, 24] MS based methods have been widely used for targeted and nontargeted lipidomics study, including identification of specific lipid classes using shotgun MS[25] and analysis of complex lipids (e.g., glycerolipids, glycerophospholipids, and glycolipids).[26-29] Particularly, combined with chemical reactions, MS has been used to pinpoint C=C bond sites in unsaturated lipids based on three different reactions. (1) Paternò–Büchi (PB) reaction. PB reaction is a classical photochemical derivatization that can specifically form adducts at C=C bonds under UV irradiation. Both acetone and

benzophenone have been used as the PB reagents to study unsaturated lipids. For example, Yu[28, 30] and Liu[29] have utilized tandem MS (MS/MS) to analyze adducts formed in the PB reactions to identify the structure of unsaturated lipids. (2) Ozone-induced dissociation (OzID). This technique can directly utilize ozonolysis, an organic reaction allowing for the cleavage of alkene double bonds using ozone, or combine it with CID (collision induced dissociation) to elucidate C=C bonds in unsaturated lipids.[31] (3) Meta-chloroperoxy benzoic acid (m-CPBA) epoxidation reaction. m-CPBA is an oxidant that can convert alkene to epoxide. Both Li[32] and Hsu[20] have used m-CPBA in reactions with unsaturated lipids to form products with triatomic rings, which generated two diagnostic ion pairs (with 16 Da mass difference) to determine the C=C bond positions.

4.2.4.2 The novel approach for unsaturated lipid isomers identification at single-cell level

Using PB, m-CPBA, and ozonolysis reactions as mentioned above, MS determination of C=C bonds in unsaturated lipids has been carried out in bulk analysis (e.g., lipids prepared solutions and lipids extractions form cells, tissues, and plasma).[28, 30, 32, 33] However, the corresponding studies at the single-cell level remain unexplored due to extremely small amount analytes in a single cell (e.g., a few pLs)[34] and the absence of appropriate techniques. Single cell MS (SCMS) methods have been rapidly developed for metabolomics and proteomics studies of a broad range of cells, including plant cells, mammalian cells, and yeasts.[35-37]. Under vacuum conditions, matrix-assisted desorption/ionization (MALDI) MS[38] and secondary ion MS (SIMS) are commonly used for single-cell analysis. In recent years, a variety of ambient based MS methods have been developed for single-cell analysis. The representative examples include single-cell video-MS[39], induced nanoESI (InESI) MS[40], probe electrospray ionization (PESI)[41], the

Single-probe,[42-45] and the T-probe.[46] Cell attachment (e.g., onto a substrate) is generally required for most SCMS techniques. However, the requirement of cell attachment prior to MS analysis largely limits the type of cells in studies. In addition, cell attachment may alter cell status and their molecular compositions.[47] A number of ambient MS techniques have been developed to analyze single non-adherent cells, such as mass cytometry[48], drop-on-demand inkjet printing coupled with PESI [49], the redesigned T-probe [34], integrated cell manipulation platform (ICMP)/Single-probe secondary ion MS (SIMS),[50] and techniques coupled with microfluidic chips.[51, 52] However, none of the existing SCMS methods has been used for studies of C=C bond positions in unsaturated lipids at the single-cell level.

Here, we used the glass micropipette needles to perform PB reactions of single cells followed up by MS determination of C=C bonds' positions in unsaturated lipids (Figure 4-2). The micropipette needle is produced by combing a fused silica capillary with a pulled

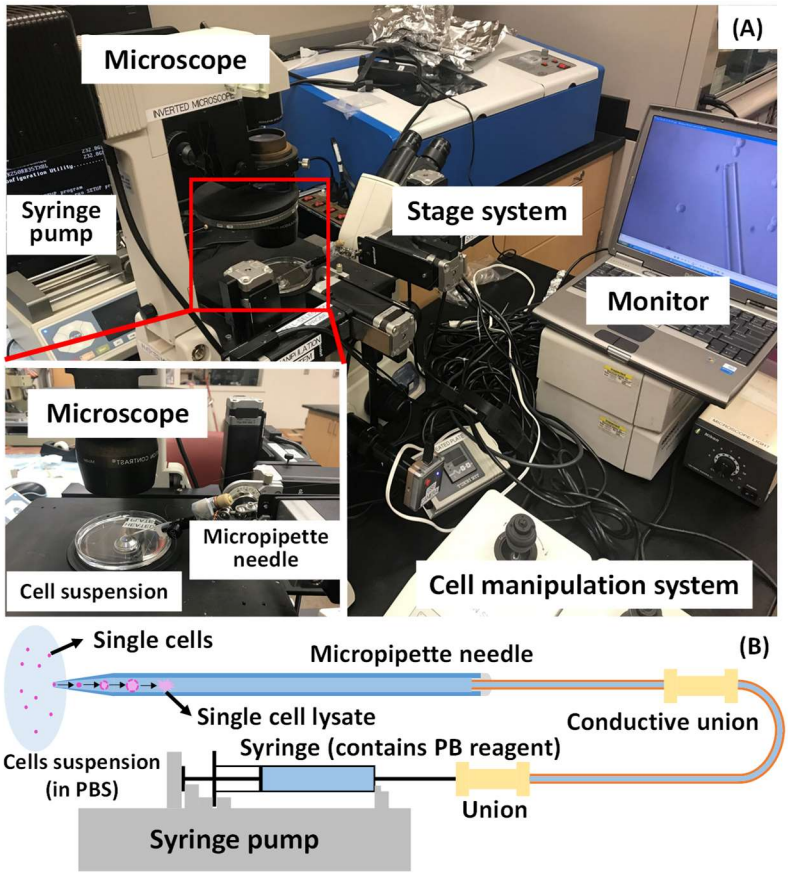


Figure 4-2. *(A) Experimental set-up of the micropipette needle for single-cell sampling. An inverted microscope was used to provide a visual guide during the experiment, and the cell manipulation system was used to control the micropipette needle to aim the targeted cell. Micropipette needle was connected with a syringe using capillary and unions. The syringe pump controlled the syringe to suck the targeted cell into the pipette. (B) Sketch of single-cell sampling using micropipette needle.*

glass micropipette (Figures 4-2B and 4-3D). The fused silica capillary is connected with a syringe to provide solution containing cell lysis solvent and the PB reagent. The

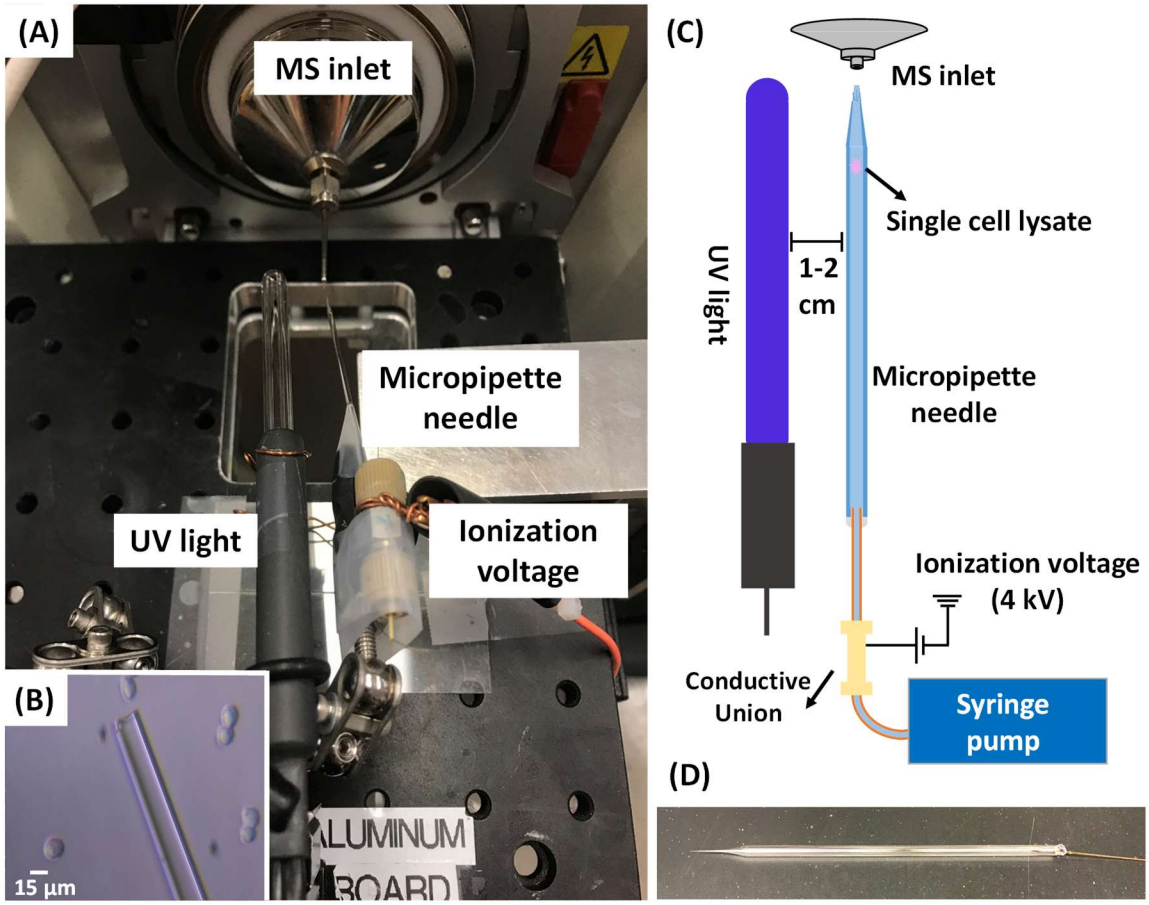


Figure 4-3. *(A) Experimental set-up of the micropipette needle for C=C bond identification at the single-cell level. The mercury UV light was placed next to the micropipette needle, and the ionization voltage was applied on the micropipette needle. (B) Sampling a suspended HCT-116 cell under the microscope. (C) Schematics of single-cell sampling and SCMS analysis. (D) Photo of a micropipette needle.*

micropipette needle plays multiple functions, including cell selection, cell lysis, micro-reactor for PB reaction, and nano-ESI emitter for ionization (Figure 4-3). To conduct the PB reactions of single cells, the reagent (i.e., acetone or benzophenone solution tone) was drawn into the glass micropipette. Using an integrated cell manipulation system,[52] which contains two Eppendorf cell manipulation systems, an inverted microscope (Nikon

Eclipse TE300, Tokyo, Japan), and a syringe pump, a target cell was selected and sucked into the glass micropipette, in which the cell underwent a rapid lysis process (Figure 4-2). A mercury lamp was placed next to the micropipette needle to provide UV irradiation and induce PB reactions with unsaturated lipids (Figure 4-3). For MS analysis, the ionization voltage was applied onto the conductive union to generate nano-ESI at the tip of the micropipette needle. Two types of SCMS experiments, including the regular (no UV irradiation) and reactive (after 15 minutes of UV irradiation) methods, were conducted for the same cell to acquire comprehensive information for studying unsaturated lipids.

4.3 Method

4.3.1 Fabrication of the micropipette needle

The micropipette needle (tip size ~15 um) was pulled from a glass capillary tube (size: 0.8 x 90 mm, Kimble Chase Life Science and Research Products, Rockwood, TN) using a pipette puller (KOPF, Tujunga, CA). UV epoxy (Prime-Dent, Chicago, IL) was used to connect the micropipette needle to a fused silica capillary (OD: 150 μm, ID: 75 μm, Polymicro Technologies, Phoenix, AZ). A syringe was connected to the fused silica capillary via a conductive union (IDEX Health & Science LLC, Oak Harbor, WA).

4.3.2 Preparation of SCMS solutions

In the reactive SCMS studies, the solvent has three major functions: inducing cell lysis, performing PB reactions, and playing the role of the ionization solvent. First, the deoxygenation of solvents was performed to minimize side reactions while promoting PB reactions.[29, 53] An Erlenmeyer flask (with stopper) containing pure acetone or ACN (acetonitrile) was placed on the ice and vacuumed for 30 min, followed by bubbling nitrogen for 30 min.[29] This process was repeated for three times to deplete oxygen from

solvents. Next, the solution containing PB reagents was prepared and added in the micropipette needle. Two different reagents, benzophenone solution (5 mM benzophenone in ACN with 0.1 % formic acid) and acetone, have been tested in our studies to compare their performance.

4.3.3 Reactive SCMS experiments

Using an Eppendorf cell manipulation system and a syringe pump, a target cell was sucked into the glass micropipette (flowrate 10 µL/min) containing pre-filled acetone or benzophenone solution (Figure 4-2). Additional solution was drawn into the micropipette needle to ensure cell lysis. The syringe pump was turned on to deliver (flowrate 0.2 µL/min) the single-cell lysate towards the nano-ESI emitter. A DC ionization voltage (+4 kV in the positive ion mode or –4 kV in the negative ion mode) was applied on a conductive union and transmitted through the solvent to induce ionization of cell lysis at the tip of the micropipette for MS analysis. Due to the long signal duration time of a single cell (20-30 minutes), both the regular (no UV irradiation) and the reactive (after UV irradiation) SCMS experiments can be conducted for the same single cell. Specifically, after accomplishing data acquisition of the regular SCMS experiment, the ionization energy was turned off and the syringe pump was paused. The UV lamp (BHK, Ontario, CA) was then turned on to generate UV radiation and initiate PB reactions between the reagents and unsaturated cellular lipids. After 15 mins of reaction, the UV light was turned

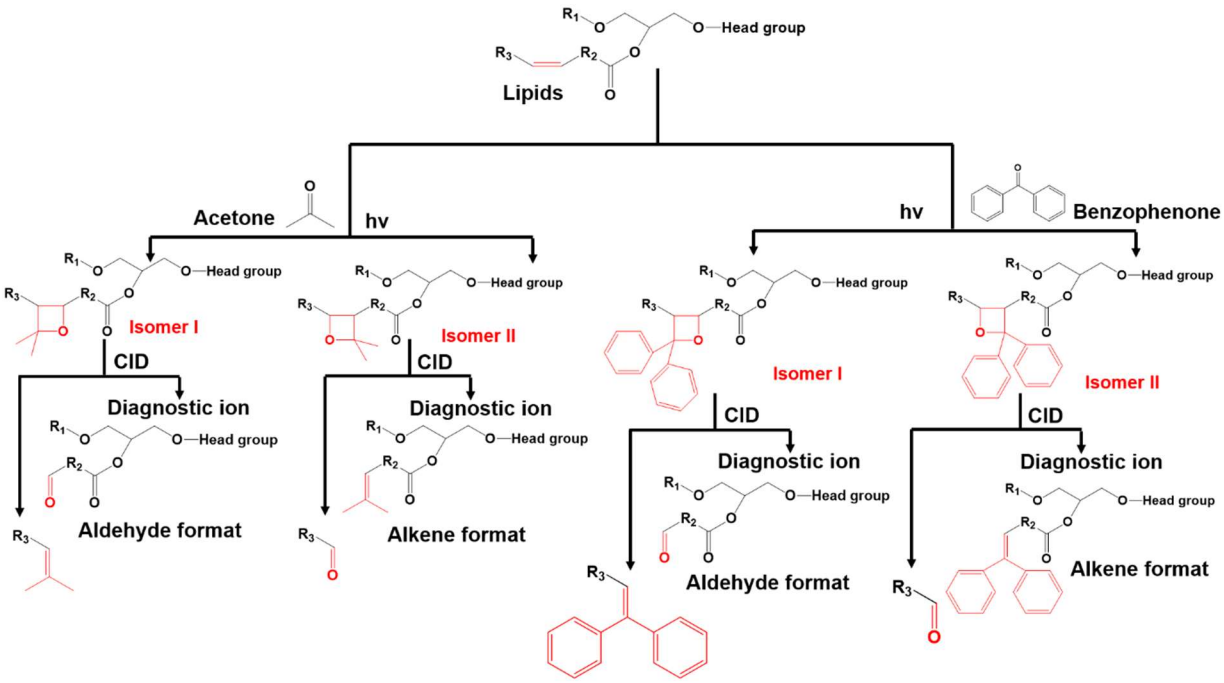


Figure 4-4. *Mechanism of PB reactions and the formation of diagnostic ion pairs (aldehyde and alkene formats) in CID.*

off, and then the reactive SCMS experiment was started by turning on the ionization voltage and resuming the syringe pump. Products from the PB reactions were analyzed using both MS scan (to obtain accurate *m/z* values of all ions) and tandem MS (MS/MS) analysis (to acquire fragments of selected ions). As illustrated in Figure 4-4, the PB reaction at each C=C bond can produce two isomers (i.e., Isomers I and II), which then produce one pair of diagnostic ions during CID, i.e., aldehyde and alkene ions can be generated from Isomer I and Isomer II, respectively.

4.3.4 Cells culture and sample preparation

The human colon cancer cell line, HCT-116, was chosen as a model system in the current study. Cells were cultured using a standard protocol as briefly described following.[42] Cells were cultured in McCoy's 5A medium, detached from Petri dish using trypsin, rinsed by

PBS (phosphate-buffered saline), centrifuged (1000 rmp, 10 min, three times), and then resuspended in PBS. Cell density was controlled to be around $5x10^4$ cells/mL, and ~7 mL of the cell suspension solution was transferred to a culture dish for the following SCMS analysis. The cell lysis sample was prepared using standard protocols for comparative studies.[54] The detailed procedure was shown in the Support Information.

4.4 Result and Discussion

4.4.1 Sampling solvent selection

Previous studies utilized both acetone and benzophenone as the PB reagents in studies of unsaturated lipids in bulk samples.[28, 29] Acetone and acetonitrile are common organic solvents generally used to prepare lysate. Thus, acetone and benzophenone solution (5 mM in acetonitrile) were selected in the current studies to induce cell lysis and PB reactions. Because a small amount of PBS is inevitably drawn into the micropipette needle during single-cell sampling, a dilution of cell lysis solution can occur, potentially resulting in reduced cell lysis efficiency. For example, our previous studies show that acetonitrile can induce rapid cell lysis (< 15 s) when its concentration is >80 %, whereas lower concentrations result in slower lysis processes.[34] Thus, we prepared cell lysis solutions using acetone and acetonitrile without adding other solvents commonly used in MS studies such as water and methanol. Because benzophenone concentration can affect the yield of products from the PB reactions,[29] we prepared a series of acetonitrile solutions containing benzophenone (i.e., 0.5, 2.0, 5.0, and 10.0 mM) to optimize the PB reaction conditions in SCMS studies. Our experiments indicated that PB products were not observed using 0.5 and 2 mM benzophenone solutions. Although both 5 and 10 mM benzophenone induced PB reactions, the later one generated more undesired side

products. Thus, 5 mM benzophenone was selected as the optimum concentration for both the regular and reactive SCMS experiments. To generate PB products in the reactive SCMS experiments, UV irradiation (~15 minutes) was necessary for both PB reagents. Relatively abundant ions (e.g., intensity > 10^4) were selected for MS/MS analysis.

4.4.2 Characterization of the micropipette needle

To evaluate the sensitivity of the micropipette needle, we measured the limit of detection (LOD) of a number of standard compounds relevant to our studies. The LODs were determined as 1.0, 0.1, and 0.1 pM, for irinotecan, verapamil, and a phosphatidylcholine (PC (16:0/18:1)), respectively, which are comparable with the results obtained using standard nano-ESI source (Table S4-1). [34, 46]

4.4.3 Workflow of data analysis

To efficiently analyze the experimental data, we wrote two different Python scripts to determine the locations of C=C bonds in lipids through three steps: screening the potential lipids and their corresponding PB products, predicting the fragmentation of PB products, and identifying C=C bonds in lipids. First, we screened the potential lipids and their corresponding PB products using the Script A, as shown in Figure S4-1. Briefly, relatively abundant ions (intensity > 10^4) were retained from SCMS data in both the “regular” (without UV irradiation) and “reactive” (15-min UV irradiation) groups. Script A was used to search for the *m/z* values with a mass difference of 58.0418 (using acetone reagent) or 182.0731 (using benzophenone reagent) between the “regular” and “reactive” groups ($(m/z)_{reactive}$ - $(m/z)_{regular}$ = 58.0418 or 182.0731, within 20 ppm), and to generate a list of *m/z* pairs. In each *m/z* pair, the $(m/z)_{regular}$ was regarded as a candidate of a potential lipid, whereas the $(m/z)_{reactive}$ was considered as the candidate of the corresponding PB product.

Then, METLIN [55] was used to find all potential lipids for each (m/z)regular, whereas those (m/z)regular values that cannot be found in METLIN were re-moved from the list along with their corresponding (m/z)reactive. An updated list of m/z pairs with potential identifications was then generated, and MS/MS experiments were conducted for ions in this list (intensity > 104). Second, we predicted the diagnostic fragments of all potential PB products obtained from the previous step using the Script B (Figure S4-2). All featured fragments (i.e., m/z values) representing the head groups, tails, and adducts (i.e., H+, Na+, and K+) of each PB product were predicted according to the potential lipids generated from METLIN database searching. Last, we determined locations of C=C bonds in unsaturated lipids by comparing the predicted fragments in the second step and experimental MS/MS spectra, which were measured from selected ions using both CID (for diagnostic ions) and HCD (for lipids head groups) modes.

According to the METLIN database searching, all lipids detected in our experiments potentially belong to phospholipids. Phospholipids contain two fatty acid tails and a hydrophilic head with a phosphate group. For ions with the same *m/z* value, differences in these two fatty acid tails can generate multiple lipid isomers that can produce the same diagenetic ions in MS/MS (Table S4-2). To further elucidate the structure of each fatty acid tail, SCMS experiments were also conducted in the negative ion mode, in which ammonium acetate (10 mM) was added in the solvent to enhance the ion intensities. Acetate adducts of phospholipids were detected, and their fragments were used to determine the fatty acid chains in these phospholipids[28] (Figure S4-3).

4.4.4 Determination of C=C bond locations in unsaturated lipids of single cells

Determining the exact structures of large numbers of unsaturated lipids in single cells is challenging due to multiple factors, including extremely complex compositions of cellular

Table 4-1. ***Analysis of unsaturated lipids in single cells.***

Ion mod	[1](*m/z*)Exp	[2](*m/z*)Cal	[3]Error (ppm	[4]Reagent	[5](*m/z*)Prod	Identified lipids	Diagnostic ions (*m/z*)
+	760.5899	760.5856	5.7	Ph2CO	942.6542	PC (16:0/18:1 (9))*	650.4362, 800.5195
+	760.5821	760.5856	-4.6	ACE	818.6579	PC (16:0/18:1 (9))*	650.4359, 676.4872
+	732.5506	732.5543	-5.1	ACE	790.5902	PC (16:0/16:1 (9))*	650.4357, 676.4882
+	729.5892	729.5910	-2.5	ACE	787.6395	SM(d18:1/18:1(9))*	645.4260,729.3963
+	756.5475	756.5500	-3.3	ACE	814.5931	PC (16:1(7)/18:2(9,12))*	646.6411, 672.4830, 728.5173
+	780.5482	780.5543	-7.8	ACE	838.5899	PC (16:1(9)/20:4(5,8,11,14))*	712.5525, 714.5693, 738.8998, 780.4312
+	784.5746	784.5855	-13.9	ACE	842.6530	PC (16:0/20:3(11,14,17))*	700.4511, 728.4319, 784.4609
+	786.5971	786.6012	-5.2	ACE	844.7043	PC (18:1(15)/18:1(15))*	660.4500, 662.4649, 786.4759
+	787.6745	787.6693	6.6	ACE	845.6319	SM(d16:1/24:0)	661.462
+	782.5654	782.5699	-5.8	ACE	840.6057	PC (16:0/18:1 (9))*	656.5559, 672.4178, 698.4372, 782.5636
+	754.5334	754.5387	-7.0	ACE	812.5792	PC (14:0/20:4(5,8,11,14))*	566.3104, 628.5224, 644.4230, 687.4790, 728.6622, 754.4146
+	810.5944	810.6012	-8.5	ACE	868.6410	PC (16:0/18:4(9,11,13,15))*	700.4489,726.5560,756.5484, 782.5640
-	253.2162	253.2173	-4.3	Ph_2CO	435.1712	FA (16:1 (9))	171.1232
-	281.2485	281.2486	-0.4	Ph_2CO	463.3290	FA (18:1 (9))	171.3439, 321.0381
-	253.2174	253.2173	0.4	ACE	311.1686	FA (16:1 (9))	197.0279
-	281.2495	281.2486	3.2	ACE	339.1998	FA (18:1 (9))	197.0279

[1]m/z measured in experiments; [2]m/z from calculations; [3]mass error between measured and calculated values; [4]PB reagents include Ph2CO (benzophenone) and ACE (acetone); [5]PB products of lipids; *species determined as multiple unsaturated lipids. Details are shown in the Support Information Table S5-12, and S14-16.

species, small sample amounts, and the lack of complete structure information of all lipids in the current database. Nevertheless, our technique can be used as an analytical tool to identify structures or confine the detected species to limited numbers of isomers. We conducted comprehensive data analysis and tentatively determined 16 unsaturated lipids at the single-cell level in the current study (Table 4-1). Among them, PB products of three ions (m/z 760.5821, 253.2162, and 281.2485) were detected using both acetone and benzo-phenone as the reagents, whereas the rest species were only observed using acetone in the experiment. The presence of benzophenone (5 mM) likely affected the detection sensitivity of lipids (Figure S4). Our results may indicate that acetone is a more effective PB reagent to identify lipids C=C bond at the single-cell level.

Here, we presented an example, in which *m/z* 760.5821 was identified as PC (16:0/18:1(9)), with details to illustrate the workflow of locating C=C bonds in unsaturated lipids through comprehensive data analysis. First, we obtained all potential species with the *m/z* of 760.5821 ($(m/z)_{regular}$ = 760.5821). This peak is commonly detected in the regular SCMS experiment, and its potential PB adducts with acetone ($(m/z)_{reactive}$ 818.6579) and benzophenone ($(m/z)_{reactive}$ 942.6542) were extracted from experimental data using the Script A (Figure S4-1). We then searched for the potential species with the *m/z* of 760.5821 obtained from METLIN searching and discovered that among all 36 potential lipids, 20 of them are phosphatidylcholines (PCs) and the rest 16 species are phosphatidylethanolamines (PEs) (Table S4-3). Second, the structure identification of lipids and corresponding PB products was performed based on their MS/MS fragments. The MS/MS spectra of *m/z* 760.5821 in both HCD and CID modes are shown in Figures S4-5B and S4-5D. Because *m/z* 184.0724 is the head group of PC or sphingomyelin (SM),

[56, 57] we excluded PEs from the list of potential candidates (Table S4-3). We then used the Script B to predict the featured fragments of the potential PB products based on the type of lipids, and results were listed in Table S4-2. Last, we determined the position of the C=C bond in the unsaturated lipid. The comparison between the experimental MS/MS of *m/z* 818.6579 and the predicted list led to the discovery of diagnostic ion pairs of *m/z* 650.4359 and *m/z* 676.4872 (i.e., ∆26) using acetone as the PB reagent (Figure 4-5A, Table S4-2).[28] However, five lipids (Table S4-2) can generate the same diagnostic ion pair (*m/z* 650/676). To narrow down the potential candidates, we performed MS/MS analysis of *m/z* 818.59 (acetate adduct of *m/z* 760.5821) in the negative mode and determined the fatty acid tails of m/z 760.5821 (Table S4-4). Combining all the above results, the ion m/z 760.5821 was identified as PC (16:0/18:1(9)) (Table S4-5). This identification was further confirmed by comparing its MS/MS fragments with those obtained from standard compound PC (16:0/18:1(9)) measured in our experiments (Figure S4-5).

As illustrated in Figure 4-4, the PB products at one C=C bond can produce a pair of diagnostic ions during fragmentation. In our experiments, nine different peaks of the PB products (Table S4-5 to S4-13) generated one or two pairs of diagnostic ions, with a mass difference of ∆26 (acetone) or ∆150 (150.0836, benzophenone[29]), in MS/MS analysis (Figures 4-5, S4-6, and S4-7). The production of two pairs of diagnostic ions likely due to the coexistence of isomeric lipids with C=C bond at different locations. For example, MS/MS experiment of *m/z* 868.6410 (the acetone PB product of *m/z* 810.5944) produced two pairs of diagnostic ions with a mass difference of ∆26: *m/z* 700.4489/726.5560 and 756.5484/782.5640 (Figure S4-6B). Previous studies found that a featured ion *m/z*

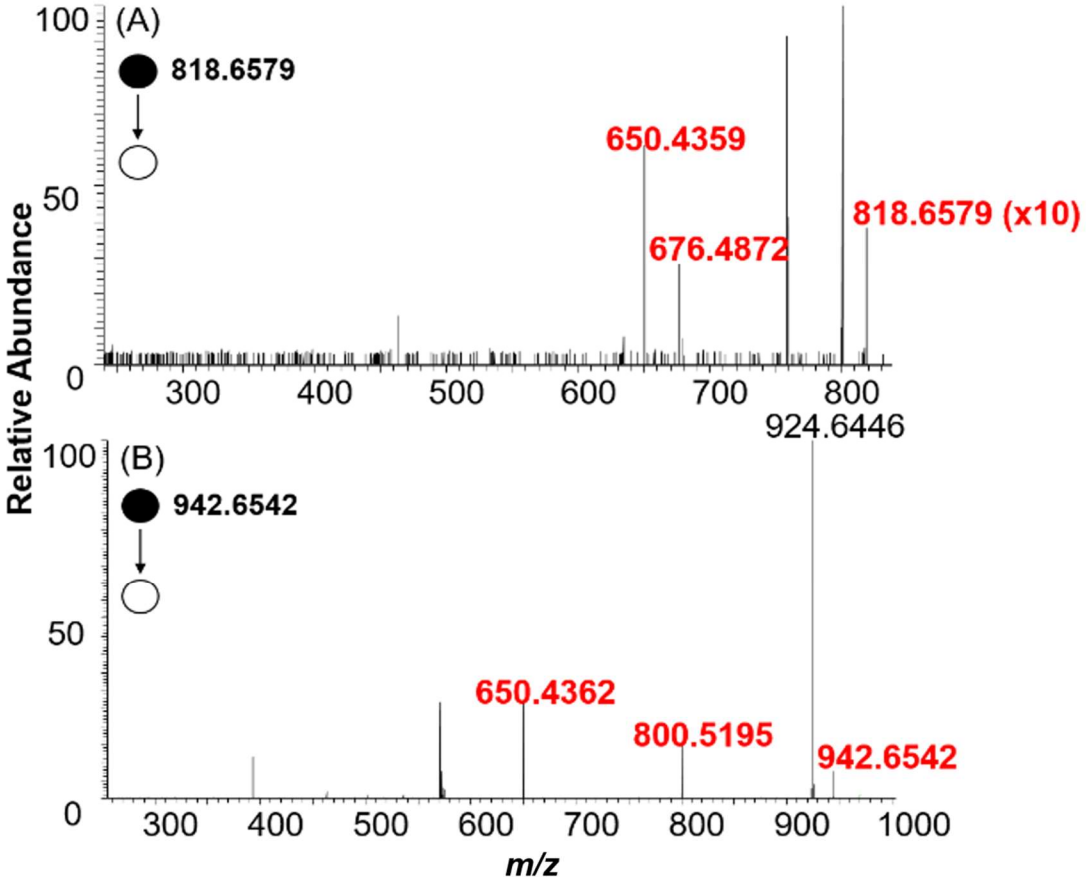


Figure 4-5. *(A) MS/MS spectra of PB product of m/z 760.5899 (m/z 818.6579) using acetone as the PB reagent detected at single-cell level. Ions labeled in red font are diagnostic ions (m/z 650.4359 and m/z 676.4872). (B) MS/MS spectra of the PB product of m/z 760.5821 (m/z 942.6542) using benzophenone as the PB reagent detected from a single cell. Ions labeled in red font are diagnostic ions (m/z 650.4362 and m/z 800.5195).*

146.9807 was produced from the head-groups of sodiated PCs, SMs, or PEs in CID.[58, 59] MS/MS spectra of the corresponding lipid(s) (*m/z* 810.5944) in the regular SCMS experiment also contained the peak of *m/z* 146.9807 (Figure S4-6A), supporting the prediction that the ion *m/z* 810.5944 belongs to one or multiple Na^+ adducts of PCs, SMs, or PEs. By searching for the potential species in METLIN database, we were able to

exclude SMs and PEs from the list while keeping the rest PCs as potential candidates. Using the Script B, we predicted the diagnostic ions of the PB products of all potential PCs (Table S4-6) and compared with experimental observation (Figure S4-6B), in which two pairs of diagnostic ions (*m/z* 700.4489/726.5560 and 756.5484/782.5640) were detected. Because all potential PCs acquired from METLIN contain only one C=C bond, our results may indicate the coexistence of isomers with different locations of a C=C bond. Combining the results from PB reactions (positive ion mode) and information of fatty acid tails (negative ion mode, Table S4-4), these potential isomers were determined as seven unsaturated PCs as listed in Table S4-6: PC (16:0/20:1(11)), PC (18:0/18:1(13)), PC (18:0/18:1(9)), PC (18:1(9)/18:0), PC (20:1(11)/16:0), PC (14:0/22:1(13)), and PC (14:1(9)/22:0).

Interestingly, our experimental results indicate that the relative signal intensities of two diagnostic ions in a pair are different: more than half of the aldehyde ions are more abundant than the alkene ions. These differences are likely attributed to the relatively higher abundances of Isomer I than Isomer II produced in the PB reactions. Similar results have been reported in previous studies of bulk samples.[28] In addition to paired diagnostic ions, we observed that the PB products of four lipids (*m/z* 814.5931, 838.5899, 840.6057, and 812.5792) produced unpaired diagnostic ions (Tables S4-9 to S4-12). This is likely due to the relatively low concentrations of these lipids in single cells, and the abundances of their PB products were insufficient to produce detectable diagnostic ion pairs. The rest seven lipids PB products (*m/z* 787.6395, 842.6530, 844.7043, 845.6319, 435.1712 (negative mode), 311.1686 (negative mode) and 339.1998 (negative mode)) also produced unpaired diagnostic ions. We totally analyzed 17 and nine single cells in the

positive and negative ion modes, respectively. The results of these ions are summarized in Tables S4-14 to S4-20, and MS/MS spectra of these PB products and their corresponding lipids are shown in Figure S4-8.

4.4.5 Comparison studies of cell lysates and single cells

Lipidomics studies are generally conducted using lysates prepared from bulk biological samples (e.g., populations of cells, tissues, and plasma extraction) through multiple steps (e.g., cell lysis, centrifuging, supernatant transfer, drying, and reconcentration), which may affect their molecular compositions due to the potential variance of sample preparation protocols[1]. In contrast, entire cellular contents from individual cells are retained in our SCMS experiments, minimizing the influence of sample preparation variance on composition analysis.[42] To evaluate the difference between these two approaches to the identification of the C=C bond, we conducted MS measurements of cell lysates and compared the results with those obtained at the single-cell level. Cell lysates were prepared and loaded into the micropipette needle for MS analysis, and data were collected before (no UV) and after the PB reactions (after 15 min of UV irradiation). Data analysis was performed using the same procedures as those used to process single cell results (see details in the Supporting Information). In general, MS/MS spectra of PB products obtained from the cell lysates were more complex than those from single cells (Figures S4-9 and S4-10), likely due to larger amounts of cellular contents in cell lysates. On the other hand, more cellular contents allowed for the analysis of additional PB products, including those with relatively lower abundances. For example, *m/z* 790.5902 (the PB product of *m/z* 732.5506) produced two pairs of diagnostic ions with a difference of *m/z* 26 (*m/z* 650.4354/676.4868 and 622.4042/648.4544) using cell lysate (Figure S4-

9B, Table S4-21), whereas only one pair of diagnostic ions (*m/z* 650.4357/676.4882) were detected from single cells. According to MS/MS spectra (Figure S4-9A) and METLIN database, the PB product *m/z* 732.5506 was produced from PCs containing one C=C bond, indicating that the peak detected in single cells is attributed to multiple isomers. Therefore, traditional MS analysis of lysate can provide complementary information for single cell studies. Similar analyses of other ions using both cell lysates and single cells were conducted, as summarized in Table S4-22 and Figure S4-10.

Although enhanced ion signal intensities were obtained from cell lysates, larger amounts of cellular contents resulted in more undesired products from PB side reactions. Previous studies indicate that abundant lipids can react with PB reagents to generate side products, which may have very similar *m/z* values as the regular PB products or induce the retro-PB reactions, i.e., decomposition of PB products back into reactants in CID[28, 33], resulting in interference for C=C bond analysis.[28, 60] For example, paired diagnostic ions in CID analysis of both *m/z* 868.6410 and 838.5899 were not observed using cell lysate, but they were detected at the single-cell level, providing structure information for C=C bond analysis (Tables S4-6 and S4-11, Figures S4-6 and S4-7D).

4.5 Conclusion

We report a simple SCMS analysis device, the micropipette needle, that can accommodate PB reactions to deter-mine C=C bond positions in unsaturated lipids at the single-cell level. HCT-116 cell line was used as a model, and individual cells were drawn into a micropipette needle to induce rapid cell lysis after mixing with acetone or acetonitrile solution containing benzophenone. To determine C=C bond loca-tions in unsaturated lipids, the micropipette needle was then used a nano-ESI emitter and coupled to a mass

spectrometer to conduct both regular and reactive SCMS analyses of the same single cell. The regular SCMS measurement provided molecular analysis of single-cell lysate without PB reactions. When conducting a reactive SCMS experiment, the lysis solution also played the role of the PB reagent by reacting with unsaturated lipids at C=C bonds under UV irradiation. Python scripts were used to analyze data obtained from both regular and reactive SCMS experiments to screen potential lipids and their corresponding PB products. Assisted by MS/MS analysis of candidate PB product ions, C=C bond locations were determined to identify unsaturated lipids at the single-cell level. Experiments were conducted in both positive and negative ion modes to obtain comprehensive structure information. Comparative studies between cell lysates and single cells were performed, and we found that bulk sample analysis can provide complementary information for single-cell studies. However, limited by a number of factors (e.g., complex compositions of cellular contents with limited amounts, lack of separation, and requirement of abundant PB product ions for MS/MS analysis), our current method is more effective for structure identification of unsaturated lipids and fatty acids with relatively high abundances and simple structures (e.g., with one or two C=C bonds). In addition, to generate abundant PB products, the throughput of reactive SCMS is primarily restricted by the time (15 min) needed for UV irradiation. The reaction time can likely be shorten using micropipette needles produced from thin-wall glass capillaries or other materials with higher UV transmission (e.g., quartz). Although a common cancer cell line was used as a model system in the current proof-of-concept studies, other systems (e.g., rare cells and heterogeneous cells) can be studied using this technique to answer specific biological questions that are intractable from bulk analysis. In addition, our techniques can be

potentially used for broad ranges of reactive SCMS studies, in which other chemical reactions can be utilized to enhance the molecular analysis of single cells or trace amounts of biological samples.

Reference

1. Altschuler, S. J.; Wu, L. F., Cellular heterogeneity: do differences make a difference? *Cell* 2010, *141* (4), 559-563.
2. McNaught, A. D.; Wilkinson, A., *Compendium of chemical terminology*. Blackwell Science Oxford: 1997; Vol. 1669.
3. Bailwad, S. A.; Singh, N.; Jani, D. R.; Patil, P.; Singh, M.; Deep, G.; Singh, S., Alterations in serum lipid profile patterns in oral cancer: correlation with histological grading and tobacco abuse. *Oral Health Dent Manag* 2014, *13* (3), 573-9.
4. Fahy, E.; Subramaniam, S.; Brown, H. A.; Glass, C. K.; Merrill Jr, A. H.; Murphy, R. C.; Raetz, C. R.; Russell, D. W.; Seyama, Y.; Shaw, W., A comprehensive classification system for lipids. *European journal of lipid science and technology* 2005, *107* (5), 337-364.
5. Fahy, E.; Cotter, D.; Sud, M.; Subramaniam, S., Lipid classification, structures and tools. *Biochimica et Biophysica Acta (BBA)-Molecular and Cell Biology of Lipids* 2011, *1811* (11), 637-647.
6. Morrison, R., Soil lipids. In *Organic geochemistry*, Springer: 1969; pp 558-575.
7. Ouellette, R. J.; Rawn, J. D., *Organic chemistry: structure, mechanism, and synthesis*. Elsevier: 2014.
8. Choi, M.-K.; Song, I.-S., Recent advances in the formulation of sphingolipid anticancer therapeutics. *Journal of Pharmaceutical Investigation* 2020, 1-13.
9. Jensen-Urstad, A. P.; Semenkovich, C. F., Fatty acid synthase and liver triglyceride metabolism: housekeeper or messenger? *Biochimica et Biophysica Acta (BBA)-Molecular and Cell Biology of Lipids* 2012, *1821* (5), 747-753.
10. Wertz, P. In *Epidermal lipids*, Seminars in dermatology, 1992; pp 106-113.
11. Wymann, M. P.; Schneiter, R., Lipid signalling in disease. *Nature reviews Molecular cell biology* 2008, *9* (2), 162-176.
12. Sun, M.; Yang, Z., Metabolomic Studies of Live Single Cancer Stem Cells Using Mass Spectrometry. *Anal. Chem.* 2018, *91* (3), 2384-2391.
13. Li, J.; Condello, S.; Thomes-Pepin, J.; Ma, X.; Xia, Y.; Hurley, T. D.; Matei, D.; Cheng, J.-X., Lipid desaturation is a metabolic marker and therapeutic target of ovarian cancer stem cells. *Cell stem cell* 2017, *20* (3), 303-314. e5.
14. Mukherjee, A.; Kenny, H. A.; Lengyel, E., Unsaturated fatty acids maintain cancer cell stemness. *Cell stem cell* 2017, *20* (3), 291-292.
15. Tirinato, L.; Pagliari, F.; Limongi, T.; Marini, M.; Falqui, A.; Seco, J.; Candeloro, P.; Liberale, C.; Di Fabrizio, E., An overview of lipid droplets in cancer and cancer stem cells. *Stem Cells Int.* 2017, *2017*, 1656053.
16. Murata, N.; Wada, H., Acyl-lipid desaturases and their importance in the tolerance and acclimatization to cold of cyanobacteria. *Biochem. J.* 1995, *308* (Pt 1), 1-8.
17. Cybulski, L. E.; Del Solar, G.; Craig, P. O.; Espinosa, M.; De Mendoza, D., Bacillus subtilis DesR functions as a phosphorylation-activated switch to control membrane lipid fluidity. *J. Biol. Chem.* 2004, *279* (38), 39340-39347.
18. Antonny, B.; Vanni, S.; Shindou, H.; Ferreira, T., From zero to six double bonds: phospholipid unsaturation and organelle function. *Trends Cell Biol.* 2015, *25* (7), 427-436.

19. Lesa, G. M.; Palfreyman, M.; Hall, D. H.; Clandinin, M. T.; Rudolph, C.; Jorgensen, E. M.; Schiavo, G., Long chain polyunsaturated fatty acids are required for efficient neurotransmission in C. elegans. *J. Cell Sci.* 2003, *116* (24), 4965-4975.
20. Ting, H.-C.; Chen, L.-T.; Chen, J.-Y.; Huang, Y.-L.; Xin, R.-C.; Chan, J.-F.; Hsu, Y.-H. H., Double bonds of unsaturated fatty acids differentially regulate mitochondrial cardiolipin remodeling. *Lipids Health Dis.* 2019, *18* (1), 53.
21. Kelley, N. S.; Hubbard, N. E.; Erickson, K. L., Conjugated linoleic acid isomers and cancer. *Nutr. J.* 2007, *137* (12), 2599-2607.
22. Hrelia, S.; Biagi, P. L.; Lorenzini, A.; Jimenez, J. A. L.; Horrobin, D. F.; Bordoni, A., Essential fatty acid metabolism in cardiomyocytes grown in media enriched with different N-6/N-3 fatty acid combinations. *IUBMB Life* 1997, *41* (2), 423-430.
23. Hu, T.; Zhang, J. L., Mass-spectrometry-based lipidomics. *J. Sep. Sci.* 2018, *41* (1), 351-372.
24. Köfeler, H. C.; Fauland, A.; Rechberger, G. N.; Trötzmüller, M., Mass spectrometry based lipidomics: an overview of technological platforms. *Metabolites* 2012, *2* (1), 19-38.
25. Han, X.; Yang, K.; Gross, R. W., Multi-dimensional mass spectrometry-based shotgun lipidomics and novel strategies for lipidomic analyses. *Mass Spectrom. Rev.* 2012, *31* (1), 134-178.
26. Quehenberger, O.; Armando, A. M.; Brown, A. H.; Milne, S. B.; Myers, D. S.; Merrill, A. H.; Bandyopadhyay, S.; Jones, K. N.; Kelly, S.; Shaner, R. L., Lipidomics reveals a remarkable diversity of lipids in human plasma. *J. Lipid Res.* 2010, *51* (11), 3299-3305.
27. Andreyev, A. Y.; Fahy, E.; Guan, Z.; Kelly, S.; Li, X.; McDonald, J. G.; Milne, S.; Myers, D.; Park, H.; Ryan, A., Subcellular organelle lipidomics in TLR-4-activated macrophages. *J. Lipid Res.* 2010, *51* (9), 2785-2797.
28. Ma, X.; Chong, L.; Tian, R.; Shi, R.; Hu, T. Y.; Ouyang, Z.; Xia, Y., Identification and quantitation of lipid C= C location isomers: A shotgun lipidomics approach enabled by photochemical reaction. *Proc. Natl. Acad. Sci.* 2016, *113* (10), 2573-2578.
29. Xu, T.; Pi, Z.; Song, F.; Liu, S.; Liu, Z., Benzophenone used as the photochemical reagent for pinpointing C= C locations in unsaturated lipids through shotgun and liquid chromatography-mass spectrometry approaches. *Anal. Chim. Acta* 2018, *1028*, 32-44.
30. Ma, X.; Zhao, X.; Li, J.; Zhang, W.; Cheng, J.-X.; Ouyang, Z.; Xia, Y., Photochemical tagging for quantitation of unsaturated fatty acids by mass spectrometry. *Anal. Chem.* 2016, *88* (18), 8931-8935.
31. Thomas, M. C.; Mitchell, T. W.; Harman, D. G.; Deeley, J. M.; Nealon, J. R.; Blanksby, S. J., Ozone-induced dissociation: Elucidation of double bond position within mass-selected lipid ions. *Anal. Chem.* 2008, *80* (1), 303-311.
32. Feng, Y.; Chen, B.; Yu, Q.; Li, L., Identification of double bond position isomers in unsaturated lipids by m-CPBA epoxidation and mass spectrometry fragmentation. *Anal. Chem.* 2019, *91* (3), 1791-1795.
33. Ma, X.; Xia, Y., Pinpointing double bonds in lipids by Paternò-Büchi reactions and mass spectrometry. *Angew Chem. Int. Ed.* 2014, *53* (10), 2592-2596.
34. Zhu, Y.; Liu, R.; Yang, Z., Redesigning the T-probe for Mass Spectrometry Analysis of Online Lysis of Non-adherent Single Cells. *Anal. Chim. Acta* 2019, *1084*, 53-59.
35. Yang, Y.; Huang, Y.; Wu, J.; Liu, N.; Deng, J.; Luan, T., Single-cell analysis by ambient mass spectrometry. *Trends Anal. Chem.* 2017, *90*, 14-26.

36. Sun, M.; Yang, Z.; Wawrik, B., Metabolomic fingerprints of individual algal cells using the single-probe mass spectrometry technique. *Front. Plant Sci.* **2018,** *9*, 571.
37. Duncan, K. D.; Fyrestam, J.; Lanekoff, I., Advances in mass spectrometry based single-cell metabolomics. *Analyst* **2019,** *144* (3), 782-793.
38. Dueñas, M. E.; Essner, J. J.; Lee, Y. J., 3D MALDI mass spectrometry imaging of a single cell: spatial mapping of lipids in the embryonic development of zebrafish. *Sci. Rep.* **2017,** *7* (1), 14946.
39. Tsuyama, N.; Mizuno, H.; Tokunaga, E.; Masujima, T., Live single-cell molecular analysis by video-mass spectrometry. *Anal. Sci.* **2008,** *24* (5), 559-561.
40. Zhu, H.; Zou, G.; Wang, N.; Zhuang, M.; Xiong, W.; Huang, G., Single-neuron identification of chemical constituents, physiological changes, and metabolism using mass spectrometry. *Proc. Natl. Acad. Sci.* **2017,** *114* (10), 2586-2591.
41. Gong, X.; Zhao, Y.; Cai, S.; Fu, S.; Yang, C.; Zhang, S.; Zhang, X., Single cell analysis with probe ESI-mass spectrometry: detection of metabolites at cellular and subcellular levels. *Anal. Chem.* **2014,** *86* (8), 3809-3816.
42. Pan, N.; Rao, W.; Kothapalli, N. R.; Liu, R.; Burgett, A. W.; Yang, Z., The single-probe: a miniaturized multifunctional device for single cell mass spectrometry analysis. *Anal. Chem.* **2014,** *86* (19), 9376-9380.
43. Rao, W.; Pan, N.; Yang, Z., Applications of the single-probe: mass spectrometry imaging and single cell analysis under ambient conditions. *J. Vis. Exp.* **2016,** (112), e53911.
44. Sun, M.; Yang, Z.; Wawrik, B., Metabolomic fingerprints of individual algal cells using the single-probe mass spectrometry technique. *Frontiers in Plant Science* **2018,** *9*, 571.
45. Liu, R.; Zhang, G.; Yang, Z., Towards rapid prediction of drug-resistant cancer cell phenotypes: single cell mass spectrometry combined with machine learning. *Chem. Commun.* **2019,** *55* (5), 616-619.
46. Liu, R.; Pan, N.; Zhu, Y.; Yang, Z., T-probe: An integrated microscale device for online in situ single cell analysis and metabolic profiling using mass spectrometry. *Anal. Chem.* **2018,** *90* (18), 11078-11085.
47. Katz, B.-Z.; Zamir, E.; Bershadsky, A.; Kam, Z.; Yamada, K. M.; Geiger, B., Physical state of the extracellular matrix regulates the structure and molecular composition of cell-matrix adhesions. *Mol. Biol. Cell* **2000,** *11* (3), 1047-1060.
48. Bandura, D. R.; Baranov, V. I.; Ornatsky, O. I.; Antonov, A.; Kinach, R.; Lou, X.; Pavlov, S.; Vorobiev, S.; Dick, J. E.; Tanner, S. D., Mass cytometry: technique for real time single cell multitarget immunoassay based on inductively coupled plasma time-of-flight mass spectrometry. *Anal. Chem.* **2009,** *81* (16), 6813-6822.
49. Chen, F.; Lin, L.; Zhang, J.; He, Z.; Uchiyama, K.; Lin, J.-M., Single-cell analysis using drop-on-demand inkjet printing and probe electrospray ionization mass spectrometry. *Anal. Chem.* **2016,** *88* (8), 4354-4360.
50. Passarelli, M. K.; Newman, C. F.; Marshall, P. S.; West, A.; Gilmore, I. S.; Bunch, J.; Alexander, M. R.; Dollery, C. T., Single-cell analysis: visualizing pharmaceutical and metabolite uptake in cells with label-free 3D mass spectrometry imaging. *Anal. Chem.* **2015,** *87* (13), 6696-6702.
51. Mao, S.; Zhang, W.; Huang, Q.; Khan, M.; Li, H.; Uchiyama, K.; Lin, J. M., In Situ Scatheless Cell Detachment Reveals Correlation between Adhesion Strength and Viability at Single - Cell Resolution. *Angew Chem. Int. Ed.* **2018,** *57* (1), 236-240.

52. Standke, S. J.; Colby, D. H.; Bensen, R. C.; Burgett, A. W.; Yang, Z., Mass Spectrometry Measurement of Single Suspended Cells Using a Combined Cell Manipulation System and a Single-Probe Device. *Anal. Chem.* 2019, *91* (3), 1738-1742.
53. Stinson, C. A.; Xia, Y., A method of coupling the Paternò–Büchi reaction with direct infusion ESI-MS/MS for locating the C [double bond, length as m-dash] C bond in glycerophospholipids. *Analyst* 2016, *141* (12), 3696-3704.
54. Floch, J., A simple method for the isolation and purification of total lipids from animal tissues. *J. biol. Chem.* 1957, *226*, 497-509.
55. Smith, C. A.; O'Maille, G.; Want, E. J.; Qin, C.; Trauger, S. A.; Brandon, T. R.; Custodio, D. E.; Abagyan, R.; Siuzdak, G., METLIN: a metabolite mass spectral database. *Ther. Drug Monit.* 2005, *27* (6), 747-751.
56. Karnezis, T.; Fisher, H. C.; Neumann, G. M.; Stone, B. A.; Stanisich, V. A., Cloning and characterization of the phosphatidylserine synthase gene of Agrobacterium sp. strain ATCC 31749 and effect of its inactivation on production of high-molecular-mass (1⟶3)-β-d-glucan (curdlan). *J. bacteriol.* 2002, *184* (15), 4114-4123.
57. Brügger, B.; Erben, G.; Sandhoff, R.; Wieland, F. T.; Lehmann, W. D., Quantitative analysis of biological membrane lipids at the low picomole level by nano-electrospray ionization tandem mass spectrometry. *Proc. Natl. Acad. Sci.* 1997, *94* (6), 2339-2344.
58. Zemski Berry, K. A.; Hankin, J. A.; Barkley, R. M.; Spraggins, J. M.; Caprioli, R. M.; Murphy, R. C., MALDI imaging of lipid biochemistry in tissues by mass spectrometry. *Chem. Rev.* 2011, *111* (10), 6491-6512.
59. Chughtai, K.; Jiang, L.; Greenwood, T. R.; Glunde, K.; Heeren, R. M., Mass spectrometry images acylcarnitines, phosphatidylcholines, and sphingomyelin in MDA-MB-231 breast tumor models. *J. Lipid Res.* 2013, *54* (2), 333-344.
60. Zhang, W.; Zhang, D.; Chen, Q.; Wu, J.; Ouyang, Z.; Xia, Y., Online photochemical derivatization enables comprehensive mass spectrometric analysis of unsaturated phospholipid isomers. *Nat. Commun.* 2019, *10* (1), 79.

Appendix I: Support Information of Chapter 3

Fabrication of the redesigned T-probe

The fabrication process of the redesigned T-probe is based on our earlier publication with major modifications, as shown in Figure S3-1.

(1) Preparation of the fused silica capillaries. The same size of fused silica capillary (O.D. 150 μm, I.D. 75 μm; Polymicro Technologies, Phoenix, AZ) was used to prepare the solve-providing capillary, the cell sampling probe, and the nano-ESI emitter. Both the sampling probe and the nano-ESI emitter were pulled using the flame to create sharp tips (~ 14 μm), allowing for smooth suction of a whole cell from the sampling tip and maintaining a stable electrospray at the tip of the nano-ESI emitter. The length of the sampling probe is 8 mm, and the nano-ESI emitter is 5.5 cm.

(2) Engraving T-shaped grooves on a PC slide. Similar to the fabrication of the T-probe, a polycarbonate (PC) slide was selected due to its cost-efficiency, safety, and chemical damage resistance.[1] A regular PC slide (75 mm × 25 mm, P11011P, Science Supply Solutions, Elk Grove Village, IL) was graved using a Computer Numeric Control (CNC; CNC 3020, LiYang Welding Equipment Co., Ltd, Shenzhen, China) micro-engraver. An end mill with a small size (diameter = 0.1 mm) was selected to produce a set of T-shaped grooves with uniform sizes (width ~150 μm, and depth ~130 μm) on the surface. The T-shaped grooves were used to retain the positions of those three capillaries in the following steps.

(3) Salinization treatment of PC slides. Two PC slides with identical dimensions (i.e., one pristine and one containing the engraved T-shaped groove) were needed to fabricate a T-probe. Bis [3-(trimethoxysilyl) propyl] amine (Bis-TPA), a salinizing reagent that can increase the surface hydrophilicity of PC slides[2], was used to improve the binding affinity between PC slides. In our fabrication process, 1 % of bis-TPA (Tokyo Chemical Industry Co., LTD, Japan, Tokyo) solution was used to treat both PC slides (i.e., pristine and engraved) for 20 min prior to the probe assembly.

(4) Probe assembly. Three capillaries were carefully embedded in the grooves on a PC slide to form a T-shaped layout. The solvent-providing capillary and nano-ESI emitter were aligned, whereas the sampling probe was vertically positioned at the T-junction. The other Bis-TPA treated PC slide (no grooves) was used to sandwich those three capillaries.

(5) Thermal binding. The sandwiched structure obtained from the previous step was retained using two glass slides, which were clamped using a paper binder. We placed such assembly in an oven at 100 oC for 30 min allowing for the thermal binding process. The probe was harvested after removing the glass slides and then glued on a trapezoidal glass slide for convenient use in the following SCMS experiments.

Cells culture and SCMS sample preparation

In this study, human colon cancer cell line, HCT-116, was chosen as the model system for SCMS experiments using the redesigned T-probe. HCT-116 cells were cultured under standard experimental conditions. When cells reached ~80% confluence in culture plate,

we subcultured them into a 12-well plate containing an autoclaved micro cover glass slide (diameter = 18 mm) in each well using the protocol reported earlier.[3] After overnight incubation (condition of incubation: 5% CO_2, 37 ^oC, humidified) in the incubator (HERAcell, Thermo Scientific), cells were ready for further sample preparation procedures as described in the following.

Before sampling control cells (without irinotecan treatment) or treated cells (treated with 18 μM of irinotecan solution for 45 min), several steps were taken to detach and wash cells. First, attached cells were rinsed with PBS, followed by trypsinization (200 μL of the trypsin-EDTA solution was added in each well). Next, 1.2 mL of McCoy's 5A medium was used to quench trypsinization before sampling. Last, we transferred 50 μL of the cell suspension to a glass slide, which can be used for the following SCMS analysis.

Cell lysis

HCT-116 cell lysate samples were used to verify our findings at the single-cell level. The cell culture procedure and drug treatment conditions used for the preparation of HCT-116 cell lysate samples were identical to those used in the SCMS sample preparation. For the preparation of control cell lysate (without drug treatment), 10 mL of HCT-116 cells in the culture plate (~5.6×10^6 cells) were washed by 5 mL of PBS before 2 mL of trypsin-EDTA solution was added to detach those cells. In parallel, irinotecan treated cells were treated using the same condition as used in the SCMS sample preparation protocol (18 μM, 45 min). Control and treated cells were first washed with PBS, and trypsinization was then quenched by adding 8 mL of culture medium. Afterward, 1.5 mL of cell suspension solution was pipetted into a 2 mL tube and centrifuged (10 min at 13000 rpm) followed by washing with 1 mL of PBS solution for three times. Cell lysis procedure (including both

control and irinotecan treated cells) was performed using a standard protocol.[4] First, cell lysis was conducted using 1 mL of lysis buffer (methanol: chloroform: water = 1:1:1) and vortexed for 10 mins on ice. Next, the sample was centrifuged at 14,000 rpm for 15 min before subjecting the supernatant (aqueous and organic phase, separately) for drying in SpeedVac concentrator (Thermo Scientific, MA). After solvent evaporation, 500 μL of methanol was used to re-dissolve the cell lysate, and 250 μL of the sample was fulfilled into a syringe. Last, we injected the cell lysate sample into MS inlet at the same flow rate (0.5 μL/min) as used in the redesigned T-probe SCMS analysis.

Data pre-treatment

The background includes instrumental noise (i.e., ions with intensity < 10^3) and interfering species detected from the culture medium. Here we developed a customized Python script to eliminate instrumental noise and reduce interfering species (Figure S3). After background subtraction, the intensities of ions were normalized to the total ion chromatogram (TIC), followed by data alignment accomplished using Geena 2 (http://bioinformatics.hsanmartino.it/geena2).[5]

Supporting Tables

Table S3-1. ***Limit of detections (LODs) of standard compounds (nM).***

Compounds	Redesigned T-probe	T-probe[6]	Single probe[7]	Nano-ESI[6]
irinotecan	0.1	0.1	/	0.1
leucine enkephalin	0.1	1	/	0.8
PC (18:1/16:0)	10	10	5	5

Table S3-2. ***Top 30 most abundant metabolites detected in untreated (control) cells at the single-cell level.***

m/z	Tentative Labeling	Adducts	Δppm
198.0962	4-hydroxy Nonenal-d3	$[M + K]^+$	4
199.9951	2-(hydroxyimino)- Pentanedioic acid	$[M + K]^+$	2
203.0538	Theobromine	$[M + Na]^+$	0
221.1662	1-Tridecene	$[M + K]^+$	1
352.0273	Oxine-copper	$[M + H]^+$	1
361.2336	S 1033	$[M + H]^+$	5
365.1078	Ser-His-OH	$[M + H]^+$	3
413.2686	Boviquinone 4	$[M + H]^+$	0
427.2843*	TEI 9647	$[M + H]^+$	0
429.2132	Taraxacolide 1-O-b-D-glucopyranoside	$[M + H]^+$	3
455.3157*	Coenzyme Q4	$[M + H]^+$	0
518.3247	PC (18:3)	$[M + H]^+$	1
546.3563	LysoPC (20:3)	$[M + H]^+$	1
671.5778	CE (20:5)	$[M + H]^+$	2
687.5721	9-HODE cholesteryl este	$[M + Na]^+$	4
780.5559*	PC (36:5)	$[M + H]^+$	2
781.5588	PE-Cer (d40:2)	$[M + K]^+$	4
782.5712*	PC (34:1)	$[M + Na]^+$	2
783.5758	SM (d37:1)	$[M + K]^+$	2
804.5573*	PC (38:7)	$[M + H]^+$	4
806.5723*	PC (38:6)	$[M + H]^+$	3
808.5871*	PC (38:5)	$[M + H]^+$	2
810.6018*	PC (36:1)	$[M + H]^+$	1
811.6073	SM (d39:1)	$[M + K]^+$	2
832.5851*	PC (40:7)	$[M + H]^+$	0
834.6037*	PE (43:6)	$[M + H]^+$	3
840.5781*	PS (40:4)	$[M + H]^+$	4
846.5989	PE (44:7)	$[M + H]^+$	2
847.5244	PG (O-40:6)	$[M + K]^+$	2
874.6309	PE (46:7)	$[M + H]^+$	1

*Identified metabolites through MS/MS analysis either at the single-cell level (through online MS/MS analysis) or at the population level (through nanoESI-MS/MS analysis).

Table S3-3. ***Top 30 most abundant metabolites detected in irinotecan treated cells at the single-cell level.***

m/z	Tentative Labeling	Adducts	Δppm
221.1662	1-Tridecene	$[M + K]^+$	1
365.1078	Ser-His-OH	$[M + H]^+$	3
413.2686	Boviquinone 4	$[M + H]^+$	0
429.2132	Taraxacolide 1-O-b-D-glucopyranoside	$[M + H]^+$	3
503.2029	Myxothiazol Z	$[M + H]^+$	0
518.3247	PC (18:3)	$[M + H]^+$	1
546.3563	LysoPC (20:3)	$[M + H]^+$	1
587.2890*	Irinotecan	$[M + H]^+$	4
609.2708	Irinotecan	$[M + Na]^+$	4
671.5778	CE (20:5)	$[M + H]^+$	2
687.5721	9-HODE cholesteryl este	$[M + Na]^+$	4
729.4094	PG (30:2)	$[M + K]^+$	1
743.4070	PA (37:7)	$[M + K]^+$	2
743.4425	PA (P-38:6)	$[M + K]^+$	1
745.4230	PA (37:6)	$[M + K]^+$	3
765.4199	Avermectin A1a monosaccharide	$[M + Na]^+$	1
775.4149	Angiotensin IV	$[M + H]^+$	1
780.5547*	PC (36:5)	$[M + H]^+$	1
781.5588	PE-Cer (d40:2)	$[M + K]^+$	4
782.5712*	PC (34:1)	$[M + Na]^+$	2
783.5758	SM (d37:1)	$[M + K]^+$	2
785.4177	Ustilagic acid	$[M + H]^+$	1
787.4333	PI (29:2)	$[M + Na]^+$	4
789.4498	PI (29:1)	$[M + Na]^+$	3
804.5573*	PC (38:7)	$[M + H]^+$	4
806.5723*	PC (38:6)	$[M + H]^+$	3
807.4610	PG (36:5)	$[M + K]^+$	4
808.5865*	PC (38:5)	$[M + H]^+$	1
809.4465	Ginsenoside F5	$[M + K]^+$	2
810.6018*	PC (36:1)	$[M + H]^+$	1

*Identified metabolites through MS/MS analysis either at the single-cell level (through online MS/MS analysis) or at the population level (through nanoESI-MS/MS analysis).

Table S3-4. ***Significantly changed cellular metabolites after drug treatment discovered through two-sample t-test.***

m/z	Name	p-value	Regulation
455.1850	Valtratum	0.05	Down
455.3139*	Coenzyme Q4	0.01	Down
457.2560	PG (14:0)	0.01	Down
507.2205	Limonoate	0.05	Down
523.2592	Gallopamil	0.04	Down
525.2623	Hydrocortisone cypionate	0.03	Down
553.3773	3-Hydroxyvecuronium	< 0.01	Down
587.2873*	Irinotecan	< 0.01	Up
780.5551*	PC (36:5)	< 0.01	Down
781.5589	PE-Cer (d40:2)	< 0.01	Up
784.5830*	PC (36:3)	0.01	Down
798.5626	PS (O-38:4)	< 0.01	Up
799.5710	PE-Cer (d40:1)	< 0.01	Up
806.5672*	PC (38:6)	0.01	Down
840.5771*	PS (40:4)	0.04	Up
841.5700	PG (P-39:1)	0.04	Up
843.6431	PG (O-40:0)	< 0.01	Down
862.6230	Galabiosylceramide (d34:1)	< 0.01	Down
863.5810	PG (41:4)	0.02	Down
874.6293	PE (46:7)	< 0.01	Down
877.5700	PG (P-42:4)	0.01	Down
888.6440	PC (44:7)	0.02	Down
955.7187	TG (37:5)	< 0.01	Down
957.7261	TG (37:4)	< 0.01	Down
1091.2790	Acaciabiuronic acid	0.04	Up

*Identified metabolites through MS/MS analysis either at the single-cell level (through online MS/MS analysis) or at the population level (through nanoESI-MS/MS analysis).

Supporting Figures

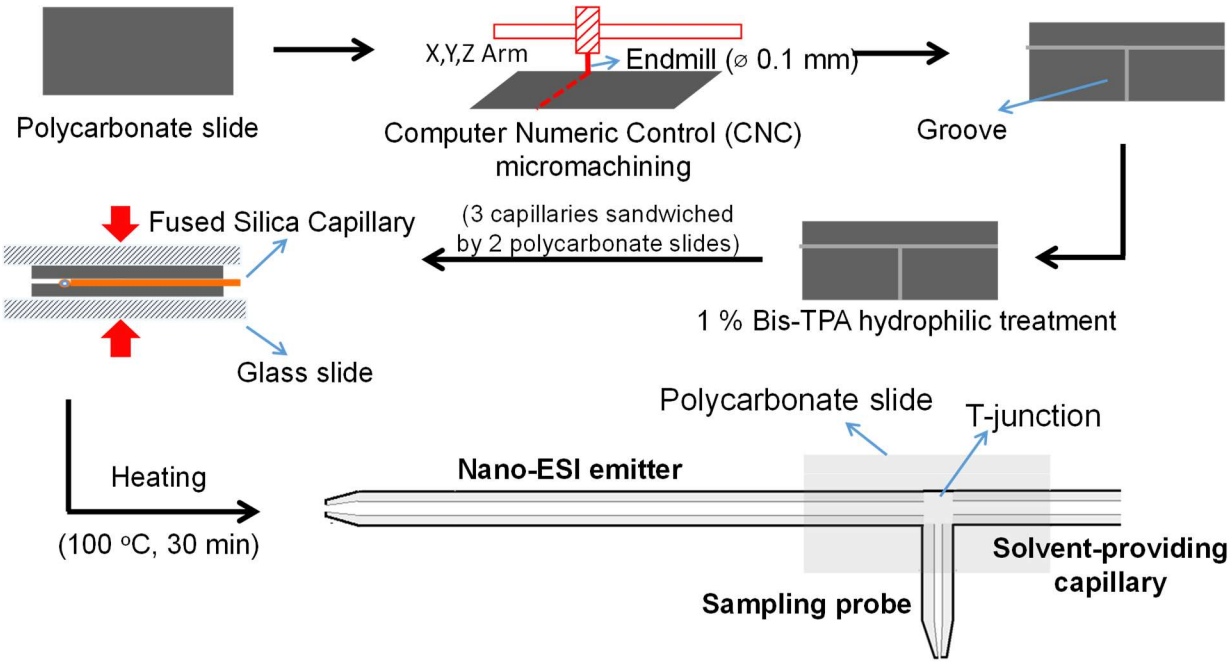


Figure S3-1. *The fabrication workflow of the redesigned T-probe. A Computer Numeric Control (CNC) micromachine was used to engrave a set of T-shaped grooves on one of the polycarbonate (PC) slide. Two PC slides were treated by 1 % Bis [3-(trimethoxysilyl) propyl] amine (Bis-TPA) to increase their binding affinity. Three capillaries were positioned in the T-shaped grooves and followed by the thermal binding process in the oven.*

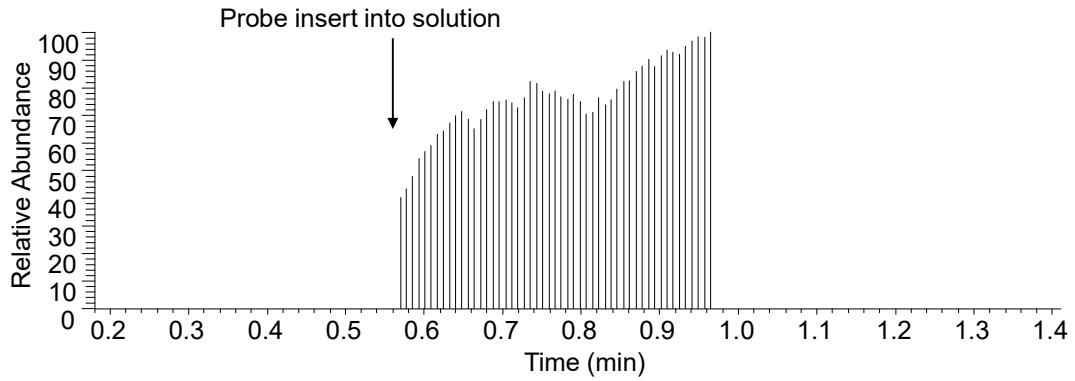


Figure S3-2. *Testing the performance of the redesigned T-probe using the standard leucine enkephalin solution.*

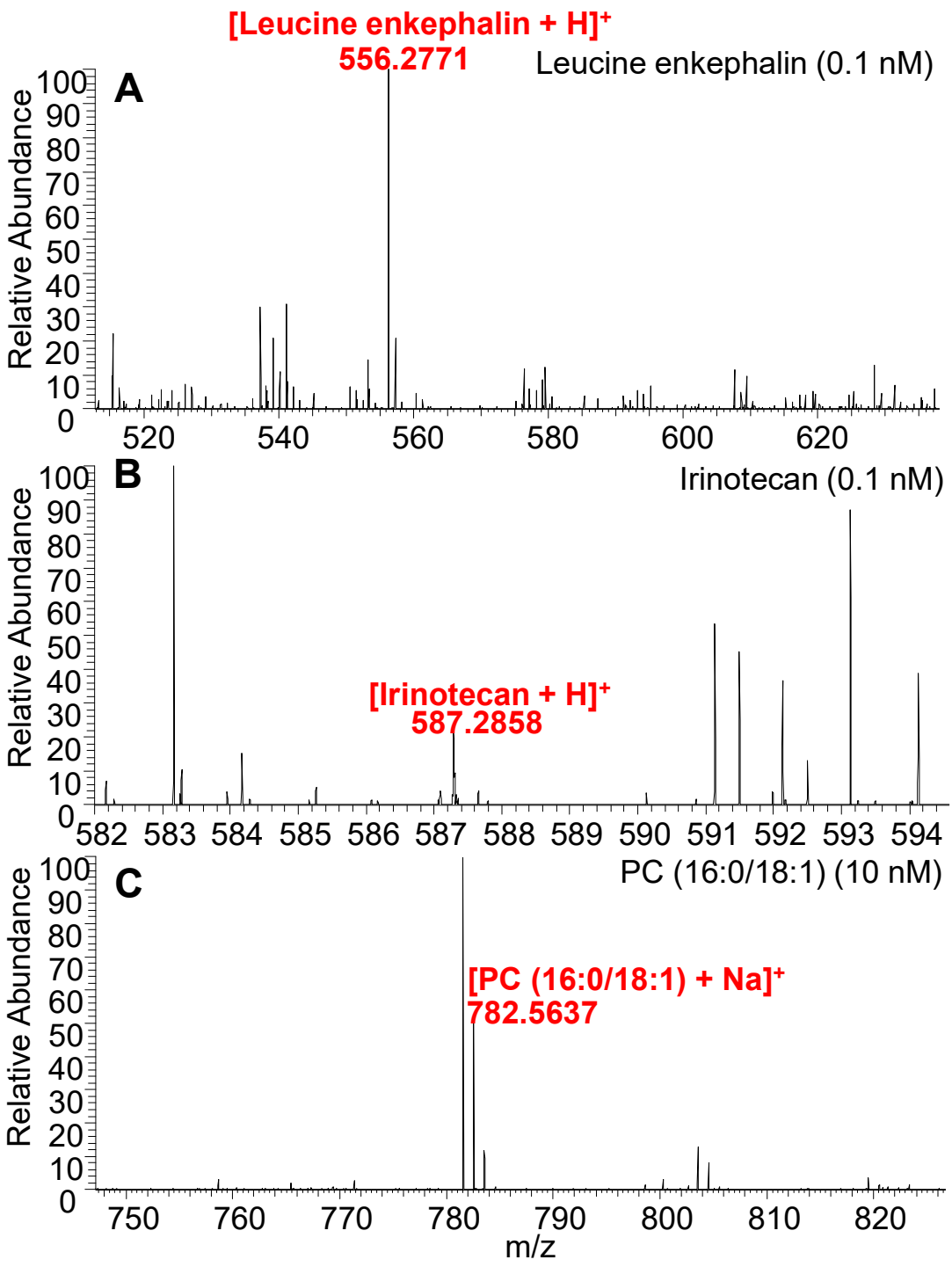


Figure S3-3. *Evaluation of the LODs of the redesigned T-probe using standard solutions of (A) leucine enkephalin (0.1 nM), (B) irinotecan (0.1 nM), and (C) PC (16:0/18:1) (10 nM).*

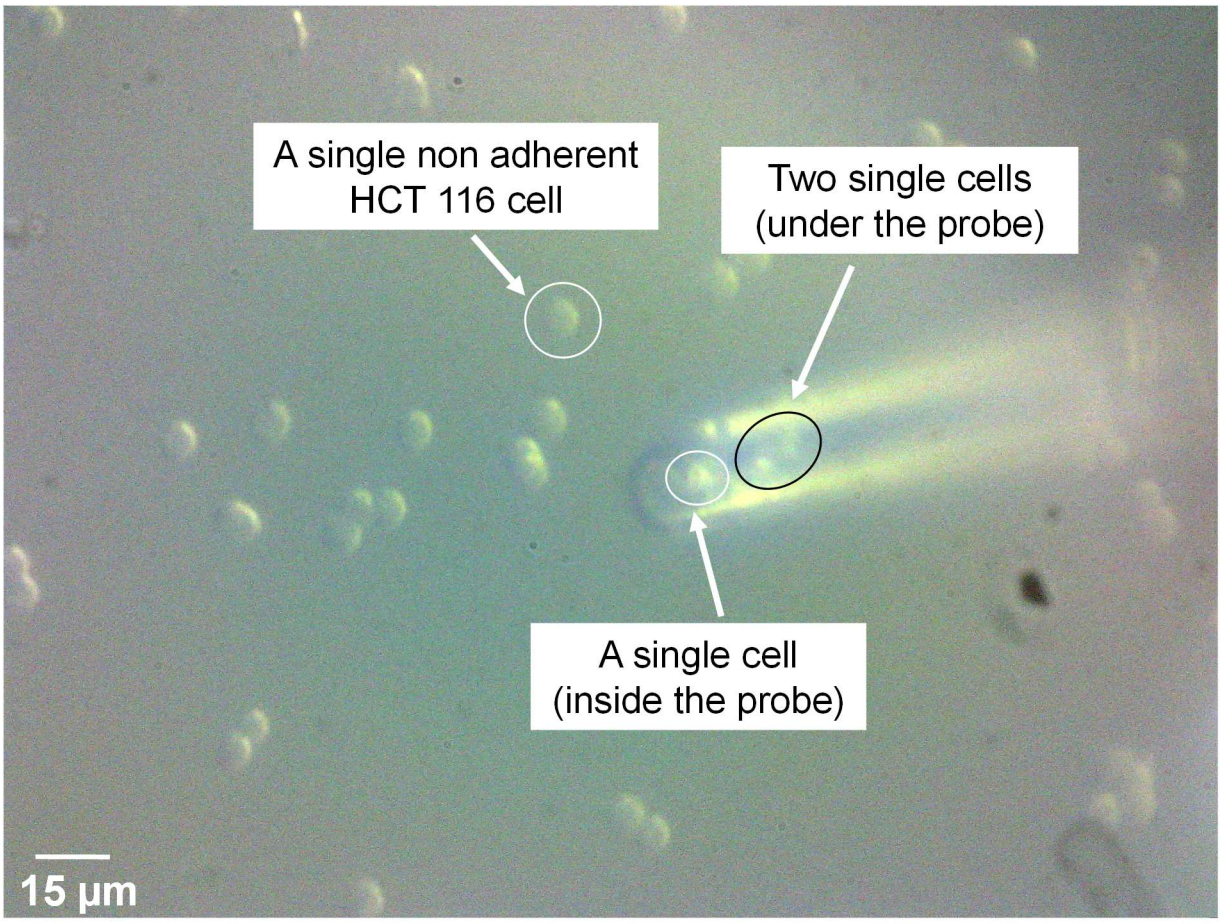


Figure S3-4. *Sampling a suspended HCT-116 cell under the microscope for the SCMS experiment.*

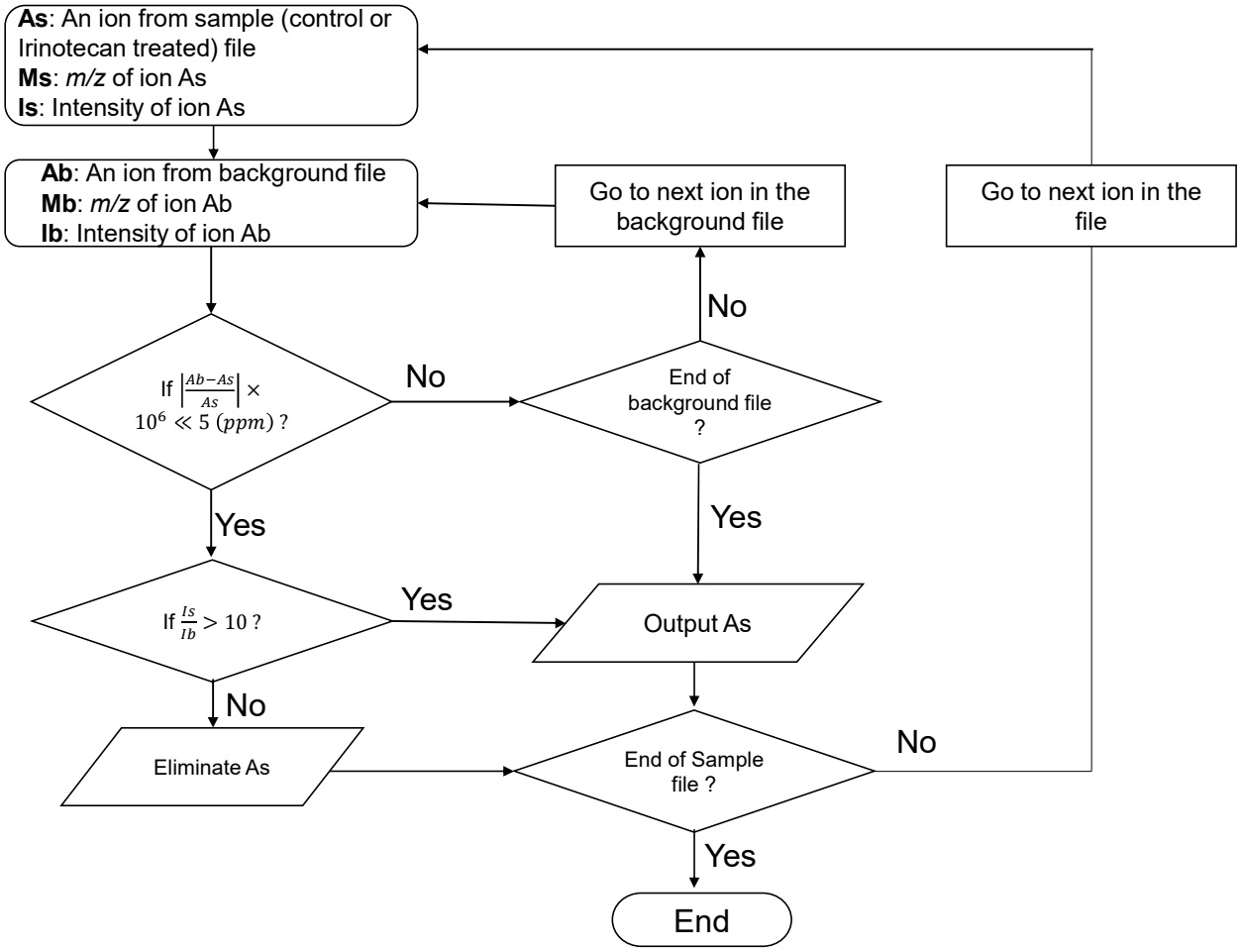


Figure S3-5. *The flowchart of the in-house developed Python script for the SCMS background subtraction.*

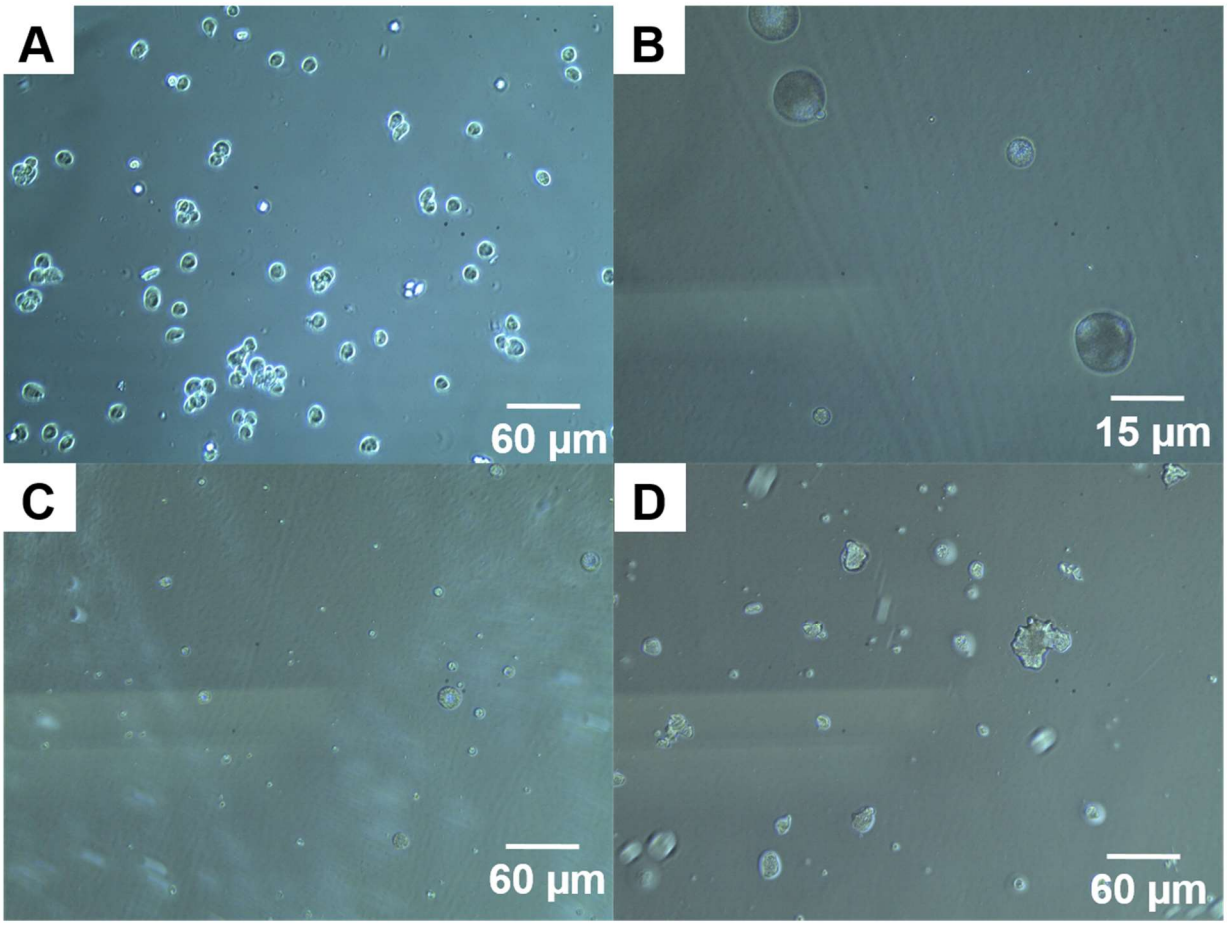


Figure S3-6. *Observation of cell lysis in different solvents under the microscope. (A) Live HCT-116 cells (with bright edges) in the culture medium. Cell lysis can be observed in (B) acetonitrile (95%)/culture medium (5%) within 3 seconds, (C) acetonitrile (90%)/culture medium (10%) within 3 seconds, and (D) acetonitrile (80%)/culture medium (20%) within 12 seconds*

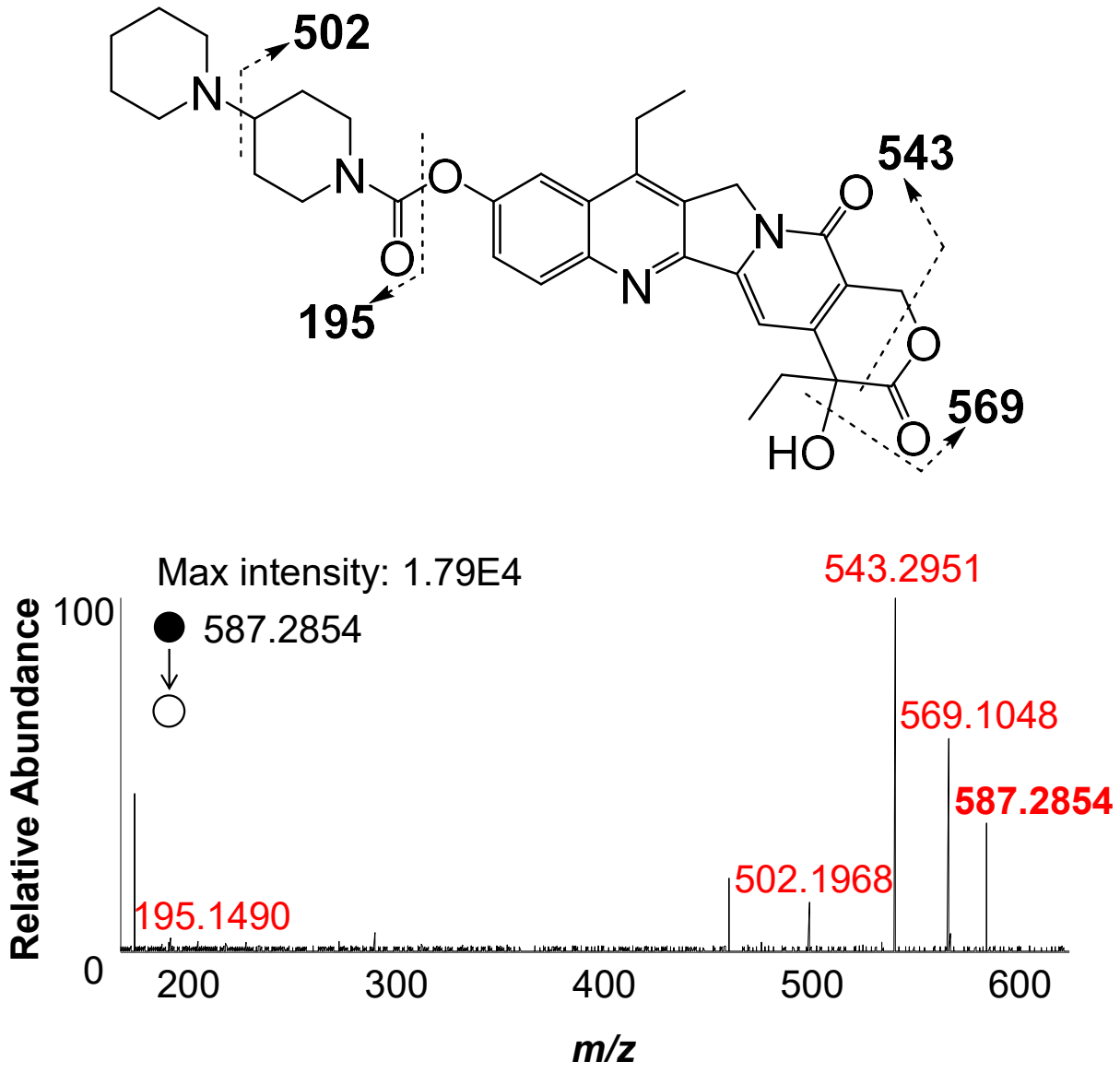


Figure S3-7. *Online MS/MS spectra of irinotecan detected from a single cell treated with irinotecan. The ions highlighted in red (m/z 569, m/z 543, m/z 502, and m/z 195) are fragments consistent with reported studies.*[8]

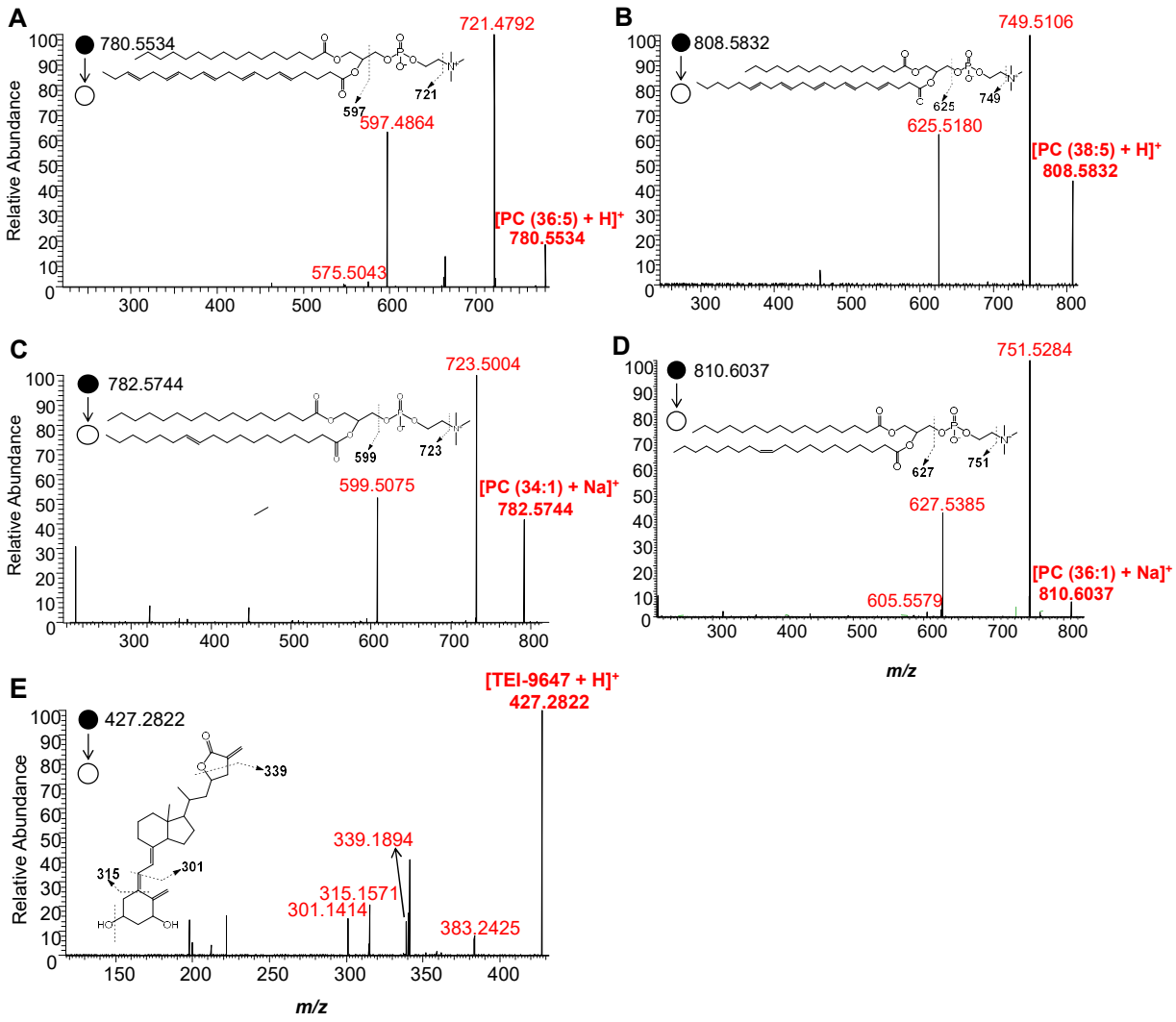
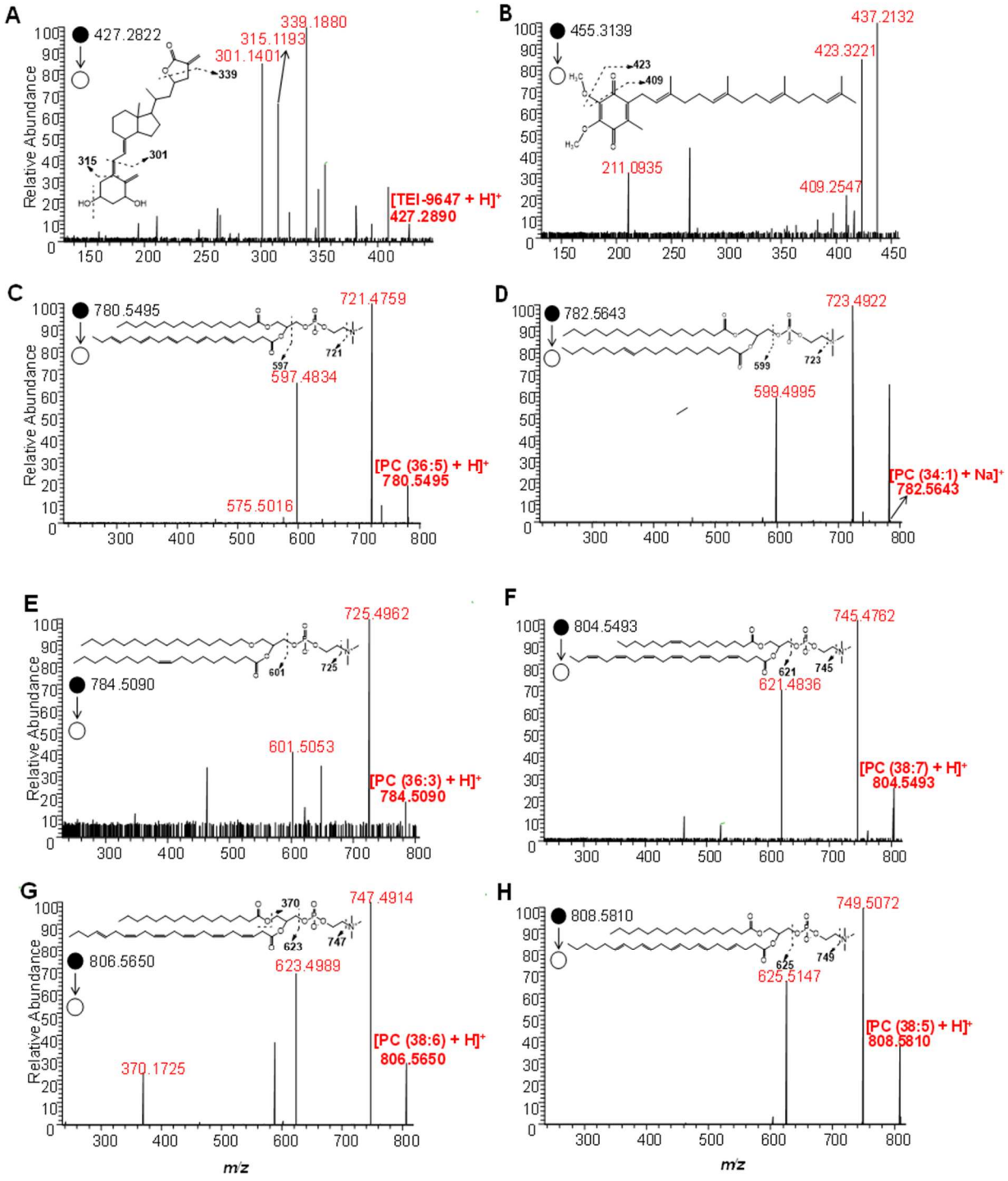


Figure S3-8. *Online MS/MS analysis of cellular species at the single cell level, including (A) PC (36:5) (m/z 780.5534), (B) PC (38:5) (m/z 808.5832), (C) PC (34:1) (m/z 782.5744), (D) PC (36:1) (m/z 810.6037), and (E) TEI9647 (m/z 427.2822). The m/z values labelled in red are consistent with in silico data reported in HMDB and METLIN.*


A
427.2822
339.1880
315.1193
301.1401
339
315
301
[TEI-9647 + H]+
427.2890
Relative Abundance
B
455.3139
437.2132
423.3221
423
409
211.0935
409.2547
C
780.5495
721.4759
597.4834
[PC (36:5) + H]+
780.5495
575.5016
D
782.5643
723.4922
599.4995
[PC (34:1) + Na]+
782.5643
E
784.5090
725.4962
601.5053
[PC (36:3) + H]+
784.5090
F
804.5493
745.4762
621.4836
[PC (38:7) + H]+
804.5493
G
806.5650
747.4914
623.4989
370.1725
[PC (38:6) + H]+
806.5650
H
808.5810
749.5072
625.5147
[PC (38:5) + H]+
808.5810
m/z

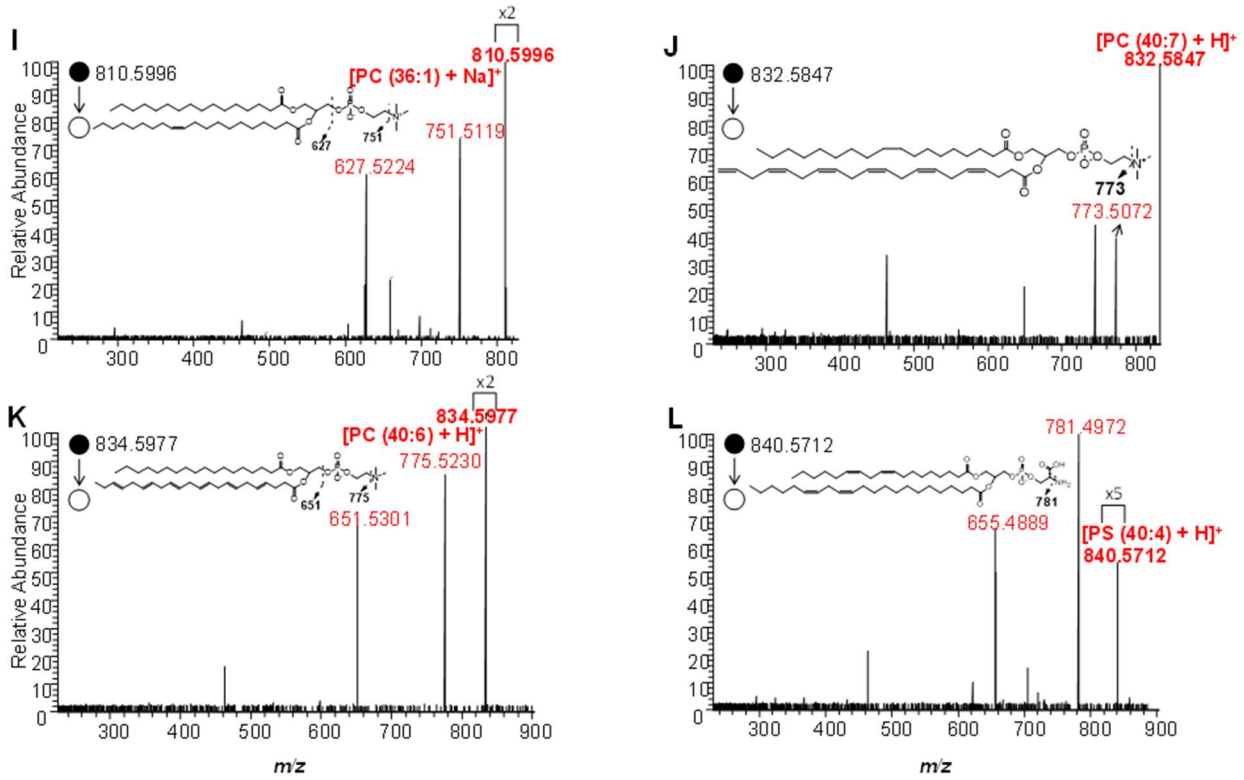


Figure S3-9. *NanoESI-MS/MS analysis of 12 cellular species detected in the lysate prepared using cells in the control group, including (A) TEI-9647 (m/z 427.2890), (B) Coenzyme Q4 (m/z 455.3139), (C) PC (36:5) (m/z 780.5534), (D) PC (34:1) (m/z 782.5643), (E) PC (O- 34:1) (m/z 784.5090), (F) PC (38:7) (m/z 804.5493), (G) PC (38:6) (m/z 806.5650), (H) PC (38:5) (m/z 808.5810), (I) PC (38:4) (m/z 810.5996), (J) PC (40:7) (m/z 832.5847), (K) PC (40:6) (m/z 834.5977), and (L) PC (40:4) (m/z 840.5712). The m/z values labelled in red are consistent with in silico data reported in HMDB and METLIN.*

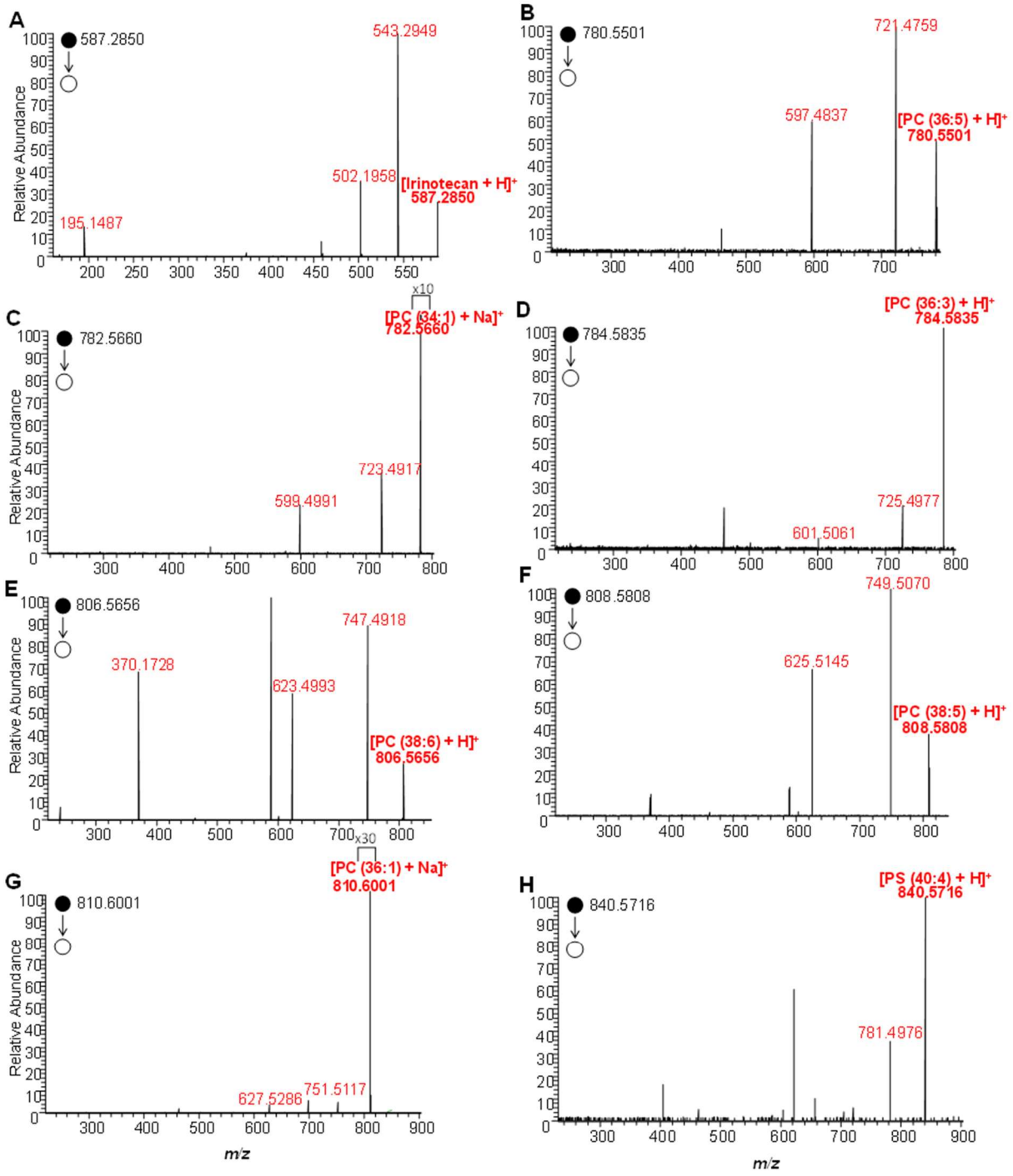


Figure S3-10. *MS/MS analysis of 8 cellular species detected in the lysate prepared using cells in irinotecan treatment groups. (A) Irinotecan (m/z 587.2850), (B) PC (36:5) (m/z 780.5501), (C) PC (34:1) (m/z 782.5660), (D) PC (O- 34:1) (m/z 784.5835), (E) PC*

(38:6) (m/z 806.5656), (F) PC (38:5) (m/z 808.5808), (G) PC (38:4) (m/z 810.6001), and (H) PC (40:4) (m/z 840.5716). The m/z values labelled in red are consistent with in silico data reported in HMDB and METLIN.

References

1. Shi, G.; Li, F.; Tian, H., Advances and application of polycarbonate in automobile windows and aero glass. *Mater. Rev* 2006, *20*, 404-407.
2. Jang, M.; Park, C. K.; Lee, N. Y., Modification of polycarbonate with hydrophilic/hydrophobic coatings for the fabrication of microdevices. *Sensors and Actuators B: Chemical* 2014, *193*, 599-607.
3. Pan, N.; Rao, W.; Kothapalli, N. R.; Liu, R.; Burgett, A. W.; Yang, Z., The single-probe: a miniaturized multifunctional device for single cell mass spectrometry analysis. *Analytical chemistry* 2014, *86* (19), 9376-9380.
4. Folch, J.; Lees, M.; Sloane Stanley, G., A simple method for the isolation and purification of total lipids from animal tissues. *J biol Chem* 1957, *226* (1), 497-509.
5. Romano, P.; Profumo, A.; Rocco, M.; Mangerini, R.; Ferri, F.; Facchiano, A., Geena 2, improved automated analysis of MALDI/TOF mass spectra. *BMC bioinformatics* 2016, *17* (4), 61.
6. Liu, R.; Pan, N.; Zhu, Y.; Yang, Z., T-Probe: An Integrated Microscale Device for Online In Situ Single Cell Analysis and Metabolic Profiling Using Mass Spectrometry. *Analytical chemistry* 2018, *90* (18), 11078-11085.
7. Pan, N.; Rao, W.; Standke, S. J.; Yang, Z., Using dicationic ion-pairing compounds to enhance the single cell mass spectrometry analysis using the single-probe: a microscale sampling and ionization device. *Analytical chemistry* 2016, *88* (13), 6812-6819.
8. Sun, M.; Tian, X.; Yang, Z., Microscale Mass Spectrometry Analysis of Extracellular Metabolites in Live Multicellular Tumor Spheroids. *Analytical chemistry* 2017, *89* (17), 9069-9076.

Appendix II: Support Information of Chapter 4

Cell lysis preparation

HCT-116 cells were cultured in complete McCoy's 5A medium under standard experimental conditions (5% CO_2, 37 ℃, humidified) in the incubator (HERAcell, Thermo Scientific). HCT-116 cells (cell density: 9* 10^5/mL) were washed using 5 mL of PBS to eliminate dead cells, and then detached from culture plate using 2 mL of trypsin-EDTA solution. Trypsinization lasted for 2 min in the incubator and then quenched by 8 mL of culture medium. 1 mL of cell suspension solution was pipetted into a 2 mL tube and centrifuged (10 min at 13000 rpm). The supernatant was removed after centrifugation, and cells were washed by 5 mL PBS solution. Repeat previous steps for three times. The procedure of cell lysis was using a standard protocol.[1] The lysis buffer was methanol with chloroform at a ratio of 1:1. Using lysis buffer to conducted cell lysis and vortexed for 10 min on ice. The cell lysis solution was centrifuged at 14,000 rpm for 15 min at 4 ℃ to eliminate sediment form cell lysis solution. The supernatant was dried in SpeedVac concentrator (Thermo Scientific, MA). After solvent evaporation, cell lysis tubes were stored at -80℃.

Lipids C=C bond identification using cell lysate

Before the experiment, 300 μL of ACN was used to redissolve the cell lysate. The same flow rate (0.2 μL/min) was used as in the SCMS analysis to infuse cell lysate in MS analysis. First, HCT-116 cell lysates were analyzed using the micropipette coupled to the mass spectrometer, and the data (both MS scan and MS/MS) were collected as the "control" group. Second, after 15 min UV irradiation of the same sample, experiments

were resumed to collect data as the “reactive” group. The procedures of the data analysis part were same as those used in single-cell results.

Supporting Tables

Table S4-1. ***Limit of detections (LODs) of standard compounds (pM).***

Compounds	Micropipette needle	Redesigned T-probe[2]	T-probe[3]	Single-probe[4]	Nano-ESI[3]
Irinotecan	10	100	100	/	100
Leucine enkephalin	/	100	1000	/	800
PC (16:0/18:1)	0.1	10000	10000	5000	5000
Verapamil	0.1	/	/	/	/

Table S4-2. ***Potential lipids with m/z 760.58 determined from acetone PB reaction at the single-cell level.***

Lipids	PB products	Adduct	Double bond position	*m/z* of predicted fragments	MS/MS match[1]
PC (16:0/18:1(9))	Isomer I	H^+	Chain2 Δ9	650.5	Y
	Isomer II	H^+	Chain2 Δ9	676.6	Y
PC (16:1(7)/18:0)	Isomer I	H^+	Chain1 Δ7	650.5	Y
	Isomer II	H^+	Chain1 Δ7	676.6	Y
PC (18:1(9)/16:0)	Isomer I	H^+	Chain1 Δ9	650.5	Y
	Isomer II	H^+	Chain1 Δ9	676.6	Y
PC (14:0/20:1(11))	Isomer I	H^+	Chain2 Δ11	650.5	Y
	Isomer II	H^+	Chain2 Δ11	676.6	Y
PC (20:1(11)/14:0)	Isomer I	H^+	Chain1 Δ11	650.5	Y
	Isomer II	H^+	Chain1 Δ11	676.6	Y
PC (16:0/18:1(11))	Isomer I	H^+	Chain2 Δ11	678.6	N
	Isomer II	H^+	Chain2 Δ11	704.6	N
PC (16:0/18:1(6))	Isomer I	H^+	Chain2 Δ6	608.5	N
	Isomer II	H^+	Chain2 Δ6	634.5	N
PC (16:1(9)/18:0)	Isomer I	H^+	Chain1 Δ9	678.6	N
	Isomer II	H^+	Chain1 Δ9	704.6	N
PC (14:1(9Z)/20:0)	Isomer I	H^+	Chain1 Δ9	706.6	N
	Isomer II	H^+	Chain1 Δ9	732.7	N
PC (18:0/16:1(9))	Isomer I	H^+	Chain2 Δ9	678.6	N
	Isomer II	H^+	Chain2 Δ9	704.6	N
PC (18:1(11)/16:0)	Isomer I	H^+	Chain1 Δ11	678.6	N
	Isomer II	H^+	Chain1 Δ11	704.6	N
PC (20:0/14:1(9))	Isomer I	H^+	Chain2 Δ9	706.6	N

	Isomer II	H^+	Chain2 Δ9	732.7	N
PC (12:0/22:1(11))	Isomer I	H^+	Chain2 Δ11	622.5	N
	Isomer II	H^+	Chain2 Δ11	648.6	N
PC (15:0/19:1(9))	Isomer I	H^+	Chain2 Δ9	636.5	N
	Isomer II	H^+	Chain2 Δ9	662.6	N
PC (15:1(9)/19:0)	Isomer I	H^+	Chain1 Δ9	692.6	N
	Isomer II	H^+	Chain1 Δ9	718.7	N
PC (17:0/17:1(9))	Isomer I	H^+	Chain2 Δ9	664.6	N
	Isomer II	H^+	Chain2 Δ9	690.6	N
PC (17:1(9)/17:0)	Isomer I	H^+	Chain1 Δ9	664.6	N
	Isomer II	H^+	Chain1 Δ9	690.6	N
PC (19:0/15:1(9))	Isomer I	H^+	Chain2 Δ9	692.6	N
	Isomer II	H^+	Chain2 Δ9	718.7	N
PC (19:1(9)/15:0)	Isomer I	H^+	Chain1 Δ9	636.5	N
	Isomer II	H^+	Chain1 Δ9	662.6	N
PC (22:1(11)/12:0)	Isomer I	H^+	Chain1 Δ11	622.5	N
	Isomer II	H^+	Chain1 Δ11	648.6	N

[1]Comparison with experimental MS/MS spectra of the corresponding PB products.

Table S4-3. ***Potential lipids (m/z 760.58) identified from acetone PB products (m/z 818.6579). Species in the shade were eliminated based on the analysis of headgroups obtained from MS/MS.***

Lipids name	Adduct
PC (16:0/18:1(11))	H^+
PC (16:0/18:1(6))	H^+
PC (16:0/18:1(9))	H^+
PC (16:1(7)/18:0)	H^+
PC (16:1(9)/18:0)	H^+
PC (18:1(9)/16:0)	H^+
PC (14:0/20:1(11))	H^+
PC (14:1(9)/20:0)	H^+
PC (18:0/16:1(9))	H^+
PC (18:1(11)/16:0)	H^+
PC (20:0/14:1(9))	H^+
PC (20:1(11)/14:0)	H^+
PC (12:0/22:1(11))	H^+
PC (15:0/19:1(9))	H^+
PC (15:1(9)/19:0)	H^+
PC (17:0/17:1(9))	H^+
PC (17:1(9)/17:0)	H^+
PC (19:0/15:1(9))	H^+
PC (19:1(9)/15:0)	H^+
PC (22:1(11)/12:0)	H^+
PE (15:0/22:1(11))	H^+
PE (15:1(9)/22:0)	H^+
PE (16:1(9)/21:0)	H^+
PE (17:0/20:1(11))	H^+
PE (17:1(9)/20:0)	H^+
PE (18:0/19:1(9))	H^+
PE (18:1(9)/19:0)	H^+
PE (19:0/18:1(9))	H^+
PE (19:1(9)/18:0)	H^+
PE (20:0/17:1(9))	H^+
PE (20:1(11)/17:0)	H^+
PE (21:0/16:1(9))	H^+
PE (22:0/15:1(9))	H^+
PE (22:1(11)/15:0)	H^+
PE (15:0/22:1(13))	H^+
PE (22:1(13)/15:0)	H^+

Table S4-4. ***Determination of fatty acid tails in lipids (negative ion mode) from single cells and cell lysates.***

m/z (lipids)	*m/z* (acetate adducts of lipids)	Sample	*m/z* of side chains	Fatty acid tails
760.59	818.59	Single cell	255,281	C 16:0, C 18:1
		Cell lysate	253,255,281,283	C 16:1, C 16:0, C 18:1, C 18:0
810.6	868.61	Single cell	255, 279, 281, 339	C 16:0, C18:2, C 18:1, C 22:0
		Cell lysate	255, 283, 339	C 16:0, C 18:0, C 22:0
732.55	790.56	Single cell	253, 281	C 16:1, C 18:1
		Cell lysate	253,255,281,283	C 16:1, C 16:0,C 18:1, C 18:0
782.57	840.57	Single cell	255,281	C 16:0, C 18:1
		Cell lysate	255, 279, 283	C 16:0, C 18:2, C 18:0
754.54	812.54	Single cell	239, 279, 281, 283	C 15:1, C 16:0, C18:2, C 18:1, C 18:0
		Cell lysate	239, 255, 279, 281, 283	C 15:1, C18:2, C 18:1, C 18:0
780.55	838.56	Single cell	253, 281, 307	C 16:1, C 18:1, C 20:2
		Cell lysate	255, 277, 281	C 16:0, C 18:3, C 18:1
756.55	814.56	Single cell	253, 267, 279, 283, 339	C 16:1, C 17:1, C 18:2, C18:0, C 22:0
		Cell lysate	255, 281, 283	C 16:0, C 18:1, C 18:0
784.59	842.59	Single cell	255, 279, 281, 283, 305	C 16:0, C18:2, C 18:1, C 18:0, C 20:3
		Cell lysate	255, 283	C 16:0, C 18:0
786.6	844.61	Single cell	253, 281, 339	C 16:1, C 18:1, C 22:0
		Cell lysate	255, 281, 283	C 16:0, C 18:1, C 18:0

Table S4-5. ***Potential species (m/z 760.58) with the same predicted fragments as m/z 818.62 (acetone PB products) at the single-cell level.***

Lipids	PB product isomers	Adducts	C=C bond position	*m/z* of predicted fragments	Carbon number match*
PC (16:0/18:1(9))**	Isomer I	H^+	Chain2 Δ9	650.54	Y
	Isomer II	H^+	Chain2 Δ9	676.59	
PC (18:1(9)/16:0)**	Isomer I	H^+	Chain1 Δ9	650.54	Y
	Isomer II	H^+	Chain1 Δ9	676.59	
PC (16:1(7)/18:0)	Isomer I	H^+	Chain1 Δ7	650.54	Y***
	Isomer II	H^+	Chain1 Δ7	676.59	
PC (14:0/20:1(11))	Isomer I	H^+	Chain2 Δ11	650.54	N
	Isomer II	H^+	Chain2 Δ11	676.59	
PC (20:1(11)/14:0)	Isomer I	H^+	Chain1 Δ11	650.54	N
	Isomer II	H^+	Chain1 Δ11	676.59	

*Comparison with results in Table S4.

**Identified species with matched MS/MS fragments (from prediction) and carbon numbers in fatty acid tails.

***Agreement is only obtained from cell lysates (not from single cells)

Table S4-6. ***Predicted diagnostic ions from m/z 868.64 (acetone PB products of m/z 810.60) at the single-cell level.***

Lipids[1]	PB products	Adduct	Double bond position	*m/z* of predicted fragments	MS/MS match[2]	Carbon number match[3]
PC (16:0/20:1(11))	Isomer I	Na^+	Chain2 Δ11	700.6	Y	Y
	Isomer II	Na^+	Chain2 Δ11	726.6	Y	
PC (18:0/18:1(13))	Isomer I	Na^+	Chain2 Δ13	756.6	Y	Y
	Isomer II	Na^+	Chain2 Δ13	782.7	Y	
PC (18:0/18:1(9))	Isomer I	Na^+	Chain2 Δ9	700.6	Y	Y
	Isomer II	Na^+	Chain2 Δ9	726.6	Y	
PC (18:1(9)/18:0)	Isomer I	Na^+	Chain1 Δ9	700.6	Y	Y
	Isomer II	Na^+	Chain1 Δ9	726.6	Y	
PC (20:1(11)/16:0)	Isomer I	Na^+	Chain1 Δ11	700.6	Y	Y
	Isomer II	Na^+	Chain1 Δ11	726.6	Y	
PC (14:1(9)/22:0)	Isomer I	Na^+	Chain1 Δ9	756.6	Y	Y
	Isomer II	Na^+	Chain1 Δ9	782.7	Y	
PC (22:0/14:1(9))	Isomer I	Na^+	Chain2 Δ9	756.6	Y	Y
	Isomer II	Na^+	Chain2 Δ9	782.7	Y	
PC (14:0/22:1(13))	Isomer I	Na^+	Chain2 Δ13	700.6	Y	N
	Isomer II	Na^+	Chain2 Δ13	726.6	Y	
PC (22:1(13)/14:0)	Isomer I	Na^+	Chain1 Δ13	700.6	Y	N
	Isomer II	Na^+	Chain1 Δ13	726.6	Y	
PC (18:0/18:1(12))	Isomer I	Na^+	Chain2 Δ12	742.6	N	Y
	Isomer II	Na^+	Chain2 Δ12	768.7	N	
PC (18:0/18:1(16))	Isomer I	Na^+	Chain2 Δ16	798.7	N	Y
	Isomer II	Na^+	Chain2 Δ16	824.8	N	
PC (18:0/18:1(6))	Isomer I	Na^+	Chain2 Δ6	658.5	N	Y
	Isomer II	Na^+	Chain2 Δ6	684.6	N	

PC (18:0/18:1(7))	Isomer I	Na^+	Chain2 Δ7	672.5	N	Y
	Isomer II	Na^+	Chain2 Δ7	698.6	N	
PC (16:1(9)/20:0)	Isomer I	Na^+	Chain1 Δ9	728.6	N	Y
	Isomer II	Na^+	Chain1 Δ9	754.7	N	
PC (18:0/18:1(11))	Isomer I	Na^+	Chain2 Δ11	728.6	N	Y
	Isomer II	Na^+	Chain2 Δ11	754.7	N	
PC (18:1(11)/18:0)	Isomer I	Na^+	Chain1 Δ11	728.6	N	Y
	Isomer II	Na^+	Chain1 Δ11	754.7	N	
PC (20:0/16:1(9))	Isomer I	Na^+	Chain2 Δ9	728.6	N	Y
	Isomer II	Na^+	Chain2 Δ9	754.7	N	

[1]Species labeled in red front indicate Identified species with matched MS/MS fragments (from prediction) and carbon numbers in fatty acid tails.

[2]Comparison with experimental MS/MS spectra of the corresponding PB products.

[3]Comparison with results in Table S4.

Table S4-7. ***Predicted diagnostic ions from m/z 942.65 (benzophenone PB products of m/z 760.58) at the single-cell level.***

Lipids[1]	PB products	Adduct	Double bond position	*m/z* of predicted fragments	MS/MS match[2]	Carbon number match[3]
PC (18:1(9)/16:0)	Isomer I	H^+	Chain1 Δ9	650.54	**Y**	**Y**
	Isomer II	H^+	Chain1 Δ9	800.62	**Y**	
PC (16:0/18:1(9))	Isomer I	H^+	Chain2 Δ9	650.54	**Y**	**Y**
	Isomer II	H^+	Chain2 Δ9	800.62	**Y**	
PC (16:1(7)/18:0)	Isomer I	H^+	Chain1 Δ7	650.54	Y	Y*
	Isomer II	H^+	Chain1 Δ7	800.62	Y	
PC (20:1(11)/14:0)	Isomer I	H^+	Chain1 Δ11	650.54	Y	N
	Isomer II	H^+	Chain1 Δ11	800.62	Y	
PC (14:0/20:1(11))	Isomer I	H^+	Chain2 Δ11	650.54	Y	N
	Isomer II	H^+	Chain2 Δ11	800.62	Y	
PC (16:0/18:1(11))	Isomer I	H^+	Chain2 Δ11	678.58	N	Y
	Isomer II	H^+	Chain2 Δ11	828.66	N	
PC (16:0/18:1(6))	Isomer I	H^+	Chain2 Δ6	608.48	N	Y
	Isomer II	H^+	Chain2 Δ6	758.56	N	
PC (18:1(11)/16:0)	Isomer I	H^+	Chain1 Δ11	678.58	N	Y
	Isomer II	H^+	Chain1 Δ11	828.66	N	
PC (16:1(9)/18:0)	Isomer I	H^+	Chain1 Δ9	678.58	N	Y*
	Isomer II	H^+	Chain1 Δ9	828.66	N	
PC (18:0/16:1(9))	Isomer I	H^+	Chain2 Δ9	678.58	N	Y*
	Isomer II	H^+	Chain2 Δ9	828.66	N	
PC (14:1(9)/20:0)	Isomer I	H^+	Chain1 Δ9	706.62	N	N
	Isomer II	H^+	Chain1 Δ9	856.70	N	

PC (20:0/14:1(9))	Isomer I	H^+	Chain2 Δ9	706.62	N	N
	Isomer II	H^+	Chain2 Δ9	856.70	N	
PC (12:0/22:1(11))	Isomer I	H^+	Chain2 Δ11	622.50	N	N
	Isomer II	H^+	Chain2 Δ11	772.58	N	
PC (15:0/19:1(9))	Isomer I	H^+	Chain2 Δ9	636.52	N	N
	Isomer II	H^+	Chain2 Δ9	786.60	N	
PC (15:1(9)/19:0)	Isomer I	H^+	Chain1 Δ9	692.60	N	N
	Isomer II	H^+	Chain1 Δ9	842.68	N	
PC (17:0/17:1(9))	Isomer I	H^+	Chain2 Δ9	664.56	N	N
	Isomer II	H^+	Chain2 Δ9	814.64	N	
PC (17:1(9)/17:0)	Isomer I	H^+	Chain1 Δ9	664.56	N	N
	Isomer II	H^+	Chain1 Δ9	814.64	N	
PC (19:0/15:1(9))	Isomer I	H^+	Chain2 Δ9	692.60	N	N
	Isomer II	H^+	Chain2 Δ9	842.68	N	
PC (19:1(9)/15:0)	Isomer I	H^+	Chain1 Δ9	636.52	N	N
	Isomer II	H^+	Chain1 Δ9	786.60	N	
PC (22:1(11)/12:0)	Isomer I	H^+	Chain1 Δ11	622.50	N	N
	Isomer II	H^+	Chain1 Δ11	772.58	N	

[1]Species labeled in red front indicate Identified species with matched MS/MS fragments (from prediction) and carbon numbers in fatty acid tails.

[2]Comparison with experimental MS/MS spectra of the corresponding PB products.

[3]Comparison with results in Table S4.

*Agreement is only obtained from cell lysates (not from single cells).

Table S4-8. ***Predicted diagnostic ions from m/z 790.59 (acetone PB products of m/z 732.55) at the single-cell level.***

Lipids[1]	PB products	Adducts	Double bond position	*m/z* of predicted fragments	MS/MS match[2]	Carbon number match[3]
PC (16:0/16:1(9))	Isomer I	H^+	Chain2 Δ9	650.5	**Y**	**Y**
	Isomer II	H^+	Chain2 Δ9	676.6	**Y**	
PC (14:0/18:1(11))	Isomer I	H^+	Chain2 Δ11	650.5	**Y**	**Y**
	Isomer II	H^+	Chain2 Δ11	676.6	**Y**	
PC (16:1(9)/16:0)	Isomer I	H^+	Chain1 Δ9	650.5	**Y**	**Y**
	Isomer II	H^+	Chain1 Δ9	676.6	**Y**	
PC (18:1(11)/14:0)	Isomer I	H^+	Chain1 Δ11	650.5	**Y**	**Y**
	Isomer II	H^+	Chain1 Δ11	676.6	**Y**	
PC (12:0/20:1(11))	Isomer I	H^+	Chain2 Δ11	622.5	N	N
	Isomer II	H^+	Chain2 Δ11	648.6	N	
PC (13:0/19:1(9))	Isomer I	H^+	Chain2 Δ9	608.5	N	N
	Isomer II	H^+	Chain2 Δ9	634.5	N	
PC (15:0/17:1(9))	Isomer I	H^+	Chain2 Δ9	636.5	N	N
	Isomer II	H^+	Chain2 Δ9	662.6	N	
PC (15:1(9)/17:0)	Isomer I	H^+	Chain1 Δ9	664.6	N	N
	Isomer II	H^+	Chain1 Δ9	690.6	N	
PC (17:0/15:1(9))	Isomer I	H^+	Chain2 Δ9	664.6	N	N
	Isomer II	H^+	Chain2 Δ9	690.6	N	

PC (17:1(9)/15:0)	Isomer I	H^+	Chain1 Δ9	636.5	N	N
	Isomer II	H^+	Chain1 Δ9	662.6	N	
PC (19:1(9)/13:0)	Isomer I	H^+	Chain1 Δ9	608.5	N	N
	Isomer II	H^+	Chain1 Δ9	634.5	N	
PC (20:1(11)/12:0)	Isomer I	H^+	Chain1 Δ11	622.5	N	N
	Isomer II	H^+	Chain1 Δ11	648.6	N	
PC (14:0/18:1(9))	Isomer I	H^+	Chain2 Δ9	622.5	N	Y
	Isomer II	H^+	Chain2 Δ9	648.6	N	
PC (18:1(9)/14:0)	Isomer I	H^+	Chain1 Δ9	622.5	N	Y
	Isomer II	H^+	Chain1 Δ9	648.6	N	
PC (14:1(9)/18:0)	Isomer I	H^+	Chain1 Δ9	678.6	N	Y*
	Isomer II	H^+	Chain1 Δ9	704.6	N	
PC (18:0/14:1(9))	Isomer I	H^+	Chain2 Δ9	678.6	N	Y*
	Isomer II	H^+	Chain2 Δ9	704.6	N	

[1]Species labeled in red front indicate Identified species with matched MS/MS fragments (from prediction) and carbon numbers in fatty acid tails.

[2]Comparison with experimental MS/MS spectra of the corresponding PB products.

[3]Comparison with results in Table S4.

*Agreement is only obtained from cell lysates (not from single cells).

Table S4-9. ***Predicted diagnostic ions from m/z 840.60 (acetone PB products of m/z 782.56) at the single-cell level.***

Lipids[1]	PB products	adduct	Double bond position	m/z of predicted fragments	MS/MS match[2]	carbon number match[3]
PC (16:0/18:1(9))	Isomer I	Na	Chain2 Δ9	672.5	**Y**	**Y**
	Isomer II	Na	Chain2 Δ9	698.6	**Y**	
PC (18:1(9)/16:0)	Isomer I	Na	Chain1 Δ9	672.5	**Y**	**Y**
	Isomer II	Na	Chain1 Δ9	698.6	**Y**	
PC (16:0/18:1(6))	Isomer I	Na	Chain2 Δ6	630.5	N	**Y**
	Isomer II	Na	Chain2 Δ6	656.5	**Y**	
PC (16:1(7)/18:0)	Isomer I	Na	Chain1 Δ7	672.5	Y	Y*
	Isomer II	Na	Chain1 Δ7	698.6	Y	
PC (14:0/20:1(11))	Isomer I	Na	Chain2 Δ11	672.5	Y	N
	Isomer II	Na	Chain2 Δ11	698.6	Y	
PC (20:1(11)/14:0)	Isomer I	Na	Chain1 Δ11	672.5	Y	N
	Isomer II	Na	Chain1 Δ11	698.6	Y	
PC (16:1(9)/18:0)	Isomer I	Na	Chain1 Δ9	700.6	N	Y*
	Isomer II	Na	Chain1 Δ9	726.6	N	
PC (18:0/16:1(9))	Isomer I	Na	Chain2 Δ9	700.6	N	Y*
	Isomer II	Na	Chain2 Δ9	726.6	N	
PC (16:0/18:1(11))	Isomer I	Na	Chain2 Δ11	700.6	N	Y
	Isomer II	Na	Chain2 Δ11	726.6	N	
PC (18:1(11)/16:0)	Isomer I	Na	Chain1 Δ11	700.6	N	Y
	Isomer II	Na	Chain1 Δ11	726.6	N	
PC (14:1(9)/20:0)	Isomer I	Na	Chain1 Δ9	728.6	N	N
	Isomer II	Na	Chain1 Δ9	754.7	N	
PC (20:0/14:1(9))	Isomer I	Na	Chain2 Δ9	728.6	N	N
	Isomer II	Na	Chain2 Δ9	754.7	N	
PC (12:0/22:1(11))	Isomer I	Na	Chain2 Δ11	644.5	N	N

	Isomer II	Na	Chain2 Δ11	670.5	N	
PC (15:0/19:1(9))	Isomer I	Na	Chain2 Δ9	658.5	N	N
	Isomer II	Na	Chain2 Δ9	684.6	N	
PC (15:1(9)/19:0)	Isomer I	Na	Chain1 Δ9	714.6	N	N
	Isomer II	Na	Chain1 Δ9	740.6	N	
PC (17:0/17:1(9))	Isomer I	Na	Chain2 Δ9	686.5	N	N
	Isomer II	Na	Chain2 Δ9	712.6	N	
PC (17:1(9)/17:0)	Isomer I	Na	Chain1 Δ9	686.5	N	N
	Isomer II	Na	Chain1 Δ9	712.6	N	
PC (19:0/15:1(9))	Isomer I	Na	Chain2 Δ9	714.6	N	N
	Isomer II	Na	Chain2 Δ9	740.6	N	
PC (19:1(9)/15:0)	Isomer I	Na	Chain1 Δ9	658.5	N	N
	Isomer II	Na	Chain1 Δ9	684.6	N	
PC (22:1(11)/12:0)	Isomer I	Na	Chain1 Δ11	644.5	N	N
	Isomer II	Na	Chain1 Δ11	670.5	N	

[1]Species labeled in red front indicate Identified species with matched MS/MS fragments (from prediction) and carbon numbers in fatty acid tails.

[2]Comparison with experimental MS/MS spectra of the corresponding PB products.

[3]Comparison with results in Table S4.

*Agreement is only obtained from cell lysates (not from single cells).

Table S4-10. ***Predicted diagnostic ions from m/z 812.57 (acetone PB products of m/z 754.53) at the single-cell level***

Lipids[1]	PB products	adduct	Double bond position	*m/z* of predicted fragments	MS/MS Match[2]	Double bond position	*m/z* of predicted fragments	MS/MS Match[2]	Double bond position	*m/z* of predicted fragments	MS/MS Match[2]	Double bond position	*m/z* of predicted fragments	MS/MS Match[2]	Carbon number match[3]
PC (16:0/18:4(9,11,13,15))	Isomer I	H^+	Chain2 Δ11	676.6	N	Chain2 Δ13	702.6	N	Chain2 Δ15	728.6	Y	Chain2 Δ9	650.5	N	**Y**
	Isomer II	H^+	Chain2 Δ11	702.6	N	Chain2 Δ13	728.6	N	Chain2 Δ15	754.7	Y	Chain2 Δ9	676.6	N	
PC (18:4(9,11,13,15)/16:0)	Isomer I	H^+	Chain1 Δ11	676.6	N	Chain1 Δ13	702.6	N	Chain1 Δ15	728.6	Y	Chain1 Δ9	650.5	N	**Y**
	Isomer II	H^+	Chain1 Δ11	702.6	N	Chain1 Δ13	728.6	Y	Chain1 Δ15	754.7	Y	Chain1 Δ9	676.6	N	
PC (16:0/18:4(6,9,12,15))	Isomer I	H^+	Chain2 Δ12	688.6	N	Chain2 Δ15	728.6	Y	Chain2 Δ6	608.5	N	Chain2 Δ9	648.5	N	**Y**
	Isomer II	H^+	Chain2 Δ12	714.6	N	Chain2 Δ15	754.7	Y	Chain2 Δ6	634.5	N	Chain2 Δ9	674.6	N	
PC (16:2(2,4)/18:2(2,4))	Isomer I	H^+	Chain1 Δ2	576.4	N	Chain1 Δ4	602.4	N	Chain2 Δ2	548.4	N	Chain2 Δ4	574.4	N	**Y**
	Isomer II	H^+	Chain1 Δ2	602.5	N	Chain1 Δ4	628.5	Y	Chain2 Δ2	574.4	N	Chain2 Δ4	600.4	N	
PC (18:2(9,12)/16:2(5,8))	Isomer I	H^+	Chain1 Δ12	686.5	Y	Chain1 Δ9	646.5	N	Chain2 Δ5	618.5	N	Chain2 Δ8	658.5	N	**Y**
	Isomer II	H^+	Chain1 Δ12	712.6	N	Chain1 Δ9	672.6	N	Chain2 Δ5	644.5	Y	Chain2 Δ8	684.6	N	
PC (14:0/18:1(9))	Isomer I	Na^+	Chain2 Δ9	644.5	Y										**Y**
	Isomer II	Na^+	Chain2 Δ9	670.5	N										
PC (18:1(9)/14:0)	Isomer I	Na^+	Chain1 Δ9	644.5	Y										**Y**
	Isomer II	Na^+	Chain1 Δ9	670.5	N										
PC (14:0/20:4(8,11,14,17))	Isomer I	H^+	Chain2 Δ11	648.5	N	Chain2 Δ14	688.6	N	Chain2 Δ17	728.6	Y	Chain2 Δ8	608.5	N	N
	Isomer II	H^+	Chain2 Δ11	674.6	N	Chain2 Δ14	714.6	N	Chain2 Δ17	754.7	Y	Chain2 Δ8	634.5	N	
PC (16:1(9)/18:3(9,12,15))	Isomer I	H^+	Chain1 Δ9	672.5	N	Chain2 Δ12	688.6	N	Chain2 Δ15	728.6	Y	Chain2 Δ9	648.5	N	N
	Isomer II	H^+	Chain1 Δ9	698.6	N	Chain2 Δ12	714.6	N	Chain2 Δ15	754.7	Y	Chain2 Δ9	674.6	N	
PC (18:3(9,12,15)/16:1(9))	Isomer I	H^+	Chain1 Δ12	688.6	N	Chain1 Δ15	728.6	Y	Chain1 Δ9	648.5	N	Chain2 Δ9	672.5	N	N
	Isomer II	H^+	Chain1 Δ12	714.6	N	Chain1 Δ15	754.7	Y	Chain1 Δ9	674.6	N	Chain2 Δ9	698.6	N	

PC (20:4(8,11,14,17)/14:0)	Isomer I	H^+	Chain1 Δ11	648.5	N	Chain1 Δ14	688.6	N	Chain1 Δ17	728.6	Y	Chain1 Δ8	608.5	N	N
	Isomer II	H^+	Chain1 Δ11	674.6	N	Chain1 Δ14	714.6	N	Chain1 Δ17	754.7	Y	Chain1 Δ8	634.5	N	
PC (14:0/20:4(5,8,11,14))	Isomer I	H^+	Chain2 Δ11	646.5	N	Chain2 Δ14	686.5	Y	Chain2 Δ5	566.4	Y	Chain2 Δ8	606.5	N	N
	Isomer II	H^+	Chain2 Δ11	672.6	N	Chain2 Δ14	712.6	N	Chain2 Δ5	592.5	N	Chain2 Δ8	632.5	N	
PC (17:2(9,12)/17:2(9,12))	Isomer I	H^+	Chain1 Δ12	700.6	N	Chain1 Δ9	660.5	N	Chain2 Δ12	700.6	N	Chain2 Δ9	660.5	N	N
	Isomer II	H^+	Chain1 Δ12	726.6	N	Chain1 Δ9	686.6	Y	Chain2 Δ12	726.6	N	Chain2 Δ9	686.6	Y	
PC (14:1(9)/20:3(5,8,11))	Isomer I	H^+	Chain1 Δ9	700.6	N	Chain2 Δ11	644.5	Y	Chain2 Δ5	564.4	N	Chain2 Δ8	604.4	N	N
	Isomer II	H^+	Chain1 Δ9	726.6	N	Chain2 Δ11	670.5	N	Chain2 Δ5	590.5	N	Chain2 Δ8	630.5	N	
PC (14:1(9)/20:3(8,11,14))	Isomer I	H^+	Chain1 Δ9	700.6	N	Chain2 Δ11	646.5	N	Chain2 Δ14	686.5	Y	Chain2 Δ8	606.5	N	N
	Isomer II	H^+	Chain1 Δ9	726.6	N	Chain2 Δ11	672.6	N	Chain2 Δ14	712.6	N	Chain2 Δ8	632.5	N	
PC (16:1(9)/18:3(6,9,12))	Isomer I	H^+	Chain1 Δ9	672.5	N	Chain2 Δ12	686.5	Y	Chain2 Δ6	606.5	N	Chain2 Δ9	646.5	N	N
	Isomer II	H^+	Chain1 Δ9	698.6	N	Chain2 Δ12	712.6	N	Chain2 Δ6	632.5	N	Chain2 Δ9	672.6	N	
PC (18:3(6,9,12)/16:1(9))	Isomer I	H^+	Chain1 Δ12	686.5	Y	Chain1 Δ6	606.5	N	Chain1 Δ9	646.5	N	Chain2 Δ9	672.5	N	N
	Isomer II	H^+	Chain1 Δ12	712.6	N	Chain1 Δ6	632.5	N	Chain1 Δ9	672.6	N	Chain2 Δ9	698.6	N	
PC (20:3(5,8,11)/14:1(9))	Isomer I	H^+	Chain1 Δ11	644.5	Y	Chain1 Δ5	564.4	N	Chain1 Δ8	604.4	N	Chain2 Δ9	700.6	N	N
	Isomer II	H^+	Chain1 Δ11	670.5	N	Chain1 Δ5	590.5	N	Chain1 Δ8	630.5	N	Chain2 Δ9	726.6	N	
PC (20:3(8,11,14)/14:1(9))	Isomer I	H^+	Chain1 Δ11	646.5	N	Chain1 Δ14	686.5	Y	Chain1 Δ8	606.5	N	Chain2 Δ9	700.6	N	N
	Isomer II	H^+	Chain1 Δ11	672.6	N	Chain1 Δ14	712.6	N	Chain1 Δ8	632.5	N	Chain2 Δ9	726.6	N	
PC (20:4(5,8,11,14)/14:0)	Isomer I	H^+	Chain1 Δ11	646.5	N	Chain1 Δ14	686.5	Y	Chain1 Δ5	566.4	Y	Chain1 Δ8	606.5	N	N
	Isomer II	H^+	Chain1 Δ11	672.6	N	Chain1 Δ14	712.6	N	Chain1 Δ5	592.5	N	Chain1 Δ8	632.5	N	
PC (12:0/22:4(7,10,13,16))	Isomer I	H^+	Chain2 Δ10	606.5	N	Chain2 Δ13	646.5	N	Chain2 Δ16	686.5	Y	Chain2 Δ7	566.4	Y	N
	Isomer II	H^+	Chain2 Δ10	632.5	N	Chain2 Δ13	672.6	N	Chain2 Δ16	712.6	N	Chain2 Δ7	592.5	N	
PC (22:4(7,1	Isomer I	H^+	Chain1 Δ10	606.5	N	Chain1 Δ13	646.5	N	Chain1 Δ16	686.5	Y	Chain1 Δ7	566.4	Y	N

0,13,16)/12:0)	Isomer II	H^+	Chain1 Δ10	632.5	N	Chain1 Δ13	672.6	N	Chain1 Δ16	712.6	N	Chain1 Δ7	592.5	N	
PC (12:0/20:1(11))	Isomer I	Na	Chain2 Δ11	644.5	Y										N
	Isomer II	Na	Chain2 Δ11	670.5	N										
PC (15:1(9)/17:0)	Isomer I	Na	Chain1 Δ9	686.5	Y										N
	Isomer II	Na	Chain1 Δ9	712.6	N										
PC (17:0/15:1(9))	Isomer I	Na	Chain2 Δ9	686.5	Y										N
	Isomer II	Na	Chain2 Δ9	712.6	N										
PC (20:1(11)/12:0)	Isomer I	Na	Chain1 Δ11	644.5	Y										N
	Isomer II	Na	Chain1 Δ11	670.5	N										
PC (18:4(6,9,12,15)/16:0)	Isomer I	H	Chain1 Δ12	688.6	N	Chain1 Δ15	728.6	N	Chain1 Δ6	608.5	N	Chain1 Δ9	648.5	N	Y
	Isomer II	H	Chain1 Δ12	714.6	N	Chain1 Δ15	754.7	N	Chain1 Δ6	634.5	N	Chain1 Δ9	674.6	N	
PC (16:0/16:1(9))	Isomer I	Na	Chain2 Δ9	672.5	N										Y
	Isomer II	Na	Chain2 Δ9	698.6	N										
PC (14:0/18:1(11))	Isomer I	Na	Chain2 Δ11	672.5	N										Y
	Isomer II	Na	Chain2 Δ11	698.6	N										
PC (14:1(9)/18:0)	Isomer I	Na	Chain1 Δ9	700.6	N										Y
	Isomer II	Na	Chain1 Δ9	726.6	N										
PC (16:1(9)/16:0)	Isomer I	Na	Chain1 Δ9	672.5	N										Y
	Isomer II	Na	Chain1 Δ9	698.6	N										
PC (18:0/14:1(9))	Isomer I	Na	Chain2 Δ9	700.6	N										Y
	Isomer II	Na	Chain2 Δ9	726.6	N										
PC (18:1(11)/14:0)	Isomer I	Na	Chain1 Δ11	672.5	N										Y
	Isomer II	Na	Chain1 Δ11	698.6	N										

PC (13:0/19:1(9))	Isomer I	Na	Chain2 Δ9	630.5	N		N
	Isomer II	Na	Chain2 Δ9	656.5	N		
PC (15:0/17:1(9))	Isomer I	Na	Chain2 Δ9	658.5	N		N
	Isomer II	Na	Chain2 Δ9	684.6	N		
PC (17:1(9)/15:0)	Isomer I	Na	Chain1 Δ9	658.5	N		N
	Isomer II	Na	Chain1 Δ9	684.6	N		
PC (19:1(9)/13:0)	Isomer I	Na	Chain1 Δ9	630.5	N		N
	Isomer II	Na	Chain1 Δ9	656.5	N		

[1]Species labeled in red front indicate Identified species with matched MS/MS fragments (from prediction) and carbon numbers in fatty acid tails.

[2]Comparison with experimental MS/MS spectra of the corresponding PB products.

[3]Comparison with results in Table S4.

Table S4-11. ***Predicted diagnostic ions from m/z 838.59 (acetone PB products of m/z 780.55) at the single-cell level***

Lipids[1]	PB products	Adduct	Double bond position	*m/z* of predicted fragments	MS/MS Match[2]	Double bond position	*m/z* of predicted fragments	MS/MS Match[2]	Double bond position	*m/z* of predicted fragments	MS/MS Match[2]	Double bond position	*m/z* of predicted fragments	MS/MS Match[2]	Double bond position	*m/z* of predicted fragments	MS/MS Match[2]	Carbon number match[3]
PC (16:1(9)/20:4(5,8,11,14))	H^+	Isomer I	Chain1 Δ9	698.5	N	Chain2 Δ11	672.5	N	Chain2 Δ14	712.6	Y	Chain2 Δ5	592.4	N	Chain2 Δ8	632.5	N	**Y**
	H^+	Isomer II	Chain1 Δ9	724.6	N	Chain2 Δ11	698.6	N	Chain2 Δ14	738.6	Y	Chain2 Δ5	618.5	N	Chain2 Δ8	658.5	N	
PC (16:1(7)/20:4(5,8,11,14))	H^+	Isomer I	Chain1 Δ7	670.5	N	Chain2 Δ11	672.5	N	Chain2 Δ14	712.6	Y	Chain2 Δ5	592.4	N	Chain2 Δ8	632.5	N	**Y**
	H^+	Isomer II	Chain1 Δ7	696.6	N	Chain2 Δ11	698.6	N	Chain2 Δ14	738.6	Y	Chain2 Δ5	618.5	N	Chain2 Δ8	658.5	N	
PC (20:4(5,8,11,14)/16:1(9))	H^+	Isomer I	Chain1 Δ11	672.5	N	Chain1 Δ14	712.6	Y	Chain1 Δ5	592.4	N	Chain1 Δ8	632.5	N	Chain2 Δ9	698.5	N	**Y**
	H^+	Isomer II	Chain1 Δ11	698.6	N	Chain1 Δ14	738.6	Y	Chain1 Δ5	618.5	N	Chain1 Δ8	658.5	N	Chain2 Δ9	724.6	N	
PC (16:1(9)/20:4(8,11,14,17))	H^+	Isomer I	Chain1 Δ9	698.5	N	Chain2 Δ11	674.5	N	Chain2 Δ14	714.6	Y	Chain2 Δ17	754.6	N	Chain2 Δ8	634.5	N	**Y**
	H^+	Isomer II	Chain1 Δ9	724.6	N	Chain2 Δ11	700.6	N	Chain2 Δ14	740.6	N	Chain2 Δ17	780.7	Y	Chain2 Δ8	660.6	N	
PC (18:1(11)/18:4(6,9,12,15))	H^+	Isomer I	Chain1 Δ11	698.5	N	Chain2 Δ12	714.6	Y	Chain2 Δ15	754.6	N	Chain2 Δ6	634.5	N	Chain2 Δ9	674.5	N	**Y**
	H^+	Isomer II	Chain1 Δ11	724.6	N	Chain2 Δ12	740.6	N	Chain2 Δ15	780.7	Y	Chain2 Δ6	660.6	N	Chain2 Δ9	700.6	N	
PC (18:1(9)/18:4(6,9,12,15))	H^+	Isomer I	Chain1 Δ9	670.5	N	Chain2 Δ12	714.6	Y	Chain2 Δ15	754.6	N	Chain2 Δ6	634.5	N	Chain2 Δ9	674.5	N	**Y**
	H^+	Isomer II	Chain1 Δ9	696.6	N	Chain2 Δ12	740.6	N	Chain2 Δ15	780.7	Y	Chain2 Δ6	660.6	N	Chain2 Δ9	700.6	N	
PC (18:4(6,9,12,15)/18:1(11))	H^+	Isomer I	Chain1 Δ12	714.6	Y	Chain1 Δ15	754.6	N	Chain1 Δ6	634.5	N	Chain1 Δ9	674.5	N	Chain2 Δ11	698.5	N	**Y**
	H^+	Isomer II	Chain1 Δ12	740.6	N	Chain1 Δ15	780.7	Y	Chain1 Δ6	660.6	N	Chain1 Δ9	700.6	N	Chain2 Δ11	724.6	N	
PC (18:4(6,9,1	H^+	Isomer I	Chain1 Δ12	714.6	Y	Chain1 Δ15	754.6	N	Chain1 Δ6	634.5	N	Chain1 Δ9	674.5	N	Chain2 Δ9	670.5	N	**Y**

2,15)/18:1(9))	H^+	Isomer II	Chain1 Δ12	740.6	N	Chain1 Δ15	780.7	Y	Chain1 Δ6	660.6	N	Chain1 Δ9	700.6	N	Chain2 Δ9	696.6	N	
PC (20:4(8,11,14,17)/16:1(9))	H^+	Isomer I	Chain1 Δ11	674.5	N	Chain1 Δ14	714.6	Y	Chain1 Δ17	754.6	N	Chain1 Δ8	634.5	N	Chain2 Δ9	698.5	N	Y
	H^+	Isomer II	Chain1 Δ11	700.6	N	Chain1 Δ14	740.6	N	Chain1 Δ17	780.7	Y	Chain1 Δ8	660.6	N	Chain2 Δ9	724.6	N	
PC (14:0/20:2(11,14))	Na	Isomer I	Chain2 Δ11	672.5	N	Chain2 Δ14	712.6	Y										Y
	Na	Isomer II	Chain2 Δ11	698.6	N	Chain2 Δ14	738.6	Y										
PC (20:2(11,14)/14:0)	Na	Isomer I	Chain1 Δ11	672.5	N	Chain1 Δ14	712.6	Y										Y
	Na	Isomer II	Chain1 Δ11	698.6	N	Chain1 Δ14	738.6	Y										
PC (18:2(9,12)/18:3(6,9,12))	H^+	Isomer I	Chain1 Δ12	712.6	Y	Chain1 Δ9	672.5	N	Chain2 Δ12	712.6	Y	Chain2 Δ6	632.5	N	Chain2 Δ9	672.5	N	Y*
	H^+	Isomer II	Chain1 Δ12	738.6	Y	Chain1 Δ9	698.6	N	Chain2 Δ12	738.6	Y	Chain2 Δ6	658.5	N	Chain2 Δ9	698.6	N	
PC (18:2(9,12)/18:3(9,12,15))	H^+	Isomer I	Chain1 Δ12	712.6	Y	Chain1 Δ9	672.5	N	Chain2 Δ12	714.6	Y	Chain2 Δ15	754.6	N	Chain2 Δ9	674.5	N	Y*
	H^+	Isomer II	Chain1 Δ12	738.6	Y	Chain1 Δ9	698.6	N	Chain2 Δ12	740.6	N	Chain2 Δ15	780.7	Y	Chain2 Δ9	700.6	N	
PC (18:3(6,9,12)/18:2(9,12))	H^+	Isomer I	Chain1 Δ12	712.6	Y	Chain1 Δ6	632.5	N	Chain1 Δ9	672.5	N	Chain2 Δ12	712.6	Y	Chain2 Δ9	672.5	N	Y*
	H^+	Isomer II	Chain1 Δ12	738.6	Y	Chain1 Δ6	658.5	N	Chain1 Δ9	698.6	N	Chain2 Δ12	738.6	Y	Chain2 Δ9	698.6	N	
PC (16:0/20:5(5,8,11,14,17))	H^+	Isomer I	Chain2 Δ11	674.5	N	Chain2 Δ14	714.6	Y	Chain2 Δ17	754.6	N	Chain2 Δ5	594.5	N	Chain2 Δ8	634.5	N	Y*
	H^+	Isomer II	Chain2 Δ11	700.6	N	Chain2 Δ14	740.6	N	Chain2 Δ17	780.7	Y	Chain2 Δ5	620.5	N	Chain2 Δ8	660.6	N	
PC (20:5(5,8,11,14,17)/16:0)	H^+	Isomer I	Chain1 Δ11	674.5	N	Chain1 Δ14	714.6	Y	Chain1 Δ17	754.6	N	Chain1 Δ5	594.5	N	Chain1 Δ8	634.5	N	Y*
	H^+	Isomer II	Chain1 Δ11	700.6	N	Chain1 Δ14	740.6	N	Chain1 Δ17	780.7	Y	Chain1 Δ5	620.5	N	Chain1 Δ8	660.6	N	
PC (16:0/18:2(10,12))	Na	Isomer I	Chain2 Δ10	686.5	N	Chain2 Δ12	712.6	Y										Y*

	Na	Isomer II	Chain2 Δ10	712.6	Y	Chain2 Δ12	738.6	Y										
PC (16:0/18:2(9,12))	Na	Isomer I	Chain2 Δ12	712.6	Y	Chain2 Δ9	672.5	N										Y*
	Na	Isomer II	Chain2 Δ12	738.6	Y	Chain2 Δ9	698.6	N										
PC (18:2(9,12)/16:0)	Na	Isomer I	Chain1 Δ12	712.6	Y	Chain1 Δ9	672.5	N										Y*
	Na	Isomer II	Chain1 Δ12	738.6	Y	Chain1 Δ9	698.6	N										
PC (14:0/22:5(4,7,10,13,16))	H^+	Isomer I	Chain2 Δ10	632.5	N	Chain2 Δ13	672.5	N	Chain2 Δ16	712.6	Y	Chain2 Δ4	552.4	N	Chain2 Δ7	592.4	N	N
	H^+	Isomer II	Chain2 Δ10	658.5	N	Chain2 Δ13	698.6	N	Chain2 Δ16	738.6	Y	Chain2 Δ4	578.5	N	Chain2 Δ7	618.5	N	
PC (14:1(9)/22:4(7,10,13,16))	H^+	Isomer I	Chain1 Δ9	726.6	N	Chain2 Δ10	632.5	N	Chain2 Δ13	672.5	N	Chain2 Δ16	712.6	Y	Chain2 Δ7	592.4	N	N
	H^+	Isomer II	Chain1 Δ9	752.6	N	Chain2 Δ10	658.5	N	Chain2 Δ13	698.6	N	Chain2 Δ16	738.6	Y	Chain2 Δ7	618.5	N	
PC (22:4(7,10,13,16)/14:1(9))	H^+	Isomer I	Chain1 Δ10	632.5	N	Chain1 Δ13	672.5	N	Chain1 Δ16	712.6	Y	Chain1 Δ7	592.4	N	Chain2 Δ9	726.6	N	N
	H^+	Isomer II	Chain1 Δ10	658.5	N	Chain1 Δ13	698.6	N	Chain1 Δ16	738.6	Y	Chain1 Δ7	618.5	N	Chain2 Δ9	752.6	N	
PC (22:5(4,7,10,13,16)/14:0)	H^+	Isomer I	Chain1 Δ10	632.5	N	Chain1 Δ13	672.5	N	Chain1 Δ16	712.6	Y	Chain1 Δ4	552.4	N	Chain1 Δ7	592.4	N	N
	H^+	Isomer II	Chain1 Δ10	658.5	N	Chain1 Δ13	698.6	N	Chain1 Δ16	738.6	Y	Chain1 Δ4	578.5	N	Chain1 Δ7	618.5	N	
PC (18:3(9,12,15)/18:2(9,12))	H^+	Isomer I	Chain1 Δ12	714.6	Y	Chain1 Δ15	754.6	N	Chain1 Δ9	674.5	N	Chain2 Δ12	712.6	Y	Chain2 Δ9	672.5	N	N
	H^+	Isomer II	Chain1 Δ12	740.6	N	Chain1 Δ15	780.7	Y	Chain1 Δ9	700.6	N	Chain2 Δ12	738.6	Y	Chain2 Δ9	698.6	N	
PC (14:0/22:5(7,10,13,16,19))	H^+	Isomer I	Chain2 Δ10	634.5	N	Chain2 Δ13	674.5	N	Chain2 Δ16	714.6	Y	Chain2 Δ19	754.6	N	Chain2 Δ7	594.5	N	N
	H^+	Isomer II	Chain2 Δ10	660.6	N	Chain2 Δ13	700.6	N	Chain2 Δ16	740.6	N	Chain2 Δ19	780.7	Y	Chain2 Δ7	620.5	N	
PC (22:5(7,10,	H^+	Isomer I	Chain1 Δ10	634.5	N	Chain1 Δ13	674.5	N	Chain1 Δ16	714.6	Y	Chain1 Δ19	754.6	N	Chain1 Δ7	594.5	N	N

13,16,19)/14:0)	H^+	Isomer II	Chain1 Δ10	660.6	N	Chain1 Δ13	700.6	N	Chain1 Δ16	740.6	N	Chain1 Δ19	780.7	Y	Chain1 Δ7	620.5	N	
PC (12:0/22:2(13,16))	Na	Isomer I	Chain2 Δ13	672.5	N	Chain2 Δ16	712.6	Y										N
	Na	Isomer II	Chain2 Δ13	698.6	N	Chain2 Δ16	738.6	Y										
PC (15:1(9)/19:1(9))	Na	Isomer I	Chain1 Δ9	712.6	Y	Chain2 Δ9	656.5	N										N
	Na	Isomer II	Chain1 Δ9	738.6	Y	Chain2 Δ9	682.5	N										
PC (19:1(9)/15:1(9))	Na	Isomer I	Chain1 Δ9	656.5	N	Chain2 Δ9	712.6	Y										N
	Na	Isomer II	Chain1 Δ9	682.5	N	Chain2 Δ9	738.6	Y										
PC (22:2(13,16)/12:0)	Na	Isomer I	Chain1 Δ13	672.5	N	Chain1 Δ16	712.6	Y										N
	Na	Isomer II	Chain1 Δ13	698.6	N	Chain1 Δ16	738.6	Y										
PC (17:0/17:2(9,12))	Na	Isomer I	Chain2 Δ12	726.6	N	Chain2 Δ9	686.5	N										N
	Na	Isomer II	Chain2 Δ12	752.6	N	Chain2 Δ9	712.6	Y										
PC (17:2(9,12)/17:0)	Na	Isomer I	Chain1 Δ12	726.6	N	Chain1 Δ9	686.5	N										N
	Na	Isomer II	Chain1 Δ12	752.6	N	Chain1 Δ9	712.6	Y										
PE (15:1(9)/22:1(11))	Na	Isomer I	Chain1 Δ9	712.6	Y	Chain2 Δ11	642.5	N										N
	Na	Isomer II	Chain1 Δ9	738.6	Y	Chain2 Δ11	668.5	N										
PE (17:0/20:2(11,14))	Na	Isomer I	Chain2 Δ11	672.5	N	Chain2 Δ14	712.6	Y										N
	Na	Isomer II	Chain2 Δ11	698.6	N	Chain2 Δ14	738.6	Y										
PE (18:2(9,12)/19:0)	Na	Isomer I	Chain1 Δ12	712.6	Y	Chain1 Δ9	672.5	N										N

	Na	Isomer II	Chain1 Δ12	738.6	Y	Chain1 Δ9	698.6	N											
PE (19:0/18:2(9,12))	Na	Isomer I	Chain2 Δ12	712.6	Y	Chain2 Δ9	672.5	N											N
	Na	Isomer II	Chain2 Δ12	738.6	Y	Chain2 Δ9	698.6	N											
PE (20:2(11,14)/17:0)	Na	Isomer I	Chain1 Δ11	672.5	N	Chain1 Δ14	712.6	Y											N
	Na	Isomer II	Chain1 Δ11	698.6	N	Chain1 Δ14	738.6	Y											
PE (22:1(11)/15:1(9))	Na	Isomer I	Chain1 Δ11	642.5	N	Chain2 Δ9	712.6	Y											N
	Na	Isomer II	Chain1 Δ11	668.5	N	Chain2 Δ9	738.6	Y											
PE (15:0/22:2(13,16))	Na	Isomer I	Chain2 Δ13	672.5	N	Chain2 Δ16	712.6	Y											N
	Na	Isomer II	Chain2 Δ13	698.6	N	Chain2 Δ16	738.6	Y											
PE (22:2(13,16)/15:0)	Na	Isomer I	Chain1 Δ13	672.5	N	Chain1 Δ16	712.6	Y											N
	Na	Isomer II	Chain1 Δ13	698.6	N	Chain1 Δ16	738.6	Y											
PE (17:2(9,12)/20:0)	Na	Isomer I	Chain1 Δ12	726.6	N	Chain1 Δ9	686.6	N											N
	Na	Isomer II	Chain1 Δ12	752.6	N	Chain1 Δ9	712.6	Y											
PE (20:0/17:2(9,12))	Na	Isomer I	Chain2 Δ12	726.6	N	Chain2 Δ9	686.6	N											N
	Na	Isomer II	Chain2 Δ12	752.6	N	Chain2 Δ9	712.6	Y											
PC (18:4(2,4,6,11)/18:1(11))	H^+	Isomer I	Chain1 Δ11	698.5	N	Chain1 Δ2	578.4	N	Chain1 Δ4	604.4	N	Chain1 Δ6	630.5	N	Chain2 Δ11	698.5	N		Y
	H^+	Isomer II	Chain1 Δ11	724.6	N	Chain1 Δ2	604.5	N	Chain1 Δ4	630.5	N	Chain1 Δ6	656.5	N	Chain2 Δ11	724.6	N		
PC (16:1(2)/18:1(9))	Na	Isomer I	Chain1 Δ2	600.4	N	Chain2 Δ9	670.5	N											Y

	Na	Isomer II	Chain1 Δ2	626.5	N	Chain2 Δ9	696.6	N		
PC (16:1(7)/18:1(9))	Na	Isomer I	Chain1 Δ7	670.5	N	Chain2 Δ9	670.5	N		Y
	Na	Isomer II	Chain1 Δ7	696.6	N	Chain2 Δ9	696.6	N		
PC (16:1(9)/18:1(9))	Na	Isomer I	Chain1 Δ9	698.5	N	Chain2 Δ9	670.5	N		Y
	Na	Isomer II	Chain1 Δ9	724.6	N	Chain2 Δ9	696.6	N		
PC (16:1(9)/18:1(11))	Na	Isomer I	Chain1 Δ9	698.5	N	Chain2 Δ11	698.5	N		Y
	Na	Isomer II	Chain1 Δ9	724.6	N	Chain2 Δ11	724.6	N		
PC (18:1(11)/16:1(9))	Na	Isomer I	Chain1 Δ11	698.5	N	Chain2 Δ9	698.5	N		Y
	Na	Isomer II	Chain1 Δ11	724.6	N	Chain2 Δ9	724.6	N		
PC (18:1(9)/16:1(9))	Na	Isomer I	Chain1 Δ9	670.5	N	Chain2 Δ9	698.5	N		Y
	Na	Isomer II	Chain1 Δ9	696.6	N	Chain2 Δ9	724.6	N		
PC (16:0/18:2(11,13))	Na	Isomer I	Chain2 Δ11	700.6	N	Chain2 Δ13	726.6	N		Y*
	Na	Isomer II	Chain2 Δ11	726.6	N	Chain2 Δ13	752.6	N		
PC (16:0/18:2(2,4))	Na	Isomer I	Chain2 Δ2	574.4	N	Chain2 Δ4	600.4	N		Y*
	Na	Isomer II	Chain2 Δ2	600.4	N	Chain2 Δ4	626.5	N		
PC (16:0/18:2(6,9))	Na	Isomer I	Chain2 Δ6	630.5	N	Chain2 Δ9	670.5	N		Y*
	Na	Isomer II	Chain2 Δ6	656.5	N	Chain2 Δ9	696.6	N		
PC (16:0/18:2(9,11))	Na	Isomer I	Chain2 Δ11	698.5	N	Chain2 Δ9	672.5	N		Y*

	Na	Isomer II	Chain2 Δ11	724.6	N	Chain2 Δ9	698.6	N		
PC (18:1(9)/16:1(3))	Na	Isomer I	Chain1 Δ9	670.5	N	Chain2 Δ3	614.4	N		Y*
	Na	Isomer II	Chain1 Δ9	696.6	N	Chain2 Δ3	640.5	N		
PC (18:2(2,4)/16:0)	Na	Isomer I	Chain1 Δ2	574.4	N	Chain1 Δ4	600.4	N		Y*
	Na	Isomer II	Chain1 Δ2	600.4	N	Chain1 Δ4	626.5	N		
PC (18:2(6,9)/16:0)	Na	Isomer I	Chain1 Δ6	630.5	N	Chain1 Δ9	670.5	N		Y*
	Na	Isomer II	Chain1 Δ6	656.5	N	Chain1 Δ9	696.6	N		
PC (17:1(10)/17:1(10))	Na	Isomer I	Chain1 Δ10	698.5	N	Chain2 Δ10	698.5	N		N
	Na	Isomer II	Chain1 Δ10	724.6	N	Chain2 Δ10	724.6	N		
PC (17:1(9)/17:1(9))	Na	Isomer I	Chain1 Δ9	684.5	N	Chain2 Δ9	684.5	N		N
	Na	Isomer II	Chain1 Δ9	710.6	N	Chain2 Δ9	710.6	N		
PC (18:0/16:2(2,4))	Na	Isomer I	Chain2 Δ2	602.4	N	Chain2 Δ4	628.4	N		N
	Na	Isomer II	Chain2 Δ2	628.5	N	Chain2 Δ4	654.5	N		
PC (14:1(9)/20:1(11))	Na	Isomer I	Chain1 Δ9	726.6	N	Chain2 Δ11	670.5	N		N
	Na	Isomer II	Chain1 Δ9	752.6	N	Chain2 Δ11	696.6	N		
PC (20:1(11)/14:1(9))	Na	Isomer I	Chain1 Δ11	670.5	N	Chain2 Δ9	726.6	N		N
	Na	Isomer II	Chain1 Δ11	696.6	N	Chain2 Δ9	752.6	N		
PE (17:1(9)/20:1(11))	Na	Isomer I	Chain1 Δ9	684.5	N	Chain2 Δ11	670.5	N		N

	Na	Isomer II	Chain1 Δ9	710.6	N	Chain2 Δ11	696.6	N		
PE (18:1(9)/19:1(9))	Na	Isomer I	Chain1 Δ9	670.5	N	Chain2 Δ9	656.5	N		N
	Na	Isomer II	Chain1 Δ9	696.6	N	Chain2 Δ9	682.5	N		
PE (19:1(9)/18:1(9))	Na	Isomer I	Chain1 Δ9	656.5	N	Chain2 Δ9	670.5	N		N
	Na	Isomer II	Chain1 Δ9	682.5	N	Chain2 Δ9	696.6	N		
PE (20:1(11)/17:1(9))	Na	Isomer I	Chain1 Δ11	670.5	N	Chain2 Δ9	684.5	N		N
	Na	Isomer II	Chain1 Δ11	696.6	N	Chain2 Δ9	710.6	N		

[1]Species labeled in red front indicate Identified species with matched MS/MS fragments (from prediction) and carbon numbers in fatty acid tails.

[2]Comparison with experimental MS/MS spectra of the corresponding PB products.

[3]Comparison with results in Table S4.

*Agreement is only obtained from cell lysates (not from single cells).

Table S4-12. ***Predicted diagnostic ions from m/z 814.49 (acetone PB products of m/z 756.54) at the single-cell level***

Lipids[1]	PB products	Adduct	Double bond position	*m/z* of predicted fragments	MS/MS Match[2]	Double bond position	*m/z* of predicted fragments	MS/MS Match[2]	Double bond position	*m/z* of predicted fragments	MS/MS Match[2]	Carbon number match[3]
PC (16:1(7)/18:2(9,12))	Isomer I	H^+	Chain1 Δ7	646.5	**Y**	Chain2 Δ12	688.6	N	Chain2 Δ9	648.5	N	**Y**
	Isomer II	H^+	Chain1 Δ7	672.6	**Y**	Chain2 Δ12	714.6	N	Chain2 Δ9	674.6	N	
PC (17:2(9,12)/17:1(9))	Isomer I	H^+	Chain1 Δ12	702.6	N	Chain1 Δ9	662.5	N	Chain2 Δ9	660.5	N	**Y**
	Isomer II	H^+	Chain1 Δ12	728.6	**Y**	Chain1 Δ9	688.6	N	Chain2 Δ9	686.6	N	
PC (17:1(9)/17:2(9,12))	Isomer I	H^+	Chain1 Δ9	660.5	N	Chain2 Δ12	702.6	N	Chain2 Δ9	662.5	N	**Y**
	Isomer II	H^+	Chain1 Δ9	686.6	N	Chain2 Δ12	728.6	**Y**	Chain2 Δ9	688.6	N	
PC (14:0/20:3(5,8,11))	Isomer I	H^+	Chain2 Δ11	646.5	Y	Chain2 Δ5	566.4	N	Chain2 Δ8	606.5	N	N
	Isomer II	H^+	Chain2 Δ11	672.6	Y	Chain2 Δ5	592.5	N	Chain2 Δ8	632.5	N	
PC (14:1(9)/20:2(11,14))	Isomer I	H^+	Chain1 Δ9	702.6	N	Chain2 Δ11	648.5	N	Chain2 Δ14	688.6	N	N
	Isomer II	H^+	Chain1 Δ9	728.6	Y	Chain2 Δ11	674.6	N	Chain2 Δ14	714.6	N	
PC (20:3(5,8,11)/14:0)	Isomer I	H^+	Chain1 Δ11	646.5	Y	Chain1 Δ5	566.4	N	Chain1 Δ8	606.5	N	N
	Isomer II	H^+	Chain1 Δ11	672.6	Y	Chain1 Δ5	592.5	N	Chain1 Δ8	632.5	N	
	Isomer I	H^+	Chain1 Δ9	674.5	N	Chain2 Δ12	688.6	N	Chain2 Δ9	648.5	N	Y

PC (16:1(9)/18:2(9,12))	Isomer II	H^+	Chain1 Δ9	700.6	N	Chain2 Δ12	714.6	N	Chain2 Δ9	674.6	N	
PC (18:2(9,12)/16:1(9))	Isomer I	H^+	Chain1 Δ12	688.6	N	Chain1 Δ9	648.5	N	Chain2 Δ9	674.5	N	Y
	Isomer II	H^+	Chain1 Δ12	714.6	N	Chain1 Δ9	674.6	N	Chain2 Δ9	700.6	N	
PC (18:3(6,9,12)/16:0)	Isomer I	H^+	Chain1 Δ12	688.6	N	Chain1 Δ6	608.5	N	Chain1 Δ9	648.5	N	Y*
	Isomer II	H^+	Chain1 Δ12	714.6	N	Chain1 Δ6	634.5	N	Chain1 Δ9	674.6	N	
PC (18:3(9,12,15)/16:0)	Isomer I	H^+	Chain1 Δ12	690.6	N	Chain1 Δ15	730.6	N	Chain1 Δ9	650.5	N	Y*
	Isomer II	H^+	Chain1 Δ12	716.6	N	Chain1 Δ15	756.7	N	Chain1 Δ9	676.6	N	
PC (16:0/18:3(5,9,12))	Isomer I	H^+	Chain2 Δ12	688.6	N	Chain2 Δ5	594.5	N	Chain2 Δ9	648.5	N	Y*
	Isomer II	H^+	Chain2 Δ12	714.6	N	Chain2 Δ5	620.5	N	Chain2 Δ9	674.6	N	
PC (16:0/18:3(6,9,12))	Isomer I	H^+	Chain2 Δ12	688.6	N	Chain2 Δ6	608.5	N	Chain2 Δ9	648.5	N	Y*
	Isomer II	H^+	Chain2 Δ12	714.6	N	Chain2 Δ6	634.5	N	Chain2 Δ9	674.6	N	
PC (16:0/18:3(9,12,15))	Isomer I	H^+	Chain2 Δ12	690.6	N	Chain2 Δ15	730.6	N	Chain2 Δ9	650.5	N	Y*
	Isomer II	H^+	Chain2 Δ12	716.6	N	Chain2 Δ15	756.7	N	Chain2 Δ9	676.6	N	
PC (20:2(11,14)/14:1(9))	Isomer I	H^+	Chain1 Δ11	648.5	N	Chain1 Δ14	688.6	N	Chain2 Δ9	702.6	N	N
	Isomer II	H^+	Chain1 Δ11	674.6	N	Chain1 Δ14	714.6	N	Chain2 Δ9	728.6	Y	

PC (15:0/19:3(9,12,15))	Isomer I	H^+	Chain2 Δ12	676.6	N	Chain2 Δ15	716.6	N	Chain2 Δ9	636.5	N	N
	Isomer II	H^+	Chain2 Δ12	702.6	N	Chain2 Δ15	742.7	N	Chain2 Δ9	662.6	N	
PC (14:0/20:3(8,11,14))	Isomer I	H^+	Chain2 Δ11	648.5	N	Chain2 Δ14	688.6	N	Chain2 Δ8	608.5	N	N
	Isomer II	H^+	Chain2 Δ11	674.6	N	Chain2 Δ14	714.6	N	Chain2 Δ8	634.5	N	
PC (20:3(8,11,14)/14:0)	Isomer I	H^+	Chain1 Δ11	648.5	N	Chain1 Δ14	688.6	N	Chain1 Δ8	608.5	N	N
	Isomer II	H^+	Chain1 Δ11	674.6	N	Chain1 Δ14	714.6	N	Chain1 Δ8	634.5	N	

[1]Species labeled in red front indicate Identified species with matched MS/MS fragments (from prediction) and carbon numbers in fatty acid tails.

[2]Comparison with experimental MS/MS spectra of the corresponding PB products.

[3]Comparison with results in Table S4.

*Agreement is only obtained from cell lysates (not from single cells).

Table S4-13. ***Predicted diagnostic ions from m/z 463.33 (benzophenone PB products of m/z 281.25) at the single-cell level***

Lipids[1]	PB products	Adduct	Double bond position	*m/z* of predicted fragments	MS/MS Match[2]
FA (18:1(9))	Isomer I	H^-	Chain1 Δ9	171.1	**Y**
	Isomer II	H^-	Chain1 Δ9	321.2	**Y**
FA (18:1(2))	Isomer I	H^-	Chain1 Δ2	73.0	N
	Isomer II	H^-	Chain1 Δ2	223.1	N
FA (18:1(3))	Isomer I	H^-	Chain1 Δ3	87.0	N
	Isomer II	H^-	Chain1 Δ3	237.1	N
FA (18:1(4))	Isomer I	H^-	Chain1 Δ4	101.0	N
	Isomer II	H^-	Chain1 Δ4	251.1	N
FA (18:1(5))	Isomer I	H^-	Chain1 Δ5	115.1	N
	Isomer II	H^-	Chain1 Δ5	265.1	N
FA (18:1(6))	Isomer I	H^-	Chain1 Δ6	129.1	N
	Isomer II	H^-	Chain1 Δ6	279.2	N
FA (18:1(7))	Isomer I	H^-	Chain1 Δ7	143.1	N
	Isomer II	H^-	Chain1 Δ7	293.2	N
FA (18:1(8))	Isomer I	H^-	Chain1 Δ8	157.1	N
	Isomer II	H^-	Chain1 Δ8	307.2	N
FA (18:1(10))	Isomer I	H^-	Chain1 Δ10	185.2	N
	Isomer II	H^-	Chain1 Δ10	335.2	N
FA (18:1(11))	Isomer I	H^-	Chain1 Δ11	199.2	N
	Isomer II	H^-	Chain1 Δ11	349.3	N
FA (18:1(12))	Isomer I	H^-	Chain1 Δ12	213.2	N
	Isomer II	H^-	Chain1 Δ12	363.3	N
FA (18:1(13))	Isomer I	H^-	Chain1 Δ13	227.2	N

	Isomer II	H^-	Chain1 Δ13	377.3	N
FA (18:1(14))	Isomer I	H^-	Chain1 Δ14	241.2	N
	Isomer II	H^-	Chain1 Δ14	391.3	N
FA (18:1(15))	Isomer I	H^-	Chain1 Δ15	255.3	N
	Isomer II	H^-	Chain1 Δ15	405.3	N
FA (18:1(16))	Isomer I	H^-	Chain1 Δ16	269.3	N
	Isomer II	H^-	Chain1 Δ16	419.4	N
FA (18:1(17))	Isomer I	H^-	Chain1 Δ17	283.3	N
	Isomer II	H^-	Chain1 Δ17	433.4	N

[1]Species labeled in red front indicate Identified species with matched MS/MS fragments (from prediction) and carbon numbers in fatty acid tails.

[2]Comparison with experimental MS/MS spectra of the corresponding PB products.

Table S4-14. ***Predicted diagnostic ions from m/z 787.64 (acetone PB products of m/z 729.59) at the single-cell level***

Lipids[1]	PB products	Adduct	Double bond position	*m/z* of predicted fragments	MS/MS Match[2]	Double bond position	*m/z* of predicted fragments	MS/MS Match[2]
SM (d18:1(4)/18:1(9Z))	H^+	Isomer I	Chain1 Δ4	549.4	N	Chain2 Δ9	619.5	N
	H^+	Isomer II	Chain1 Δ4	575.5	N	Chain2 Δ9	645.6	**Y**
SM (d16:1(4)/20:1(11))	H^+	Isomer I	Chain1 Δ4	577.5	N	Chain2 Δ11	619.5	N
	H^+	Isomer II	Chain1 Δ4	603.5	N	Chain2 Δ11	645.6	**Y**
SM (d18:0/18:2(9,12))	H^+	Isomer I	Chain2 Δ12	661.6	N	Chain2 Δ9	621.6	N
	H^+	Isomer II	Chain2 Δ12	687.7	N	Chain2 Δ9	647.6	N
SM (d18:2(4,14)/18:0)	H^+	Isomer I	Chain1 Δ4	551.5	N	Chain1 Δ14	689.6	N
	H^+	Isomer II	Chain1 Δ4	577.5	N	Chain1 Δ14	715.7	N
SM (d19:1(4)/17:1(9))	H^+	Isomer I	Chain1 Δ4	535.4	N	Chain2 Δ9	633.6	N
	H^+	Isomer II	Chain1 Δ4	561.5	N	Chain2 Δ9	659.6	N

[1]Species labeled in red front indicate Identified species with matched MS/MS fragments (from prediction) and carbon numbers in fatty acid tails.

[2]Comparison with experimental MS/MS spectra of the corresponding PB products.

Table S4-15. ***Predicted diagnostic ions from m/z 842.65 (acetone PB products of m/z 784.57) at the single-cell level***

Lipids[1]	PB products	Adduct	Double bond position	*m/z* of predicted fragments	MS/MS Match[2]	Double bond position	*m/z* of predicted fragments	MS/MS Match[2]	Double bond position	*m/z* of predicted fragments	MS/MS Match[2]	Carbon number match
PC (16:0/20:3(11,14,17))	Isomer I	H^+	Chain2 Δ11	678.6	N	Chain2 Δ14	718.6	N	Chain2 Δ17	758.7	N	**Y**
	Isomer II	H^+	Chain2 Δ11	704.6	N	Chain2 Δ14	744.7	N	Chain2 Δ17	784.7	**Y**	
PC (16:0/20:3(5,8,11))	Isomer I	H^+	Chain2 Δ11	674.5	N	Chain2 Δ5	594.5	N	Chain2 Δ8	634.5	N	**Y**
	Isomer II	H^+	Chain2 Δ11	700.6	**Y**	Chain2 Δ5	620.5	N	Chain2 Δ8	660.6	N	
PC (16:0/20:3(5,8,11))	Isomer I	H^+	Chain2 Δ11	674.5	N	Chain2 Δ5	594.5	N	Chain2 Δ8	634.5	N	**Y**
	Isomer II	H^+	Chain2 Δ11	700.6	**Y**	Chain2 Δ5	620.5	N	Chain2 Δ8	660.6	N	
PC (18:0/18:3(9,12,15))	Isomer I	H^+	Chain2 Δ12	718.6	N	Chain2 Δ15	758.7	N	Chain2 Δ9	678.6	N	**Y**
	Isomer II	H^+	Chain2 Δ12	744.7	N	Chain2 Δ15	784.7	**Y**	Chain2 Δ9	704.6	N	
PC (18:1(9)/18:2(6,9))	Isomer I	H^+	Chain1 Δ9	674.5	N	Chain2 Δ6	634.5	N	Chain2 Δ9	674.5	N	**Y**
	Isomer II	H^+	Chain1 Δ9	700.6	**Y**	Chain2 Δ6	660.6	N	Chain2 Δ9	700.6	**Y**	
PC (18:1(9)/18:2(9,12))	Isomer I	H^+	Chain1 Δ9	674.5	N	Chain2 Δ12	716.6	N	Chain2 Δ9	676.6	N	**Y**
	Isomer II	H^+	Chain1 Δ9	700.6	**Y**	Chain2 Δ12	742.7	N	Chain2 Δ9	702.6	N	
PC (18:1(11)/18:2(9,12))	Isomer I	H^+	Chain1 Δ11	702.6	N	Chain2 Δ12	716.6	N	Chain2 Δ9	676.6	N	**Y**
	Isomer II	H^+	Chain1 Δ11	728.6	**Y**	Chain2 Δ12	742.7	N	Chain2 Δ9	702.6	N	
PC (18:2(9,12)/18:1(11))	Isomer I	H^+	Chain1 Δ12	716.6	N	Chain1 Δ9	676.6	N	Chain2 Δ11	702.6	N	**Y**
	Isomer II	H^+	Chain1 Δ12	742.7	N	Chain1 Δ9	702.6	N	Chain2 Δ11	728.6	**Y**	
PC (18:2(9,12)/18:1(9))	Isomer I	H^+	Chain1 Δ12	716.6	N	Chain1 Δ9	676.6	N	Chain2 Δ9	674.5	N	**Y**
	Isomer II	H^+	Chain1 Δ12	742.7	N	Chain1 Δ9	702.6	N	Chain2 Δ9	700.6	**Y**	
PC (18:3(9,12,15)/18:0)	Isomer I	H^+	Chain1 Δ12	718.6	N	Chain1 Δ15	758.7	N	Chain1 Δ9	678.6	N	**Y**
	Isomer II	H^+	Chain1 Δ12	744.7	N	Chain1 Δ15	784.7	**Y**	Chain1 Δ9	704.6	N	
PC (20:3(5,8,11)/16:0)	Isomer I	H^+	Chain1 Δ11	674.5	N	Chain1 Δ5	594.5	N	Chain1 Δ8	634.5	N	**Y**
	Isomer II	H^+	Chain1 Δ11	700.6	**Y**	Chain1 Δ5	620.5	N	Chain1 Δ8	660.6	N	
	Isomer I	H^+	Chain1 Δ11	676.6	N	Chain1 Δ14	716.6	N	Chain2 Δ9	702.6	N	N

PC (20:2(11,14)/ 16:1(9))	Isomer II	H^+	Chain1 Δ11	702.6	N	Chain1 Δ14	742.7	N	Chain2 Δ9	728.6	Y	
PC (16:1(9)/20:2 (11,14))	Isomer I	H^+	Chain1 Δ9	702.6	N	Chain2 Δ11	676.6	N	Chain2 Δ14	716.6	N	N
	Isomer II	H^+	Chain1 Δ9	728.6	Y	Chain2 Δ11	702.6	N	Chain2 Δ14	742.7	N	
PC (16:0/20:3(8, 11,14))	Isomer I	H^+	Chain2 Δ11	676.6	N	Chain2 Δ14	716.6	N	Chain2 Δ8	636.5	N	Y
	Isomer II	H^+	Chain2 Δ11	702.6	N	Chain2 Δ14	742.7	N	Chain2 Δ8	662.6	N	
PC (18:0/18:3(6, 9,12))	Isomer I	H^+	Chain2 Δ12	716.6	N	Chain2 Δ6	636.5	N	Chain2 Δ9	676.6	N	Y
	Isomer II	H^+	Chain2 Δ12	742.7	N	Chain2 Δ6	662.6	N	Chain2 Δ9	702.6	N	
PC (18:3(6,9,12) /18:0)	Isomer I	H^+	Chain1 Δ12	716.6	N	Chain1 Δ6	636.5	N	Chain1 Δ9	676.6	N	Y
	Isomer II	H^+	Chain1 Δ12	742.7	N	Chain1 Δ6	662.6	N	Chain1 Δ9	702.6	N	
PC (20:3(8,11,1 4)/16:0)	Isomer I	H^+	Chain1 Δ11	676.6	N	Chain1 Δ14	716.6	N	Chain1 Δ8	636.5	N	Y
	Isomer II	H^+	Chain1 Δ11	702.6	N	Chain1 Δ14	742.7	N	Chain1 Δ8	662.6	N	
PC (14:1(9)/22:2 (13,16))	Isomer I	H^+	Chain1 Δ9	730.6	N	Chain2 Δ13	676.6	N	Chain2 Δ16	716.6	N	N
	Isomer II	H^+	Chain1 Δ9	756.7	N	Chain2 Δ13	702.6	N	Chain2 Δ16	742.7	N	
PC (22:2(13,16)/ 14:1(9))	Isomer I	H^+	Chain1 Δ13	676.6	N	Chain1 Δ16	716.6	N	Chain2 Δ9	730.6	N	N
	Isomer II	H^+	Chain1 Δ13	702.6	N	Chain1 Δ16	742.7	N	Chain2 Δ9	756.7	N	
PC (17:2(9,12)/1 9:1(9))	Isomer I	H^+	Chain1 Δ12	730.6	N	Chain1 Δ9	690.6	N	Chain2 Δ9	660.5	N	N
	Isomer II	H^+	Chain1 Δ12	756.7	N	Chain1 Δ9	716.6	N	Chain2 Δ9	686.6	N	
PC (19:1(9)/17:2 (9,12))	Isomer I	H^+	Chain1 Δ9	660.5	N	Chain2 Δ12	730.6	N	Chain2 Δ9	690.6	N	N
	Isomer II	H^+	Chain1 Δ9	686.6	N	Chain2 Δ12	756.7	N	Chain2 Δ9	716.6	N	

[1]Species labeled in red front indicate Identified species with matched MS/MS fragments (from prediction) and carbon numbers in fatty acid tails.

[2]Comparison with experimental MS/MS spectra of the corresponding PB products.

[3]Comparison with results in Table S4.

Table S4-16. ***Predicted diagnostic ions from m/z 844.70 (acetone PB products of m/z 786.59) at the single-cell level***

Lipids[1]	PB products	adduct	Double bond position	*m/z* of predicted fragments	MS/MS Match[2]	Double bond position	*m/z* of predicted fragments	MS/MS Match[2]	Carbon number match[3]
PC (18:1(15)/18:1(15))	Isomer I	H^+	Chain1 Δ15	760.7	N	Chain2 Δ15	760.7	N	**Y**
	Isomer II	H^+	Chain1 Δ15	786.7	**Y**	Chain2 Δ15	786.7	**Y**	
PC (18:1(6)/18:1(6))	Isomer I	H^+	Chain1 Δ6	634.5	N	Chain2 Δ6	634.5	N	**Y**
	Isomer II	H^+	Chain1 Δ6	660.6	**Y**	Chain2 Δ6	660.6	**Y**	
PC (18:1(8)/18:1(8))	Isomer I	H^+	Chain1 Δ8	662.5	**Y**	Chain2 Δ8	662.5	**Y**	**Y**
	Isomer II	H^+	Chain1 Δ8	688.6	N	Chain2 Δ8	688.6	N	
PC (17:1(9)/19:1(9))	Isomer I	H^+	Chain1 Δ9	690.6	N	Chain2 Δ9	662.5	Y	N
	Isomer II	H^+	Chain1 Δ9	716.6	N	Chain2 Δ9	688.6	N	
PC (19:1(9)/17:1(9))	Isomer I	H^+	Chain1 Δ9	662.5	Y	Chain2 Δ9	690.6	N	N
	Isomer II	H^+	Chain1 Δ9	688.6	N	Chain2 Δ9	716.6	N	
PC (18:0/18:2(6,9))	Isomer I	H^+	Chain2 Δ6	636.5	N	Chain2 Δ9	676.6	N	N
	Isomer II	H^+	Chain2 Δ6	662.6	Y	Chain2 Δ9	702.6	N	
PC (18:1(10)/18:1(10))	Isomer I	H^+	Chain1 Δ10	690.6	N	Chain2 Δ10	690.6	N	Y
	Isomer II	H^+	Chain1 Δ10	716.6	N	Chain2 Δ10	716.6	N	

PC (18:1(11)/18:1(11))	Isomer I	H^+	Chain1 Δ11	704.6	N	Chain2 Δ11	704.6	N	Y
	Isomer II	H^+	Chain1 Δ11	730.7	N	Chain2 Δ11	730.7	N	
PC (18:1(12)/18:1(12))	Isomer I	H^+	Chain1 Δ12	718.6	N	Chain2 Δ12	718.6	N	Y
	Isomer II	H^+	Chain1 Δ12	744.7	N	Chain2 Δ12	744.7	N	
PC (18:1(13)/18:1(13))	Isomer I	H^+	Chain1 Δ13	732.6	N	Chain2 Δ13	732.6	N	Y
	Isomer II	H^+	Chain1 Δ13	758.7	N	Chain2 Δ13	758.7	N	
PC (18:1(14)/18:1(14))	Isomer I	H^+	Chain1 Δ14	746.7	N	Chain2 Δ14	746.7	N	Y
	Isomer II	H^+	Chain1 Δ14	772.7	N	Chain2 Δ14	772.7	N	
PC (18:1(16)/18:1(16))	Isomer I	H^+	Chain1 Δ16	774.7	N	Chain2 Δ16	774.7	N	Y
	Isomer II	H^+	Chain1 Δ16	800.8	N	Chain2 Δ16	800.8	N	
PC (18:1(17)/18:1(17))	Isomer I	H^+	Chain1 Δ17	788.7	N	Chain2 Δ17	788.7	N	Y
	Isomer II	H^+	Chain1 Δ17	814.8	N	Chain2 Δ17	814.8	N	
PC (18:1(2)/18:1(2))	Isomer I	H^+	Chain1 Δ2	578.4	N	Chain2 Δ2	578.4	N	Y
	Isomer II	H^+	Chain1 Δ2	604.5	N	Chain2 Δ2	604.5	N	
PC (18:1(3)/18:1(3))	Isomer I	H^+	Chain1 Δ3	592.4	N	Chain2 Δ3	592.4	N	Y
	Isomer II	H^+	Chain1 Δ3	618.5	N	Chain2 Δ3	618.5	N	

PC (18:1(4)/18:1(4))	Isomer I	H^+	Chain1 Δ4	606.5	N	Chain2 Δ4	606.5	N	Y
	Isomer II	H^+	Chain1 Δ4	632.5	N	Chain2 Δ4	632.5	N	
PC (18:1(5)/18:1(5))	Isomer I	H^+	Chain1 Δ5	620.5	N	Chain2 Δ5	620.5	N	Y
	Isomer II	H^+	Chain1 Δ5	646.5	N	Chain2 Δ5	646.5	N	
PC (18:1(7)/18:1(7))	Isomer I	H^+	Chain1 Δ7	648.5	N	Chain2 Δ7	648.5	N	Y
	Isomer II	H^+	Chain1 Δ7	674.6	N	Chain2 Δ7	674.6	N	
PC (18:1(9)/18:1(9))	Isomer I	H^+	Chain1 Δ9	676.6	N	Chain2 Δ9	676.6	N	Y
	Isomer II	H^+	Chain1 Δ9	702.6	N	Chain2 Δ9	702.6	N	
PC (16:1(9)/20:1(11))	Isomer I	H^+	Chain1 Δ9	704.6	N	Chain2 Δ11	676.6	N	Y
	Isomer II	H^+	Chain1 Δ9	730.7	N	Chain2 Δ11	702.6	N	
PC (18:1(11)/18:1(9))	Isomer I	H^+	Chain1 Δ11	704.6	N	Chain2 Δ9	676.6	N	Y
	Isomer II	H^+	Chain1 Δ11	730.7	N	Chain2 Δ9	702.6	N	
PC (18:1(9)/18:1(11))	Isomer I	H^+	Chain1 Δ9	676.6	N	Chain2 Δ11	704.6	N	Y
	Isomer II	H^+	Chain1 Δ9	702.6	N	Chain2 Δ11	730.7	N	
PC (20:1(11)/16:1(9))	Isomer I	H^+	Chain1 Δ11	676.6	N	Chain2 Δ9	704.6	N	Y
	Isomer II	H^+	Chain1 Δ11	702.6	N	Chain2 Δ9	730.7	N	

PC (16:0/20:2(11,14))	Isomer I	H^+	Chain2 Δ11	678.6	N	Chain2 Δ14	718.6	N	Y*
	Isomer II	H^+	Chain2 Δ11	704.6	N	Chain2 Δ14	744.7	N	
PC (18:0/18:2(10,12))	Isomer I	H^+	Chain2 Δ10	692.6	N	Chain2 Δ12	718.6	N	Y*
	Isomer II	H^+	Chain2 Δ10	718.7	N	Chain2 Δ12	744.7	N	
PC (18:0/18:2(2,4))	Isomer I	H^+	Chain2 Δ2	580.4	N	Chain2 Δ4	606.5	N	Y*
	Isomer II	H^+	Chain2 Δ2	606.5	N	Chain2 Δ4	632.5	N	
PC (18:0/18:2(9,12))	Isomer I	H^+	Chain2 Δ12	718.6	N	Chain2 Δ9	678.6	N	Y*
	Isomer II	H^+	Chain2 Δ12	744.7	N	Chain2 Δ9	704.6	N	
PC (18:2(9,12)/18:0)	Isomer I	H^+	Chain1 Δ12	718.6	N	Chain1 Δ9	678.6	N	Y*
	Isomer II	H^+	Chain1 Δ12	744.7	N	Chain1 Δ9	704.6	N	
PC (20:2(11,14)/16:0)	Isomer I	H^+	Chain1 Δ11	678.6	N	Chain1 Δ14	718.6	N	Y*
	Isomer II	H^+	Chain1 Δ11	704.6	N	Chain1 Δ14	744.7	N	
PC (14:0/22:2(13,16))	Isomer I	H^+	Chain2 Δ13	678.6	N	Chain2 Δ16	718.6	N	N
	Isomer II	H^+	Chain2 Δ13	704.6	N	Chain2 Δ16	744.7	N	
PC (14:1(9)/22:1(13))	Isomer I	H^+	Chain1 Δ9	732.6	N	Chain2 Δ13	676.6	N	N
	Isomer II	H^+	Chain1 Δ9	758.7	N	Chain2 Δ13	702.6	N	

PC (22:1(13)/14:1(9))	Isomer I	H^+	Chain1 Δ13	676.6	N	Chain2 Δ9	732.6	N	N
	Isomer II	H^+	Chain1 Δ13	702.6	N	Chain2 Δ9	758.7	N	
PC (22:2(13,16)/14:0)	Isomer I	H^+	Chain1 Δ13	678.6	N	Chain1 Δ16	718.6	N	N
	Isomer II	H^+	Chain1 Δ13	704.6	N	Chain1 Δ16	744.7	N	
PC (14:1(9)/22:1(11))	Isomer I	H^+	Chain1 Δ9	732.6	N	Chain2 Δ11	648.5	N	N
	Isomer II	H^+	Chain1 Δ9	758.7	N	Chain2 Δ11	674.6	N	
PC (17:2(9,12)/19:0)	Isomer I	H^+	Chain1 Δ12	732.6	N	Chain1 Δ9	692.6	N	N
	Isomer II	H^+	Chain1 Δ12	758.7	N	Chain1 Δ9	718.7	N	
PC (19:0/17:2(9,12))	Isomer I	H^+	Chain2 Δ12	732.6	N	Chain2 Δ9	692.6	N	N
	Isomer II	H^+	Chain2 Δ12	758.7	N	Chain2 Δ9	718.7	N	
PC (22:1(11)/14:1(9))	Isomer I	H^+	Chain1 Δ11	648.5	N	Chain2 Δ9	732.6	N	N
	Isomer II	H^+	Chain1 Δ11	674.6	N	Chain2 Δ9	758.7	N	

[1]Species labeled in red front indicate Identified species with matched MS/MS fragments (from prediction) and carbon numbers in fatty acid tails.

[2]Comparison with experimental MS/MS spectra of the corresponding PB products.

[3]Comparison with results in Table S4.

*Agreement is only obtained from cell lysates (not from single cells).

Table S4-17. ***Predicted diagnostic ions from m/z 845.53 (acetone PB products of m/z 787.67) at the single-cell level***

Lipids[1]	PB products	Adduct	Double bond position	*m/z* of predicted fragments	MS/MS Match[2]
SM/d16:1(4)/24:0)	Isomer I	H^+	Chain1 Δ1	635.6	N
	Isomer II	H^+	Chain1 Δ1	661.6	**Y**
SM/d18:1(4)/22:0)	Isomer I	H^+	Chain1 Δ1	607.5	N
	Isomer II	H^+	Chain1 Δ1	633.6	N

[1]Species labeled in red front indicate Identified species with matched MS/MS fragments (from prediction) and carbon numbers in fatty acid tails.

[2]Comparison with experimental MS/MS spectra of the corresponding PB products.

Table S4-18. ***Predicted diagnostic ions from m/z 435.17 (benzophenone PB products of m/z 253.21) at the single-cell level.***

Lipids[1]	PB products	Adduct	Double bond position	*m/z* of predicted fragments	MS/MS Match[2]
FA (16:1 (9))	Isomer I	H^-	Chain1 Δ9	171.1	Y
	Isomer II	H^-	Chain1 Δ9	321.2	N
FA (16:1 (2))	Isomer I	H^-	Chain1 Δ2	73.0	N
	Isomer II	H^-	Chain1 Δ2	223.0	N
FA (16:1 (3))	Isomer I	H^-	Chain1 Δ3	87.0	N
	Isomer II	H^-	Chain1 Δ3	237.1	N
FA (16:1 (4))	Isomer I	H^-	Chain1 Δ4	101.0	N
	Isomer II	H^-	Chain1 Δ4	251.1	N
FA (16:1 (6))	Isomer I	H^-	Chain1 Δ6	129.1	N
	Isomer II	H^-	Chain1 Δ6	279.2	N
FA (16:1 (7))	Isomer I	H^-	Chain1 Δ7	143.1	N
	Isomer II	H^-	Chain1 Δ7	293.2	N
FA (16:1 (10))	Isomer I	H^-	Chain1 Δ10	185.2	N
	Isomer II	H^-	Chain1 Δ10	335.2	N
FA (16:1 (11))	Isomer I	H^-	Chain1 Δ11	199.2	N
	Isomer II	H^-	Chain1 Δ11	349.3	N
FA (16:1 (12))	Isomer I	H^-	Chain1 Δ12	213.2	N
	Isomer II	H^-	Chain1 Δ12	363.3	N
FA (16:1 (13))	Isomer I	H^-	Chain1 Δ13	227.2	N
	Isomer II	H^-	Chain1 Δ13	377.3	N
FA (16:1 (14))	Isomer I	H^-	Chain1 Δ14	241.2	N
	Isomer II	H^-	Chain1 Δ14	391.3	N

[1]Species labeled in red front indicate Identified species with matched MS/MS fragments (from prediction) and carbon numbers in fatty acid tails.

[2]Comparison with experimental MS/MS spectra of the corresponding PB products.

Table S4-19. ***Predicted diagnostic ions from m/z 311.16 (acetone PB products of m/z 253.21) at the single cell level.***

Lipids[1]	PB products	Adduct	Double bond position	*m/z* of predicted fragments	MS/MS match[2]
FA (16:1(9))	Isomer I	H^-	Chain1 Δ9	171.1	N
	Isomer II	H^-	Chain1 Δ9	197.2	**Y**
FA (16:1(2))	Isomer I	H^-	Chain1 Δ2	73.0	N
	Isomer II	H^-	Chain1 Δ2	99.0	N
FA (16:1(3))	Isomer I	H^-	Chain1 Δ3	87.0	N
	Isomer II	H^-	Chain1 Δ3	113.1	N
FA (16:1(4))	Isomer I	H^-	Chain1 Δ4	101.0	N
	Isomer II	H^-	Chain1 Δ4	127.1	N
FA (16:1(6))	Isomer I	H^-	Chain1 Δ6	129.1	N
	Isomer II	H^-	Chain1 Δ6	155.1	N
FA (16:1(7))	Isomer I	H^-	Chain1 Δ7	143.1	N
	Isomer II	H^-	Chain1 Δ7	169.1	N
FA (16:1(10))	Isomer I	H^-	Chain1 Δ10	185.2	N
	Isomer II	H^-	Chain1 Δ10	211.2	N
FA (16:1(11))	Isomer I	H^-	Chain1 Δ11	199.2	N
	Isomer II	H^-	Chain1 Δ11	225.2	N
FA (16:1(12))	Isomer I	H^-	Chain1 Δ12	213.2	N
	Isomer II	H^-	Chain1 Δ12	239.2	N
FA (16:1(13))	Isomer I	H^-	Chain1 Δ13	227.2	N
	Isomer II	H^-	Chain1 Δ13	253.3	N
FA (16:1(14))	Isomer I	H^-	Chain1 Δ14	241.2	N
	Isomer II	H^-	Chain1 Δ14	267.3	N

[1]Species labeled in red front indicate Identified species with matched MS/MS fragments (from prediction) and carbon numbers in fatty acid tails.

[2]Comparison with experimental MS/MS spectra of the corresponding PB products.

Table S4-20. ***Predicted diagnostic ions from m/z 339.20 (acetone PB products of m/z 281.25) at the single cell level.***

Lipids[1]	PB products	Adduct	Double bond position	*m/z* of predicted fragments	MS/MS match[2]
FA (18:1(9))	Isomer I	H^-	Chain1 Δ9	171.1	N
	Isomer II	H^-	Chain1 Δ9	197.2	**Y**
FA (18:1(2))	Isomer I	H^-	Chain1 Δ2	73.0	N
	Isomer II	H^-	Chain1 Δ2	99.0	N
FA (18:1(3))	Isomer I	H^-	Chain1 Δ3	87.0	N
	Isomer II	H^-	Chain1 Δ3	113.1	N
FA (18:1(4))	Isomer I	H^-	Chain1 Δ4	101.0	N
	Isomer II	H^-	Chain1 Δ4	127.1	N
FA (18:1(5))	Isomer I	H^-	Chain1 Δ5	115.1	N
	Isomer II	H^-	Chain1 Δ5	141.1	N
FA (18:1(6))	Isomer I	H^-	Chain1 Δ6	129.1	N
	Isomer II	H^-	Chain1 Δ6	155.1	N
FA (18:1(7))	Isomer I	H^-	Chain1 Δ7	143.1	N
	Isomer II	H^-	Chain1 Δ7	169.1	N
FA (18:1(8))	Isomer I	H^-	Chain1 Δ8	157.1	N
	Isomer II	H^-	Chain1 Δ8	183.2	N
FA (18:1(10))	Isomer I	H^-	Chain1 Δ10	185.2	N
	Isomer II	H^-	Chain1 Δ10	211.2	N
FA (18:1(11))	Isomer I	H^-	Chain1 Δ11	199.2	N
	Isomer II	H^-	Chain1 Δ11	225.2	N
FA (18:1(12))	Isomer I	H^-	Chain1 Δ12	213.2	N
	Isomer II	H^-	Chain1 Δ12	239.2	N

[1]Species labeled in red front indicate Identified species with matched MS/MS fragments (from prediction) and carbon numbers in fatty acid tails.

[2]Comparison with experimental MS/MS spectra of the corresponding PB products.

Table S4-21. ***Predicted diagnostic ions from m/z 790.59 (acetone PB products of m/z 732.55) at cell lysates level.***

Lipids[1]	PB products	Adduct	Double bond position	*m/z* of predicted fragments	MS/MS match[2]	Carbon number match[3]
PC (14:0/18:1(9))	Isomer I	H^+	Chain2 Δ9	622.5	**Y**	
	Isomer II	H^+	Chain2 Δ9	648.6	**Y**	**Y**
PC (16:0/16:1(9))	Isomer I	H^+	Chain2 Δ9	650.5	**Y**	
	Isomer II	H^+	Chain2 Δ9	676.6	**Y**	**Y**
PC (18:1(9)/14:0)	Isomer I	H^+	Chain1 Δ9	622.5	**Y**	
	Isomer II	H^+	Chain1 Δ9	648.6	**Y**	**Y**
PC (14:0/18:1(11))	Isomer I	H^+	Chain2 Δ11	650.5	**Y**	
	Isomer II	H^+	Chain2 Δ11	676.6	**Y**	**Y**
PC (16:1(9)/16:0)	Isomer I	H^+	Chain1 Δ9	650.5	**Y**	
	Isomer II	H^+	Chain1 Δ9	676.6	**Y**	**Y**
PC (18:1(11)/14:0)	Isomer I	H^+	Chain1 Δ11	650.5	**Y**	
	Isomer II	H^+	Chain1 Δ11	676.6	**Y**	**Y**
PC (12:0/20:1(11))	Isomer I	H^+	Chain2 Δ11	622.5	Y	
	Isomer II	H^+	Chain2 Δ11	648.6	Y	N
PC (20:1(11)/12:0)	Isomer I	H^+	Chain1 Δ11	622.5	Y	
	Isomer II	H^+	Chain1 Δ11	648.6	Y	N
PC (14:1(9)/18:0)	Isomer I	H^+	Chain1 Δ9	678.6	N	
	Isomer II	H^+	Chain1 Δ9	704.6	N	Y
PC (18:0/14:1(9))	Isomer I	H^+	Chain2 Δ9	678.6	N	
	Isomer II	H^+	Chain2 Δ9	704.6	N	Y
PC (13:0/19:1(9))	Isomer I	H^+	Chain2 Δ9	608.5	N	
	Isomer II	H^+	Chain2 Δ9	634.5	N	N
PC (15:0/17:1(9))	Isomer I	H^+	Chain2 Δ9	636.5	N	
	Isomer II	H^+	Chain2 Δ9	662.6	N	N

PC (15:1(9)/17:0)	Isomer I	H^+	Chain1 Δ9	664.6	N	
	Isomer II	H^+	Chain1 Δ9	690.6	N	N
PC (17:0/15:1(9))	Isomer I	H^+	Chain2 Δ9	664.6	N	
	Isomer II	H^+	Chain2 Δ9	690.6	N	N
PC (17:1(9)/15:0)	Isomer I	H^+	Chain1 Δ9	636.5	N	
	Isomer II	H^+	Chain1 Δ9	662.6	N	N
PC (19:1(9)/13:0)	Isomer I	H^+	Chain1 Δ9	608.5	N	
	Isomer II	H^+	Chain1 Δ9	634.5	N	N

[1]Species labeled in red front indicate Identified species with matched MS/MS fragments (from prediction) and carbon numbers in fatty acid tails.

[2]Comparison with experimental MS/MS spectra of the corresponding PB products.

[3]Comparison with results in Table S4.

Table S4-22. ***Comparison of C=C bond identifications between single cells and cell lysates.***

Lipids (*m/z*)	Experiment type	Head group (*m/z*)	Head group type with adduct	Product of Lipids (*m/z*)	Diagnostic ions
810.6012	Single-cell	146	$[PC + Na]^+$	868.641	700,726,756, 782
	Cell lysate	146, 184	$[PC + H]^+$, $[PC + Na]^+$		none
732.5543	Single-cell	184	$[PC + H]^+$	790.5902	650, 676
	Cell lysate	184	$[PC + H]^+$		622, 648, 650, 676
756.55	Single-cell	184	$[PC + H]^+$	814.4938	646, 672, 728
	Cell lysate	184	$[PC + H]^+$		none
760.5856	Single-cell	184	$[PC + H]^+$	818.6279	650, 676
	Cell lysate	184	$[PC + H]^+$		650, 676, 678
782.5699	Single-cell	146	$[PC + Na]^+$	840.6057	656, 672, 698, 782
	Cell lysate	146	$[PC + Na]^+$		592, 594, 656, 782
754.5387	Single-cell	146, 184	$[PC + H]^+$, $[PC + Na]^+$	812.5792	566, 628, 644, 687, 728, 754
	Cell lysate	146, 184	$[PC + H]^+$, $[PC + Na]^+$		566, 628, 754
780.5543	Single-cell	146, 184	$[PC + H]^+$, $[PC + Na]^+$	838.5899	712, 714, 738, 780
	Cell lysate	146, 185	$[PC + H]^+$, $[PC + Na]^+$		780
784.5746	Single-cell	184	$[PC + H]^+$	842.653	700, 728, 784
	Cell lysate	184	$[PC + H]^+$		784
786.6012	Single-cell	184	$[PC + H]^+$	844.7043	660, 662, 786
	Cell lysate	184	$[PC + H]^+$		786
787.6693	Single-cell	184	$[SM + H]^+$	845.5319	661
	Cell lysate	184	$[SM + H]^+$		661

Supporting Figures

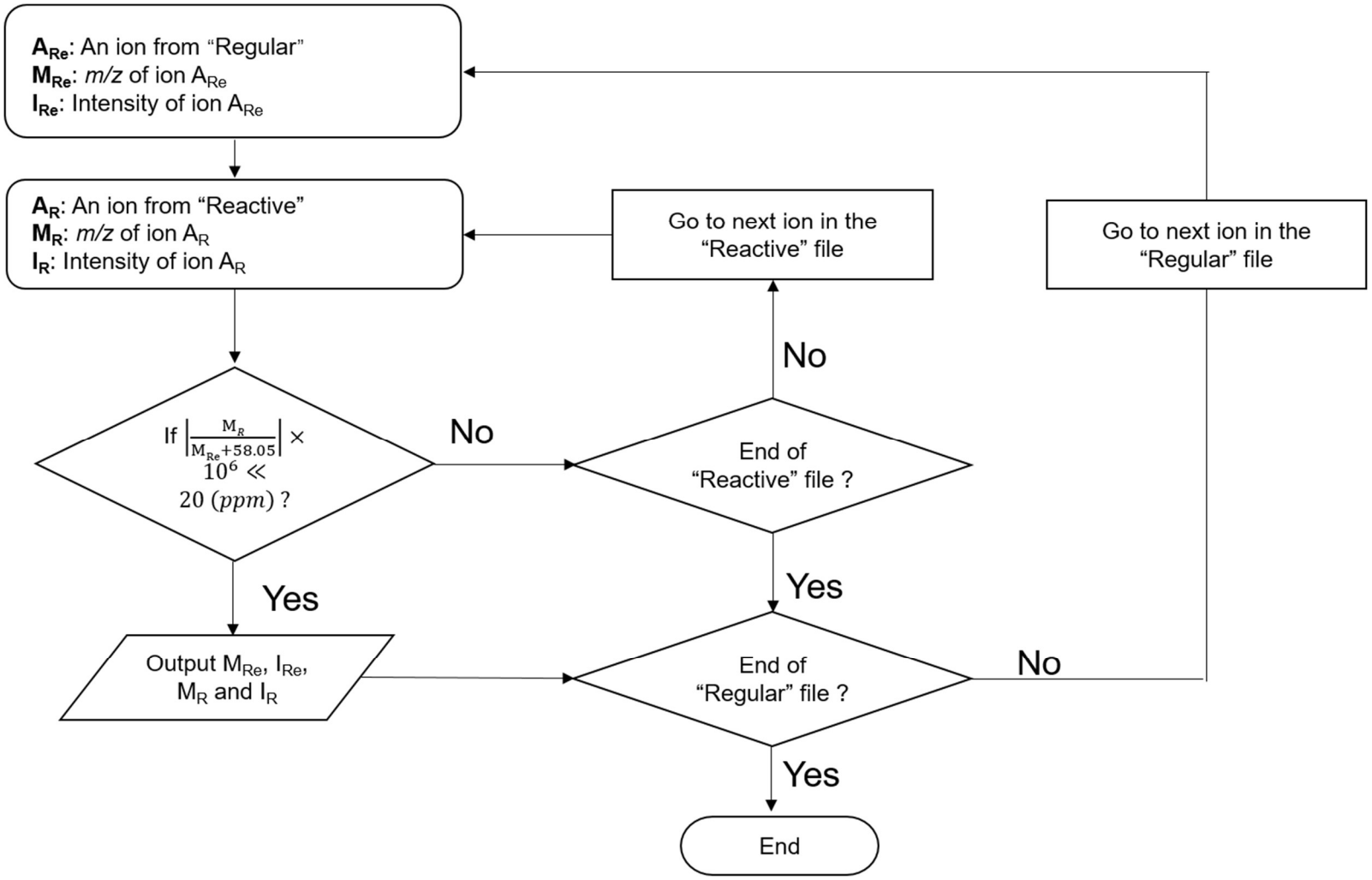
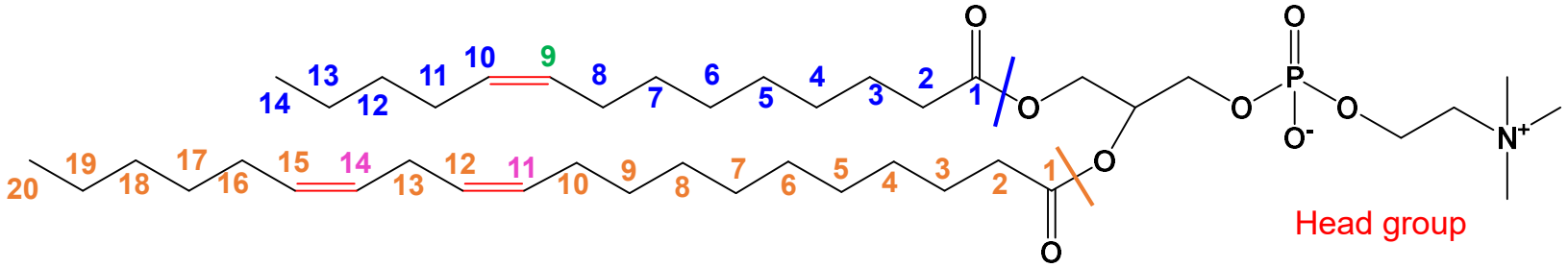


Figure S4-1. *Flowchart of the Script A for screening potential lipids and their corresponding PB products.*



PC(14:1(9)/20:2(11,14))

Head group Chain 1 Chain 2

Number of carbons

Degree of unsaturation

Position of double bonds

PC(14:1(9)/20:2(11,14))

Number of carbons

Degree of unsaturation

Position of double bonds

Using PC(14:1(9)/20:2(11,14)) as an example

m/z of the lipid = m/z of head group + m/z of Chain 1 + m/z of Chain 2 + m/z of adduct

Using PB product of PC(14:1(9)/20:2(11,14)) at Δ9 position as an example

m/z of PB product isomer I = m/z of head group + m/z of parts of Chain 1 (from Δ1 to Δ9) + m/z of Chain 2 + m/z of adduct + 16

m/z of PB product isomer II = m/z of head group + m/z of parts of Chain 1 (from Δ1 to Δ9) + m/z of Chain 2 + m/z of adduct + 42.05 (this value depends on PB reagent, acetone: 42.05; benzophenone: 166.08)

Figure S4-2. *Principles of Script B to predict the m/z of diagnostic ions of PB products*

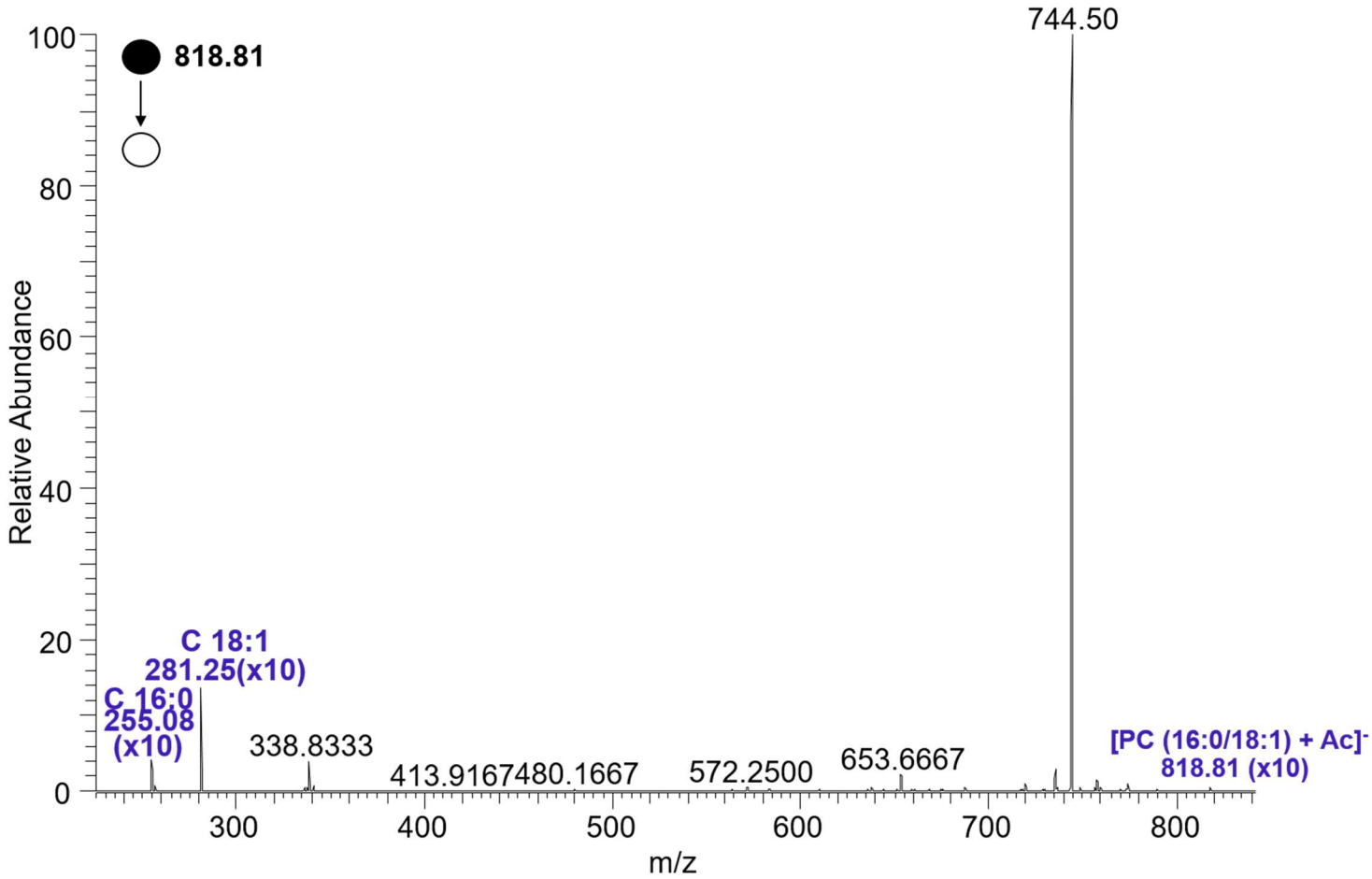


Figure S4-3. *MS/MS spectra of PC (16:0/18:1(9)) standard solution (1 μM, containing 10 mM ammonium acetate) at the negative ion mode. m/z 281.25 and m/z 255.08 are two fatty acid tails of PC (16:0/18:1(9)).*

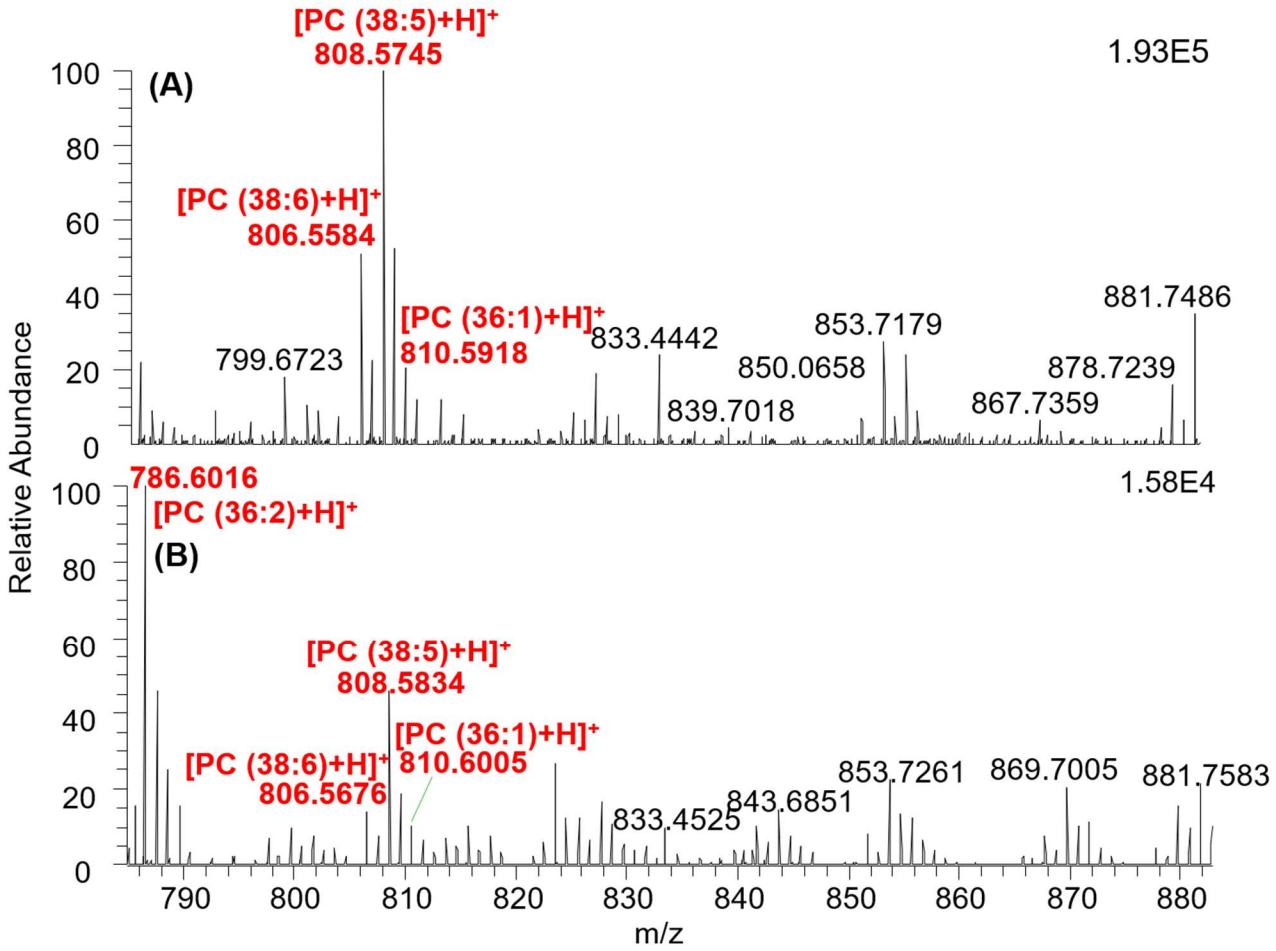


Figure S4-4. *Mass spectra (selected range) of HCT-116 single cell in (A) acetone and (B) 5 mM benzophenone solution without UV irradiation.*

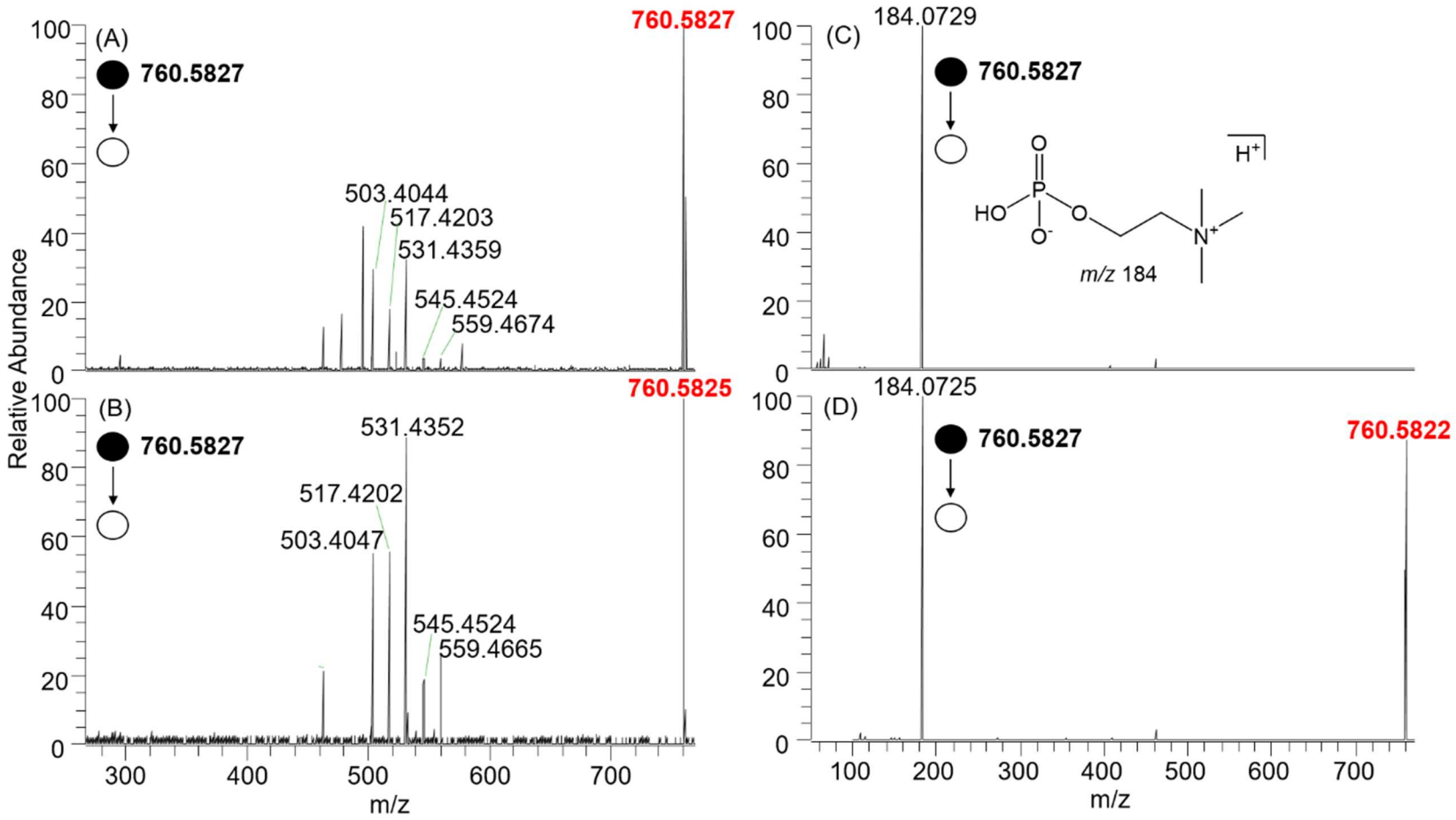


Figure S4-5. *(A) MS/MS spectra of PC (16:0/18:1(9)) detected from 10 μM PC (16:0/18:1(9)) standard solution using CID mode. (B) MS/MS spectra of PC (16:0/18:1(9)) detected at the single-cell level using CID mode. (C) MS/MS spectra of PC (16:0/18:1(9)) detected from 10 μM PC (16:0/18:1(9)) standard solution using HCD mode. (D) MS/MS spectra of PC (16:0/18:1(9)) detected at the single-cell level using HCD mode.*

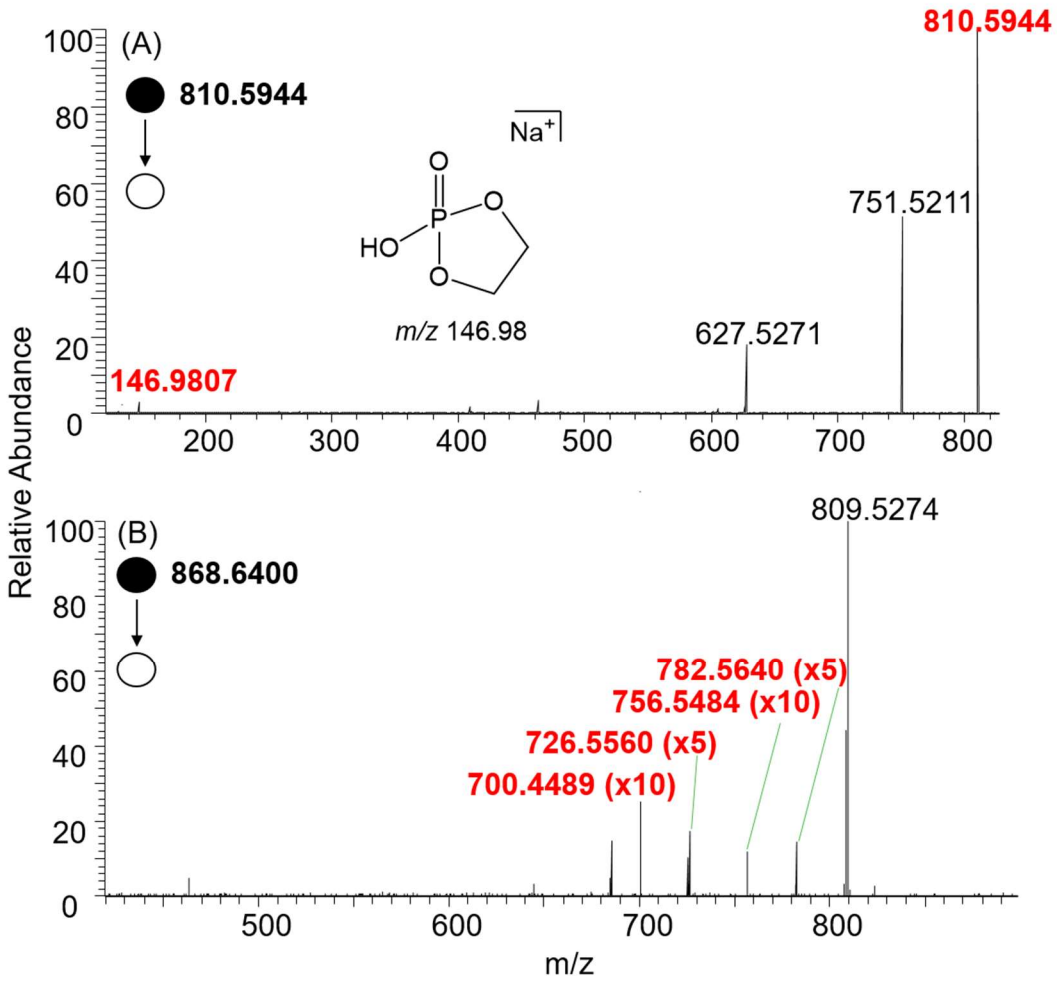


Figure S4-6. *(A) MS/MS spectra of m/z 810.59 detected at the single-cell level. (B) MS/MS spectra of m/z 868.64 (PB product of m/z 810.59) detected at the single-cell level. The peaks labelled in red are parent and diagnostic ions.*

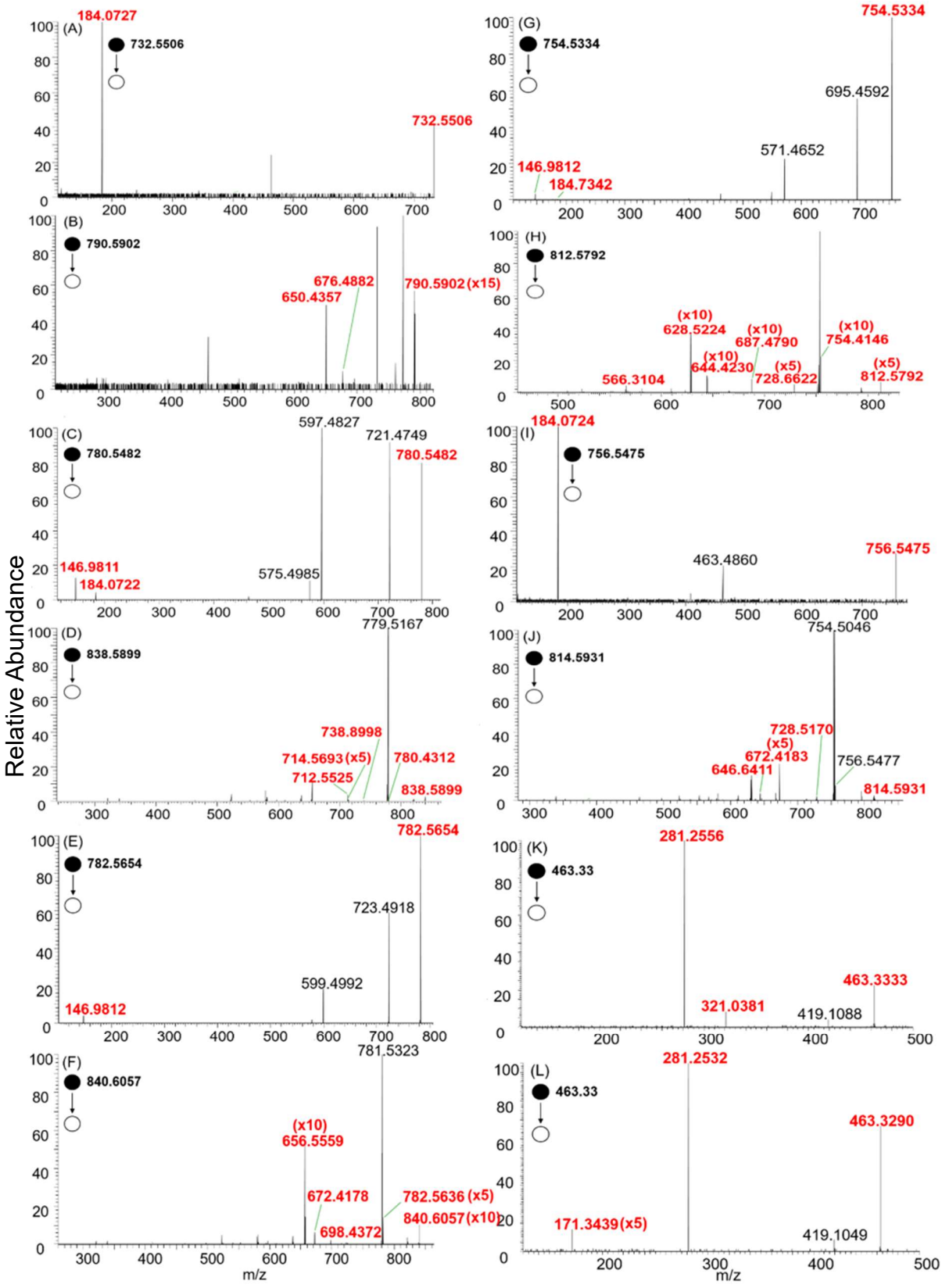

Relative Abundance
m/z
(A)
184.0727
732.5506
732.5506
(B)
790.5902
676.4882
650.4357
790.5902 (x15)
(C)
780.5482
597.4827
721.4749
780.5482
146.9811
184.0722
575.4985
(D)
838.5899
779.5167
738.8998
714.5693 (x5)
712.5525
780.4312
838.5899
(E)
782.5654
782.5654
723.4918
599.4992
146.9812
(F)
840.6057
781.5323
(x10)
656.5559
672.4178
782.5636 (x5)
840.6057 (x10)
698.4372
(G)
754.5334
754.5334
695.4592
571.4652
146.9812
184.7342
(H)
812.5792
812.5792
(x10)
628.5224
(x10)
687.4790
(x10)
754.4146
(x10)
644.4230
(x5)
728.6622
(x5)
566.3104
(I)
756.5475
184.0724
756.5475
463.4860
(J)
814.5931
754.5046
728.5170
(x5)
672.4183
646.6411
756.5477
814.5931
(K)
463.33
281.2556
463.3333
321.0381
419.1088
(L)
463.33
281.2532
463.3290
171.3439 (x5)
419.1049

Figure S4-7. *MS/MS of lipids and their corresponding PB products (with paired diagnostic ions) at the single-cell level, including (A) m/z 732.55, (B) m/z 790.59 (PB product of m/z 732.55), (C) m/z 780.54, (D) m/z 838.58 (PB product of m/z 780.54), (E) m/z 782.56, (F) m/z 840.60 (PB product of m/z 782.56), (G) m/z 754.5, (H) m/z 812.58 (PB product of m/z 754.53), (I) m/z 756.54, (J) m/z 814.59 (PB product of m/z 756.54), (K) m/z 463.33 (negative mode) and (L) m/z 463.33 (negative mode). The peaks labelled in red are parent and diagnostic ions.*

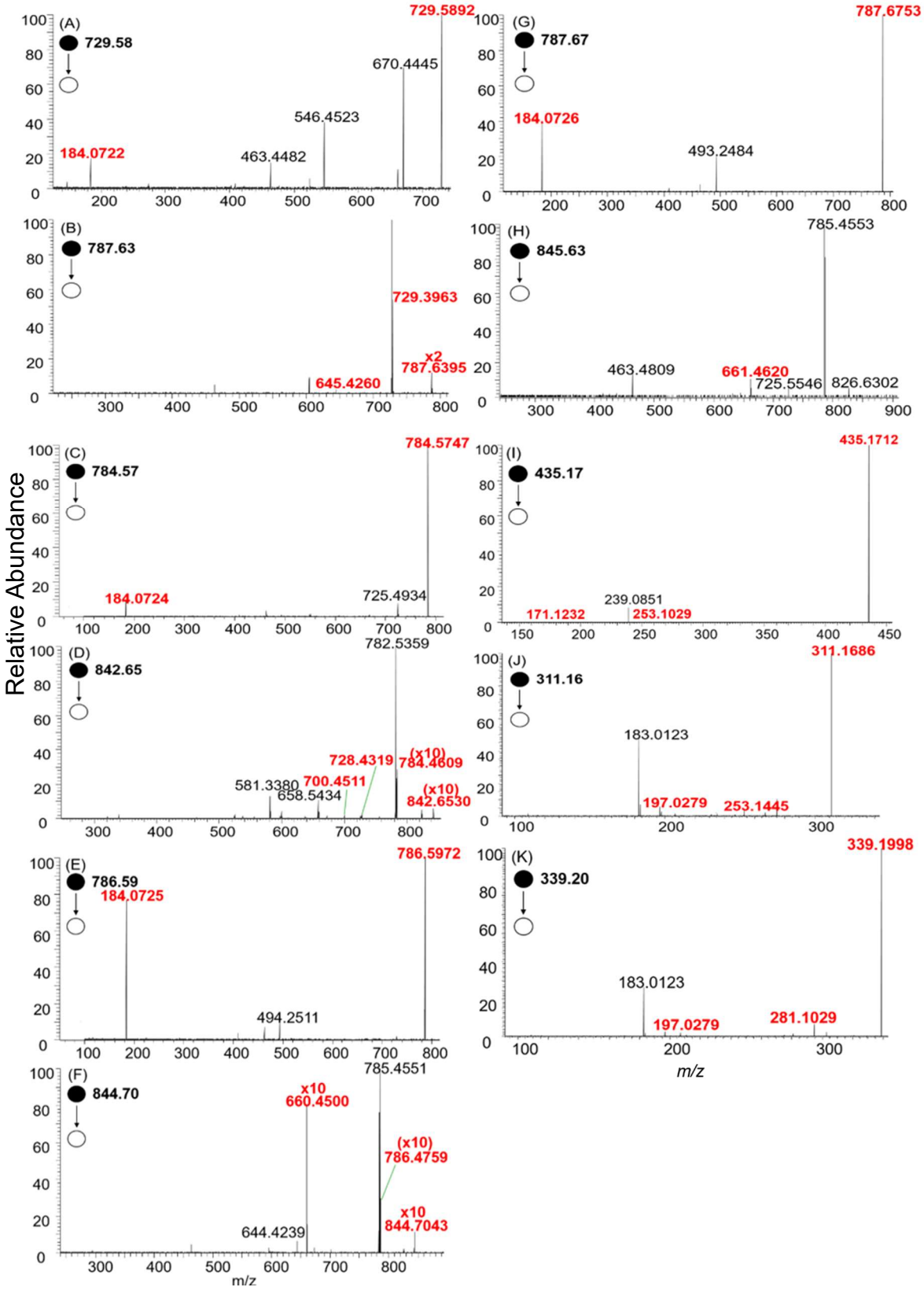

(A)
729.58
729.5892
670.4445
546.4523
463.4482
184.0722
(G)
787.67
787.6753
184.0726
493.2484
(B)
787.63
729.3963
x2
787.6395
645.4260
(H)
845.63
785.4553
463.4809
661.4620
725.5546
826.6302
(C)
784.57
784.5747
184.0724
725.4934
782.5359
(I)
435.17
435.1712
239.0851
171.1232
253.1029
(D)
842.65
728.4319
(x10)
784.4609
581.3380
700.4511
658.5434
(x10)
842.6530
(J)
311.16
311.1686
183.0123
197.0279
253.1445
(E)
786.59
184.0725
786.5972
494.2511
785.4551
(K)
339.20
339.1998
183.0123
197.0279
281.1029
(F)
844.70
x10
660.4500
(x10)
786.4759
x10
844.7043
644.4239
Relative Abundance
m/z
m/z

Figure S4-8. *MS/MS analysis of lipids and their corresponding PB products (with unpaired diagnostic ions) at the single-cell level, including (A) m/z 729.51, (B) m/z 787.63 (PB product of m/z 729.51), (C) m/z 784.57, (D) m/z 842.65 (PB product of m/z 784.57), (E) m/z 786.59, (F) m/z 844.70 (PB product of m/z 786.59), (G) m/z 787.67, (H) m/z 845.64 (PB product of m/z 787.67), (I) m/z 435.17 (negative mode), (J) m/z 311.16 (negative mode) and (K)m/z 339.19 (negative mode). The peaks labelled in red are parent and diagnostic ions.*

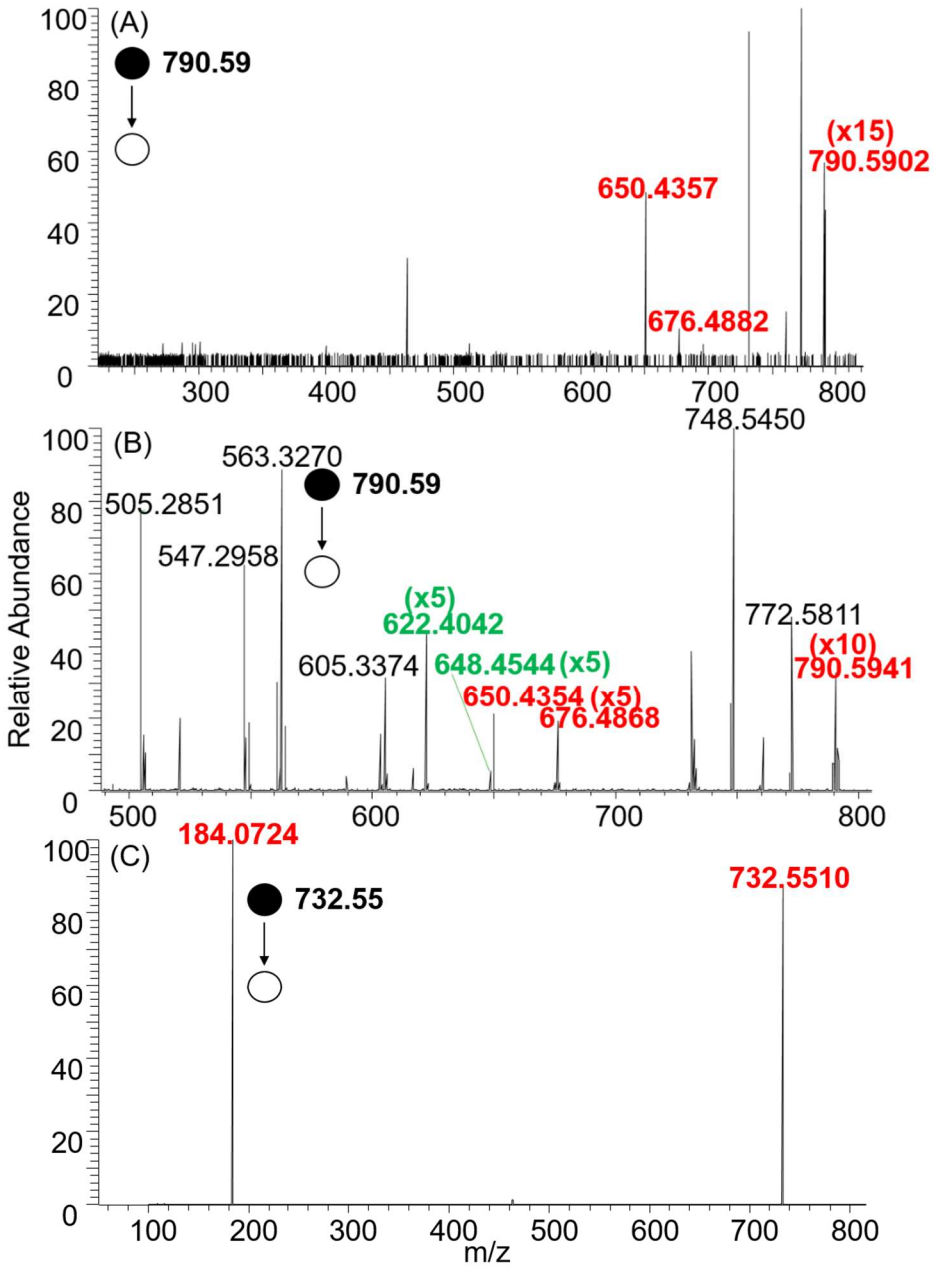
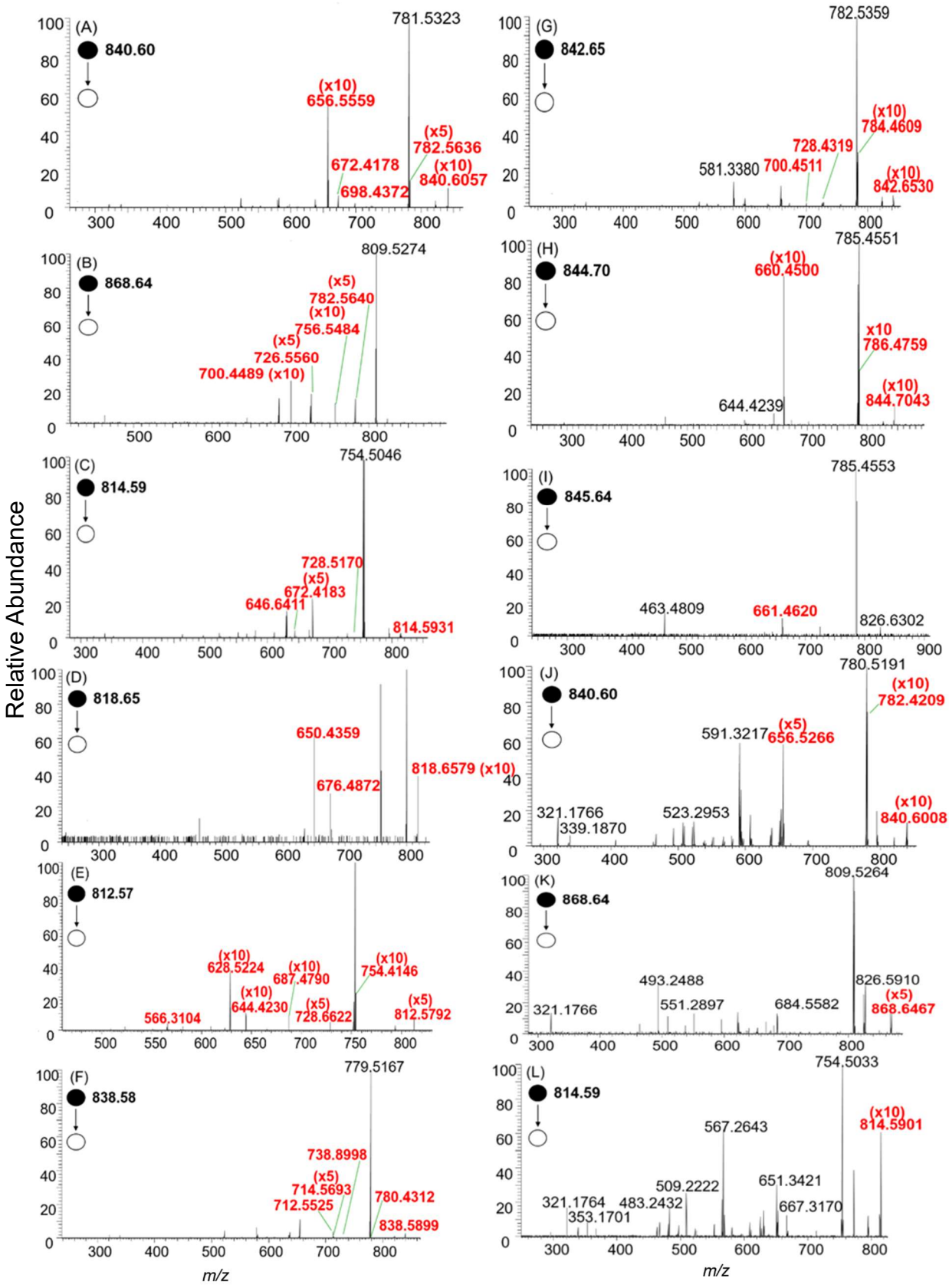


Figure S4-9. *MS/MS spectra of m/z 790.59 obtained (A) at the single-cell level and (B) from cell lysate. (C) MS/MS spectra of m/z 732.55 detected from cell lysate. The peaks labelled in red are parent and diagnostic ions.*


Relative Abundance
m/z
(A)
840.60
781.5323
(x10)
656.5559
(x5)
782.5636
672.4178
(x10)
840.6057
698.4372
(B)
868.64
809.5274
(x5)
782.5640
(x10)
756.5484
(x5)
726.5560
700.4489 (x10)
(C)
814.59
754.5046
728.5170
(x5)
672.4183
646.6411
814.5931
(D)
818.65
650.4359
818.6579 (x10)
676.4872
(E)
812.57
(x10)
628.5224
(x10)
687.4790
(x10)
754.4146
(x10)
644.4230
(x5)
728.6622
(x5)
812.5792
566.3104
(F)
838.58
779.5167
738.8998
(x5)
714.5693
712.5525
780.4312
838.5899
(G)
842.65
782.5359
(x10)
784.4609
728.4319
581.3380
700.4511
(x10)
842.6530
(H)
844.70
785.4551
(x10)
660.4500
x10
786.4759
644.4239
(x10)
844.7043
(I)
845.64
785.4553
463.4809
661.4620
826.6302
(J)
840.60
780.5191
(x10)
782.4209
591.3217
(x5)
656.5266
321.1766
339.1870
523.2953
(x10)
840.6008
(K)
868.64
809.5264
493.2488
826.5910
321.1766
551.2897
684.5582
(x5)
868.6467
(L)
814.59
754.5033
(x10)
814.5901
567.2643
509.2222
651.3421
321.1764
353.1701
483.2432
667.3170

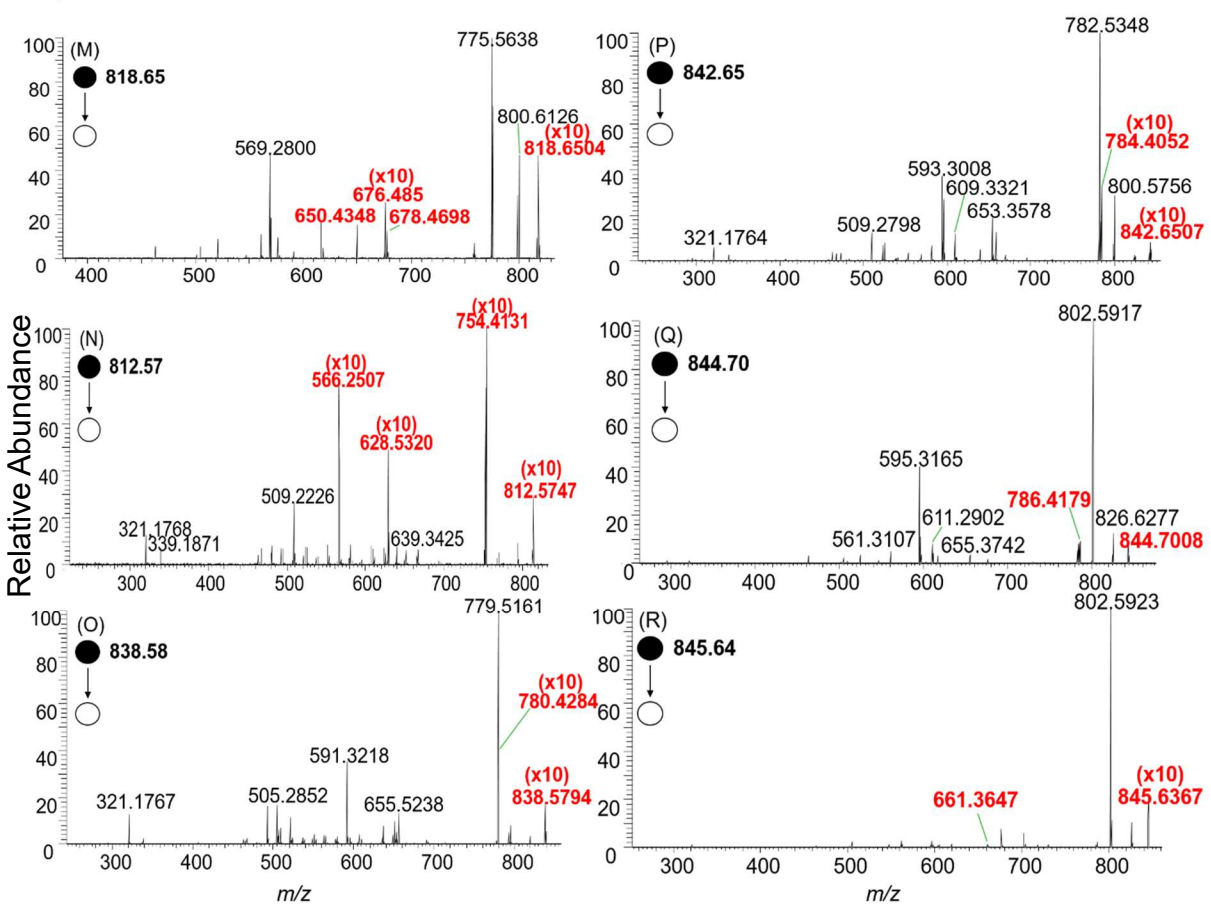


Figure S4-10. *MS/MS analysis of PB products. Results from single cells include (A) m/z 840.60, (B) m/z 868.64, (C) m/z 814.59, (D) m/z 818.65, (E) m/z 812.58, (F) m/z 838.58, (G) m/z 842.65, (H) m/z 844.67, (I) m/z 845.64, Results from cell lysates include (J) m/z 840.60, (K) m/z 868.64, (L) m/z 814.59, (M) m/z 818.65, (N) m/z 812.58, (O) m/z 838.58, (P) m/z 842.65, (Q) m/z 844.67, and (R) m/z 845.64. The peaks labelled in red are parent and diagnostic ions.*

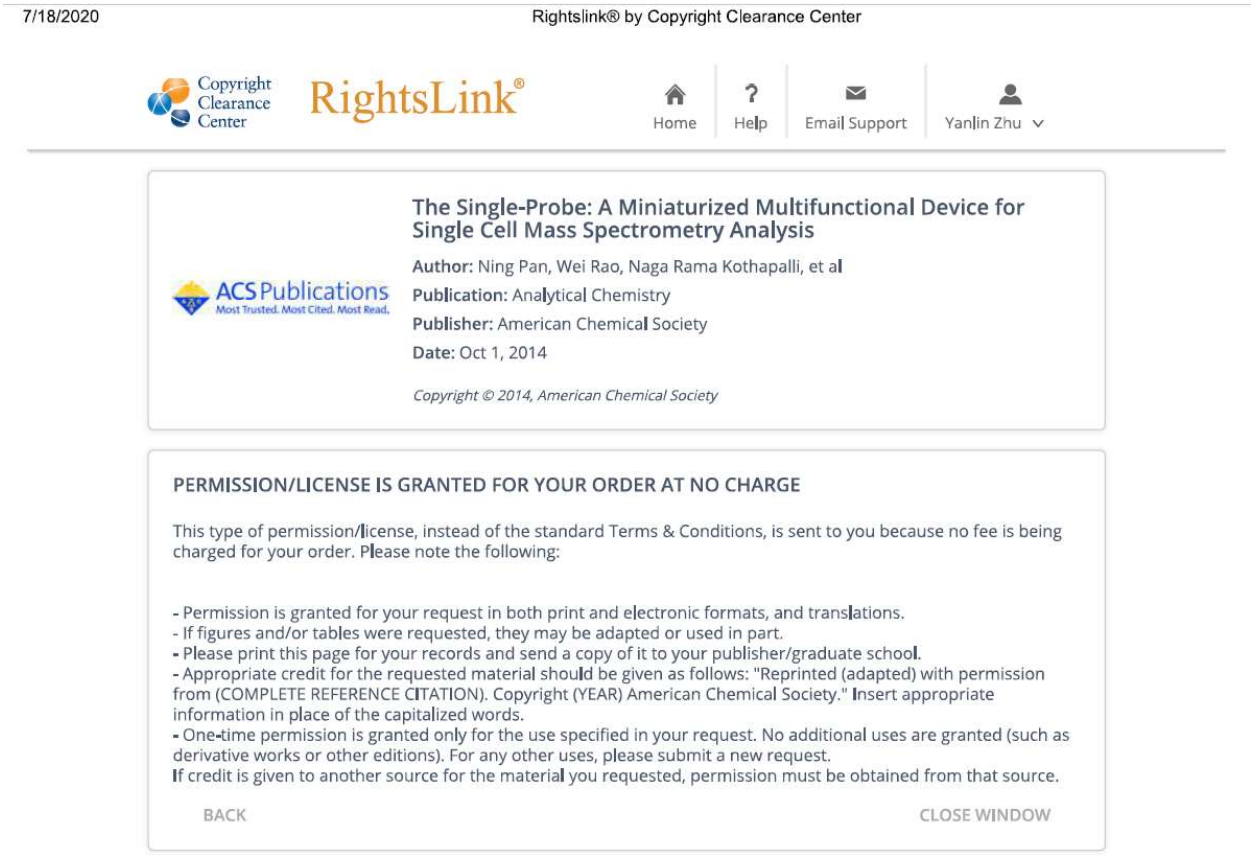
References

1 J. Floch, *J. biol. Chem.*, 1957, **226**, 497-509.
2 Y. Zhu, R. Liu and Z. Yang, *Anal. Chim. Acta*, 2019, **1084**, 53-59.
3 R. Liu, N. Pan, Y. Zhu and Z. Yang, *Anal. Chem.*, 2018, **90**, 11078-11085.
4 N. Pan, W. Rao, S. J. Standke and Z. Yang, *Analytical chemistry*, 2016, **88**, 6812-6819.

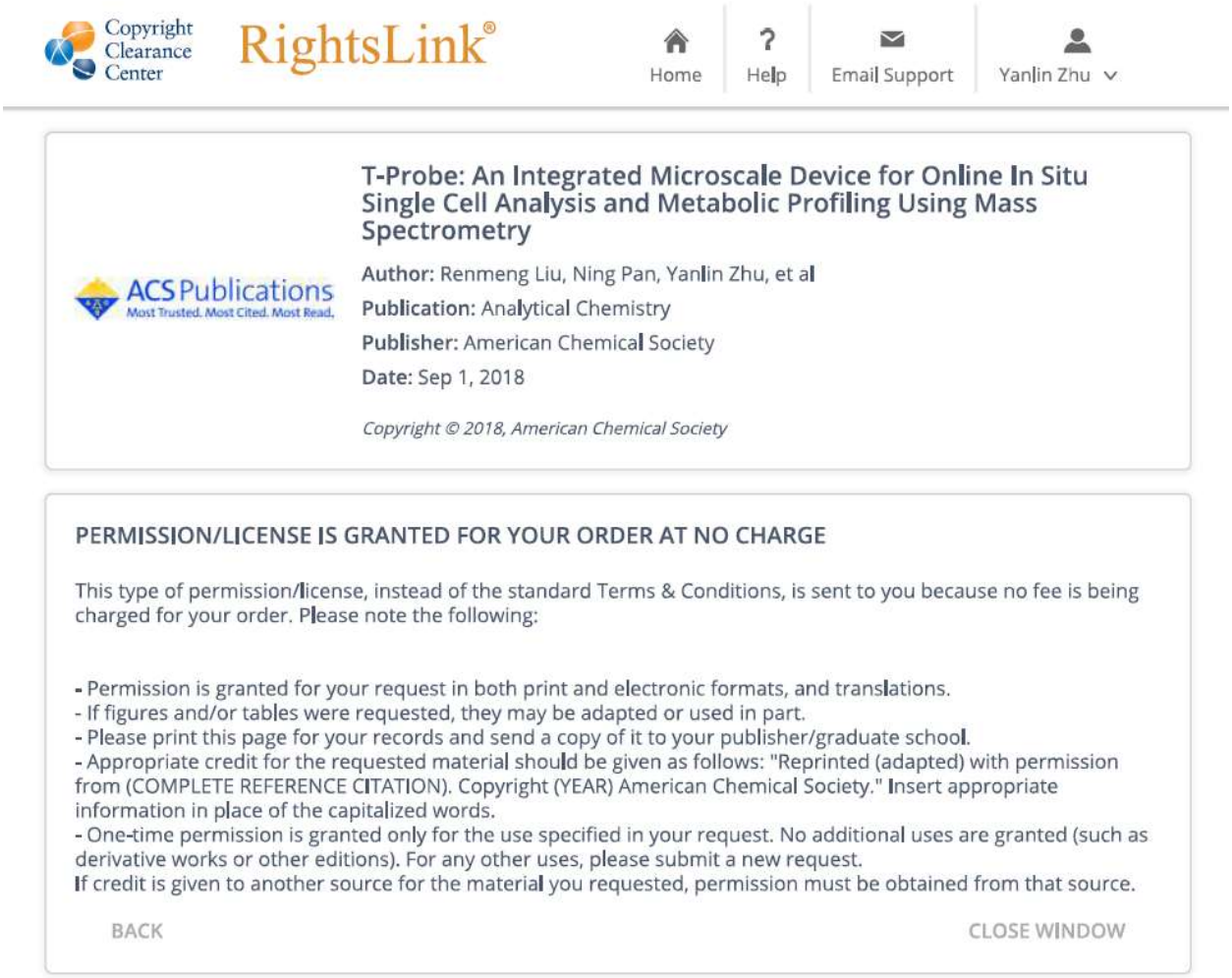
Appendix III: Copyrights

Copyrights of Chapter 1

Copyright of Figure 1-1



Copyright of Figure 1-2



Copyright of Figure 1-3

JOHN WILEY AND SONS LICENSE
TERMS AND CONDITIONS

Jul 18, 2020

This Agreement between University of Oklahoma -- Yanlin Zhu ("You") and John Wiley and Sons ("John Wiley and Sons") consists of your license details and the terms and conditions provided by John Wiley and Sons and Copyright Clearance Center.

License Number	4872000060582
License date	Jul 18, 2020
Licensed Content Publisher	John Wiley and Sons
Licensed Content Publication	Journal of Mass Spectrometry
Licensed Content Title	Live single-cell video-mass spectrometry for cellular and subcellular molecular detection and cell classification
Licensed Content Author	Tsutomu Masujima, Takanori Harada, Naohiro Tsuyama, et al
Licensed Content Date	Jul 10, 2008
Licensed Content Volume	43
Licensed Content Issue	12
Licensed Content Pages	9

Copyright of Figure 1-4



Royal Society of Chemistry - License Terms and Conditions

This is a License Agreement between Yanlin Zhu ("You") and Royal Society of Chemistry ("Publisher") provided by Copyright Clearance Center ("CCC"). The license consists of your order details, the terms and conditions provided by Royal Society of Chemistry, and the CCC terms and conditions.

All payments must be made in full to CCC.

Order Date	18-Jul-2020	**Type of Use**	Republish in a thesis/dissertation
Order license ID	1049227-1	**Publisher**	Royal Society of Chemistry
ISSN	1364-5528	**Portion**	Image/photo/illustration

LICENSED CONTENT

Publication Title	The analyst online	**Country**	United Kingdom of Great Britain and Northern Ireland
Author/Editor	Society of Public Analysts (Great Britain), Chemical Society (Great Britain), Society for Analytical Chemistry, Society of Public Analysts (Great Britain), Royal Society of Chemistry (Great Britain)	**Rightsholder**	Royal Society of Chemistry
		Publication Type	e-Journal
		URL	http://www.rsc.org/is/journals/current/an...
Date	12/31/1875		
Language	English		

REQUEST DETAILS

Portion Type	Image/photo/illustration	**Distribution**	Worldwide
Number of images / photos / illustrations	1	**Translation**	Original language of publication
Format (select all that apply)	Print, Electronic	**Copies for the disabled?**	No
Who will republish the content?	Academic institution	**Minor editing privileges?**	No
Duration of Use	Life of current edition	**Incidental promotional use?**	Yes
Lifetime Unit Quantity	Up to 9,999	**Currency**	USD
Rights Requested	Main product		

NEW WORK DETAILS

Title	DEVELOPMENT AND APPLICATION OF SINGLE CELL MASS SPECTROMETRY TECHNIQUES FOR NON-ADHERENT CELL ANALYSIS	**Institution name**	University of oklahoma
		Expected presentation date	2020-07-18
Instructor name	Yanlin Zhu		

ADDITIONAL DETAILS

Copyright of Figure 1-5

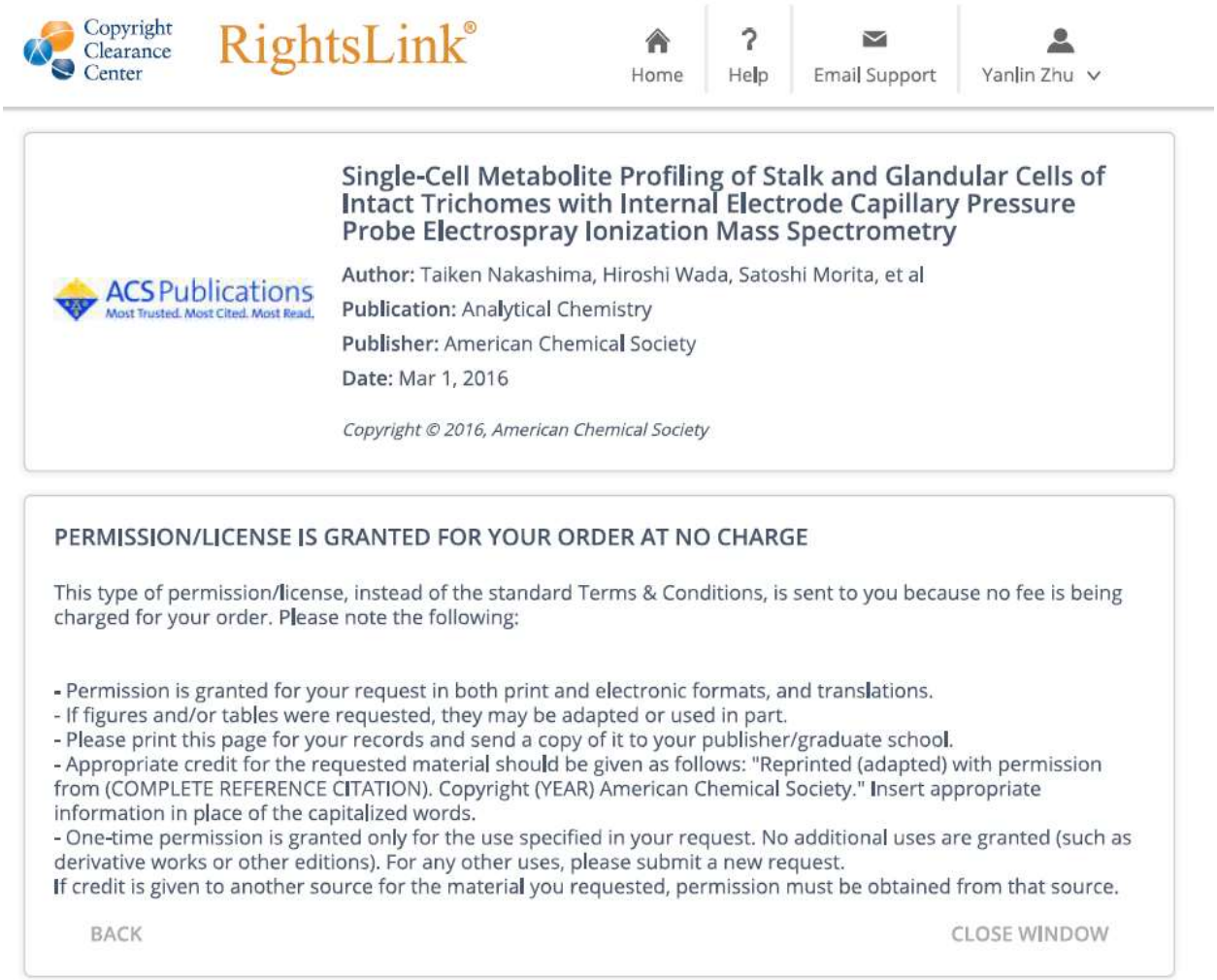
ELSEVIER LICENSE
TERMS AND CONDITIONS

Jul 18, 2020

This Agreement between University of Oklahoma -- Yanlin Zhu ("You") and Elsevier ("Elsevier") consists of your license details and the terms and conditions provided by Elsevier and Copyright Clearance Center.

License Number	4872010245102
License date	Jul 18, 2020
Licensed Content Publisher	Elsevier
Licensed Content Publication	Analytical Biochemistry
Licensed Content Title	Living cell manipulation, manageable sampling, and shotgun picoliter electrospray mass spectrometry for profiling metabolites
Licensed Content Author	Yousef Gholipour,Rosa Erra-Balsells,Kenzo Hiraoka,Hiroshi Nonami
Licensed Content Date	Feb 1, 2013
Licensed Content Volume	433
Licensed Content Issue	1
Licensed Content Pages	9
Start Page	70
End Page	78

Copyright of Figure 1-6



Copyright of Figure 1-7

AIP PUBLISHING LICENSE
TERMS AND CONDITIONS

Jul 18, 2020

This Agreement between University of Oklahoma -- Yanlin Zhu ("You") and AIP Publishing ("AIP Publishing") consists of your license details and the terms and conditions provided by AIP Publishing and Copyright Clearance Center.

License Number	4872011509934
License date	Jul 18, 2020
Licensed Content Publisher	AIP Publishing
Licensed Content Publication	Review of Scientific Instruments
Licensed Content Title	Nanomanipulation-coupled nanospray mass spectrometry as an approach for single cell analysis
Licensed Content Author	Mandy Phelps, Jason Hamilton, Guido F. Verbeck
Licensed Content Date	Dec 1, 2014
Licensed Content Volume	85
Licensed Content Issue	12
Type of Use	Thesis/Dissertation
Requestor type	Student

Copyright of Figure 1-8



Royal Society of Chemistry - License Terms and Conditions

This is a License Agreement between Yanlin Zhu ("You") and Royal Society of Chemistry ("Publisher") provided by Copyright Clearance Center ("CCC"). The license consists of your order details, the terms and conditions provided by Royal Society of Chemistry, and the CCC terms and conditions.

All payments must be made in full to CCC.

Order Date	18-Jul-2020	**Type of Use**	Republish in a thesis/dissertation
Order license ID	1049229-1	**Publisher**	Royal Society of Chemistry
ISSN	1364-5528	**Portion**	Image/photo/illustration

LICENSED CONTENT

Publication Title	The analyst online	**Country**	United Kingdom of Great Britain and Northern Ireland
Author/Editor	Society of Public Analysts (Great Britain), Chemical Society (Great Britain), Society for Analytical Chemistry, Society of Public Analysts (Great Britain), Royal Society of Chemistry (Great Britain)	**Rightsholder**	Royal Society of Chemistry
		Publication Type	e-Journal
		URL	http://www.rsc.org/is/journals/current/an...
Date	12/31/1875		
Language	English		

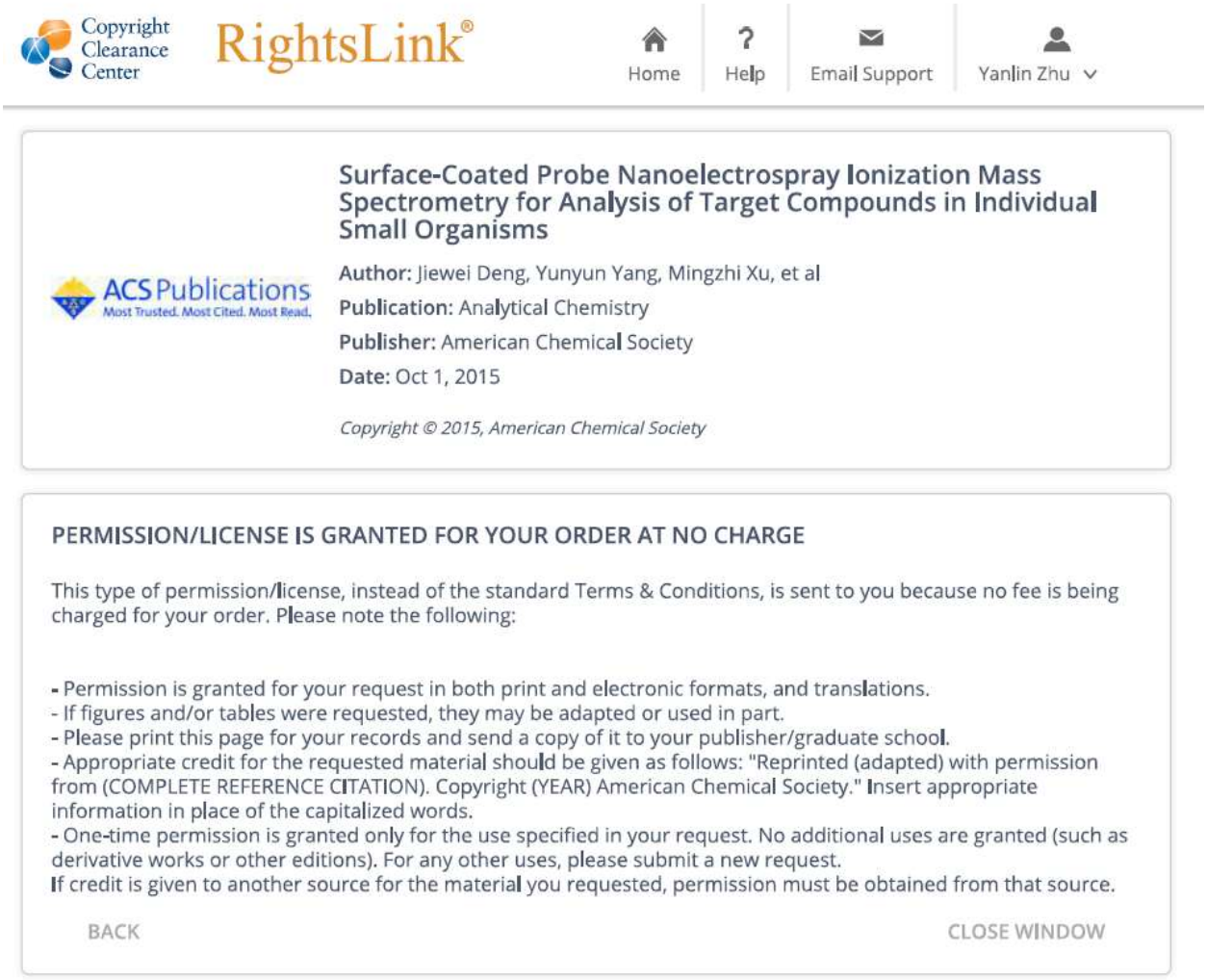
REQUEST DETAILS

Portion Type	Image/photo/illustration	**Distribution**	Worldwide
Number of images / photos / illustrations	1	**Translation**	Original language of publication
Format (select all that apply)	Print, Electronic	**Copies for the disabled?**	No
Who will republish the content?	Academic institution	**Minor editing privileges?**	No
Duration of Use	Life of current edition	**Incidental promotional use?**	Yes
Lifetime Unit Quantity	Up to 2,000,000	**Currency**	USD
Rights Requested	Main product		

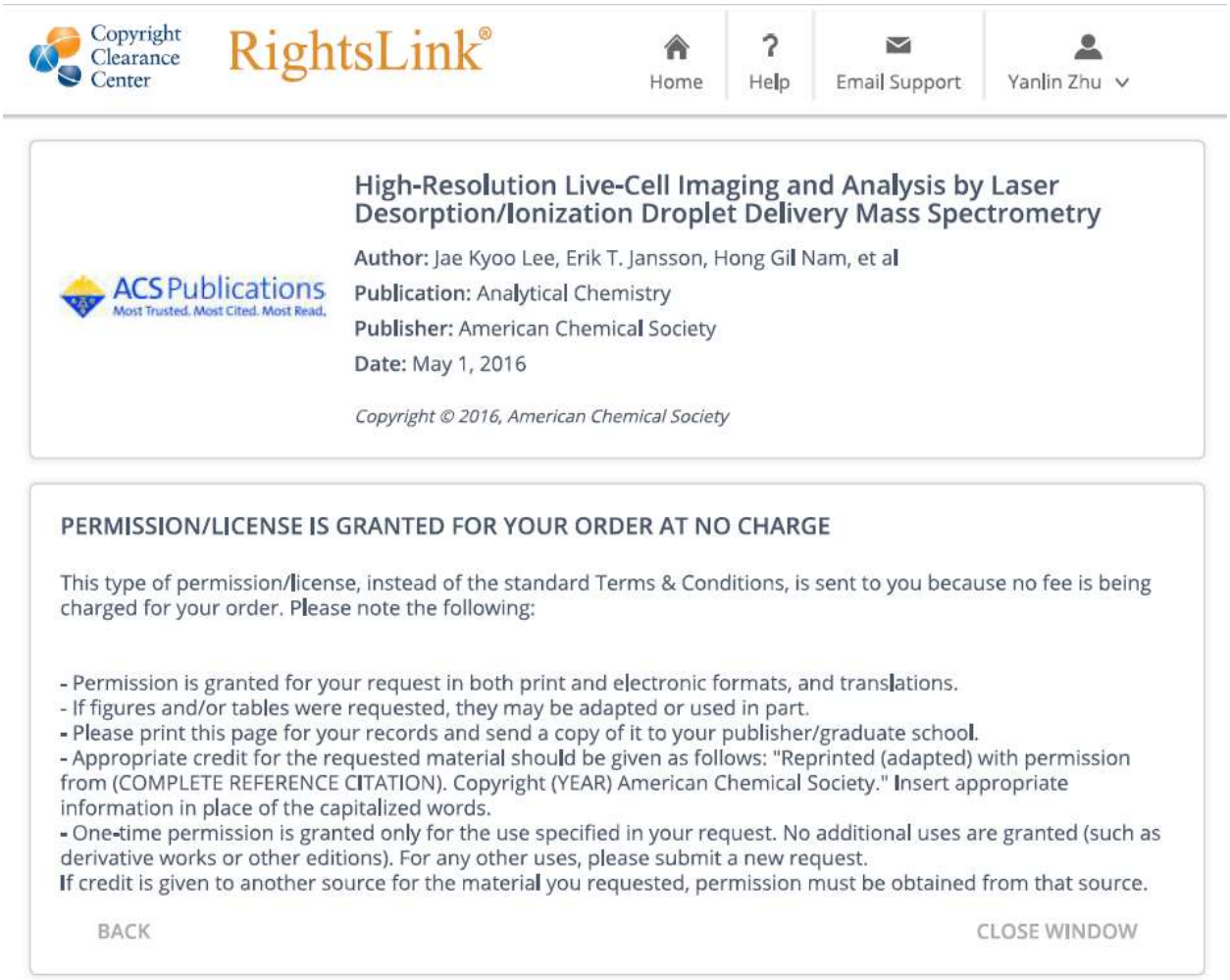
NEW WORK DETAILS

Title	DEVELOPMENT AND APPLICATION OF SINGLE CELL MASS SPECTROMETRY TECHNIQUES FOR NON-ADHERENT CELL ANALYSIS	**Institution name**	University of Oklahoma
		Expected presentation date	2020-07-18
Instructor name	Yanlin Zhu		

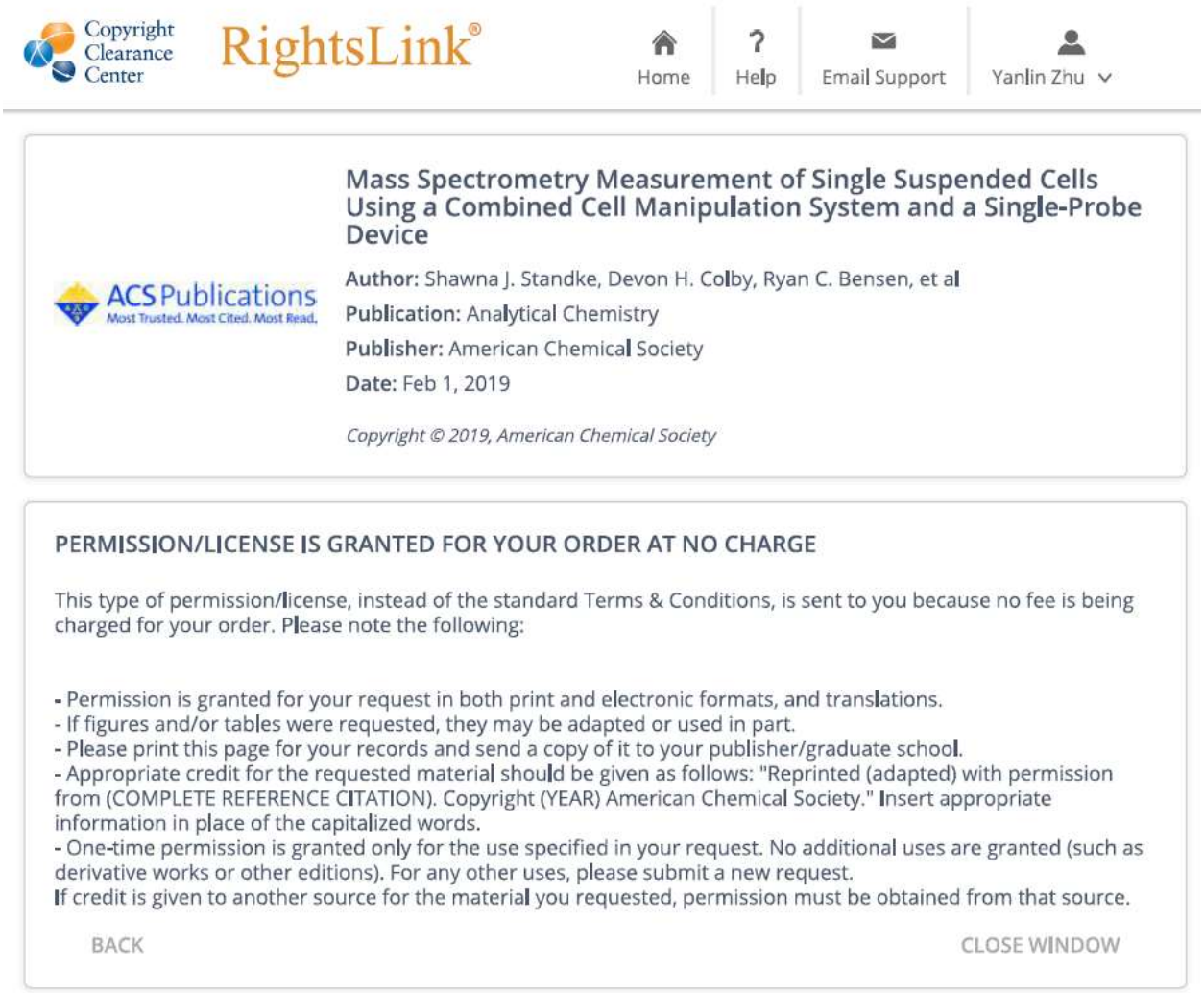
Copyright of Figure 1-9



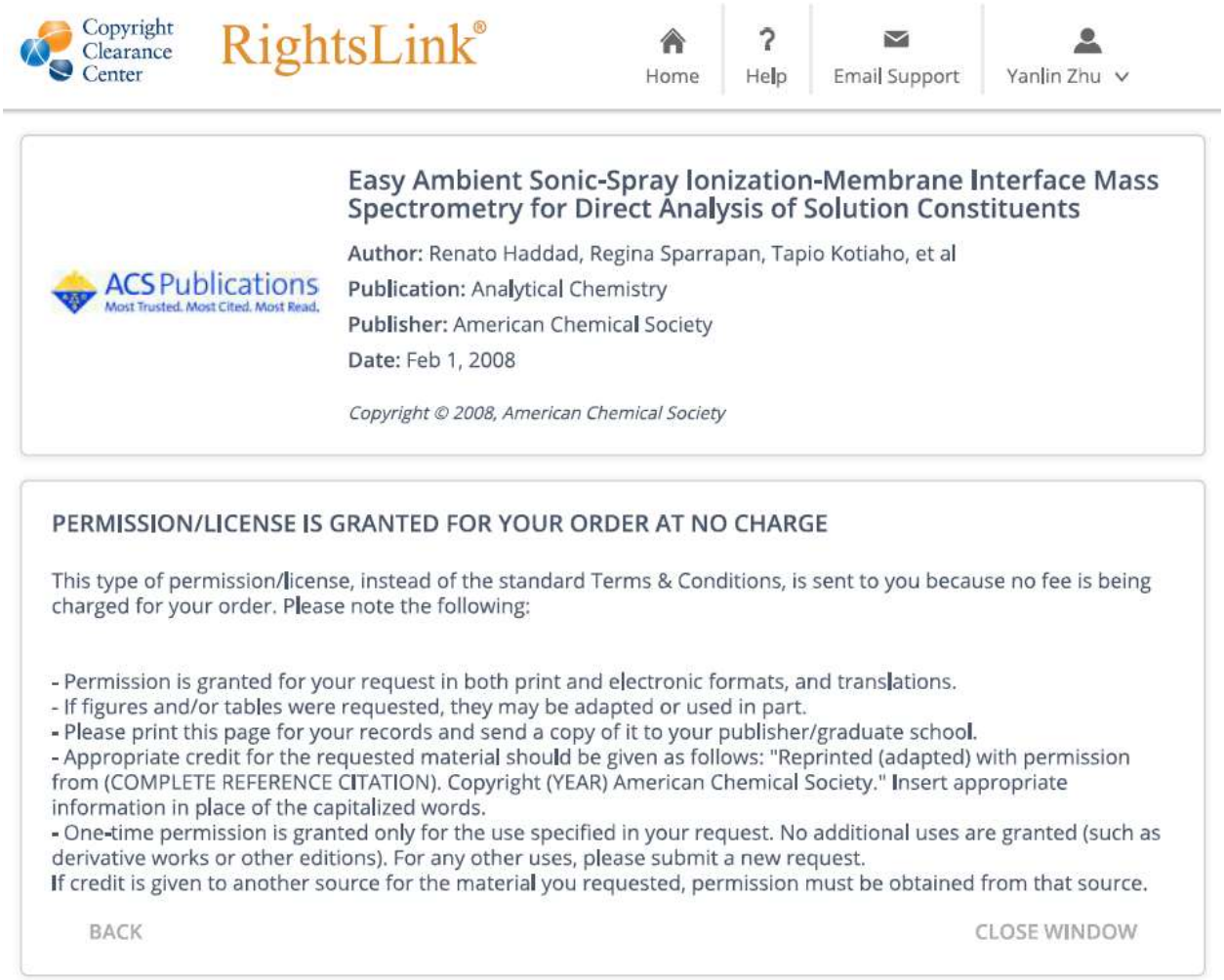
Copyright of Figure 1-10



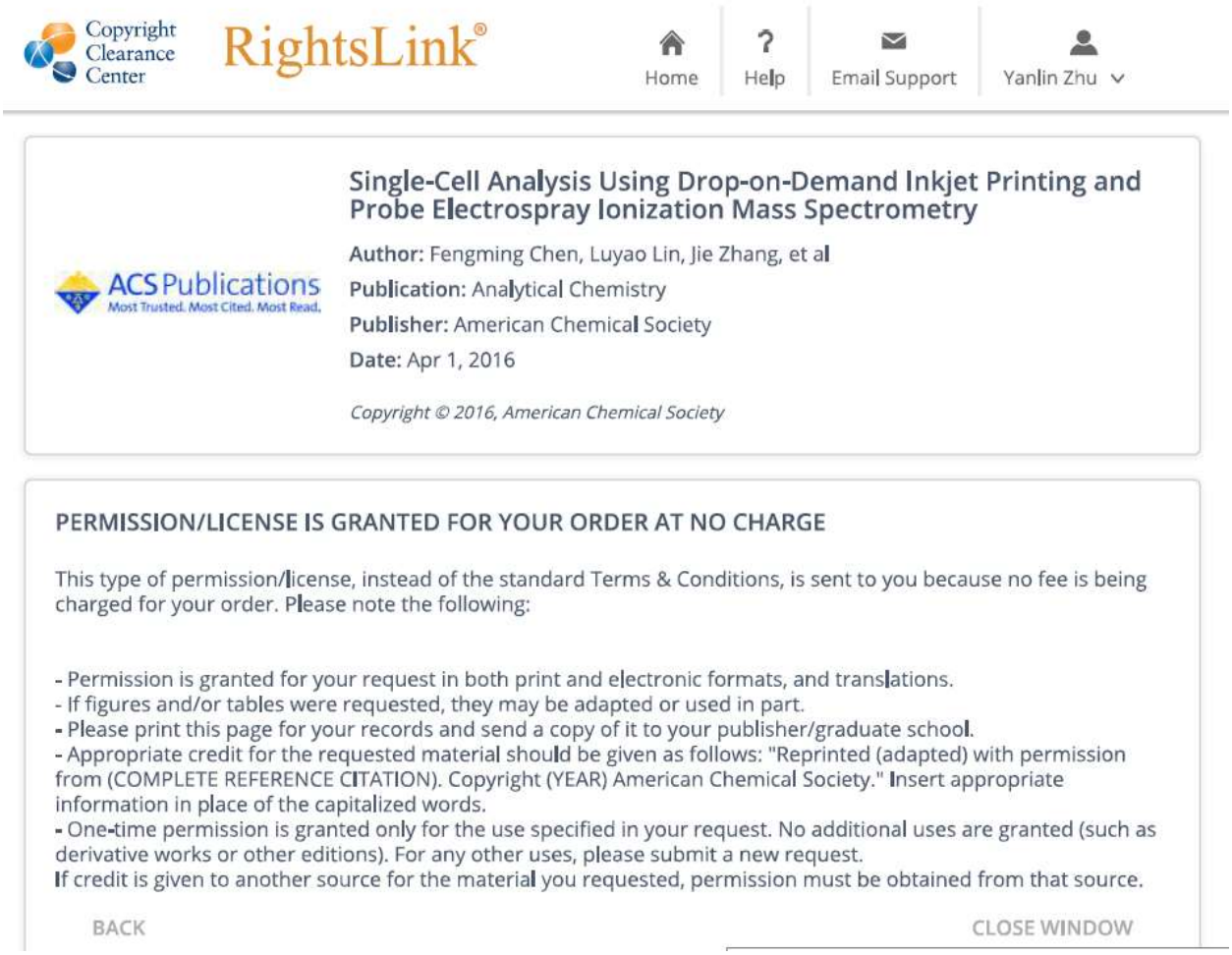
Copyright of Figure 1-11



Copyright of Figure 1-12



Copyright of Figure 1-13



Copyright of Figure 1-14

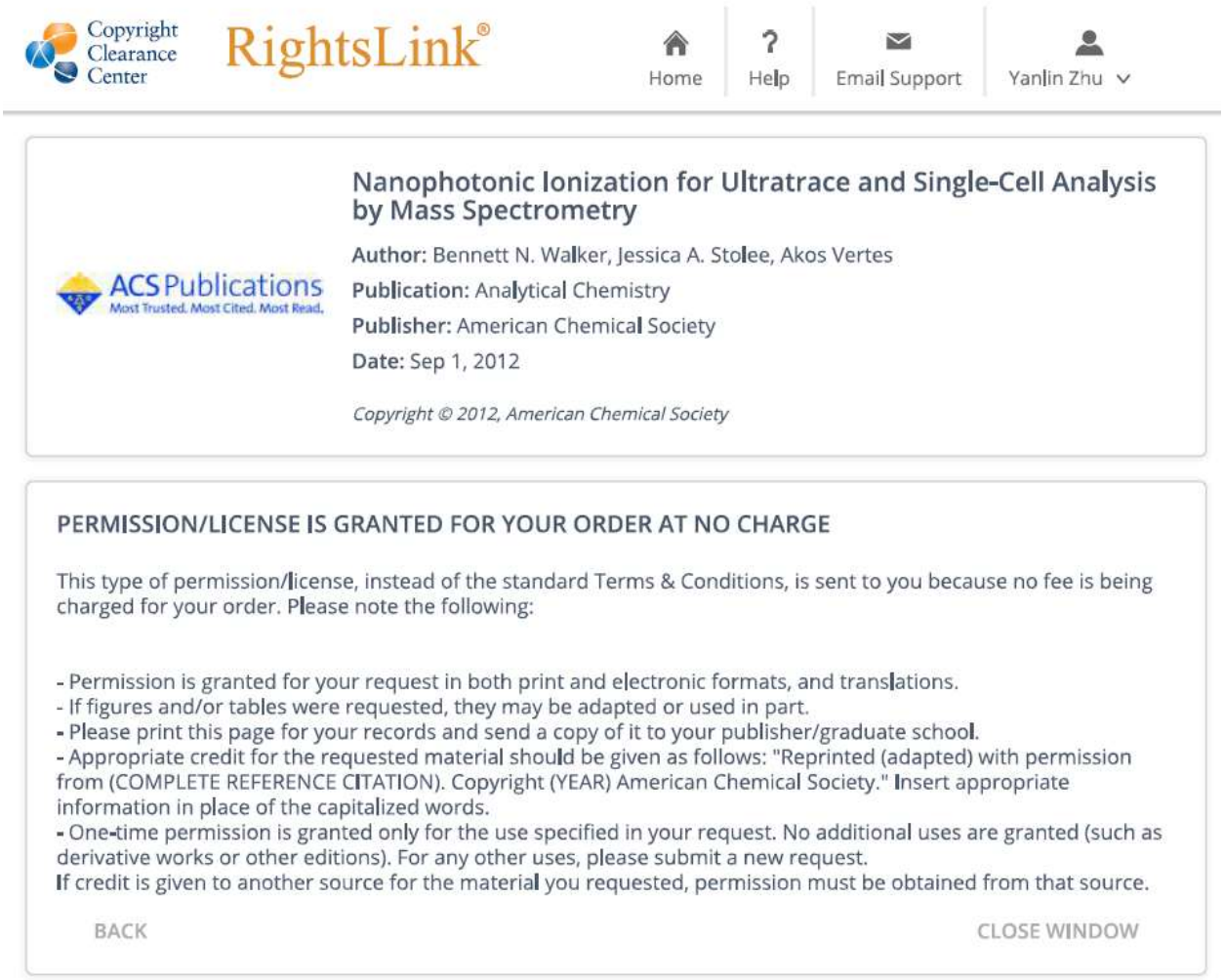
ELSEVIER LICENSE
TERMS AND CONDITIONS

Jul 18, 2020

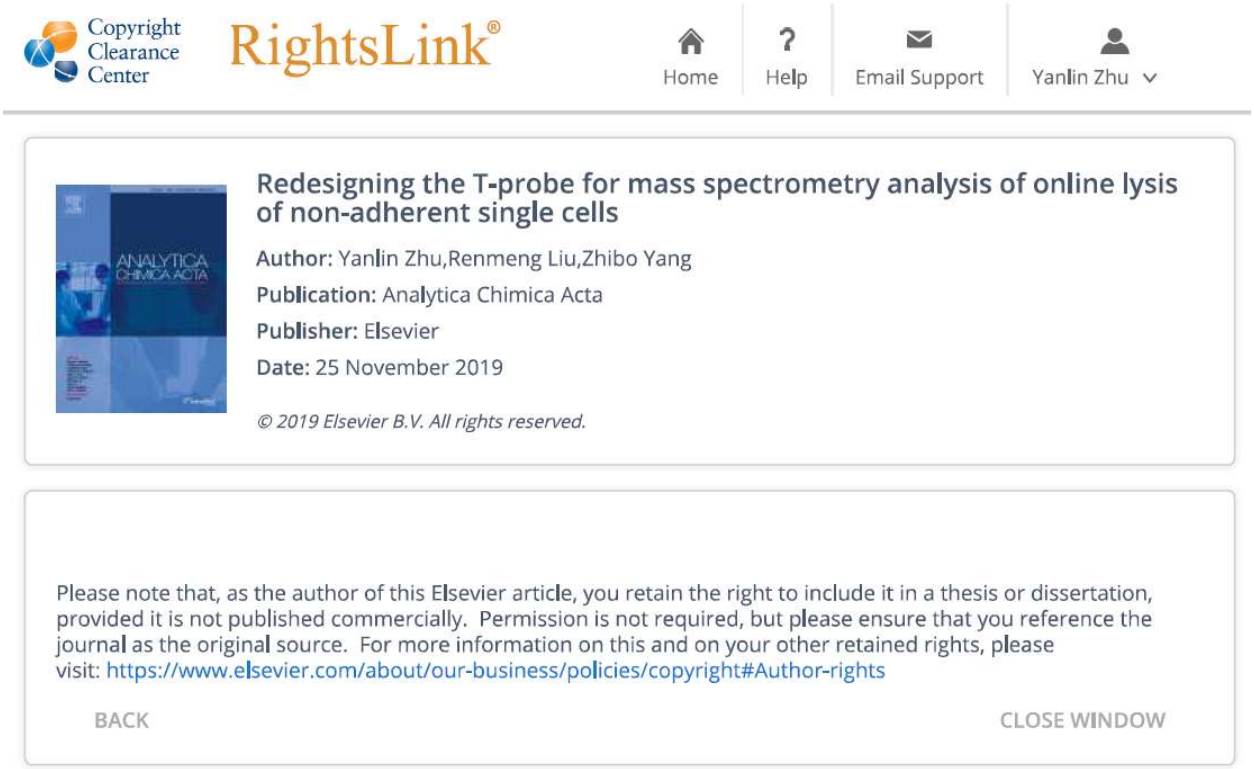
This Agreement between University of Oklahoma -- Yanlin Zhu ("You") and Elsevier ("Elsevier") consists of your license details and the terms and conditions provided by Elsevier and Copyright Clearance Center.

License Number	4872200022466
License date	Jul 18, 2020
Licensed Content Publisher	Elsevier
Licensed Content Publication	Trends in Immunology
Licensed Content Title	A deep profiler's guide to cytometry
Licensed Content Author	Sean C. Bendall,Garry P. Nolan,Mario Roederer,Pratip K. Chattopadhyay
Licensed Content Date	Jul 1, 2012
Licensed Content Volume	33
Licensed Content Issue	7
Licensed Content Pages	10
Start Page	323
End Page	332
Type of Use	reuse in a thesis/dissertation

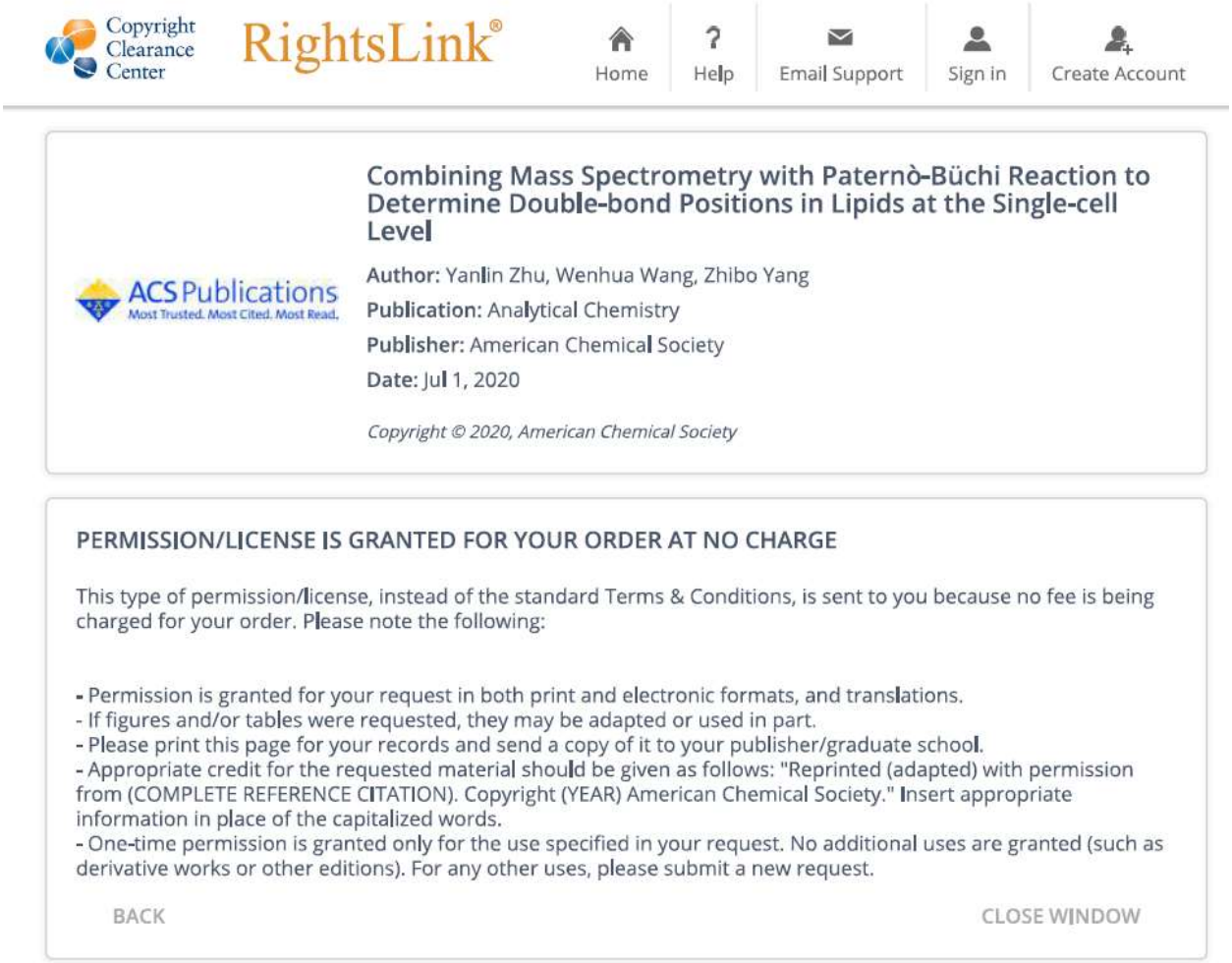
Copyright of Figure 1-15



Copyrights of Chapter 3



Copyrights of Chapter 4



Copyright Clearance Center RightsLink®

Home | Help | Email Support | Sign in | Create Account

ACS Publications
Most Trusted. Most Cited. Most Read.

Combining Mass Spectrometry with Paternò-Büchi Reaction to Determine Double-bond Positions in Lipids at the Single-cell Level

Author: Yanlin Zhu, Wenhua Wang, Zhibo Yang
Publication: Analytical Chemistry
Publisher: American Chemical Society
Date: Jul 1, 2020

Copyright © 2020, American Chemical Society

PERMISSION/LICENSE IS GRANTED FOR YOUR ORDER AT NO CHARGE

This type of permission/license, instead of the standard Terms & Conditions, is sent to you because no fee is being charged for your order. Please note the following:

- Permission is granted for your request in both print and electronic formats, and translations.
- If figures and/or tables were requested, they may be adapted or used in part.
- Please print this page for your records and send a copy of it to your publisher/graduate school.
- Appropriate credit for the requested material should be given as follows: "Reprinted (adapted) with permission from (COMPLETE REFERENCE CITATION). Copyright (YEAR) American Chemical Society." Insert appropriate information in place of the capitalized words.
- One-time permission is granted only for the use specified in your request. No additional uses are granted (such as derivative works or other editions). For any other uses, please submit a new request.

BACK CLOSE WINDOW

Copyrights of Figure 4-1

ELSEVIER LICENSE
TERMS AND CONDITIONS

Jul 19, 2020

This Agreement between University of Oklahoma -- Yanlin Zhu ("You") and Elsevier ("Elsevier") consists of your license details and the terms and conditions provided by Elsevier and Copyright Clearance Center.

License Number	4872710685815
License date	Jul 19, 2020
Licensed Content Publisher	Elsevier
Licensed Content Publication	Survey of Ophthalmology
Licensed Content Title	Beyond the cherry-red spot: Ocular manifestations of sphingolipid–mediated neurodegenerative and inflammatory disorders
Licensed Content Author	Hui Chen,Annie Y. Chan,Donald U. Stone,Nawajes A. Mandal
Licensed Content Date	January–February 2014
Licensed Content Volume	59
Licensed Content Issue	1
Licensed Content Pages	13
Start Page	64
End Page	76